Session 2(a)

General Issues on Valves I

Session Chair

Robert Kershaw
Arizona Public Service Company

Flow Loop Testing and Validation of Thermal Binding Model for Wedge Gate Valves

J. K. Wang, Desi Somogyi, P. Daniel Alvarez, M. S. Kalsi
Kalsi Engineering, Inc.

John Hosler
Electric Power Research Institute

Abstract

This paper presents a validated methodology to predict unwedging thrust for gate valves that are exposed to temperature and pressure changes between closing and opening strokes. The simplified methodology is based upon first principle models that were exercised over a wide range of variations in design parameters, operating condition parameters and thermal binding scenarios, increasing or decreasing the unwedging thrust. Flow loop tests were performed to systematically vary these parameters.

Methodology provided bounding predictions for all test data. The paper also summarizes the applicability and implementations of the methodology.

Introduction

The capability of gate valves to open can be critical to the safe operation of a nuclear power plant. The thrust required to unwedge solid and flexible wedge gate valves can increase, potentially compromising the ability to open, when subjected to temperature changes between the time the valve is closed and when it is required to open [1 through 6*]. This phenomenon is referred to as "gate valve thermal binding."

U.S. Nuclear Regulatory Commission Generic Letters 89-10 (Supplement 6) and 95-07 recommend that all U.S. nuclear power plants identify and address the potential for pressure locking and thermal binding in gate valves in safety-related systems. The industry has developed validated pressure locking methodologies [7,8,9]. However, the thermal binding phenomenon is significantly more complex, and until now, no validated thermal binding methodology has been available to predict the increase in unwedging thrust under thermal binding scenarios.

To meet this industry need, the Electric Power Research Institute (EPRI) undertook the development and validation of a gate valve thermal binding methodology, as described in earlier papers [10 and 11]. A first principles analytical model was developed that takes into account all the important parameters that contribute to the thermal binding phenomenon. The model is comprised of the mechanical and thermal model. The analytical model was exercised over a wide range

* Numerals in brackets denote references listed at the end of this paper

of valve design parameters and operating conditions resulting in the development of a simplified, closed-form, hand calculation methodology to predict unwedging thrust.

A series of tests was conducted on a gate valve under various thermal binding conditions. In addition, data were obtained from thermal binding tests performed by Omaha Public Power District (OPPD), Fort Calhoun Nuclear Plant. Analytical predictions made using the simplified methodology were compared to all available test results to validate the model. Model development, testing, and validation tasks were performed under the Kalsi Engineering, Inc. quality assurance program, which meets the requirements of 10CFR50, Appendix B. The model development and validation are documented in a four volume report [12].

This paper summarizes the development of EPRI gate valve thermal binding methodology, including a description of the mechanical model, simplified temperature prediction model, flow loop testing, and comparison of methodology predictions to test data. The paper also presents applicability and implementation of the methodology.

Thermal Binding Methodology Description

The EPRI thermal binding model is applicable to flexible wedge disc designs (Fig. 1) with or without a bonnet fluid communication feature, as well as solid wedge disc designs. The methodology does not account for traditional pressure locking conditions. Consequently, it is applicable only to valves in which the bonnet pressure is equal to or less than the upstream pressure.

Thermal Binding Scenarios

Two basic scenarios can cause a gate valve to thermally bind: *Scenario 1,* in which valve is closed hot and opened cold (CHOC), and *Scenario 2*, in which valve is closed cold and opened hot (CCOH). Additionally, the valve may be subjected to changes in upstream and downstream pressures either apart from or in conjunction with the temperature changes. It should be noted that pressure changes can influence unwedging thrust due to pressure-induced disc pinching phenomenon, as described in References 8 through 11. The methodology addresses both of these thermal binding scenarios, as well as changes in pressures.

Thermal Binding Mechanisms

The following mechanisms can influence the unwedging thrust after the valve is wedged closed and are included in the model:

- Changes in disc-to-seat interference (and contact force) due to changes in temperature as well as due to differences in coefficients of thermal expansion of disc, body, seat rings, and overlay materials,
- Differential expansion/contraction between the stem and valve topworks (i.e., upper body and yoke) due to differences in temperature and coefficients of thermal expansion,
- Changes in coefficients of friction as a function of differences between closing and opening temperatures.
- Changes in pressures upstream, downstream, and in the bonnet cavity of the valve body.

External piping loads can also influence unwedging thrust, however, they are excluded from the methodology.

Model Description

The required unwedging thrust after a valve is subjected to temperature and pressure changes under a thermal binding scenario is given by the following equation.

$$F_O = \frac{F_{sr} + F_{vert} + F_{pack} - F_p + F_w}{TRF}$$

Where

F_O = Required unwedging thrust, lb

F_{sr} = Seat frictional resistance force based on final seat reaction forces, R_1, R_2, and friction coefficient μ, before opening, lb

$= (2 R_{relx} R1 + R2 - R_1) (\mu \cos \theta - \sin \theta)$

R_{relx} = Ratio of seat unwedging/wedging seat contact forces derived from static wedging/unwedging thrust, lb

F_{vert} = Pressure load on projected areas of the wedge disc along the stem axis due to differences in bonnet, upstream and downstream pressures, lb

$= \pi A^2 \sin \theta (2 Pb - Pu - Pd)$

F_{pack} = Stem packing friction force, lb

F_p = Stem piston force, lb

F_w = Disc and stem assembly weight, lb

TRF = Torque reaction factor (dimensionless)

The important factors for calculating the unwedging thrust and their technical bases are described below.

Seat Friction Force, F_{sr}

F_{sr} is the key term that dictates increase/decrease in unwedging thrust under a thermal binding scenario. F_{sr} depends upon seat reaction forces, R_1 and R_2, and disc to seat friction coefficient μ. Changes in valve component temperatures, pressures and disc to seat friction coefficients between the time the valve is closed and when it is required to open contribute towards an increase/decrease in unwedging thrust as compared to the normal unwedging thrust. The sequence of pressure and temperature changes is also important in determining the final magnitude of F_{sr}. This requires iterative calculations that consider disc equilibrium along the pipe axis, disc equilibrium along the stem axis, and potential for further wedging of the disc due to these changes. The detailed model equations, their derivations, bases, and calculation procedures using data sheets are included in Reference 12.

Seat Contact Force Relaxation Ratio, R_{relx}

Test results show that, under constant temperature conditions, the actual stem unwedging thrust is usually lower than the theoretically predicted value for a given wedging thrust. This is due to the fact that when the stem forces are reversed from compression to tension, there is a change in the seat contact forces caused by changes in stresses in the disc and due to Poisson's ratio effect. In the thermal binding methodology (and in the EPRI MOV PPM, Ref. 13) this is defined as structural relaxation effect. R_{relx} accounts for the decrease in the seat contact force between wedging and unwedging from the theoretically calculated values due to structural relaxation effects. The magnitude of R_{relx} is calculated from static wedging/unwedging thrusts using equations described

[12]. The model also provides a bounding value for R_{relx} when test data are not available.

Disc, Body, Topworks Flexibility

To calculate changes in seat contact forces, stiffnesses of the disc, body, and valve topworks must be known. Valve body geometry is relatively complex. However, closed-form equations have been developed to calculate body stiffnesses [9-12]. These equations are based on a matrix of three-dimensional finite element analysis (FEA) results to cover variations in valve body geometries related to size, pressure class, and valve manufacturers.

The methodology also provides for closed-form equations to calculate disc stiffness. The disc stiffness equations are based upon classical formulas for plate stresses and deflections. These formulas were refined by performing a matrix of FEA's to account for elasticity of the hub and to cover variations in disc geometries based upon size, pressure class and manufacturers.

The valve topworks stiffness is calculated using stem dimensions and data from the static closing thrust signature for a MOV. Data sheets are provided in the methodology for calculating body, disc and valve topworks stiffnesses.

Disc to Seat Friction Coefficients

Under EPRI MOV PPM [13], extensive separate effects tests and flow loop tests were performed to determine friction coefficient between disc and seat faces overlaid with Stellite 6 hard facing. The friction coefficient depends upon fluid medium, fluid temperature, and contact stress. Even under the same conditions, friction coefficient can vary significantly. The EPRI thermal binding methodology provides different values for closing and for opening strokes based upon these parameters and variations in friction coefficients.

Component Temperature Predictions

The methodology provides simplified closed-form temperature algorithms for calculating component temperatures required in the model to predict unwedging thrust, based upon dimensions shown in Figure 2.

Lumped Parameter Model (LPM) and CFD Analyses

The simplified algorithms are based upon an extensive matrix of steady state thermal analyses performed using a Lumped Parameter Model (Fig. 3) that simulates thermal characteristics of a wedge gate valve both in the open and closed positions. The gate valve thermal characteristics were also modeled using a three-dimensional Computational Fluid Dynamics (CFD) approach. Figure 3 shows the detail of the lumped parameter model. Figures 4 and 5 show the details of the coupled fluid flow and heat transfer CFD model.

The LPM was developed to efficiently calculate results for a large number of analyses to address variations in valve design and operating parameters. The CFD model was developed to benchmark and verify the assumptions of heat transfer coefficients and modeling simplifications incorporated in the LPM, which is based upon simple conduction and convection equations for extended fin surfaces. Figure 6 shows typical temperature distributions for an open valve. For an open valve, the disc seat and the body are at a relatively uniform temperature and the temperature gradients are primarily in the stem and yoke. For a closed valve, significant temperature gradients are also present in the

valve disc and body from the upstream side to the downstream. Detailed comparisons of the temperature distributions and convective heat transfer film coefficients, obtained by CFD analyses in the upstream, bonnet cavity and downstream regions of the valve, confirmed the adequacy of the LPM.

The LPM was then exercised over a wide range of variations of the following parameters to provide detailed thermal maps:

Disc in the open and in the closed positions.

For closed valve, different fluid mediums in the upstream, bonnet, and downstream regions;

Key dimensions that vary with valve size, pressure class, and the manufacturer;

Valve component materials;

Fluid temperature;

Flow rate;

Insulation thickness.

In the parametric analyses, the nominal valve geometry selected was based on average dimensions from a number of valve manufacturers' designs for 6" ANSI 900 conventional wedge gate valves. The geometric variations covered wide variations in key dimensions found over the size range from 2" to 18" and pressure classes from ANSI class 150 to 2500. Typical results showing variations in temperatures with valve size for a valve exposed to 650°F are shown in Figures 7 and 8. Figure 7 is for an open valve and Figure 8 is for a closed valve with no bonnet fluid communication to upstream side.

Simplified Temperature Prediction Algorithms

Closed-form equations to calculate valve component temperatures from the LPM results of parametric thermal analysis were developed for use in the EPRI thermal binding methodology. Simplified temperature prediction algorithms predict the component temperatures based upon the fluid temperature, valve size, valve dimensional ratios that define distortions from the nominal valve proportions, the specific material combination being used for various components of the valve and whether the valve is insulated or not.

Temperature predictions for a specific valve size and geometry use the nominal valve size predictions which are modified by multiplying with a number of Adjustment Factors, A_{ij} to cover design parameters and operating parameters applicable for that analysis. The methodology provides separate graphs and tables for Adjustment Factors to cover three major categories of analysis: (1) open valve, (2) closed valve with no bonnet communication to the upstream fluid, and (3) closed valve with bonnet communication to the upstream fluid.

Figure 9 shows an example Adjustment Factor for a bonnet wall thickness ratio effect for a closed valve with no bonnet to upstream fluid communication. Figure 10 shows an adjustment factor for insulation thickness for the closed valve with no bonnet to upstream fluid communication. The simplified methodology uses piecewise linear interpolation for all geometrical ratio dependent Adjustment Factors (e.g., for bonnet wall thickness ratio effect) and discreet Adjustment Factors for some parameters (e.g., for insulation or no insulation cases and for six combinations describing fixed material choices for various valve components).

Applicability

The EPRI thermal binding model is applicable to gate valves with the following features:

Disc types: Single-piece, flexible or solid wedge.

Valve sizes: 2" to 18" (Note: Body stiffness predictions have been validated against FEA results only from 3" to 14" sizes.)

Valve materials: The methodology is applicable to the following six base material combinations; with the disc and seat faces being hard-faced with Stellite 6 in all cases.

Insulation: Both insulated and uninsulated valves

Fluid type: Steam or water

Material Combination	Body	Disc	Seat	Stem	Bonnet Cap	Yoke
1	C.S.	C.S.	C.S.	C.S.	C.S.	C.S.
2	C.S.	C.S.	C.S.	410 S.S.	C.S.	C.S.
3	C.S.	C.S.	C.S.	17-4 S.S.	C.S.	C.S.
4	C.S.	C.S.	C.S.	316 S.S.	C.S.	C.S.
5	316 S.S.	316 S.S.	316 S.S.	316 S.S.	316 S.S.	C.S.
6	316 S.S.	316 S.S.	316 S.S.	316 S.S., 410 S.S., or 17-4 S.S.	316 S.S.	316 S.S.

Fluid temperature: 35°F to 650°F

Bonnet Pressure: Valves with bonnet pressure equal to or less than the upstream pressure

Thermal binding scenarios:

(1) Valve closed hot and opened cold (CHOC) or opened at lower temperature

- With differential pressure while closing
- Without differential pressure while closing

(2) Valve closed cold and opened hot (CCOH)

- bonnet in communication with upstream side
- bonnet not in communication with upstream side

Note: The model assumes that relatively steady-state thermal conditions have been achieved. Consequently, it is considered applicable to the typical reactor heat-up and cool-down rates for pressurized water reactors (PWRs) and boiling water reactors (BWRs); rapid thermal transients are outside the scope of the model.

External piping loads: Not included in the model

Methodology Implementation

Figure 11 shows key steps in implementing the methodology. Detailed data sheets, tables and figures are provided in Reference 12 to calculate the unwedging thrust bases on all the relevant valve design parameters, data from static in-situ tests, and history of changes in fluid temperatures and pressure between wedging and unwedging. Figure 2 shows the dimensional data required to perform temperature calculations.

Flow Loop Testing

To validate the analytical model, flow loop tests were performed by EPRI to cover a wide range of thermal binding scenarios. Additionally, data were obtained from thermal binding tests performed by Omaha Public Power District (OPPD) at Wyle Test Laboratories.The test specimens and the test matrix for these flow loop tests are described below. All test data meet 10 CFR Appendix B quality assurance (QA) requirements.

Test Specimens

EPRI Test Valve is a 3-inch, Class 1500 Velan wedge gate valve (Fig. 12) in which both a flexible wedge and a solid wedge were tested (Fig. 13). The valve is of a pressure sealed bonnet design comprised of the following basic components and materials: The valve body, seat, disc and yoke were made out of carbon steel material, and the valve stem was made of 410 stainless steel. Both the disc and seat were hard-faced with Stellite 6.

OPPD Test Valve is a 2.5-inch, Class 2500 Crane-Aloyco flexible wedge gate valve with a pressure sealed bonnet design (Fig. 14). The valve is comprised of the following basic components and materials: Valve body seat disc and stem were made of 316 stainless steel and the valve had a carbon steel yoke. Both disc and seat faces were hard-faced with Stellite 6.

Test Matrix

EPRI Valve Test Matrix

EPRI Test Valve was extensively instrumented to provide external and internal temperature measurements at various locations on the valve components in addition to thrust, pressure, and differential pressure data (Fig. 15). Table 1 summarizes the overall test matrix for EPRI Test Valve. The following parameters were systematically varied in the test matrix, which consisted of 15 test cases:

Thermal binding scenarios: The valve was tested under both thermal binding scenarios, i.e., closed hot, opened cold (CHOC), and closed cold, opened hot (CCOH). The last two test cases in Table 1 are modifications of Scenario 1 in which the valve was closed hot and allowed to cool down to a lower temperature, instead of ambient temperature, before opening.

Pressure-induced disc pinching: Tests were performed with and without pressure induced disc pinching effect in conjunction with the appropriate thermal binding scenarios.

Disc stiffness: Two different disc designs, flexible and solid wedge, were used to evaluate effect of disc stiffness on unwedging thrust under similar thermal binding scenarios.

Operating temperature: Operating steam temperatures of 650°F, 450°F, and 350°F were used to determine the fluid temperature effect on unwedging thrust. The corresponding pressures for saturated steam range were approximately 2200 psi, 430 psi, and 125 psi.

Insulation: Valves operated at high temperatures are usually insulated. Test matrix covered evaluation of the effect of no insulation in one of the tests. All other tests were performed with insulated valve.

In addition to the above test cases to determine the effect of thermal binding, static wedging and unwedging tests were performed for both flexible and solid wedge discs to obtain the baseline wedging/unwedging characteristics under ambient temperature conditions. These data were used to calculate the seat contact force reduction ratio, R_{relx}, due to structural relaxation. The disc-to-seat

friction coefficients for both upstream and downstream seats were measured under the appropriate fluid temperature conditions before wedging and after unwedging.

OPPD Valve Test Matrix

Flow loop tests on OPPD Test Valve were performed by OPPD with the primary objective of determining the maximum unwedging thrust the power operated relief valve (PORV) block valves at their plant to operate under applicable thermal binding scenarios (Fig. 16). Only the exterior of valve body was instrumented with thermocouples at selected locations. No tests were performed to determine the disc-to-seat friction coefficient. The valve was not insulated in any of the tests. OPPD Test Valve thermal binding testing involved heating the valve to a steady state condition, with steam at approximately 650°F, then closing the valve and allowing it to cool to a predetermined temperature before reopening.

The first series of tests were performed in which the valve was allowed to cool down to some intermediate temperature before opening. In these tests, it was not possible to confirm that steady state conditions were reached before unwedging due to the fact that thermocouples were applied only on the outside surface of the body; no temperature measurements of the disc, stem or yoke were attempted. Additionally, cooling of the test valve in these tests was achieved by closing an upstream valve instead of bringing down the temperature of the upstream fluid to the intermediate value. Therefore, data from this series of tests were not used for validation of the methodology due to the concern that the valve component temperatures may deviate significantly from the quasi-steady state conditions.

The second series of tests allowed the valve to cool to ambient temperature and achieve steady state conditions before opening. This series of tests, consisting of three test cases, was used in the methodology validation as tabulated in Table 2. All of these wedging/unwedging strokes were performed under similar operating conditions.

Flow Loop Test Results

Figure 17 summarizes results of all thermal binding tests performed by EPRI and OPPD. The unwedging thrust after the valve is subjected to a specific thermal binding scenario is compared to the estimated baseline unwedging thrust (with no thermal binding effect). The baseline unwedging thrust in the EPRI test is estimated by assuming a constant unwedging/wedging thrust ratio for a given valve obtained by ambient testing and applying this ratio to different closing thrusts for each test case to account for different closing thrusts due to changes in torque switch trip settings.

One can see that there is a wide variation in the unwedging thrust after valve is subject to a thermal binding scenario. The wedging thrust can increase significantly, exhibit a modest increase or even decrease as compared to the estimated baseline unwedging thrust, based on ambient conditions. The maximum increase in unwedging thrust from EPRI test was found for a solid wedge, closed cold, opened hot valve that was insulated. The maximum increase in unwedging thrust for the OPPD test was found for a closed hot, opened cold case for the uninsulated valve when the valve was under a transient thermal condition.

In general, higher thrust increases were found for the solid wedge/high stiffness disc, as expected. The CCOH scenario was found to result in modest increases and, in several

cases, even a decrease in unwedging thrust for test cases in which bonnet to upstream side fluid communication is provided. This is due to the fact that fluid communication to the bonnet tends to eliminate the disc to body temperature differences. The test results also show large increases in unwedging thrust for the CCOH scenarios in which the bonnet to upstream fluid communication is not permitted. This is attributed to the higher thermal gradients in the disc and body. The results show that bonnet to upstream communication that is provided in some applications to eliminate the traditional pressure locking conditions can also significantly reduce the thermal binding effect under CCOH scenarios.

Validation Results

The thermal binding methodology was validated by comparing model predictions to test data for EPRI and OPPD test valves. Figure 18 shows the comparison of opening thrust predictions to test results for both valves. This figure shows that the methodology predictions bound the test results for all test cases. As described in the test matrix, the validation comparisons include different thermal binding scenarios, pressure-induced disc pinching effect, disc stiffness, fluid temperature, bonnet to upstream fluid communication, and insulated versus uninsulated valves.

Figure 18 also shows a relatively wide scatter of test data versus predictions. The main contributing factors to the scatter are (1) the disc-to-seat friction coefficient can vary over a wide range, as observed in the EPRI valve thermal binding tests and other industry experience including EPRI MOV Performance Prediction Program [13], and (2) the valve component temperatures cannot be precisely predicted, due to the complex nature of the heat transfer phenomenon. Actual component temperatures can vary significantly, even under the same operating conditions, due to variations in convective heat transfer coefficients caused by fluctuations in ambient conditions, e.g., the degree of air circulation, and leakage of hot fluid across the upstream seat into the bonnet cavity for valves having no intentional bonnet fluid communication feature.

In spite of these variations and the complexity of the thermal binding phenomenon, the methodology provided bounding predictions for the required opening thrust for all test cases.

Conclusions

A first-principles model for predicting the required unwedging thrust for a wedge gate valve under thermal binding conditions has been developed. The model accounts for both closed hot, opened cold and closed cold, opened hot thermal binding scenarios. The model is applicable to solid wedge and flexible wedge gate valves with or without bonnet to upstream fluid communication. The model also accounts for superimposed effect of changes in upstream, bonnet, and downstream pressures that can affect the unwedging thrust. Traditional pressure locking phenomena is not included in the methodology. The methodology provides closed-form equations for predicting unwedging thrust.

The methodology was validated by comparing model predictions for opening thrust against flow loop test data under both thermal binding scenarios: closed hot opened cold as well as closed cold opened hot. The methodology predictions were found to bound test results for all test cases. Tests included different thermal binding scenarios, pressure-induced disc pinching effect, variations in disc

stiffnesses, valve designs with and without bonnet communication to the upstream fluid, changes in fluid temperatures, and tests with and without insulation. The overall ratio of measured thrust divided by predicted thrust ranged from 0.338 to 0.957 for all test cases.

Comparisons show that predictions for closed hot opened cold scenarios are in closer agreement than the closed cold opened hot scenarios for valve designs that do not have a bonnet fluid communication to the upstream side. This is due to the fact that thermal gradients for closed valves that have hot fluid present only on the upstream side of the disk are significantly affected by conditions that can not be controlled in practice, e.g., upstream seat-to-bonnet leakage, amount of air trapped in the upstream piping or the bonnet cavity. In spite of these effects, the methodology provides bounding predictions with reasonable conservatism for all cases.

The development of a validated thermal binding methodology is a significant milestone in the industry.

Acknowledgements

EPRI and Kalsi Engineering, Inc., are grateful to Omaha Public Power District/Fort Calhoun Station plant management, and, especially, Mr. Kevin Hyde, who was responsible for performing their thermal binding tests and providing the data and support during this project.

References

1. "Pressure Locking and Thermal Binding of Safety-Related Power-Operated Gate Valves," U.S. NRC Generic Letter 95-07, August 17, 1995.

2. *Operating Experience Feedback Report –Pressure Locking and Thermal Binding of Gate Valves*, U.S. NRC NUREG-1275 Vol. 9, March 1993.

3. Earl J. Brown. **Proceedings of Workshop on Gate Valve Pressure Locking and Thermal Binding**, U.S. NRC, NUREG/CP-0146, February 1994.

4. MOV Program Pressure Locking and Thermal Binding Evaluation, PI-20, Rev. 2, Northeast Utilities Service Company, May 1995.

5. J. K. Wang and M. S. Kalsi. *Improvements in Motor-Operated Gate Valve Designs and Prediction Models for Nuclear Power Plant Systems*, U.S. NRC NUREG/CR-5807, May 1992.

6. J. M. Farrel. *Thermal Binding and Pressure Locking in Gate Valves – Velan Experience*, **Proceedings of Workshop on Gate Valve Pressure Locking and Thermal Binding**, U.S. NRC, NUREG/CP-0146, February 1994.

7. Brian D. Bunte and John F. Kelly. *Commonwealth Edison Company Pressure Locking Test Report*, **Proceedings of the Fourth NRC/ASME Symposium on Valve and Pump Testing**, U. S. NRC NUREG/CP-0152, July 1996.

8. J. K. Wang, M. S. Kalsi, and S. S. Averitt. *Enhanced Pressure Locking Methodology*, presented at EPRI Sixth Valve Technology Symposium, July 1997.

9. J. K. Wang, S. S. Averitt, and M. S. Kalsi. "Generalized Pressure Locking Methodology," Kalsi Engineering, Inc. Document No. 1698, Rev. 1, August 2000.

10. M. S. Kalsi, J. K. Wang, and D. Somogyi. *Development and Validation of a Thermal Binding Methodology for Gate Valves,*

presented at EPRI Sixth Valve Technology Symposium, July 1997.

11. M. S. Kalsi, J. K. Wang, D. Somogyi, J. Hosler, *Thermal Binding Model for Wedge Gate Valves - Analytical Predictions and Validation Test Plan,* presented at EPRI/NMAC Seventh Valve Symposium, May 1999.

12. **EPRI Gate Valve Thermal Binding Unwedging Thrust Methodology, Volumes 1 through 4**, Electric Power Research Institute, E210203, October 2001.

13. **EPRI MOV Performance Prediction Program—Gate Valve Model Report**, Electric Power Research Institute, TR-103229, August 1994.

14. **Mathcad 4.0 User's Guide**, MathSoft, Inc., 1993.

Table 1 EPRI Valve Test Cases for Methodology Validation

Test Case*	Disc	Insu-lated?	Closing Conditions		Opening Conditions	
			Pressures (P_u, P_b, P_d), psi	Fluid Temp, °F	Pressures (P_u, P_b, P_d), psi	Fluid Temp, °F
1-1, CHOC, 650	Flex	Yes	0, 0, 0	643	0, 0, 0	93
1-2, CHOC 650P	Flex	Yes	2100, 2100, 2100	638	0, 0, 0	90
1-3, CCOH, 650UB	Flex	Yes	0, 0, 0	94	0, 0, 0	649
1-4, CCOH, 650U	Flex	Yes	0, 0, 0	86	0, 0, 0	649
2-1, CHOC 650	Flex	No	0, 0, 0	649	0, 0, 0	90
3-1, CCOH, 350 UB	Solid	Yes	0, 0, 0	83	0, 0, 0	359
3-2, CHOC 350P	Solid	Yes	125, 125, 125	348	0, 0, 0	75
4-1, CCOH, 450 UB	Solid	Yes	0, 0, 0	100	0, 0, 0	447
4-1R, CCOH, 450UB	Solid	Yes	0, 0, 0	99	0, 0, 0	450
4-2, CHOC, 450P	Solid	Yes	430, 430, 430	457	0, 0, 0	62
5-1, CCOH, 650UB	Solid	Yes	0, 0, 0	89	0, 0, 0	649
5-2, CHOC, 650P	Solid	Yes	2103, 2103, 2103	650	0, 0, 0	70
6-1, CCOH, 650U	Solid	Yes	0, 0, 0	72	0, 0, 0	641
7-1, CHOL, 650P	Solid	Yes	2163, 2163, 2163	647	0, 0, 0	572
8-1, CHOL, 350P	Solid	Yes	132, 132, 132	354	0, 0, 0	272

*The following nomenclature is used to describe test cases in this table:

CHOC = Valve was closed hot and opened cold (ambient temperature).
CCOH = Valve was closed cold and opened hot
CHOL = Valve was closed hot and opened lower (75°F lower than the closing temperature)
650/450/350 = Test temperature level
P = Closed with pressure for closed hot cases
U = Heated upstream side of the disc only for closed cold cases
UB = Heated upstream side of the disc and bonnet for closed cold cases

Table 2 OPPD Valve Test Cases for Methodology Validation

Test Case	Disc	Insu-lated?	Closing Conditions		Opening Conditions	
			Pressures (P_u, P_b, P_d), psi	Fluid Temp, °F	Pressures (P_u, P_b, P_d), psi	Fluid Temp, °F
HTC2/13A	Flex	No	2262, 2262, 2262	637	0, 0, 0	73
HTC3/13B	Flex	No	2264, 2264, 2264	637	0, 0, 0	76
HTC3/13C	Flex	No	2226, 2226, 2226	632	0, 0, 0	57

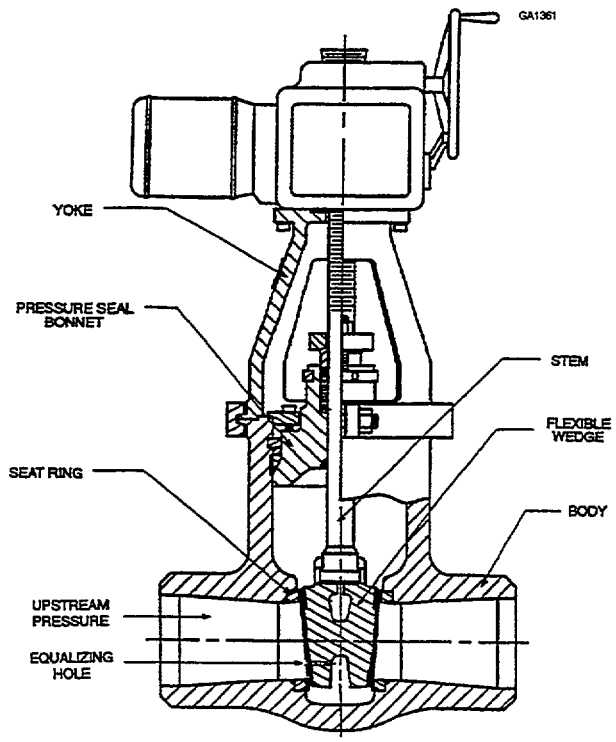

Figure 1 Typical Motor-Operated Wedge Gate Valve Assembly

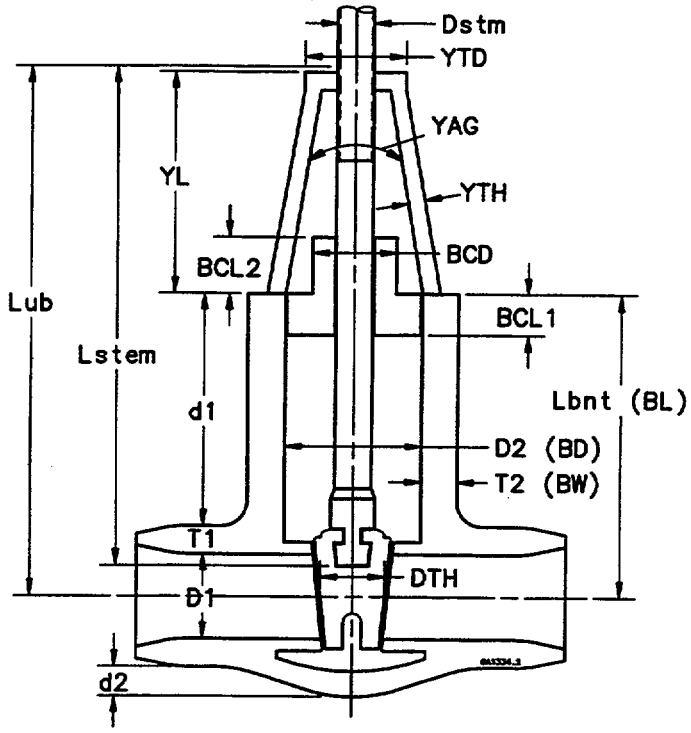

Figure 2 Dimensions required for performing Thermal Binding Calculations

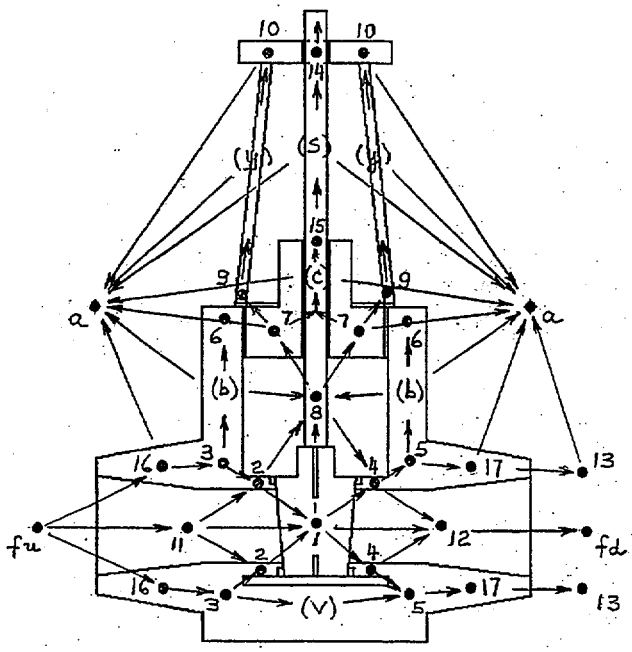

Figure 3 Schematic of the Closed Valve Lumped Parameter Thermal Model

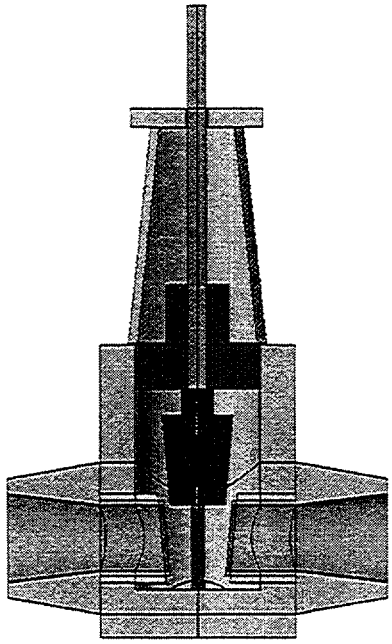

Figure 4 Simplified 3-D FEA Thermal Model of a Typical Gate Valve

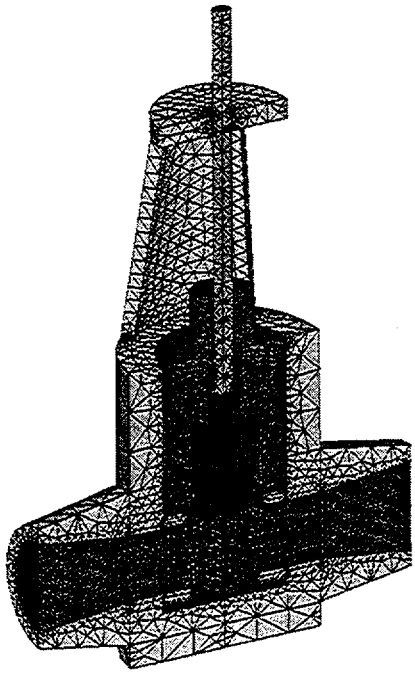

Figure 5 Open Valve Model Finite Element Meshing

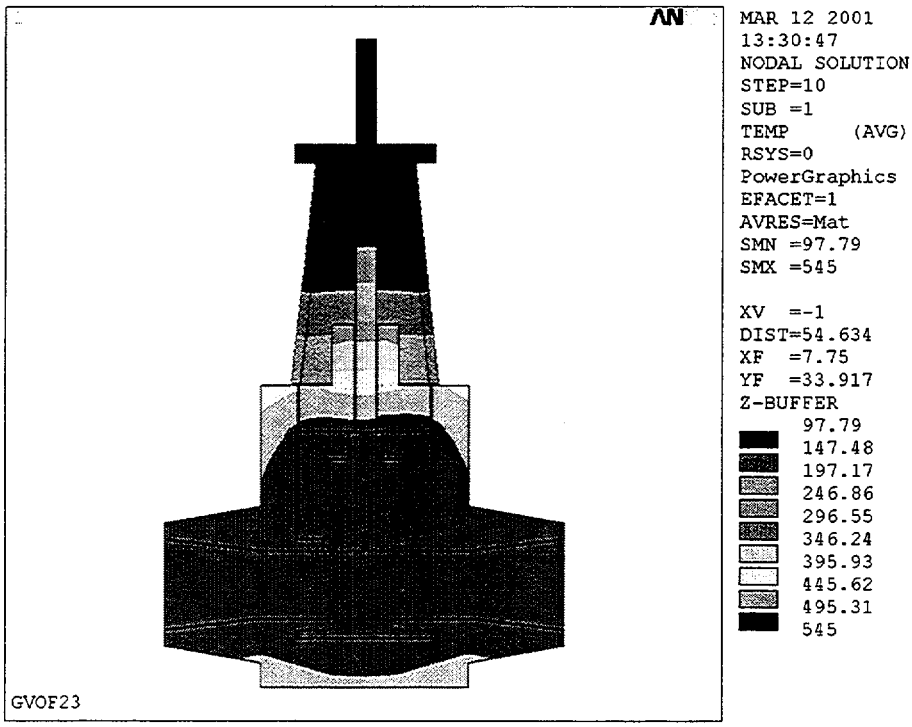

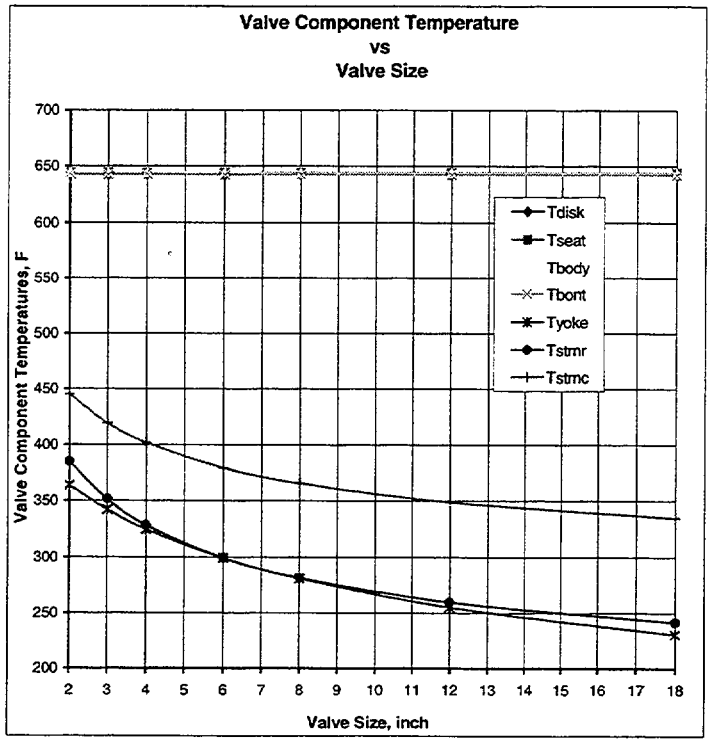

Figure 7 Valve Component Temperature Predictions for Open Valve

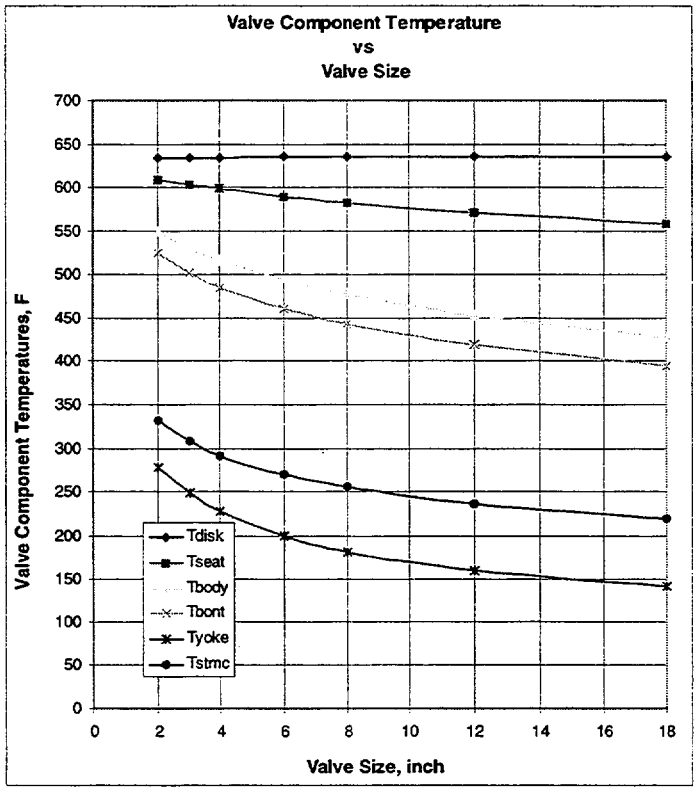

Figure 8 Valve Component Temperature Predictions for Closed Valve With No Bonnet to Upstream Fluid Communication

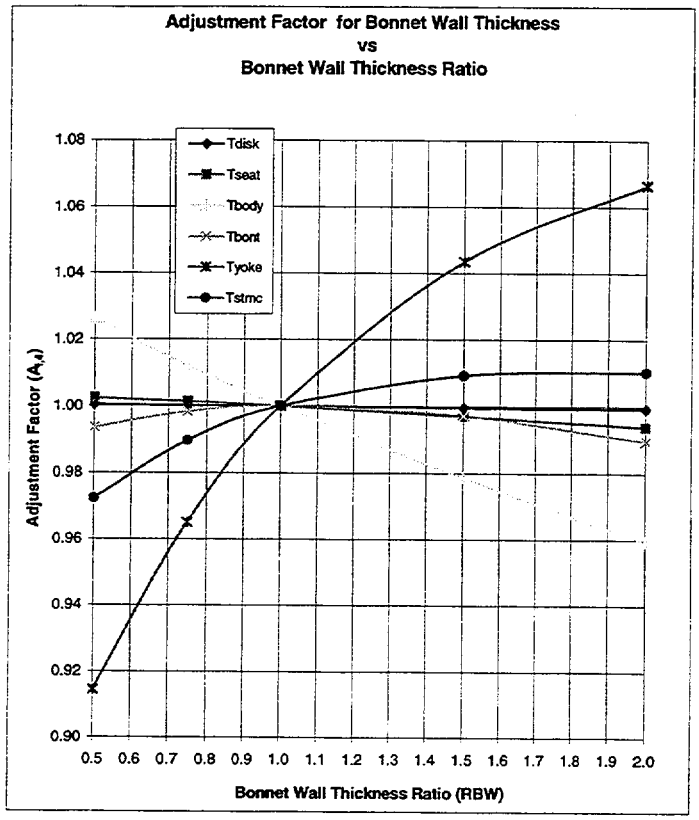

Figure 9 Example of Adjustment Factor for Bonnet Wall Thickness for Closed Valve With No Bonnet to Upstream Fluid Communication

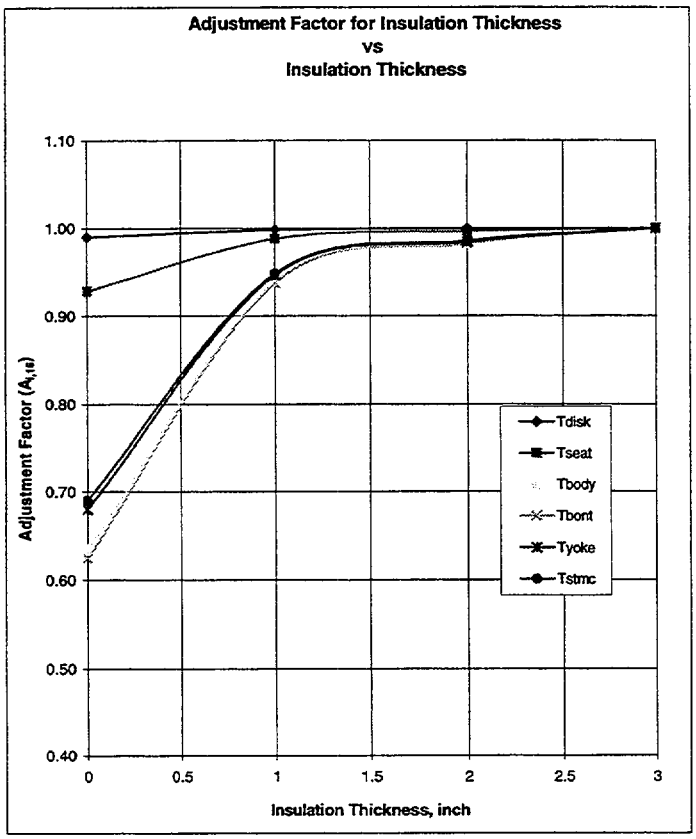

Figure 10 Example of Adjustment Factor for Insulation for Closed Valve With No Bonnet to Upstream Fluid Communication

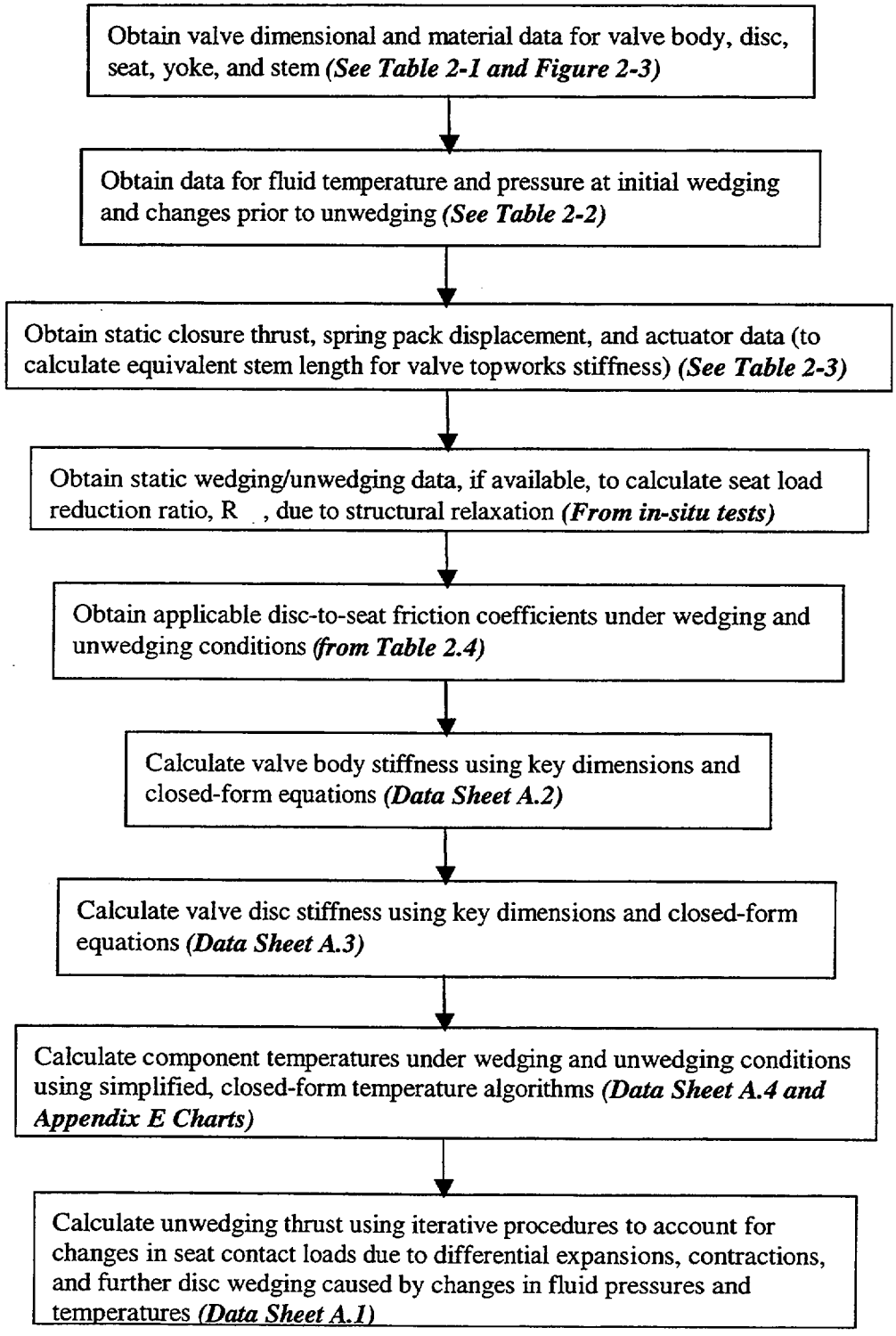

Figure 11 Thermal Binding Methodology Implementation

*Note: Tables, Figures and data sheets in this figure pertain to Ref. 12.

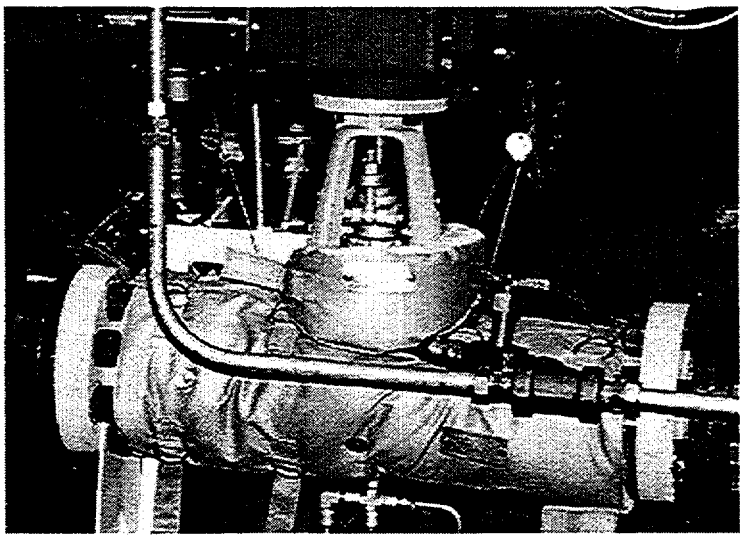

Figure 12 EPRI Valve Test Setup

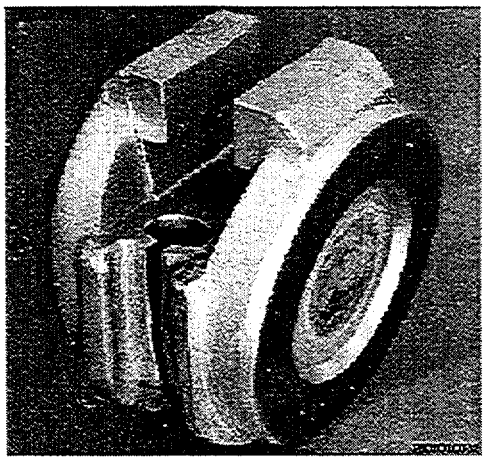

Flexible

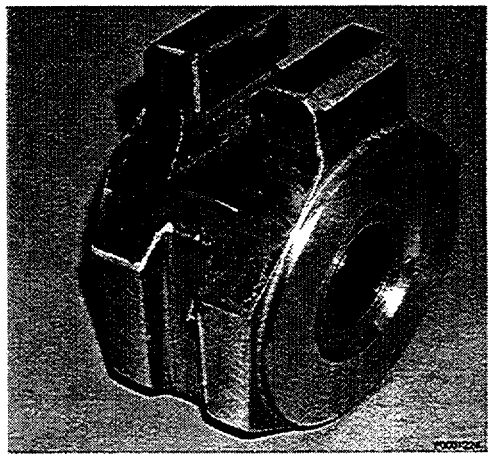

Solid

Figure 13 Flexible Wedge and Solid Wedge Discs Used in the EPRI Test Valve

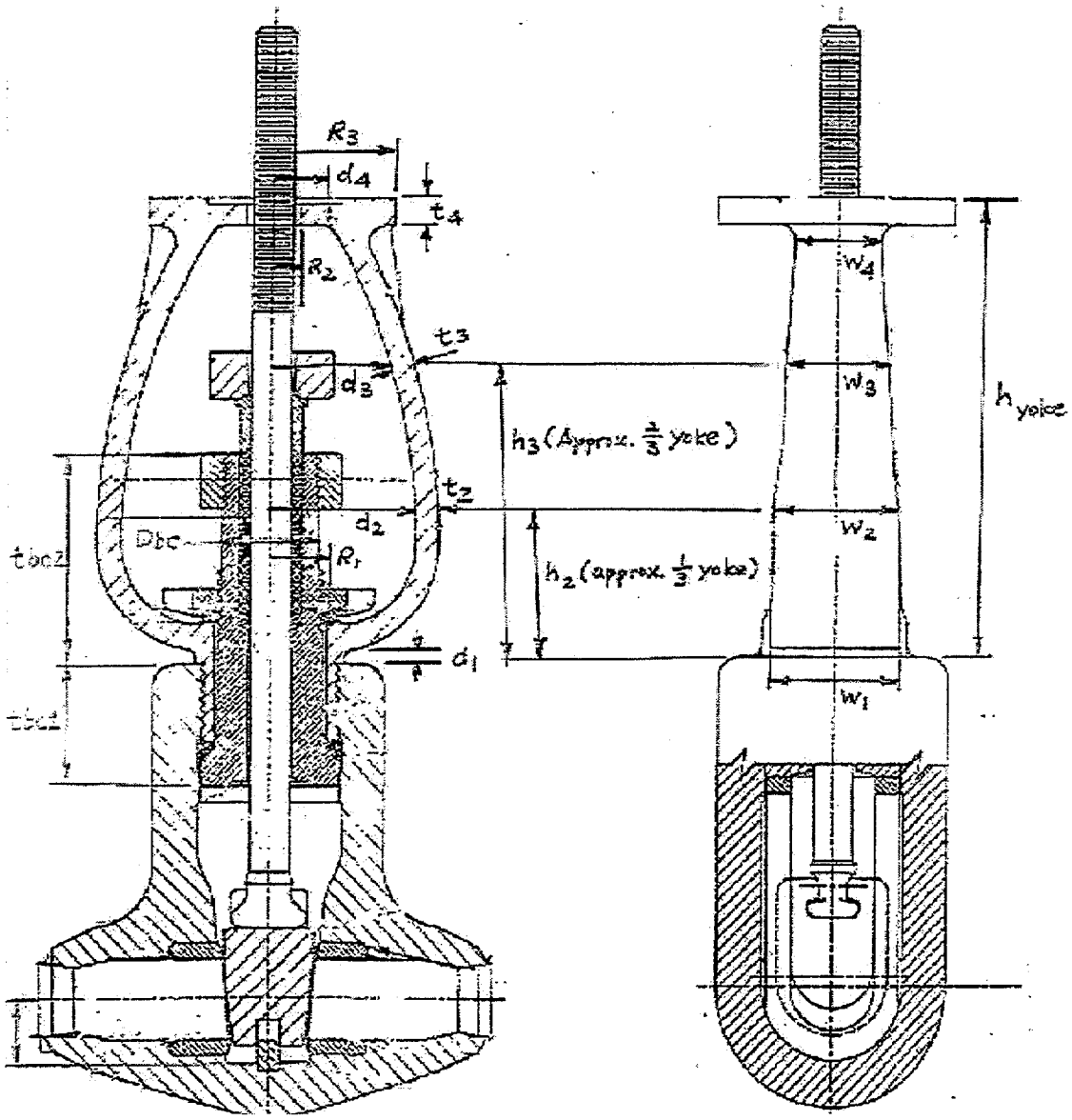

Figure 14 OPPD Test Valve

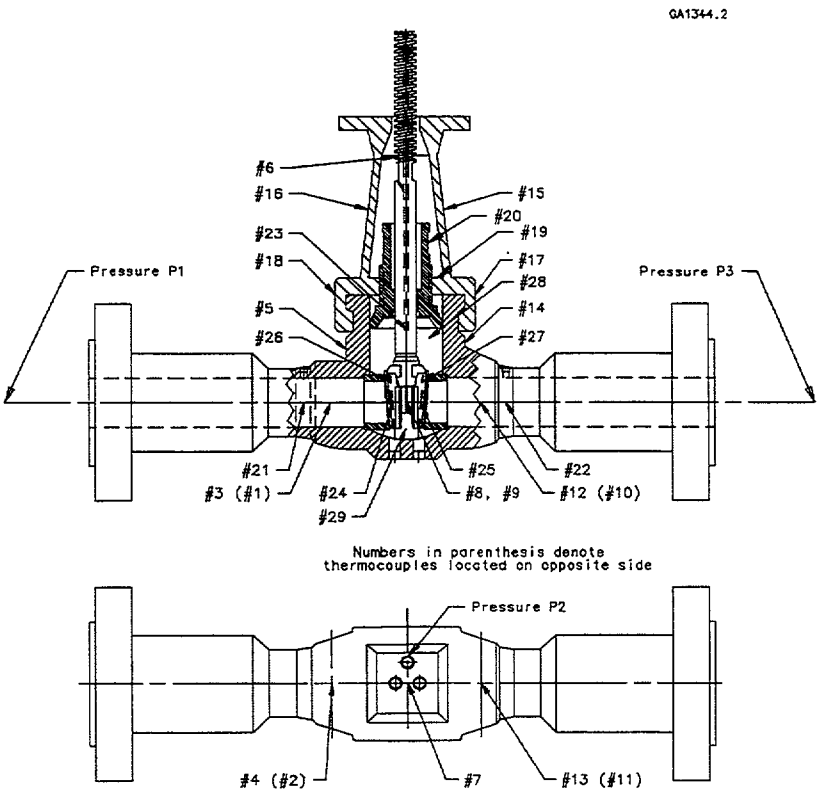

Figure 15 Thermocouple and Pressure Transducer Placement in EPRI Test Valve

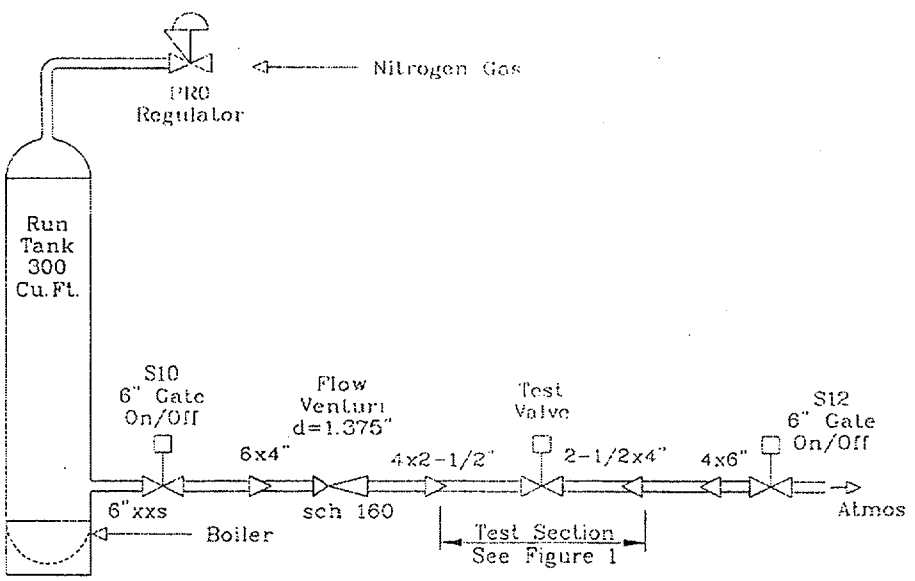

Figure 16 Flow Loop Test Setup of OPPD Test Valve

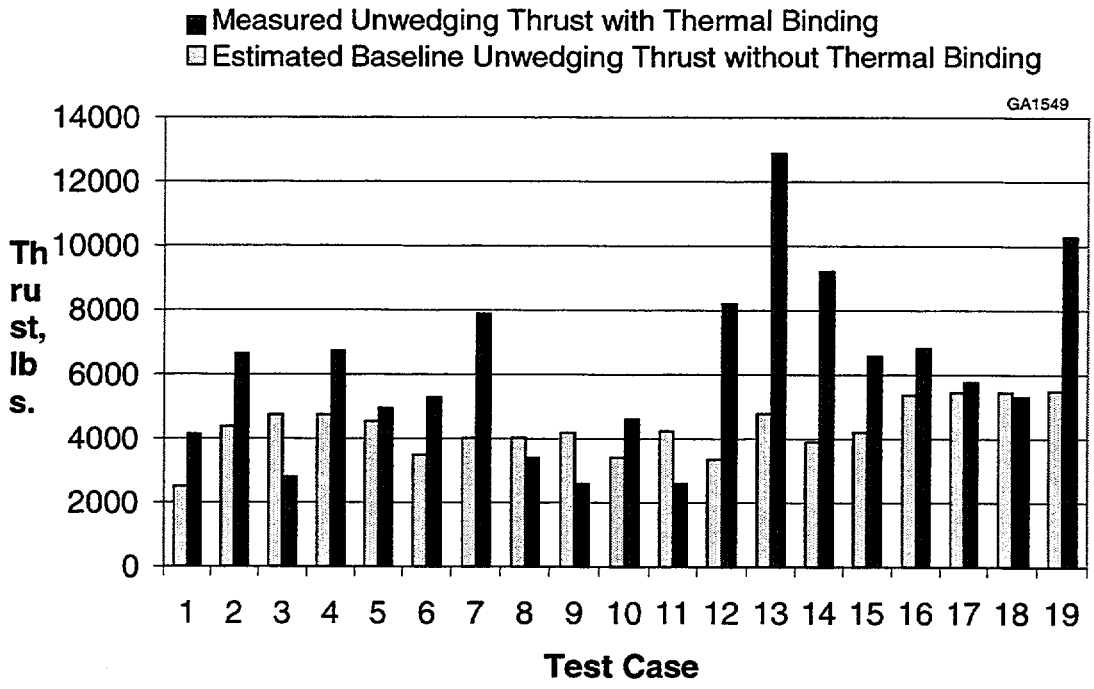

Figure 17 Comparison of Measured Unwedging Thrust for Various Thermal Binding Tests to the Estimated Baseline Wedging Thrust

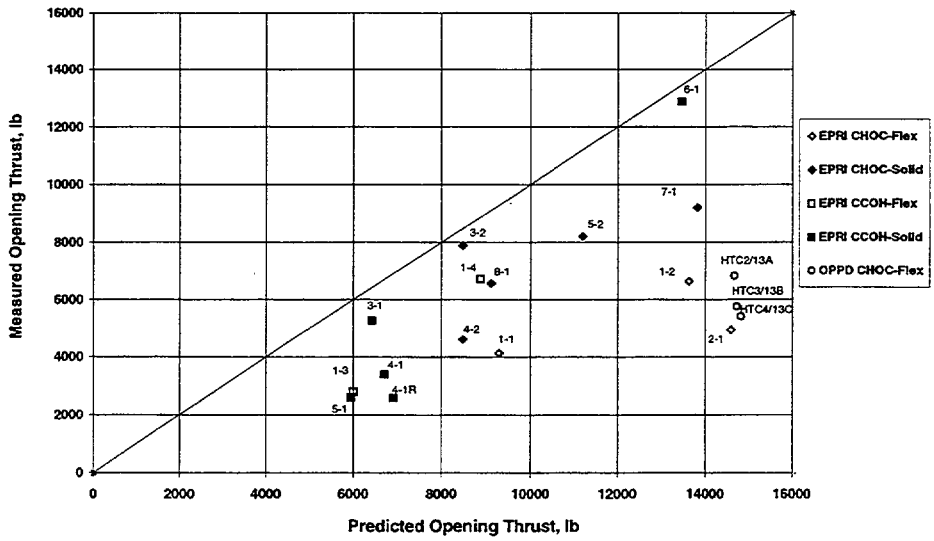

Figure 18 Comparison of Opening Thrust Predictions to Test Results Using Default Friction Coefficients and Simplified Methodology

Directional Leakage Experience With Large Butterfly Valves

Brian P. Lindenlaub, James W. Rowland, Edward H. Smith Jr., and Neil A. Thibodaux
Palo Verde Nuclear Generating Station
Arizona Public Service Company

Abstract

Recent experience at the Palo Verde Nuclear Generating Station has identified three leakage-related reliability concerns with certain large butterfly valves. The first concern is a newly-discovered failure mode for soft-seated butterfly valves in containment purge applications. The second concern involves testing discrepancies that may be encountered during reverse pressure testing of offset-stem butterfly valves. The third concern involves a packing configuration that can be susceptible to directional leakage characteristics, and thus may be unsuitable for reverse-direction leakage testing. This paper describes these three concerns, contributing factors, and corrective actions that can be taken.

Introduction

The Palo Verde Nuclear Generating Station (PVNGS) consists of 3 Combustion Engineering System 80 1250 MW pressurized water reactors located approximately 50 miles southwest of Phoenix, Arizona. During refueling outages, each unit's Containment Purge (CP) system provides ventilation to the containment building through two 42" penetrations, one for supply air (Penetration 56) and one for exhaust (Penetration 57). The CP system is shown schematically in Figure 1.

Each 42" CP penetration is equipped with two containment isolation valves (CIVs), one located inside the containment building and one located outside. Each valve is an ASME Class 2 motor-operated butterfly valve designed for nuclear air service. The valve has a vertical shaft and a single offset disc. There is no disc stop to limit disc rotation in the closed direction. The valves are oriented "back to back" in the penetration, as shown in Figure 2.

The valve seat consists of a carbon steel seat welded into the valve body. The valve seat has a very slight taper, actually a radius, to facilitate seating. A synthetic rubber seal made of Ethylene Propylene Terepolymer (EPT) is secured onto the valve disc with a segmented retaining ring and 48 retaining screws. The seating configuration is shown in Figure 3.

The valves are locked closed during power operation. A 10 CFR 50 Appendix J local leakage rate test (LLRT) is performed on the valves every 184 days per plant Technical Specifications. The LLRT is performed by pressurizing the space between the valves, which happens to test the inboard valves in the reverse direction. The combined leakage rate for both valves is determined by measuring the makeup flow required to maintain the 52 psig test pressure. The LLRT acceptance criterion is 0.05 L_a, where L_a is the maximum allowable containment leakage rate. 0.05 L_a is equivalent to 11,604 standard cubic

centimeters per minute (sccm). There are provisions for installing blind flanges on the outside of the outboard valves in case of valve leakage problems.

During an extensive investigation into leakage problems with these valves, three separate reliability concerns were identified. The first reliability concern is a newly-discovered failure mode for soft-seated butterfly valves in containment purge applications. The second concern involves testing discrepancies that may be encountered during reverse pressure testing of offset-stem butterfly valves. The third concern involves a packing configuration that can be susceptible to directional leakage characteristics, and thus may be unsuitable for reverse-direction leakage testing.

Background

Unit 1's 42" CP inboard supply CIV, 1CP3A, experienced several LLRT failures in 1999:

- 2/3/99 – As-found leakage rate exceeded 20,000 sccm. Leak detection fluid was used to identify leakage past the 1CP3A seat. After adjusting the seal retaining screws in the area of the leak, the LLRT was satisfactory.
- 8/2/99 –As-found leakage rate exceeded 20,000 sccm. After using the 1CP3A handwheel to adjust the disc position, the LLRT was satisfactory.
- 8/6/99 – Post-maintenance LLRT was performed following work on the outboard CIV, 1CP2A. The leakage rate exceeded 20,000 sccm. Leak detection fluid was used to identify leakage past the seat of 1CP3A, which had been adjusted and passed an LLRT just 4 days earlier. After adjusting the seal retaining screws in the area of the leak, the LLRT was satisfactory.

The initial investigation into these LLRT failures theorized that the valve disc was "coasting" too far past the seat. Since the valve is not equipped with positive disc stops, the valve is set up so that the MOV limit switch de-energizes the motor just before the valve is fully closed. The residual momentum of the gear train and disc then carry the disc the rest of the way into the seat. If the limit switch or the EPT seal is not adjusted precisely, the valve will coast too far (or not far enough) to seal properly. In addition, relaxation of residual torque in the gear train over time was thought to result in additional disc rotation in the closed direction.

On 9/22/99, work was performed on 1CP3A to correct this condition. The EPT disc seal was replaced, and the MOV limit switch and the new disc seal were adjusted so that the disc would "coast" just short of the center of the seat. The post-maintenance LLRT was successful, and it was believed that the valve was ready for the containment Integrated Leakage Rate Test (ILRT) scheduled about 5 weeks later at the end of the Unit 1 refueling outage.

On 10/30/99, the 42" CP CIVs were closed in preparation for the Unit 1 ILRT. Pre-ILRT LLRTs were successful on both penetrations. When the containment building was pressurized to 52 psig for the ILRT on 11/2/99, it was noticed that the pressure in penetration 56 closely followed containment pressure, indicating leakage past the inboard CIV, 1CP3A. The penetration was vented through a test connection while the containment was still pressurized in an unsuccessful attempt to seat the valve. Pressure in Penetration 56 also followed containment pressure while the containment was being depressurized. Visual inspection of the valve on 11/6/99 observed no anomalies; the seated position was found similar to the setup position of 9/22/99.

Additionally, a troubleshooting LLRT was successfully performed after the ILRT. It was obvious that the accident direction leakage observed during the ILRT did not match the results of the LLRTs (reverse-direction) performed immediately before and after the ILRT. A blind flange was installed on the outside of the penetration until a more detailed investigation could identify and correct the cause of the leakage.

An investigation team was formed to determine the cause or causes of the LLRT failures of 1CP3A and the ILRT leakage into Penetration 56 via the 1CP3A valve. After a lengthy investigation, the team identified the three distinct failure mechanisms described below.

1. Disc "Walking" Phenomenon

The most intriguing failure mechanism discovered during this investigation was the tendency for the disc to migrate, or "walk," through the seat during repeated pressurization cycles. This phenomenon is characterized by a sudden unexpected increase in the leakage rate due to the valve disc moving past the properly closed and sealed position and breaking the seal. The valve disc is "driven" through the seat by the complex frictional forces that occur during pressure cycles. It is believed that this is the mechanism that led to the LLRT failures of 1CP3A in 1999.

When the valve is closed, the EPT seals are distorted in opposite directions because of the opposing frictional forces between the seals and the body seat. A "squeegee" analogy can be used to visualize this phenomenon. When a rubber squeegee is compressed and moved across a surface, the seal yields slightly to a dragged condition due to the surface friction. When the relative motion is reversed, there is an increase in the friction between the rubber seal and the stationary surface as the seal transitions to being dragged in the opposite direction. The effect is commonly seen in automobile windshield wipers that have taken a set; they wipe smoothly in one direction but chatter, hop and skip when moved in the opposite direction. If the compression remains the same, much more force is required to push the squeegee in the reverse direction. The CP valve disc seals are stout pieces of synthetic rubber and are not as flimsy as a squeegee or a windshield wiper. Nevertheless, this analogy illustrates the distortion and frictional forces that occur, as the valve is closed and later when the disc is subjected to pressure forces.

The sequence of events that comprises the "walking" phenomenon are shown in Figure 4, which illustrates the initial position of the valve disc, disc movement during LLRT pressurization, and additional disc movement as the penetration is depressurized. Initially, opposing "squeegee" conditions are established on opposite sides of the disc after the disc is closed normally. When an axial force is imposed on the disc (such as during LLRT pressurization), the side of the EPT seal with favorable "squeegee" deformation (least sliding friction) will slide on the hard body seat. The other side, with unfavorable "squeegee" deformation (greater sliding friction), will resist movement. The net result is additional disc rotation in the "closed" direction. When the force is released (penetration de-pressurized), the valve stem springs back axially to its original position. The "squeegee" effect once again prevails and the disc is rotated further in the closed direction. This walking action will continue with each pressure cycle until the disc walks off the seat or until another resistive force arrests the walking motion.

This phenomenon was observed on several CP valves by measuring changes in disc axial

position at 8 points around the circumference of the disc during LLRTs. A graph showing typical measurements is shown in Figure 5. Two distinct disc movements are shown. First, the valve disc moves axially, outward, approximately 0.040" as air pressure is applied inside the penetration, as shown by the displacements in the 6 o'clock and 12 o'clock positions. Secondly, there was rotational movement in the closing direction, as shown by uneven displacements in the 3 o'clock and 9 o'clock positions. At the 3 o'clock position, the disc was initially at 0.040" outward and moved to 0.177" outward, for a total movement of 0.137". At the 9 o'clock position, the disc was initially at 0.065" inward and moved to 0.050" inward as pressure was applied, which was an outward movement of 0.015". Therefore, a rotational movement occurred as the penetration was being pressurized.

Additional disc rotational movement is shown in Figure 5 as the penetration was depressurized. The disc returned to its normal relaxed position (moving toward the centerline of the penetration) as LLRT pressure was removed. As expected, the valve stem returned approximately 0.040", close to its as-found depressurized position. But once again, the movement at the sides was not equal. At the 3 o'clock position, the pressurized position of the disc was 0.177" outward and moved to 0.149" (still outward), for a total inward movement of 0.028". At the 9 o'clock position, the pressurized position of the disc was 0.050" inward and moved to 0.152" inward as pressure was removed, which was an inward movement of 0.102". Therefore, another rotational movement occurred as the penetration was being depressurized.

The valve was subjected to a series of pressure cycles while additional measurements were taken. Each time, the right side moved outward as the penetration was pressurized and the left side moved inward as the penetration was depressurized, as shown in the composite graph in Figure 6. This figure clearly shows disc movement in the closed direction after every pressure cycle. In fact, the valve was walking more during the final pressure cycle than any of the previous cycles. Thus, initial theories about coasting through the seat or residual torque slowly driving the disc through the seat were disproved. Since the sealing area of the body seat is only 0.500" wide, the team concluded that the disc shown in Figure 6 would have walked off the seat after just one more pressure cycle.

Historical information also supported the "walking" theory. There had been several unexpected LLRT failures where the as-found position of the disc was beyond the closed position. These random failures often occurred after several successful LLRTs for no apparent reason.

2. Accident Direction Seat Leakage

Accident direction seat leakage is the second reliability concern addressed by the team. Under certain conditions, the inboard valves will seal when pressurized from inside of the penetration during a LLRT, but will leak when pressurized from containment during ILRT or accident conditions. This occurs because the pressure is applied in the opposite direction from an LLRT, which causes the valve disc to move axially away from the "tapered" seat, relaxing the compression on the EPT disc seal. This type of problem has been observed at other plants and was the subject of NRC Information Notice 88-73.

The valves were designed with a slight taper, actually a radius, shape to the seat. This taper is fundamentally necessary because of the offset valve stem design. The tapered seat is a

segment of the arc formed by the radius from the axis of rotation (the stem) to the outside edge of the EPT disc seal. Because of the offset, the interference between the disc seal and the body seat increases as the disc moves axially toward the body seat centerline, and decreases as it moves away. Therefore, this design has a preferential differential pressure direction. With the valves oriented back-to-back, as shown in Figure 2, the inboard valves are pushed out of the tapered seat by ILRT/ accident pressure and are pushed into the tapered seat by LLRT pressure. This failure mechanism does not affect the outboard CP CIVs because they are pushed into the taper during both LLRT and ILRT/accident pressure conditions.

The movement of the 42" valve disc is illustrated in Figure 7. This failure mechanism was confirmed by taking disc measurements as LLRT pressure was applied. A nominal 0.040" of disc movement was measured at the 12 o'clock and 6 o'clock positions. (Disc movement with ILRT pressure was not measured, but is assumed similar in magnitude because of symmetry in bearing design and applied loads.) Some axial disc movement is expected since the 52 psig differential pressure creates a 70,000 pound force on the large disc.

The team determined that the dominant factor affecting 1CP3A seat leakage during the Unit 1 ILRT (*see Background)* was improper vertical alignment of the disc. With the disc approximately 0.020" low in the valve body, previous attempts to adjust the disc seal could not compensate for the magnitude of the vertical misalignment. Furthermore, the team determined that the manufacturer's seal adjustment instructions were inadequate to account for many of the valve variables.

Following the formation of the investigation team, two more ILRTs were performed (Units 2 and 3) which provided valuable data collection opportunities. Enhanced disc seal adjustment techniques initially yielded promising results. There were no anomalies observed during the Unit 3 ILRT for the valves that were checked or set up using enhanced instructions developed by the team. Even as the scope of the investigation grew to address leakage through 8" valves of the same design, the lessons learned from the 42" valves quickly resolved the leakage problem through the smaller valves using the same enhanced instructions.

Despite the team's successes with disc seal adjustments, there was a discrepancy between the LLRT and ILRT leakage rates during the Unit 2 refueling outage, the last of the three consecutive ILRTs. Fundamentally, the leakage rates were all less than the acceptance criterion of 0.05 L_a. However, the ILRT (accident-direction) leakage was approximately five times greater than the LLRT (reverse-direction) leakage rate.

Section 6.2 of ANSI/ANS 56.8-1994 states that "Tests shall be performed so that the test pressure is applied in the same direction as that which would occur during the DBA, unless it can be shown that the results from applying the pressure in a different direction will provide equivalent or more conservative results." There was full recognition following the Unit 2 ILRT that the LLRT leakage rate was not necessarily indicative of the leakage rates expected during accident conditions, and that reverse testing the inboard CP valves would not necessarily provide "equivalent or more conservative results." Therefore it was concluded that that the normal LLRT does not comply with ANSI/ANS 56.8-1994. Blind flanges were installed as corrective action.

Factors Contributing to Disc "Walking" and Accident Direction Seat Leakage

The investigation discovered many factors that need to be controlled to ensure reliable performance of the 42" CP CIVs. Many of the factors impacting the *walking through the seat* problem were closely related to the *accident direction seat leakage* problem. In fact, the randomness of these leakage events can be explained by the numerous variables. No single problem caused all of the leakage events. Instead, condition variables, maintenance practices, operating philosophies, scheduling changes and design shortcomings occasionally aligned in a synergistic manner to cause leakage.

In addition, the team determined that some causes are related to both failure mechanisms in opposing directions. For example, greater disc seal compression enhances sealing, but increases the frictional forces involved with "walking." Thus an adjustment intended to compensate for one problem may aggravate the other problem.

Factors contributing to the failures include the following:

Adjustment of the EPT Disc Seal

The most important factor for proper sealing is adjustment of the EPT disc seal. The manufacturer's instructions for adjusting the disc seal assume the valve is lying horizontally on a shop table. This is not practical for a valve that is welded vertically. The manufacturer's instructions also assume a uniform annulus between the disc and body seat. Inspection of installed valves identified horizontal and vertical disc misalignment and out of roundness, which means that the annulus is not uniform. In addition, the manufacturer's instructions involve even tightening of the cap screws, then an additional ½ turn on each after the first contact between the EPT seal and the hard seat. This leads to uneven seal compression that increases the likelihood that the disc will walk through the seat. The team developed an improved seal adjustment method that differs slightly from the manufacturer's guidance. This improved method uses feeler gauges to ensure uniform seal compression.

Disc Vertical Alignment

Proper vertical alignment of the disc inside the body is crucial to successful operation of the valve. By manually setting the thrust collar to achieve equivalent gaps at the top and bottom of the disc, concentric vertical alignment within 0.003" could be reasonably achieved. This value is much better than the manufacturer's recommended concentricity (<0.010").

Condition of the Upper and Lower Bearings

The condition of the upper and lower bearings also affects the ability of the valve to seal. Approximately 70,000 pounds of force is applied to the disc at full test pressure. Degraded bearings can allow more axial disc movement than can be absorbed by EPT disc seal compression.

Disc Horizontal Alignment

Side-to-side disc-body misalignment by as much as 0.021" has been measured on some valves. This is much greater than the manufacturer's recommended concentricity (<0.010"). However, the design of the valve does not provide for any side-to-side adjustment of the disc inside the valve body.

Variations in EPT Disc Seal Dimensions and Composition

Variations in the dimensions and composition of the replacement seals provided by the valve manufacturer contributed to the difficulty in setting up these valves for consistent sealing.

Narrow Body Seat

The body seat is only 0.5" wide. Very little disc movement can be tolerated before leakage occurs. For example, only 0.25" of disc movement is required for a disc centered on the seat to move off the seat. For a nominal 42" valve, this corresponds to a rotational disc movement of only 0.68 degrees.

Lack of a Disc Stop

Without a mechanical stop to limit disc motion in the closed direction, pressure cycles can cause the valve to "walk" through the seat.

Body Seat Taper

The body seat of the inboard valve is oriented so that ILRT (accident direction) pressure pushes the disc out of the tapered/radiused seat. This reduces the compression on the EPT disc seal, which can lead to seat leakage.

Mechanical "Slop"

Mechanical clearances from gear lash, worm end play, and splined and keyed connections all contribute to mechanical "slop" between the disc and the valve actuator.

Limit Switch Adjustment

The smallest incremental adjustment of the actuator close limit switch in the limit switch assembly is one gear tooth. This results in a discrete disc rotation of about ¼" at the horizontal disc centerline, too much to ensure consistent precision setup of the valve.

3. Packing Directional Leakage

The third reliability problem addressed during this investigation was a directionally sensitive packing concern. The team discovered that the valve packing, if not properly compressed, could leak in one direction while sealing in the other direction. This is a concern on the inboard valves since the inboard valve packing must be capable of sealing against differential pressure in both the accident and LLRT directions.

The valve packing arrangement is shown in Figure 8. It consists of 2 sets of chevron-shaped elastomer rings, 4 rings to a set, with a lantern ring in the middle. The valve stuffing box is equipped with a leakoff line. The packing sets are oriented "back to back," with the "innermost" set optimized to prevent containment pressure from leaking INTO the penetration, and the "outermost" set optimized to prevent LLRT pressure from leaking OUT OF the penetration.

With the packing sets in this orientation, the innermost set on the inboard valve performs the accident function of preventing containment pressure from leaking into the penetration. This leakage path is shown in Figure 8. An LLRT performed by pressurizing the inside of the penetration does not verify the leak tightness of the innermost set in this direction. During an LLRT, leakage past the innermost set (non-optimized direction) can be masked by the outermost packing. As with the Accident Direction Seat Leakage problem previously described, the team concluded that the existing LLRT methodology would not adequately predict packing leakage during accident conditions.

After discovering that the LLRT did not effectively test the inboard valve packing, procedures were revised to perform a separate LLRT of the packing stuffing box through

the leakoff line. The results of the penetration LLRT and the packing LLRT were then added together to conservatively determine the total leakage for the penetration.

Testing was performed on the packing on the inboard 42" CP CIVs in all three units. The packing leakage on one valve exceeded the LLRT acceptance criterion. The compression on this packing was found to be less than the recommended value, but after shimming per the manufacturer's instructions, the subsequent packing test was acceptable.

Conclusion

A complete understanding of the interaction between the variables and the reliability of new seal adjustment techniques for these valves would require further investigation. Without a disc stop or other modification to arrest and preclude disc "walking," a technique to set up the actuator and valve would be too complex and empirical for a standard procedure. Thus, development of a practical setup method is not likely. In addition, the long-term reliability of such a setup, even if developed, is not known and cannot be easily verified. The cost of continued investigation would most certainly exceed the cost of other alternatives. Therefore the investigation team concluded that further investigation into the problems associated with the 42" CP CIVs was not warranted.

The team recommended installing blind flanges on the outside of the outboard valves during power operation and making these flanges part of the permanent plant design. The blind flanges have been used at Palo Verde in the past as a contingency action and, during this investigation, as a short term solution and backup means of isolation. Other plants have also used blind flanges on their containment purge penetrations. To address the differential pressure directionality issue, some plants have reversed the orientation of their inboard purge isolation valves. This approach was determined to be impractical at Palo Verde since the inboard valves are welded to the penetration and flanged to the ducting.

The blind flange solution directly addresses the valve seat leakage issues. It also eliminates the need to perform leakage testing on the inboard valve packing. Blind flanges are currently installed on the 42" CP penetrations in all three units. A design change is underway to update plant design and licensing documents to reflect permanent use of the blind flanges.

References

Code of Federal Regulations - Title 10, Part 50, Appendix J, "Primary Reactor Containment Leakage Testing for Water-Cooled Power Reactors"

Regulatory Guide 1.163, "Performance-Based Containment Leak-Test Program," September 1995

NEI 94-01, "Industry Guideline for Implementing Performance-Based Option of 10CFR50, Appendix J," Rev. 0.

ANSI/ANS 56.8-1994, "Containment System Leakage Testing Requirements"

NUREG-1493, "Performance-Based Containment Leak Test Program"

NRC Information Notice 88-73, "Direction Dependent Leak Characteristics of Containment Purge Valves"

NRC Circular 77-11, "Leakage of Containment Isolation Valves with Resilient Seats"

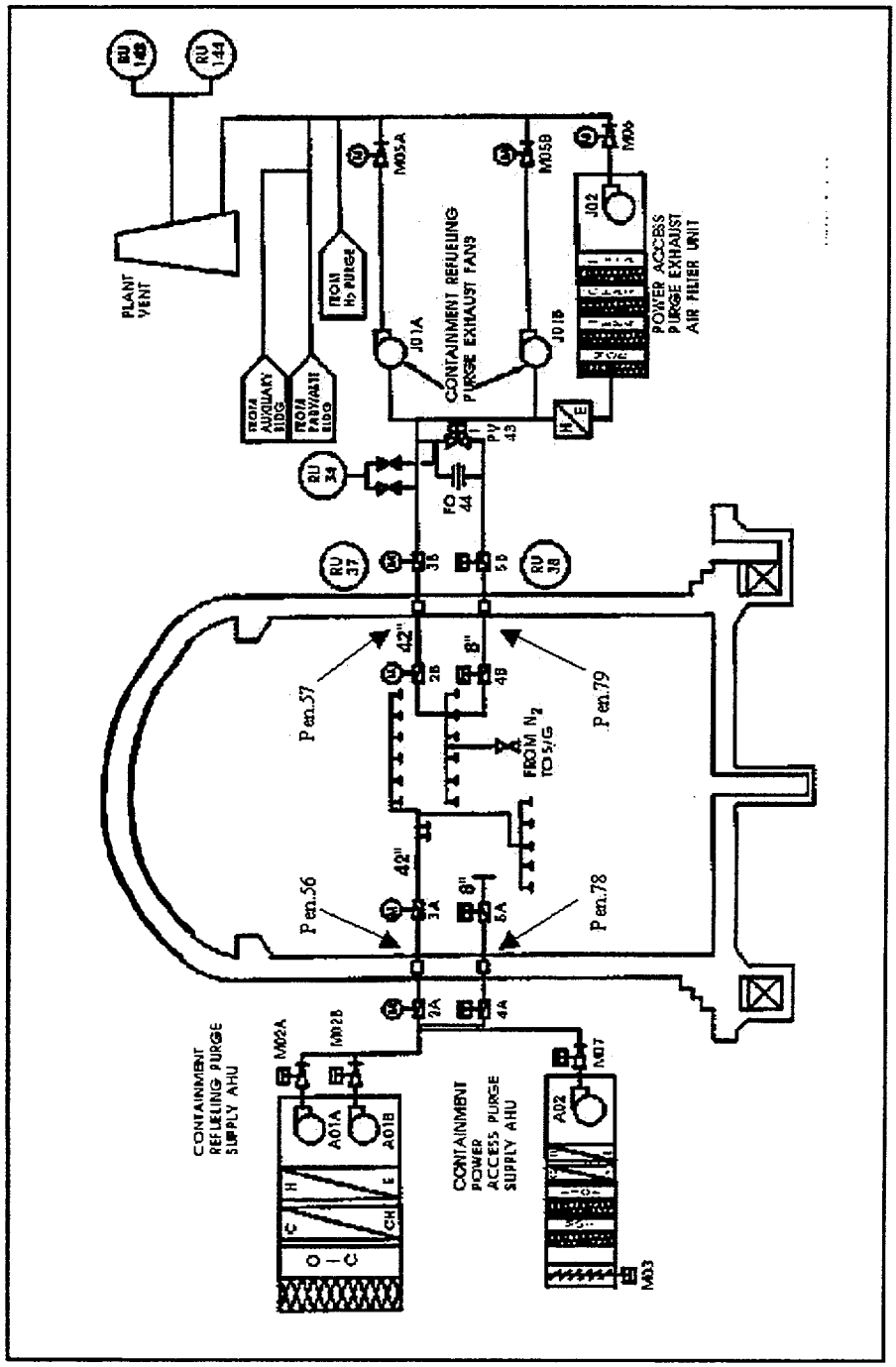

Figure 1 Containment Purge System Piping and Instrumentation Configuration

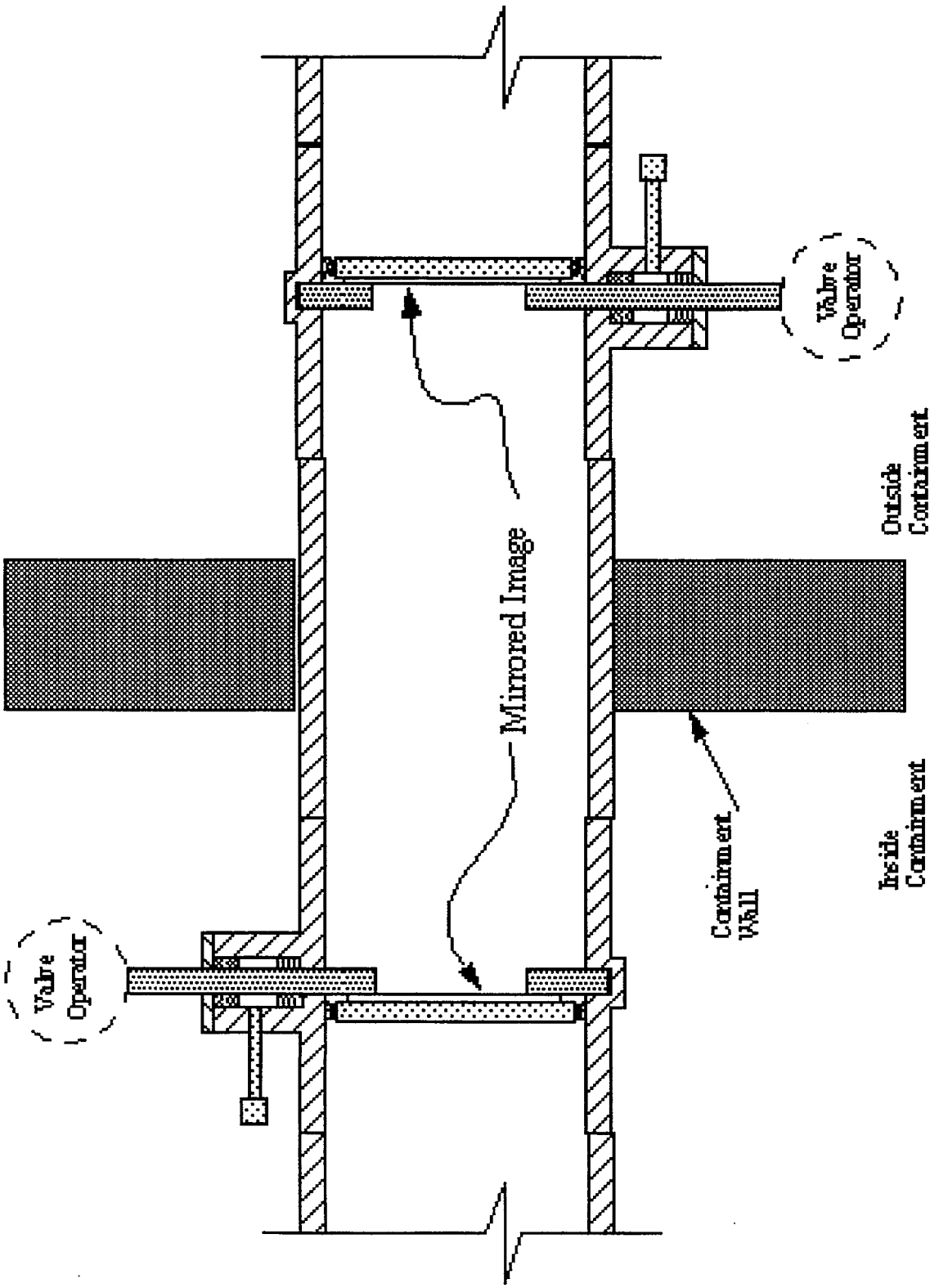

Figure 2 Purge Valve Orientation (Back to Back)

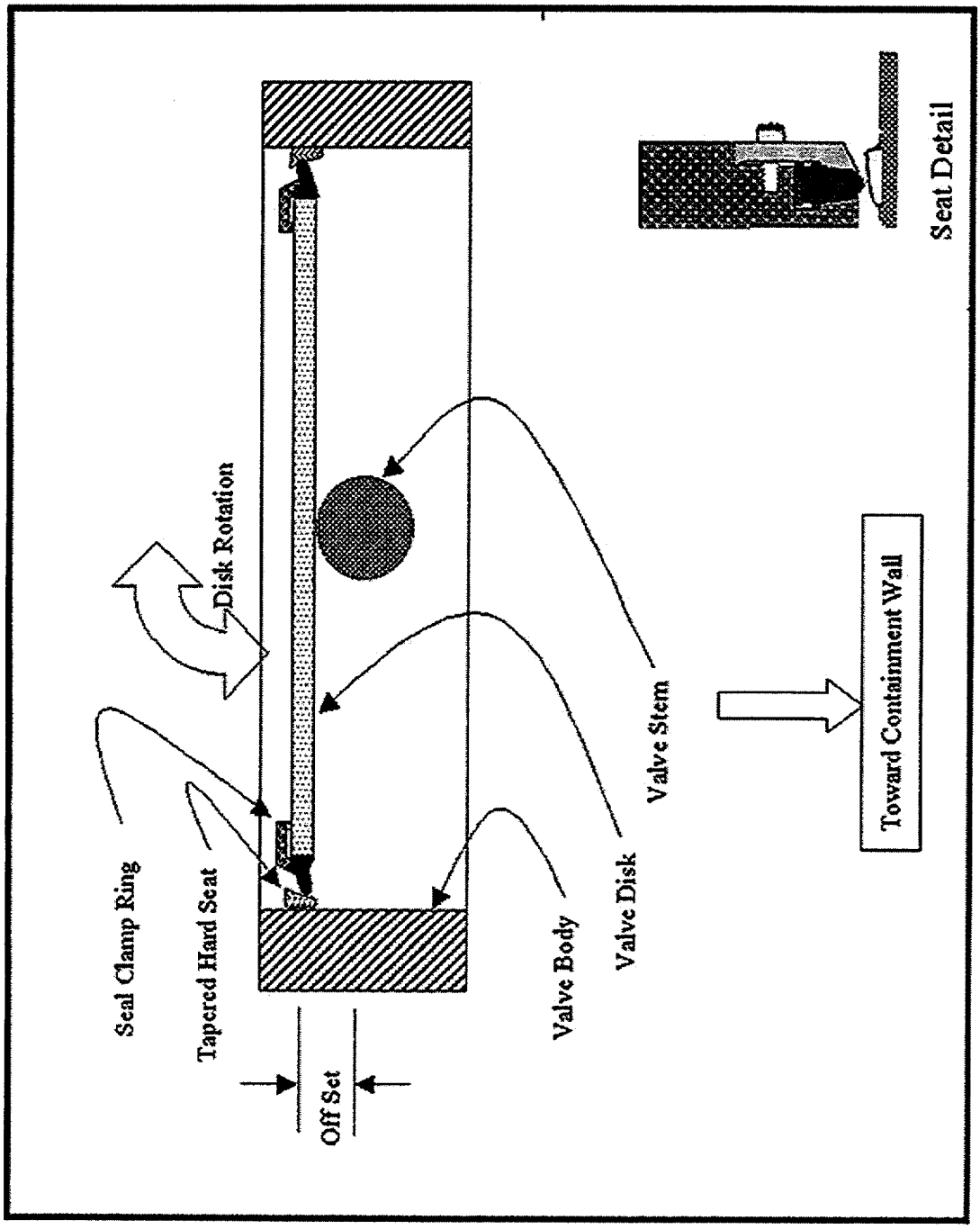

Figure 3 Purge Valve Seating Configuration

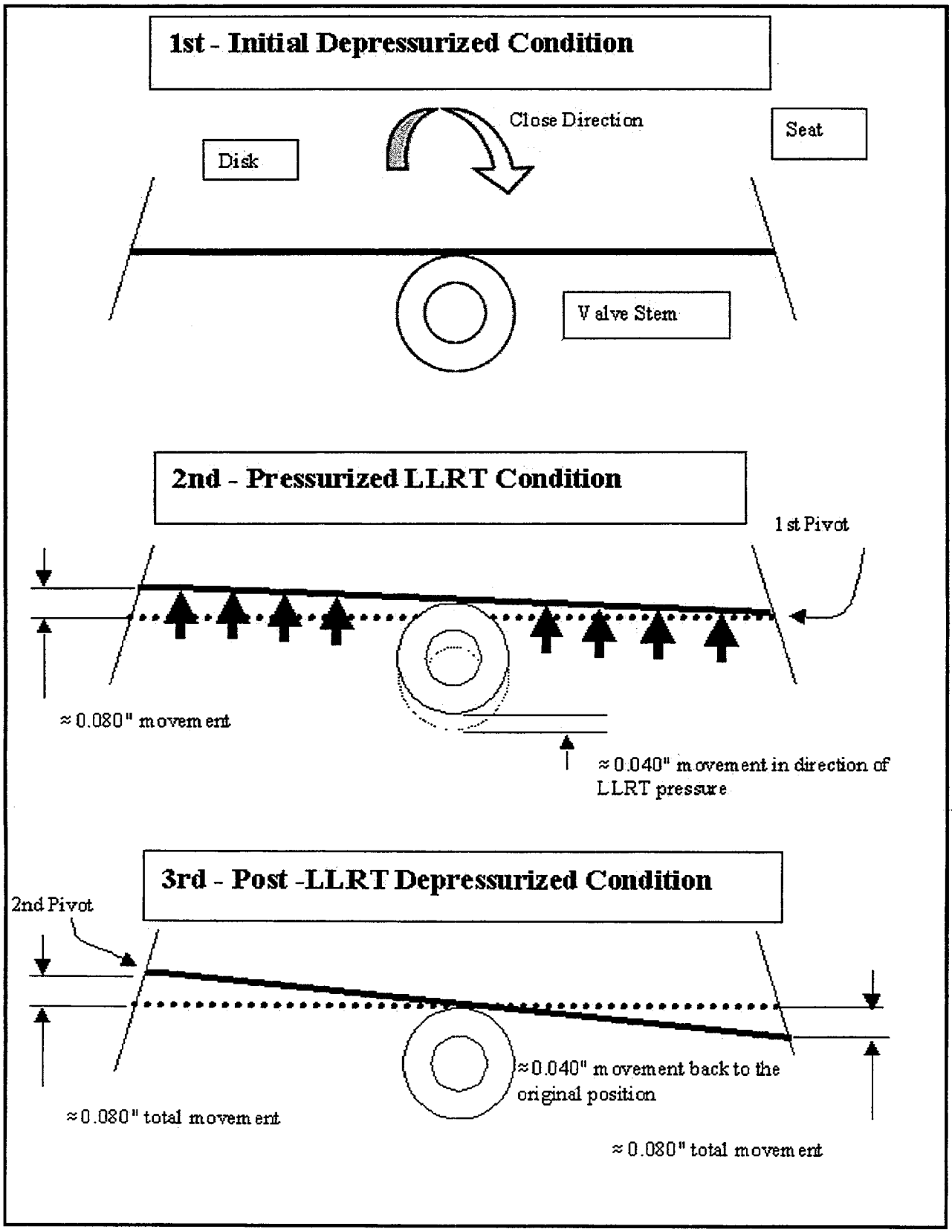

Figure 4 Valve Disk "Walking" Phenomenon

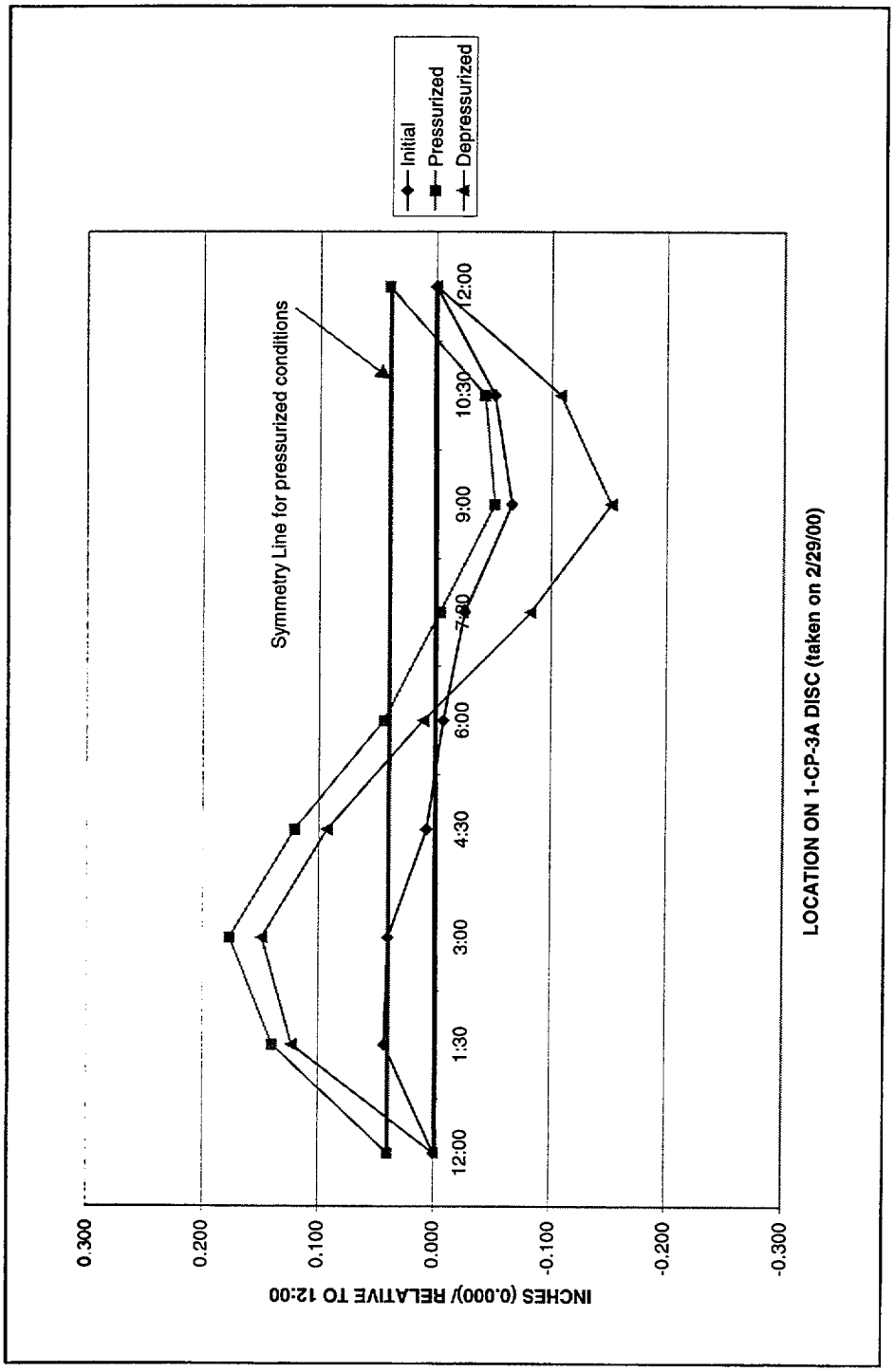

Figure 5 Graph of Valve Disk Movement - One Pressure Cycle

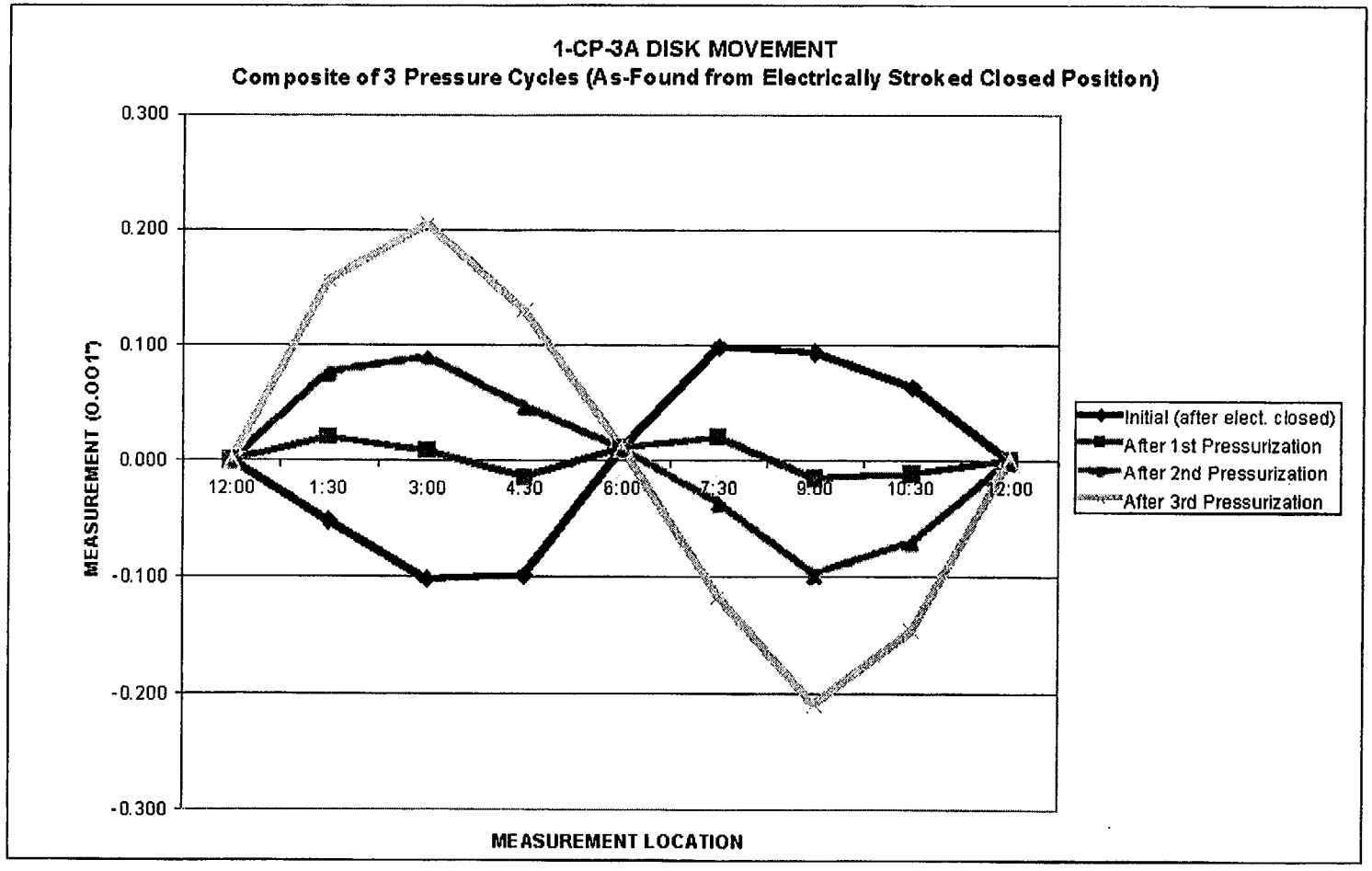

Figure 6 Graph of Valve Disk Movement - Successive Pressure Cycles

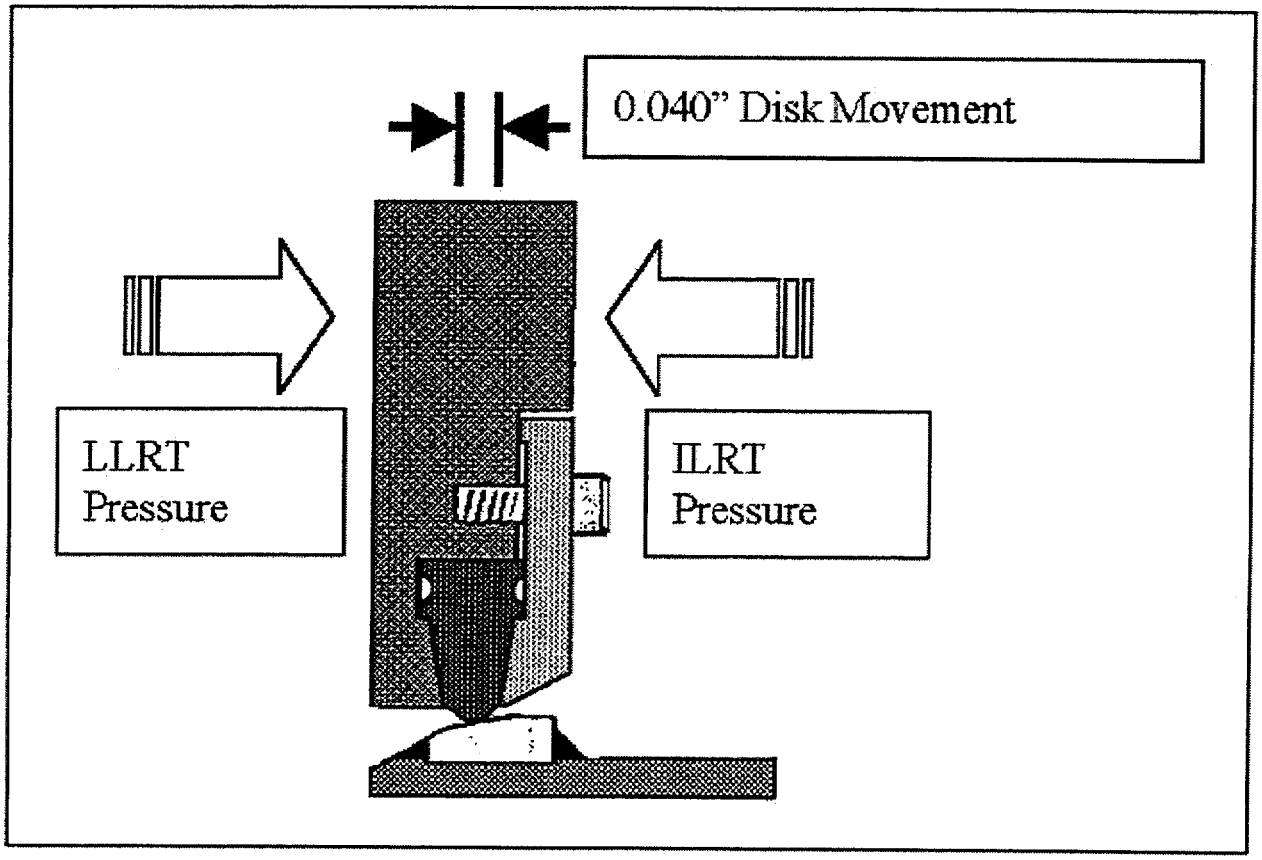

Figure 7 Diagram Showing Valve Disk Axial Movement During Pressurization

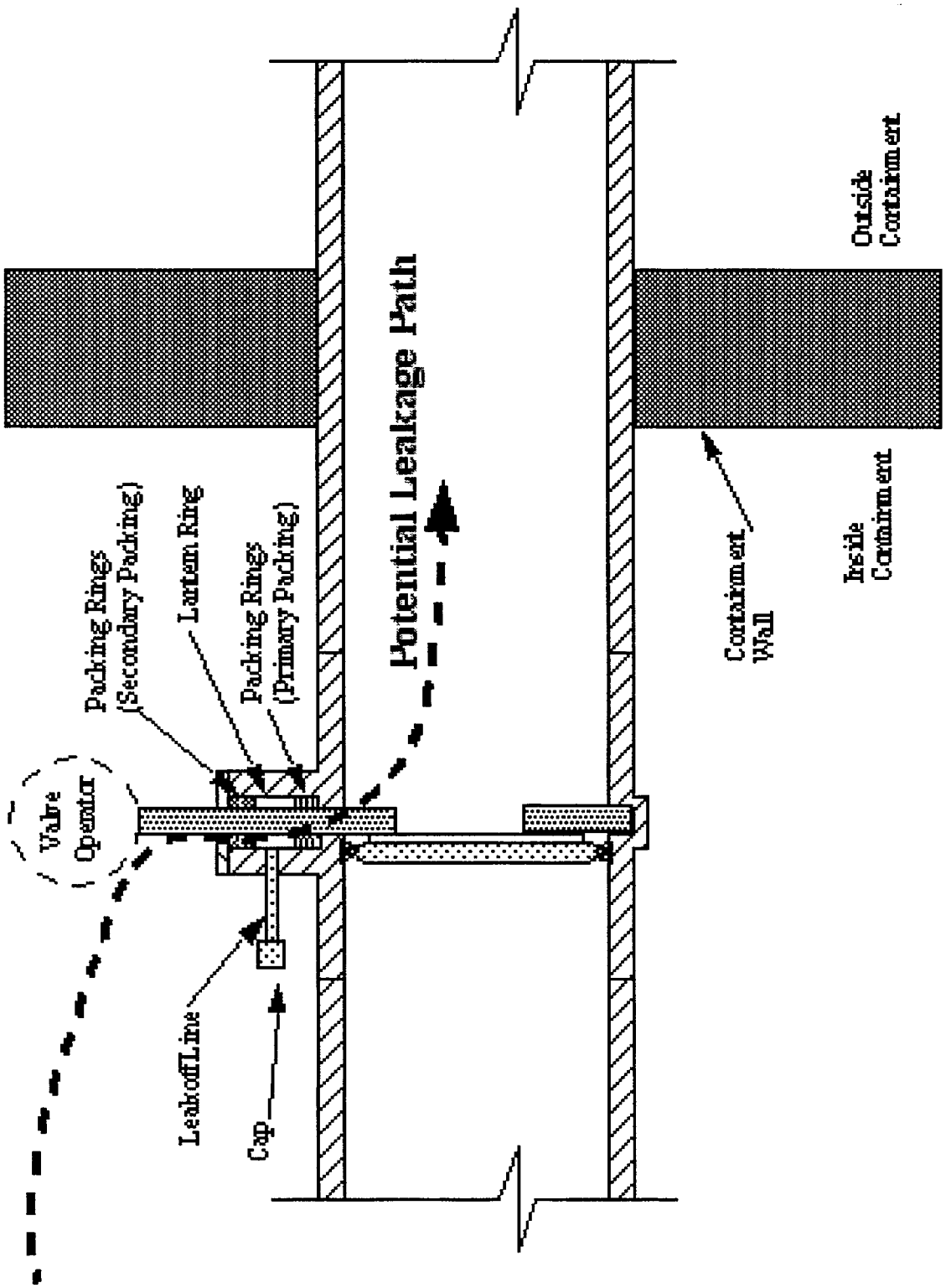

Figure 8 Valve Packing Arrangement and Potential Leak Path

Variation of Coefficient of Friction of Stellite 6 With pH

P. Coppolani, Framatome ANP
L. Cachon, Commissariat à l'Energie Atomique
J-M. Pitard Bouet – D. Hersant, Electricité de France

Abstract

Operability of motor operated gate valves with hardfaced discs and seats relies on the value of the friction coefficient of the hardfacing material. For most gate valves, the hardfacing material is Stellite 6, a cobalt based alloy.

Previous studies have shown that the value of the friction coefficient of Stellite 6 was a function of many parameters such as the temperature, the medium, the aging and the number of cycles (opening and closure).

This paper presents the results of friction testing of Stellited gate discs on Stellited seats in cold water, with pH representative of that of pressurized water reactor (PWR) auxiliary circuits.

The main results are the following ones:

In acid (pH = 5) or basic water (pH = 9), the friction coefficient increases with the number of cycles and then stabilizes at a plateau value.

In basic water, the plateau value can reach 0.65 and is maintained after stroking interruption.

In acid water, the plateau value is equal to 0.4 when cycling is made with loss of sealing between the disc and the seat. It drops from 0.4 to 0.3 after an interruption of one hour or more of the cycling before increasing again after cycling restart.

Introduction

Electricité de France (EDF), Commissariat à l'Energie Atomique (CEA) and Framatome ANP have been investigating for many years the operability of motor operated gate valves (MOVs) installed in the auxiliary circuits of the PWRs manufactured in France.

The objective is to be able to predict, as accurately as possible, the thrust and so the torque of the actuator needed to operate a valve. Two key parameters, for gate valves with adequate disc guides, are the friction factors between the stem and the stem nut and at the disc/seat interface.

For valves with discs and seats hardfaced with Stellite 6, a lot of testing has been done either by the manufacturers themselves or by private or public laboratories, and numerous values of friction coefficient are available. However, there is a very large scatter, which cannot only be explained by differences in manufacturing or composition of the Stellite 6 deposits (Ref. [1]). Further testing has shown that, in most circumstances, the friction coefficient increased with the number of cycles and then reached a plateau (Ref. [2]). However, this seemed not always to be true in an oxidizing environment such as the water of boiling water reactors (BWRs) (Ref. [3]).

Previous studies (Ref. [5]) have also shown that there was a significant decrease (about

0.2) of the Stellite 6 friction coefficient between ambient temperature and 350°C.

Those results strengthen the hypothesis that the friction coefficient of the Stellite 6 depends on the composition of the oxide or corrosion film on its surface, which itself is related to the chemistry and temperature environment.

This paper presents the results of tests performed in CEA laboratories of Cadarache, on a test bench "OPERA" to address the issue of medium pH influence on Stellite 6 friction coefficient at ambient temperature. Indeed, most safety related valves of PWRs are located on auxiliary circuits which start to operate at ambient temperature.

OPERA Test Bench

The Opera Test Bench is a friction autoclave in which were located the specimens consisting of a complete disc resting on its seat (Fig. 1).

The disc was attached to a rod, actuated by a two way hydraulic cylinder at a speed of 0.01 m/s.

The width of the seat was adjusted so as to obtain a contact pressure of 100 MPa, under a differential pressure of 16 MPa.

The friction force was measured with a thrust sensor on the pull rod and a correction was made to take into account the parasitic force due to friction of the seals and pressure on the section of the pull rod. An average value of the friction coefficient was then obtained by dividing the friction force by the force due to the differential pressure acting on a circular surface with a radius equal to the average radius of the seat.

The test bench can be operated in two modes: without or with loss of sealing at each cycle.

In the first mode, the amplitude of the cycling: 0.01 m is lower than the difference: D between the width of the stellited ring of the disc: 20 mm and the width of the seat: 3 mm.

Pressure above the disc is maintained equal to 16 MPa, while pressure in the closed cavity below the disc is kept equal to atmospheric pressure: so the disc slides on the seat under a constant differential pressure of 16 MPa.

So in this mode of operation, the cycling frequency is 1 Hz.

In the second mode, the amplitude of the cycle is slightly greater than D.

So at the end of each cycle, there is connection between the upstream side and the downstream side of the disc: therefore, the differential pressure cancels.

Then the disc is pulled back until closure of the leakage path; the volume below the disc is drained to atmosphere so as to restore the initial differential pressure of 16 MPa, and another cycle is started. The interest of this mode of operation is to reproduce more accurately the functioning of a gate valve, at the expense of a longer test duration due to the lower cycling frequency of about 0.1 Hz.

Test Program

This paper presents the results of two test programs carried out to understand the variation of Stellite 6 friction coefficient with the resting time and the chemistry of the medium.

In the first test program, which was conducted in water at a pH of about 5, the parameter was the interval of time (or resting time) between two series of cycles.

This was done to simulate the operation of a valve, which stays open (or closed) some time before two consecutive actuations.

In this test, the test bench mode of operation was the one "without loss of sealing" at each cycle.

In the second test program, the parameter was the pH of the medium. So tests were done first in basic water pH = 9 and then in acid water pH = 5. In these cases, the test bench mode of operation was the one "with loss of sealing" at each cycle.

Furthermore, a comparison was made between the two modes of operation with/or without loss of sealing.

The acid medium consisted of demineralized water, with addition of boron (about 2000 ppm) to obtain pH = 5. The basic medium was obtained by adding soda to a solution of demineralized water with 2000 ppm of boron, until reaching pH = 9

Results

Cycling without loss of sealing at each cycle, acid water: pH = 5

Fig. 2 shows the general shape of the curve of friction coefficient versus the number of cycles.

Three phases can be characterized.

The first phase corresponds to the destruction of the oxide films on the seating surfaces: it lasts about a few dozen cycles.

In phase two, the evolution of friction coefficient is low but non null: it lasts about a few hundred cycles.

Phase three corresponds to the plateau value: the friction is mostly adherence friction.

Fig. 3 shows the variation of the friction coefficient at the beginning of a cycle and at its end (plateau value) versus the time elapsed between two series of cycles. It appears that after a rest time greater than one hour, the friction coefficient drops from its maximum plateau value: 0.5 down to 0.3.

Cycling with loss of sealing at each cycle, basic water: pH = 9

The results are shown on Fig. 4. The initial friction coefficient value is low which can be explained by the fact that the specimens had remained in air for more than one year and that their surface was covered by oxide or adsorbed elements acting as solid lubricants.

After about 50 cycles, the friction coefficient reaches a plateau value of 0.6 and stays around this value $\pm$ 0.05, after several pauses in the cycling, respectively 1.3 and then 20 hours.

Cycling with loss of sealing at each cycle, acid water: pH = 5

After the completion of the basic water testing the specimens were left 1 h 30 min in air and then 30 min in acid medium of pH = 5. Cycling was then started.

It was first found that the friction coefficient had decreased from 0.6 to 0.2.

The results are shown on Fig. 4. After 40 cycles, the friction coefficient is stabilized to 0.4.

When the cycling was continued in the mode without loss of sealing and so at a higher frequency, the friction coefficients increased again and stabilized at a value of 0.5, as in the initial testing. It was also verified that, after a rest time of one hour, the friction coefficient had dropped to a value of 0.3.

So it appears that the result depends on the testing mode and on the length of time during which the seating surfaces are wet by the medium.

Visual Expertise of the Surfaces

After 300 cycles in acid water: pH = 5 and in basic water: pH = 9 the aspect of the surfaces were not the same.

After cycling in acid water the contact surfaces were polished like a mirror, suggesting a mechanism of lapping. On the contrary after cycling in basic water there were marks of adherence and abrasion.

However, in both cases, the roughness of the surfaces had remained low enough so as to keep the initial tightness.

"Sticking" test

The test was done only in acid water, after 3000 cycles in the "without loss of sealing" stroking mode. The disc was left one month on its seat with the upstream side at 16 MPa and the downstream side at atmospheric pressure.

At the end of the month, one opening was realized. During the opening, the maximum value of the friction coefficient was 0.35 (Fig. 5), instead of 0.58 at the end of the previous cycles.

So, it seems that in acid water no sticking is possible. On the contrary the evolution of the seating surfaces leads to an improvement of the sliding.

Conclusion

It appears that the friction of Stellite 6 is related to the tribo chemistry of the contact. This fact is not in contradiction with previous studies (see Ref. [3]) which shows that in hot, oxidizing media such as the ones of BWRs, the friction coefficient may increase with aging and so the risk of sticking. Indeed cases of sticking due to metallic bonding between the Stellited nozzles and discs of pilots of safety/relief valves of BWRs have been reported by NRC (Ref. [4]) and have been explained by the buildup of an oxide layer acting as a bond between the surfaces of identical composition.

On the contrary in non-oxygenated acid water, the corrosion products seem to act as a lubricant.

In summary for a gate valve operating at ambient temperature in a medium of composition similar to the one of PWRs coolant, that is to say $5 < pH < 9$ and in absence of oxygen, the results of the above tests show that:

- the friction coefficient of Stellite 6 increases with the number of cycles and then reaches a plateau value.
- In acid water; pH = 5:

  The value of the plateau is equal to 0.4

  After a resting time equal to or greater than 1 hour, the friction coefficient decreases back to 0.3

  Sticking in closed position is not possible.
- In basic water; pH = 9:

  The average value of the plateau is equal to 0.6

  The value of the plateau does not decrease significantly with the resting time.

It also appears that friction values lower than 0.3 can be found for Stellite surfaces left in contact with air and not cleaned. Those low values are no longer obtained after

maintaining and cycling the surfaces under water.

References

[1] Hardfacing – Metallurgical characteristics and utilization properties of hardfacing deposited by the fusion of cobalt-base alloys – PTAN2 – 1992 Edition AFCEN.

[2] J.F. Hosler, P.S. Damerell, M.G. Gidson, N.E. Estep, Gate Valve Performance Prediction, Third NRC/ASME Symposium on Valve and Pump testing - NUREG/CP-0137, July 1994.

[3] J.C. Watkins, K.G. Dewall, G.H. Weidenhamer, Status of Stellite 6 Friction Testing, Fifth NRC/ASME Symposium on Valve and Pump Testing - NUREG/CP-0152, July 1998.

[4] NRC IE Information Notice 86-12 – Target Rock Two stage SRV set point drift.

[5] L. Cachon et al., Tribological qualification of cobalt free coatings for pressurized water reactor primary circuit gate valve applications. Surface and coating technology 85(1996) 163-169.

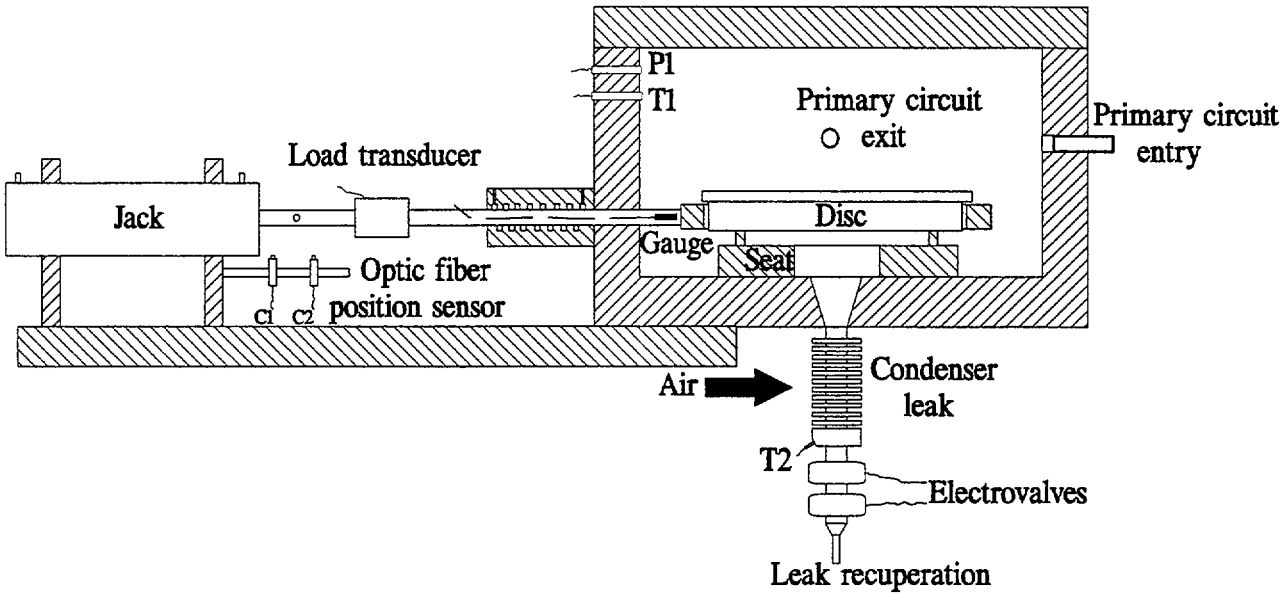

Figure 1 OPERA Test Bench

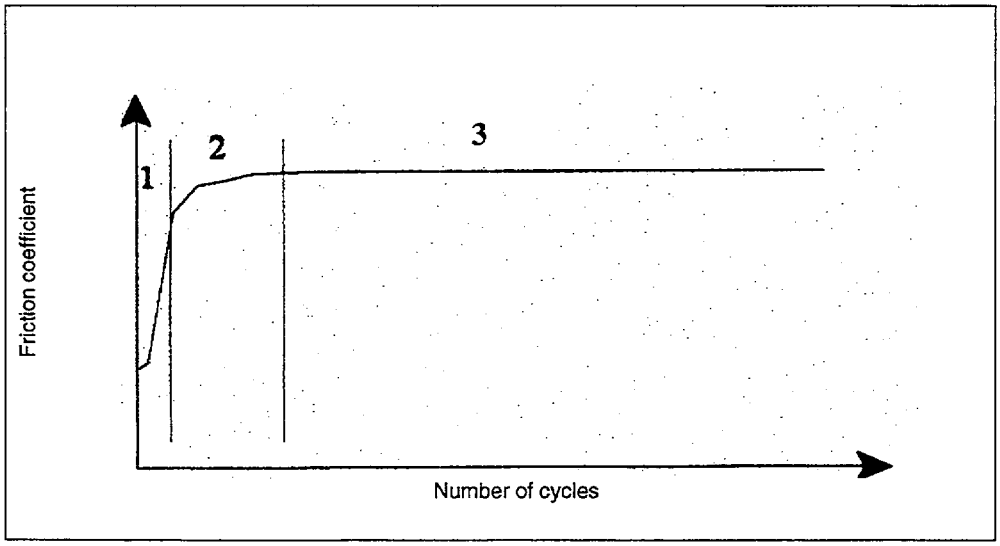

Figure 2 Typical Variation of Friction Coefficient with the Number of Cycles

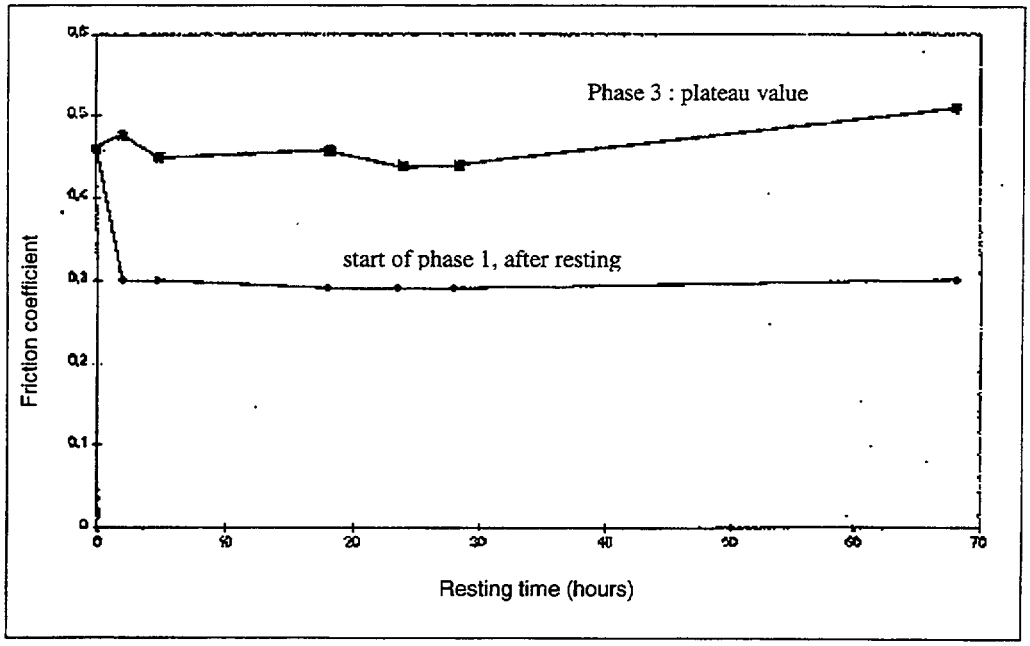

Figure 3 Variation of Friction Coefficient with the Resting Time Between Two Cycling Runs

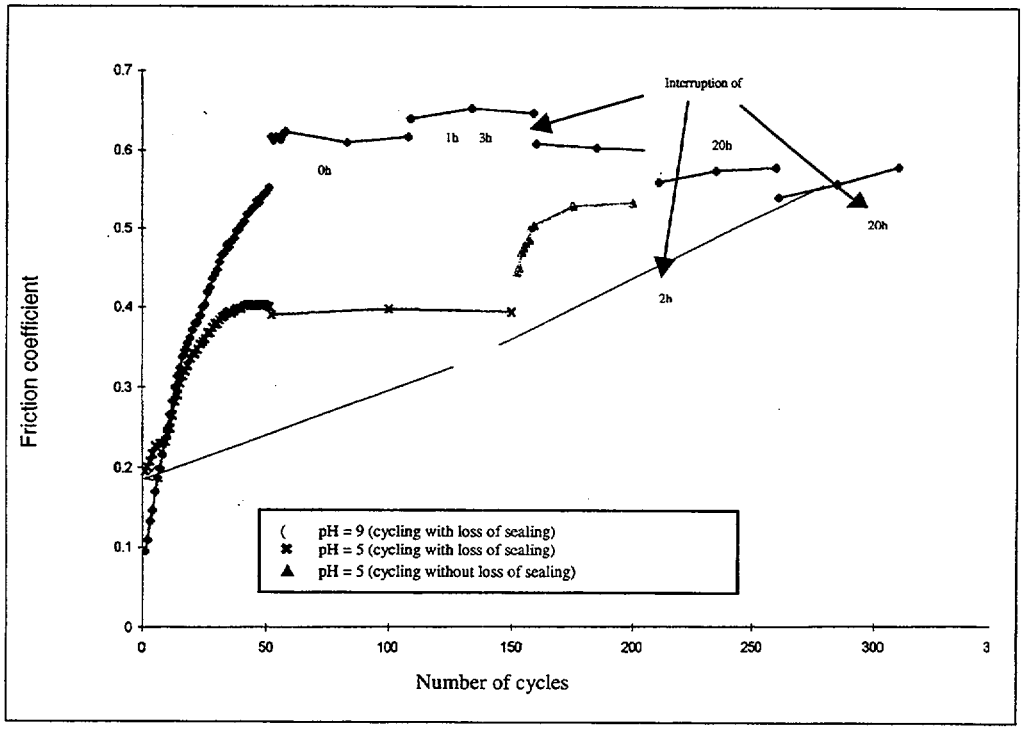

Figure 4 Evolution of Friction Coefficient with the Number of Cycles and the pH

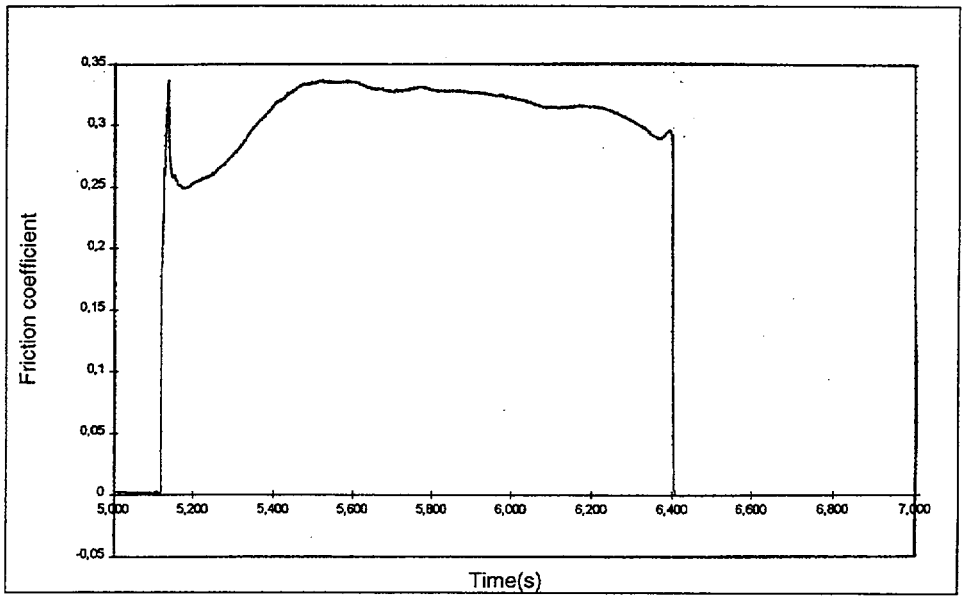

Figure 5 Friction Coefficient Variation During Opening After 1 Month Closed

QME-1 Qualification of the Edward Equiwedge Gate Valve Equipped with the Type A Gas/Hydraulic Actuator

Gregory Smyth, Wyle Laboratories
Joseph Gallagher, Edward Valve Company

Abstract

This paper discusses the analytical and test methodologies used to qualify a line of valves in accordance with ASME QME-1-1994. Four valves are used in the qualification program, and range from Size 4 to Size 26. All the valves are rated as Special Class 900 in accordance with ANSI B16.34, and are Class 2 N-Stamped per the ASME *Boiler and Pressure Vessel Code* (NC-3500). They are all gate valves with linear piston gas/hydraulic actuators. Their intended service is for Main Steam and Main Feedwater Isolation in a Pressurized Water Reactor (PWR) Nuclear Power Plant.

The paper presents an overview of the QME-1 requirements for these valves with explanations of the individual tests required by the QME-1 document. These include various inspections, fundamental frequency determination, cold and hot cycling, simultaneous end-loads with static seismic loading and flow interruption/functional capability demonstration.

The paper presents a detailed description of the testing and the results for the Size 20 Economizer Main Feedwater Isolation Valve (EMFIV). All testing was performed by Wyle Laboratories at the Huntsville Facility. Using direct stem force measurements, obtained during the various test conditions, valve factors are determined.

1.0 Introduction

Wyle Laboratories and Edward Valves are conducting an ASME QME-1 Qualification Program on four Equiwedge Gate Valves; each equipped with the Edward Type A Gas/ Hydraulic Actuator. The valves are being qualified for Main Steam and Main Feedwater Isolation Service in a PWR Nuclear Power Plant. The test program consists of the following valve and actuator combinations:

Valve Size	Actuator Size	Service
26 x 24 x 26	A-290	Main Steam Isolation Valve (MSIV)
4	A-100	Main Steam Isolation Bypass Valve (MSIBV)
20 x 16 x 20	A-260	Economizer Main Feedwater Isolation Valve (EMFIV)
8 x 6 x 8	A-100	Downcomer Main Feedwater Isolation Valve (DMFIV)

All the valves are rated as Special Class 900 in accordance with ANSI B16.34, and are Class 2 N-Stamped per the ASME *Boiler and Pressure Vessel Code* (NC-3500). The actuators are U-Stamped in accordance with Section VIII, Division 1 of the ASME *Boiler and Pressure Vessel Code.*

This paper presents an overview of the general requirements of the ASME QME-1 Standard for valves, as defined in the QV section, and as applied to these valves. Some explanation is provided for the different test types encountered in the valve test sequence. This consists of various inspections, fundamental frequency determination, cycle testing, end-loading testing, seismic testing, and flow interruption and functional capability demonstration.

As of the writing of this paper, the program is still in process. However, all of the testing on the Size 20 EMFIV has been completed and, although the test data has not been fully analyzed, the results are presented. Following completion of the program, later work will focus on a detailed analysis of the results for all four valves. Any similarities and/or differences shall be noted in the later work.

The data presented includes force measurements from stem mounted strain gages and actuator performance data. This data was obtained throughout the test program including the Flow Interruption and Capability Demonstration. Comparisons of this data are made at the various stages of the test program.

2.0 Service Conditions

These valves are for Main Steam and Main Feedwater Isolation Service in a PWR Nuclear Power Plant. Except for the Main Steam Isolation Bypass Valve, they are maintained in the fully open position during normal plant operation. The Main Steam Isolation Bypass Valve is opened during the startup of the plant, but is maintained in the fully closed position during plant operation (refer to Figure 1).

The valves are designed for the following conditions:

Valve	Normal Operating Pressure (psi)	Normal Operating Temperature (F)	Design Pressure (psi)	Design Temperature (F)
Main Steam Isolation Valve	1055	553	1382	590
Main Steam Isolation Bypass Valve	1155	564	1382	590
Economizer Main Feedwater Isolation Valve	1425	455	2050	500
Downcomer Main Feedwater Isolation Valve	1425	455	2050	500

Their safety related function is to close and provide automatic and positive isolation of the safety related piping and the containment system from the non-safety related piping; valve opening is not a safety concern. They are required to perform this function with sufficient force to achieve isolation and within a maximum closure time before, during and after normal and accident plant conditions.

3.0 Equipment Description

The test valves used in this program are Edward Equiwedge Gate Valves with Type A Actuators (refer to Figure 2). These are bidirectional valves that consist of two independent gates separated by a spacer ring. Sealing is accomplished by the taper in the gates that match the angle of the seat rings. The spacer ring maintains flexibility between the gates and prevents binding. The gates are guided throughout the stroke by tongues on their sides that fit into grooves in the body. This guiding arrangement prevents contact between the seating surfaces on the gates and seat rings until the valve is approximately 95% closed.

The seating and wear surfaces in the valve are hardfaced with a cobalt base alloy (Stellite 21). Flexible graphite is used for the stem packing and the pressure seal bonnet gasket. The valves also have provisions to prevent center cavity overpressurization. This is accomplished by a bypass arrangement on one side of the valves that equalizes the center cavity pressure to the high pressure side of the valve.

The Edward Type A Valve Actuator is a linear piston actuator composed of hydraulic, pneumatic and electrical systems (refer to Figure 3). Its circuitry is designed to perform either a fast or slow valve closure, open stroke, or exercise cycle. The exercise cycle consists of partially stroking the valve closed (generally 10%) in a slow closure mode and then reopening the valve. The piston rod attaches directly to the valve stem and, by controlling the direction and speed of the piston, the direction and speed of the valve closure element are also controlled.

The source of the valve closing force is compressed nitrogen gas contained in a volume on one end of the actuator cylinder. The pressure of the nitrogen is adjusted to suit specific applications.

The hydraulic system moves the piston in the non-critical direction (i.e., open the valve); this also compresses a fixed mass of nitrogen gas. It controls the piston speed in the critical direction (i.e., valve closure) while the gas expands to close the valve. The pneumatic system is used to develop the hydraulic force needed for opening the valve and compressing the gas. The electrical system is used to monitor, control, and verify the essential parameters and functions of the actuator.

Typical performance data for the opening and closing functions of the valve/actuator assembly are shown in Figures 4 and 5, respectively.

4.0 ASME QME-1 Requirements

4.1 Introduction to QME-1

ASME QME-1, "Qualification of Active Mechanical Equipment Used in Nuclear Power Plants," describes the requirements and guidelines for qualifying active mechanical equipment in nuclear power plants. It was first issued in 1994 as ASME QME-1-1994. However work on developing qualification standards for valves and pumps has been going on since the early 1970s with the ANSI N45 Committee.

The standard is divided into three sections:

QR General Requirements

QP Qualification of Active Pump Assemblies

QV Functional Qualification Requirements for Active Valve Assemblies for Nuclear Power Plants

Section QV specifies a method of qualification for active valve assemblies to provide assurance the valve will function over

the required range of service conditions. Section QV is an extension of ANSI B16.41-1983. The qualification is based on tests and/or analysis to demonstrate that the valve/actuator assembly can perform its function under the most adverse conditions of pressure, flow, temperature, mechanical loading, and vibration.

4.2 Edward Valves Test Sequence for ASME QME-1 Testing

Based on the range of valve sizes and service conditions for this test program, Edward Valves concluded that qualification by testing for all four valves was necessary. QVP-7000 – Parent Valve Qualification requires the following tests:

- Pre test Inspection
- Fundamental Frequency Determination
- Environmental and Aging Simulation (not performed)
- Intermediate Inspection (not performed)
- Cycle Test
- Intermediate Inspection
- End-loading and Seismic Test
- Intermediate Inspection
- Flow Interruption and Functional Capability Demonstration
- Post test Inspection

Each of these tests shall be described in the following sections. Based on the design of the valves and materials of construction, it is not necessary to perform the Environmental and Aging Simulation. In addition, it is not necessary to perform an intermediate inspection after the fundamental frequency determination. As stated in paragraph QVP-7330.1(b), the purpose of the intermediate inspection is to evaluate the test valve assembly and provide data relating the functional performance of the assembly to the various test environments. The purpose of the modal test is to measure the dynamic characteristics of the valve assembly. It does not subject the valve assembly to any adverse test environment that may result in its performance degradation.

4.3 Test Program Methodologies and Results

The test sequence is listed above. Throughout the following sections, the test methodology is typical for all four valves.

Throughout the program, the following performance and test data, as required, are continuously recorded:

Stem Force (lbs)
Test Valve Upstream Pressure (psig)
Test Valve Downstream Pressure (psig)
Actuator Gas Pressure (psig)
Actuator Hydraulic Pressure (psig)
Solenoid Voltage (VDC)
Open Limit Switch
Close Limit Switch
Fluid Temperature inside the Valve (deg F) (Cycle and Flow Test only)
Valve Body Temperature (deg F) (Cycle and Flow Test only)
Flowrate (gpm) (Cycle and Flow Test only)
Test Valve Differential Pressure (psid) (Cycle and Flow Test only)

This meets and, in some cases, exceeds the QME-1 requirements. This data will be used for future evaluations of the valve/actuator performance.

Two data acquisition systems are being used during the test programs. Both are high performance PC based data acquisition systems from DATAQ and MEGADAC. Typical sample rates are 1000 Hz for closing and 20 Hz for opening.

The stem force measurement is based on strain gage data. Wyle Laboratories installed the strain gages at a location to allow proper operation without gage damage. The strain gage output is determined using two data points. The first data point is the packing friction with the valve in the intermediate position. The second data point is the valve seating force with the valve closed. The seating force is based on the actuator gas pressure times the gas piston area. The force is also checked by review of the force in tension with the valve backseated, based on the hydraulic pressure times the rod piston diameter. If necessary, the packing friction is adjusted to ensure the backseating is acceptable.

Strain Gage type Pressure transducers are used to measure the gas, hydraulic and internal valve pressures. A digital multimeter is used to obtain the solenoid voltage measurement. Limit Switches are monitored using a nominal dc voltage supply. Stroke times are based on the change of state between the open and close limit switches. A type K thermocouple is used to monitor valve body temperature and valve fluid temperature. Flow Rate is determined using a Venturi flow meter and a differential pressure transducer across the venturi pressure ports. Valve differential pressure is calculated from the valve upstream and downstream pressure measurements. As noted in the table above, some of these parameters are only measured during the Cycle and Flow testing.

Actuator Motive Power

Throughout the qualification, QME-1 requires that the valve be cycled at minimum, nominal and maximum motive power supply to the actuator. The specific state of the motive power supply depends on the testing being performed. Generally, for the service condition being simulated, QME-1 requires the valve to be stroked under the most adverse conditions to produce maximum degradation to the equipment. Depending on the test condition, this can either occur at the minimum or maximum output of the actuator. Tests are also performed at nominal actuator power supply to establish baseline data for comparison with the other data.

The motive power settings for the Size 20 EMFIV are:

Actuator Motive Power	Solenoid Voltage (VDC)	Actuator Precharge Nitrogen Pressure Valve Closed (psi)
Minimum	90 –2,+0	1520
Nominal	125 ± 2	1628
Maximum	140 –0,+2	1735

4.3.1 Inspections (Pre-test, Intermediate and Post Test)

This inspection consists of a main seat leakage test, a packing leakage test and a baseline cold cycle stroke time test. A visual inspection and packing preload check are also performed during the pretest inspection. The post test inspection consists of the above tests and a complete disassembly and examination

of the valve internals. The results of this examination are presented in Section 4.3.7.

The valve installation is illustrated in Figure 6.

The main seat leakage test is performed in both the forward and reverse flow directions at a minimum of 2250-psig differential pressure. The main seat leakage test used the positive water displacement method. The change in length of water column over the 5 minutes test time was measured and converted to the volumetric value.

The packing and pressure seal gasket leakage test is also performed at 2250 psig minimum.

The Baseline Cold Cycle Stroke Time Test was performed as follows:

The test valve assembly was closed into a pressurized valve body (2250 psig) and opened with a minimum differential pressure of 2250 psig at minimum motive power. The test is repeated at nominal motive power.

Inspection Results for the Size 20 EMFIV:

Seat and Packing/Gasket External Leakage Test Results

Test Type	Seat Leakage - Forward (ml in 5 minutes)	Seat Leakage – Reverse (ml in 5 minutes)	Packing and External Leakage (ml in 5 minutes)
Pre-Test Inspection	13.7	27	Zero
Intermediate Inspection – following cycle test	0	1	Zero
Intermediate Inspection – following end loading / seismic test	39	124	Zero
Post Test Inspection	9.6	9.6	Zero

Force and Stroke Time Data Results

Test Type	Stroke Direction O=Open C=Close	Motive Power	Differential Pressure (psid)	Maximum Stem Force (compression - closing / tension – opening (lbs)	Stroke Time (secs)
Pre-Test Inspection	O→C	Minimum	0	107.1	3.9
	C→O	Minimum	2250	64.3	138.3
	O→C	Nominal	0	114.5	3.8
	C→O	Nominal	2270	57.44	175.8
Intermediate Inspection – following cycle test	O→C	Minimum	0	118.0	3.8
	C→O	Minimum	2300	91.5	140.5
	O→C	Nominal	0	124.0	3.65
	C→O	Nominal	2260	N/A	236.9
Intermediate Inspection – following end loading / seismic test	O→C	Minimum	0	107.1	3.8
	C→O	Minimum	2260	54.75	133.4
	O→C	Nominal	0	113.2	3.6
	C→O	Nominal	2256	56.0	142.7

Post Test Inspection	O→C	Minimum	0	103.6	3.8
	C→O	Minimum	2260	115.7	130.7
	O→C	Nominal	0	110.6	3.8
	C→O	Nominal	2270	114.0	140.7

4.3.2 Fundamental Frequency Determination

The modal survey test is performed to determine the valve resonant frequencies, mode shapes and modal damping for both the full open and full close positions of the valve for the frequency range of 10 to 100 Hz. QME-1 only requires that the lowest resonant frequency of the valve assembly be measured.

The testing method used is the Transfer Function Method. The valve was excited using impact testing techniques.

The test valves are mounted in bookend structures. For the Size 4 MSIBV and Size 8 DMFIV, the bookend structures are welded to a reaction mass to perform the testing (hard mounting). For the Size 20 EMFIV and Size 26 MSIV, the bookend structures are installed on the test fixture at Wyle Laboratories as illustrated in Figure 6 (flexible mounting). (The vertical beam structure in Figure 6 is not installed during this test.) Therefore, for these valves, the modal test is performed on the complete system (i.e., valve and test fixture).

A hard mounting could be used for the smaller valves. In this case, the ends of the valves can be considered fixed. This is verified by accelerometers mounted on the support fixture. Because of the mass of the larger valves, they could not be hard mounted. They are tested in a flexible fixture, and the resonant frequencies of the valve assemblies are then determined analytically. This is accomplished by constructing a model of the valve and fixture that match the test results. After the analytical model agrees with the test results, the effects of the fixture can be removed from the model, and the resonant frequencies of the valve assembly can be determined.

Testing is performed with the valves in both the closed and open positions. The responses are measured with triaxial accelerometers at up to 100 locations. A minimum of five excitation points are used.

The following table lists the results for the Size 20 EMFIV, and Figure 7 shows a typical mode for the valve and fixture.

Mode	Valve Closed		Valve Opened	
	Frequency (Hz)	Damping	Frequency (Hz)	Damping
1	16.434	1.112%	16.361	1.097%
2	17.630	3.005%	17.515	3.020%
3	23.281	5.036%	23.375	5.068%
4	41.700	1.912%	42.278	1.819%
5	44.422	2.553%	44.898	2.321%
6	48.068	1.684%	50.576	0.747%
7	53.618	1.967%	54.915	2.334%
8	72.458	3.853%	72.847	1.795%
9	78.785	2.219%	78.519	2.066%

4.3.3 Environmental and Aging Simulation

The valves use metal for all the pressure containing and structural components. Their performance is not degraded by environmental and aging effects such as radiation, elevated temperature and humidity. The nonmetallic parts inside the valve are the pressure seal gasket and the stem packing which are totally confined and in compressive loading. The top and bottom rings of the packing are made from braided filaments of carbon fiber. The interior packing rings and pressure seal gasket are made from flexible graphite which consists of approximately 95% carbon.

Although the packing and gasket are not considered pressure boundary components, they are essential in preventing external leakage from the valve. Published data from Union Carbide indicates that these materials can be used at temperatures up to 5400 deg F, and they show statistically insignificant changes in material properties after exposure to 170 Mrad of gamma radiation. For the specified service conditions, their qualified life is indefinite and Aging Simulation is not necessary.

4.3.4 Cycle Test

The Cycle Test is performed under both cold and hot conditions. The Cold Cycle Functional Testing is performed to demonstrate the valve assembly's capability to open and close under adverse conditions of motive power and system pressure at temperature conditions not exceeding 100 deg F. The Hot Cycle Functional Testing is performed to demonstrate the same capability at normal operating temperature.

The basis for qualification is the maximum time to open and close the valve. The valve was installed as illustrated in Figure 8.

For the cold cycle testing, the actuator is precharged to the maximum motive power and the valve is cycled three times with no internal pressure.

The actuator is then precharged to the minimum motive power. Three valve cycles are performed against an internal pressure. After closure, a differential pressure is then established across the valve and it is opened. During the open stroke, flow is maintained. For the tests on the Size 20 EMFIV, the internal pressure was 2100 psig minimum, and a flow rate of approximately 500 gpm was maintained during the open stroke.

For the hot cycle testing, the actuator is precharged to the nominal motive power. One valve cycle is performed against an internal pressure. After closure, a differential pressure is then established across the valve and it is opened. During the open stroke, flow is maintained. For the tests on the Size 20 EMFIV, the internal pressure was 2100 psig minimum, and a flow rate of approximately 200 gpm was maintained during the open stroke.

Then, the actuator is precharged to the minimum motive power. Three valve cycles are performed against an internal pressure. After closure, a differential pressure is then established across the valve and it is opened under no flow conditions. For the tests on the Size 20 EMFIV, the internal pressure was 2100 psig minimum.

The actuator is precharged to the maximum motive power. The valve is closed against an internal pressure of 2100 psig minimum.

With the valve closed, it is allowed to cool to less than 100 deg F. With the maximum actuator pressure, the valve is opened using

Force and Stroke Time Data Results

Test Type	Stroke Direction O=Open C=Close	Motive Power	Differential Pressure (psid)	Maximum Stem Force (compression - closing / tension – opening (lbs)	Stroke Time (secs)
Cold Cycle Testing	C→O	Maximum	0	36.5	162.5
	O→C	Maximum	0	127.4	3.3
	C→O	Maximum	0	34.6	160.6
	O→C	Maximum	0	131.3	3.3
	C→O	Maximum	0	33.6	163.0
	O→C	Maximum	0	130.8	3.3
	O→C	Minimum	0	111.5	3.7
	C→O	Minimum	2111	81.71	138.5
	O→C	Minimum	0	111.3	3.7
	C→O	Minimum	2119	79.4	134.8
	O→C	Minimum	0	112.7	3.6
	C→O	Minimum	2113	78.1	132.8
Hot Cycle Testing	O→C	Nominal	0	129.5	3.5
	C→O	Nominal	2104	89.9	145.0
	O→C	Minimum	0	110.7	3.65
	C→O	Minimum	2113	78.1	131.6
	O→C	Minimum	0	120.4	3.6
	C→O	Minimum	2106	79.1	132.0
	O→C	Minimum	0	121.7	3.6
	C→O	Minimum	2105	79.7	135.2
	O→C	Maximum	0	129.8	3.45
	C→O	Maximum	2145	101.2	166.6

the minimum voltage to the solenoid valves with a minimum differential pressure of 2100 psig.

4.3.5 End-loading and Seismic Test

The seismic test is intended to demonstrate the operability of the valve assembly when subjected to a loading, which is representative of the specified seismic load qualification level. The pipe-reaction end-loading test is intended to demonstrate operability of the test valve assembly while being subjected to the pipe end-loading forces for which the valve is to be qualified, along with normal service loads which include pressure and deadweight. The end loading and seismic test are combined to provide the worse case operability condition. Per QME-1, adjustments are made for the loadings to account for variations in the dimensions and material yield strength.

The test valve is mounted in the test fixture, as illustrated in Figure 9 and 10, which allows the simultaneous application of seismic and pipe end loads.

Four 45-degree rectangular rosette strain gages are mounted on the valve body near the upstream side flanged end. Strain gage data is taken throughout the test sequence to monitor the stresses on the valve body. The strain

gages are zeroed with the valve closed, the downstream end of the valve unsupported and no pressure in the valve body cavity. (This is not a requirement of QME-1.)

The test sequence consists of cycling the test valve under various actuator motive power settings with a static seismic load applied to the valve upper structure initially. With the seismic load maintained, the required end loading moment is applied to the valve ends.

The seismic loading portion of testing demonstrated the operability of the test valve assembly under the seismic load qualification level. The horizontal test force (71,600 lbs for the Size 20 EMFIV) was applied along the axis perpendicular to the valve flow axis. Per the fundamental frequency determination test results, this is the least rigid axis of the valve. The force was applied at the actuator mounting region, such that the resulting forces and moments acting on the yoke-actuator structure are at least equal to the uniform seismic acceleration of the valve assembly. A valve cycle was performed at normal motive power with 2250 psig minimum differential pressure during the unseating. Three valve cycles were performed with zero internal pressure at maximum motive power. Two valve cycles were performed at minimum motive power with 2250 psig minimum differential pressure across the valve during unseating.

With the seismic load applied, a moment of 4,797,000 in-lbs minimum (for the Size 20 EMFIV) was applied to the valve body in a direction tending to close the bonnet bore with 2760 psig internal pressure. The internal pressure was reduced to 2250 psig

Force and Stroke Time Data Results

Test Type	Stroke Direction O=Open C=Close	Motive Power	Differential Pressure (psid)	Maximum Stem Force (compression - closing / tension – opening (lbs)	Stroke Time (secs)
End Loading and Seismic	O→C	Nominal	0	113.8	3.4
	C→O	Nominal	2256	58.2	165.3
	O→C	Maximum*	0	121.4	3.4
	C→O	Maximum*	0	36.6	173.5
	O→C	Minimum	0	105.2	3.4
	C→O	Minimum	2257	61.3	134.7
	O→C	Minimum	0	107.3	3.9
	C→O	Minimum	2262	61.5	132.9
	O→C	Minimum	0	106.4	3.9
	C→O	Minimum	2257	57.7	131.5

* Data from One of the three cycles is provided here.

Seat Leakage Test Results

Test Type	Seat Leakage – Forward (ml in 5 minutes)	Seat Leakage – Reverse (ml in 5 minutes)
Seat Leakage Test	43.5	45.0

minimum and the end moment was reduced to 3,900,000 in-lbs (for the Size 20 EMFIV). The valve was closed and seat leakage testing was performed in both the forward and reverse flow directions with a minimum of 2250-psig differential pressure. The leakage was measured for 5 minutes in both the forward and reverse flow direction using the same methods discussed in Section 4.3.1.

Following the seat leakage test, the valve was opened against the rated differential pressure of 2250 psig during unseating.

Results

The open valve factor data is presented in the Section 5.0.

4.3.6 Flow Interruption and Functional Capability Demonstration

The Flow Interruption and Functional Capability Test is performed to demonstrate the test valve assembly's capability to close against simulated line rupture flow conditions. The testing is performed with the valve installed in the forward flow direction.

The general test sequence is as follows:

Minimum motive power to the actuator is established. The test is performed with water at 2100 psig minimum at 564 deg F minimum. The first flow interruption and functional capability test is performed. A seat leakage test was performed immediately following the closure, with 2100 psig differential pressure across the valve.

The motive power was adjusted to the maximum value. The test valve was opened with a differential pressure of 2100 psid.

A second flow interruption and functional capability test was performed.

4.3.7 Post Test Inspection

The Post Test Inspection consists of the same testing previously described for the Pre-test and Intermediate Inspections, but it also requires a disassembly and inspection of the valves. During this inspection, any significant damage or changes are required to be noted. For this program, the Post Test inspection concentrated on the pressure boundary and structural components of the valves.

Force and Stroke Time Data Results

Test Type	Stroke Direction O=Open C=Close	Motive Power	Differential Pressure (psid)	Maximum Stem Force (compression - closing / tension – opening (lbs)	Stroke Time (secs)
Flow Interruption	O→C	Minimum	1465	109.1	3.8
	C→O	Maximum	2106	79.0	177.6
	O→C	Minimum	1378	107.5	3.8

Seat Leakage Test Results

Test Type	Differential Pressure (psid)	Seat Leakage – Forward (ml in 30 minutes)
Seat Leakage Test	2100	132

The general condition of the body was good. The inside of the body was clean with no excessive amount of rust or corrosion. The pressure seal gasket area, gasket retainer groove and yoke lock ring groove showed no signs of deformation due to the test pressures or loads. There was normal wear on the body guide grooves due to valve cycling but there was no galling or scoring. None of the Stellite hardfacing on the seating or guiding surfaces was damaged.

Figure 11 shows the downstream gate. There are signs of wear on its seating and guiding surfaces. The condition of the gate is normal for the testing to which it was subjected. It was put in an "as new" condition after lapping/polishing. The valve stem showed no signs of scoring, pitting or deformation. The stem threads used for the actuator coupling were in good condition. The stem packing and pressure seal gasket showed no signs of extrusion or any other indication of failing. The condition of these parts was consistent with the absence of external leakage. The yoke and actuator lock rings had no indications of yielding or permanent deformation. The registers at the top and bottom of the yoke for locating the valve body and actuator were not damaged. This indicates that the loads applied to the valve during the testing did not cause any detrimental effects.

5.0 Valve Factor Discussion

Open Valve Factor

The open valve factor can be derived from the strokes that are performed under differential pressure, as follows:

The maximum opening force and differential pressure during the unseating is obtained from the test results. The open valve factor is given by:

$$\text{Valve Factor (Opening)} = \frac{\text{Max. Measured Opening Force} + (DP * A_{stem}) - F}{A_{seat} * DP}$$

Where

A_{seat} is the mean seat area = 134.17 in^2

A_{stem} is the stem cross-sectional area = 4.41 in^2

DP is the differential pressure in psi

F is the packing friction (a conservative packing force of 4000 lbs was used based on the actual test data).

The results for the complete test program are summarized as follows:

Test Type Description	Differential Pressure (psid)	Maximum Opening Force (Kip)	Temperature (deg F)	Comments	Open Valve Factor
Pre-Test Inspection	2250	64.3	Ambient		0.23
	2270	57.44	Ambient		0.21
End Loading and Seismic	2256	58.2	Ambient	With Seismic	0.21
	2257	61.3	Ambient	With Seismic	0.22
	2262	61.5	Ambient	With Seismic	0.22
	2257	57.7	Ambient	With Seismic / End Load	0.21

Intermediate Inspection	2260	54.75	Ambient		0.2
	2256	56	Ambient		0.20
Cold Cycle Testing	2111	81.71	Ambient	500 gpm	0.31
	2119	79.4	Ambient	500 gpm	0.30
	2113	78.1	Ambient	500 gpm	0.29
Hot Cycle Testing	2104	89.9	460	200 gpm	0.34
	2113	78.1	460		0.29
	2106	79.1	460		0.30
	2105	79.7	460		0.3
	2145	101.2	Ambient		0.37
Intermediate Inspection	2300	91.5	Ambient		0.32
	2260	103.42	Ambient		0.36
Flow Interruption	2106	79	541 deg F		0.30
Post Test Inspection	2260	115.7	Ambient		0.40
	2270	114	Ambient		0.39
*1 Kip = 1000 lbs force					

Closing Valve Factor

The closing valve factor was derived using the following approach:

The force is measured during the valve closing stroke at two locations. The first event is at a time early in the valve closing stroke and the second event is at the maximum closing force prior to seating. This second event represents the location of the maximum closing valve factor. The events are illustrated in Figure 12 for the first flow interruption test.

At both events during the valve closure, the force is given using the following equation:

$$\text{Force}(t) = A_{seat} * VF * DP(t) + P(t) * A_{stem} + F \quad (2)$$

Where

A_{seat} is the mean seat area = 134.17 in^2

A_{stem} is the stem cross-sectional area = 4.41 in^2

VF is the valve factor

DP is the differential pressure in psi

P is the upstream pressure in psi

F is the packing friction.

t is the time, where force, differential pressure and pressure are a function of time.

By inspection of the test results for force, differential pressure and upstream pressure can be determined at the two events. By subtracting the force equation (2) at the two events, the packing force component is eliminated.

The following table shows the required test data for the closing valve factor determination.

Events during First Flow Test	Force (lbs)	Differential Pressure (psid)	Upstream Pressure (psig)
During closing = 6.38 secs	-4,300	18.5	1226.3
At max. force prior to hardseat contact = 9.18 secs	-69,670	1328.3	1492.2

Using this data, and subtracting equation (2) for the two events gives:

$69{,}670 - 4300 = 134.17 * VF * (1328.3 - 18.5) + 4.41 * (1492.2 - 1226.3)$

Closing Valve Factor = 0.365

Similarly for the second flow interruption test, the table below provides the required test data for the closing valve factor determination.

Events during Second Flow Test	Force (lbs)	Differential Pressure (psid)	Upstream Pressure (psig)
During closing = 8.4 secs	-4,437	30	1234.3
At max. force prior to seating = 11.16 secs	-61,690	1269.2	1469.3

Using this data and subtracting equation (2) for the two events gives:

$61{,}690 - 4437 = 134.17 * VF * (1269.2 - 30) + 4.41 * (1469.3 - 1234.3)$

Closing Valve Factor = 0.338

The valve factors determined in this section are based on the actual measured strain gage values. A formal error analysis has not been performed on this data. The overall thrust accuracy is related to factors such as the pressure measurement accuracy, the internal friction in the actuator and strain gage variations.

6.0 Conclusions

This paper presented the test methodology for QME-1 qualification of the Edward Equiwedge Gate Valve for Containment Isolation Service. The test results obtained by Wyle Laboratories for the Size 20 EMFIV shows that it successfully met the QME-1 requirements. Wyle Laboratories is obtaining similar data on the other three valve sizes.

After the publication of Generic Letter 89-10, many utilities developed qualification programs for their specific applications. The intent of QME-1 is to establish a common standard for qualifying active valves for use in nuclear plants. However, this standard does not have enough flexibility for specific applications, such as the requirement for opening against line rupture flow. For the valves involved in this program, this test is not representative of the service conditions.

Additionally, the standard does not address valve preconditioning. To properly evaluate valve performance over its life, a certain amount of cycles under normal conditions should be performed prior to conducting the static load and flow interruption tests. The exact amount of preconditioning under the associated service conditions should be considered.

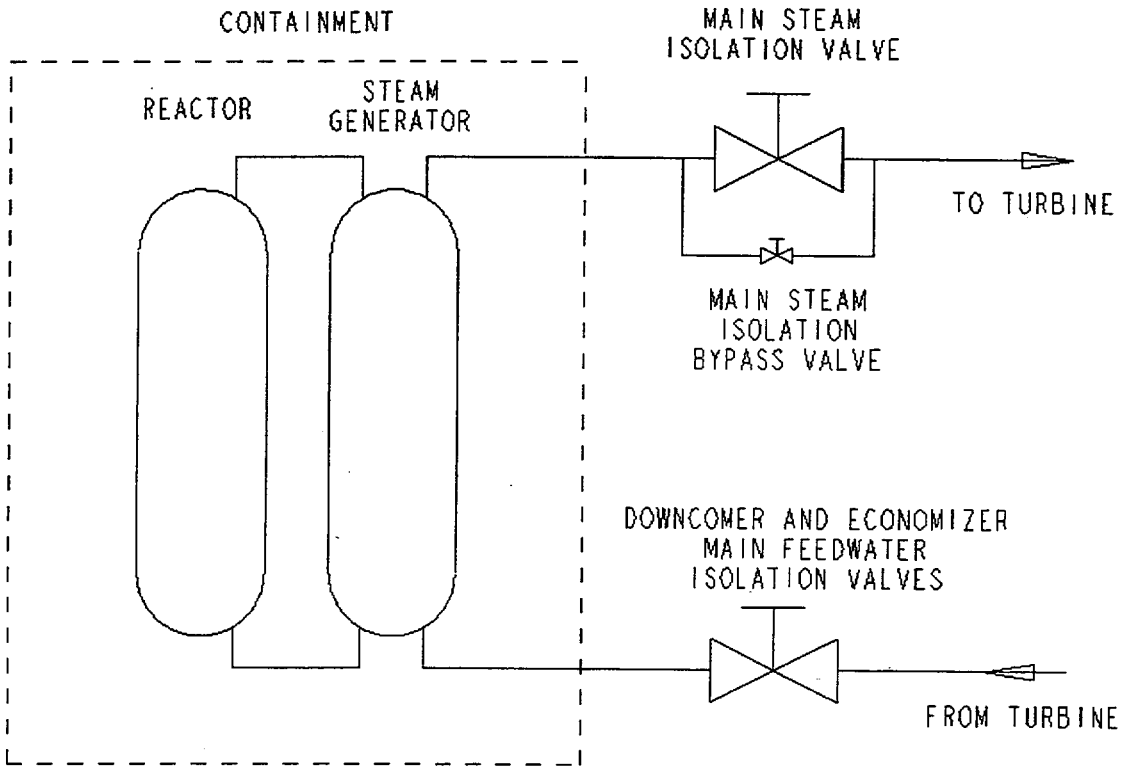

Figure 1 – Schematic for the Main Steam and Main Feedwater Isolation Valves in a PWR Nuclear Power Plant

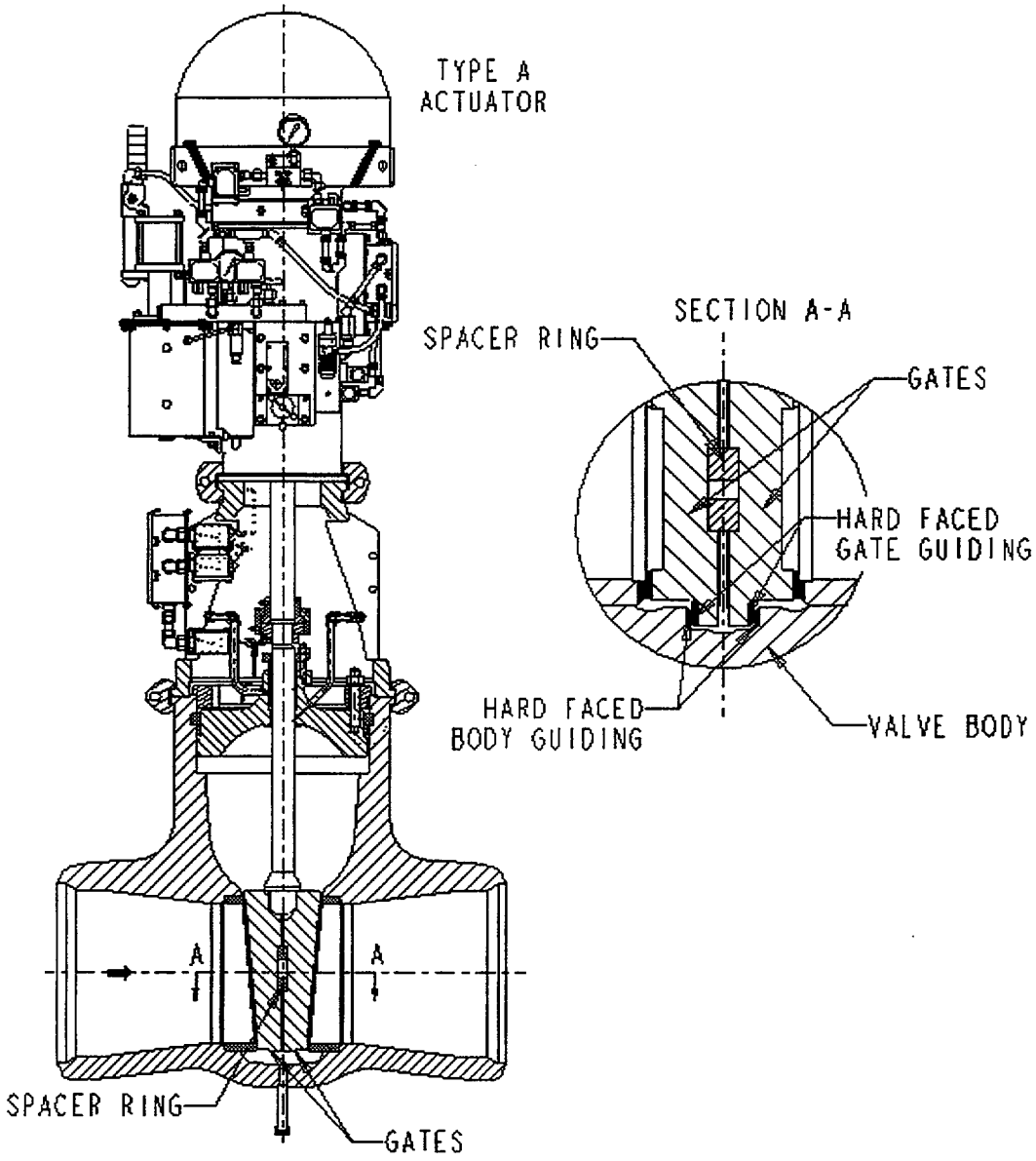

Figure 2 – Cross-section of the Edward Equiwedge Gate Valve with a Type A Actuator

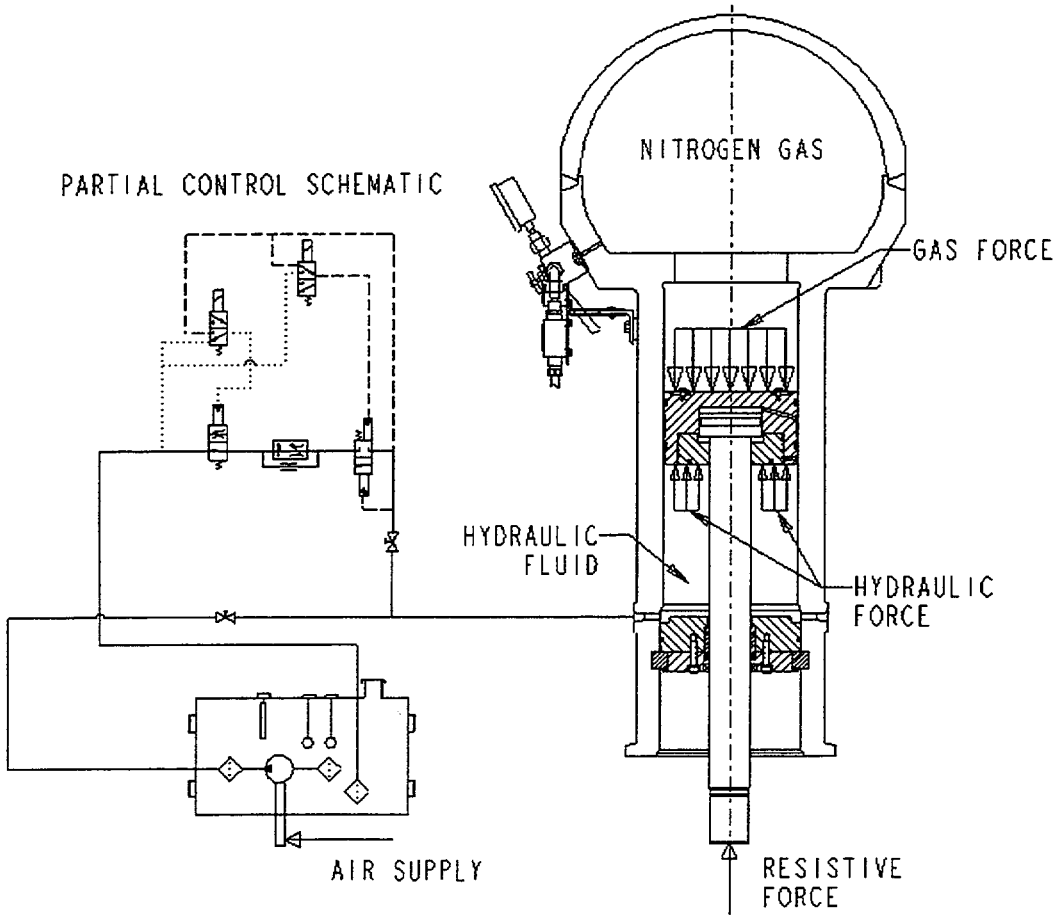

Figure 3 – Cross-section and Partial Control Schematic of the Edward Valves Type A Actuator

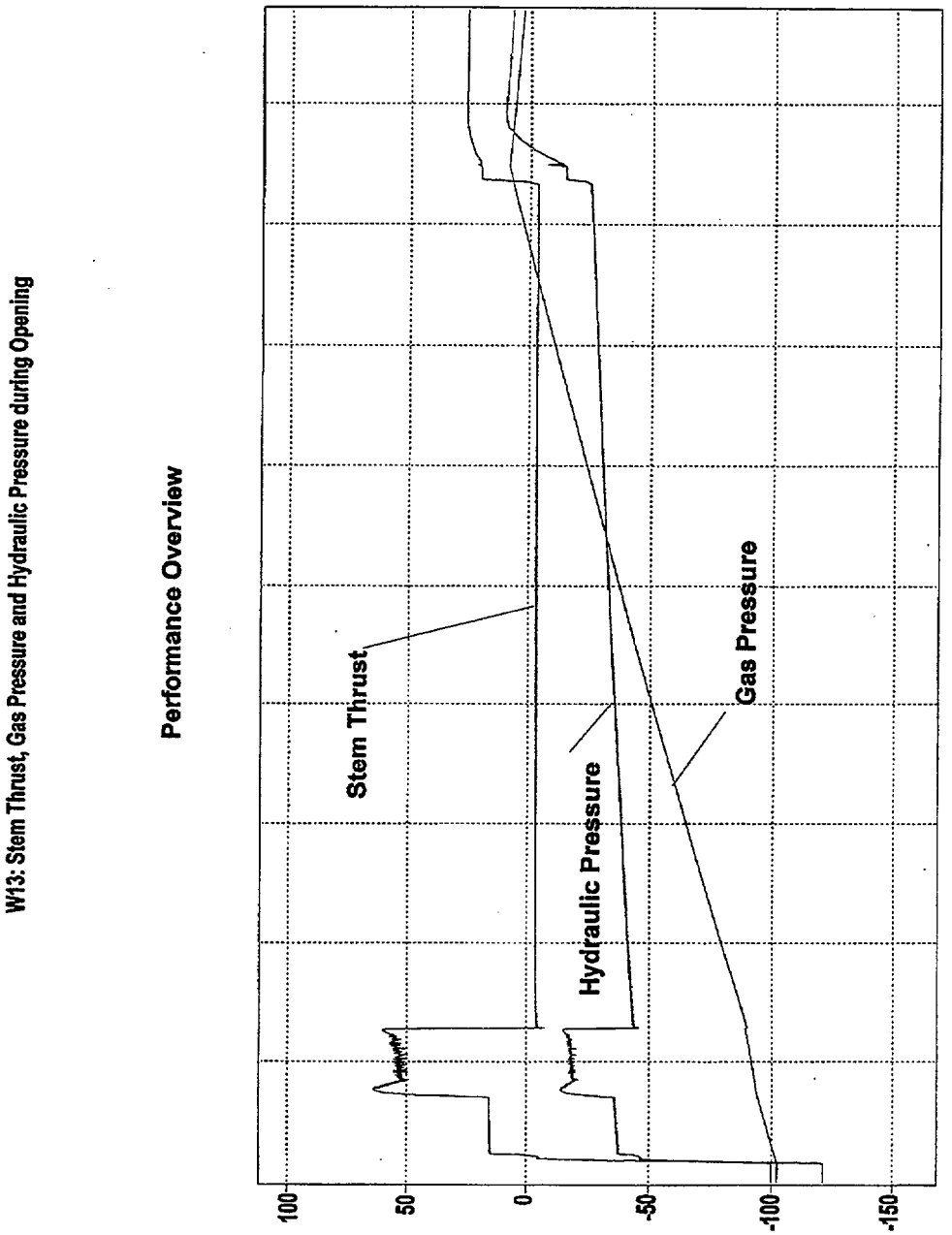

Figure 4 – Typical Performance Data During the Opening Stroke

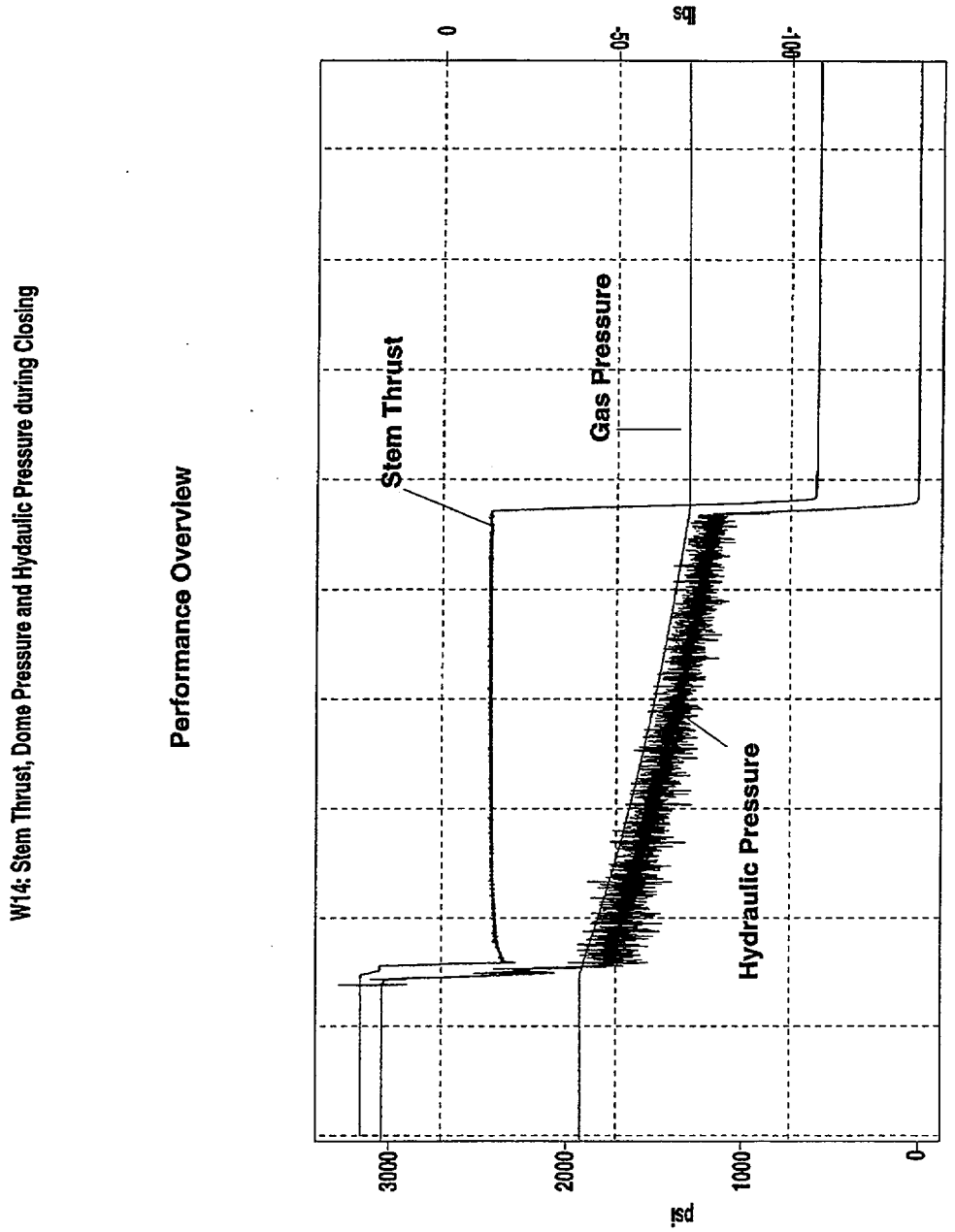

Figure 5 – Typical Performance Data During the Closing Stroke

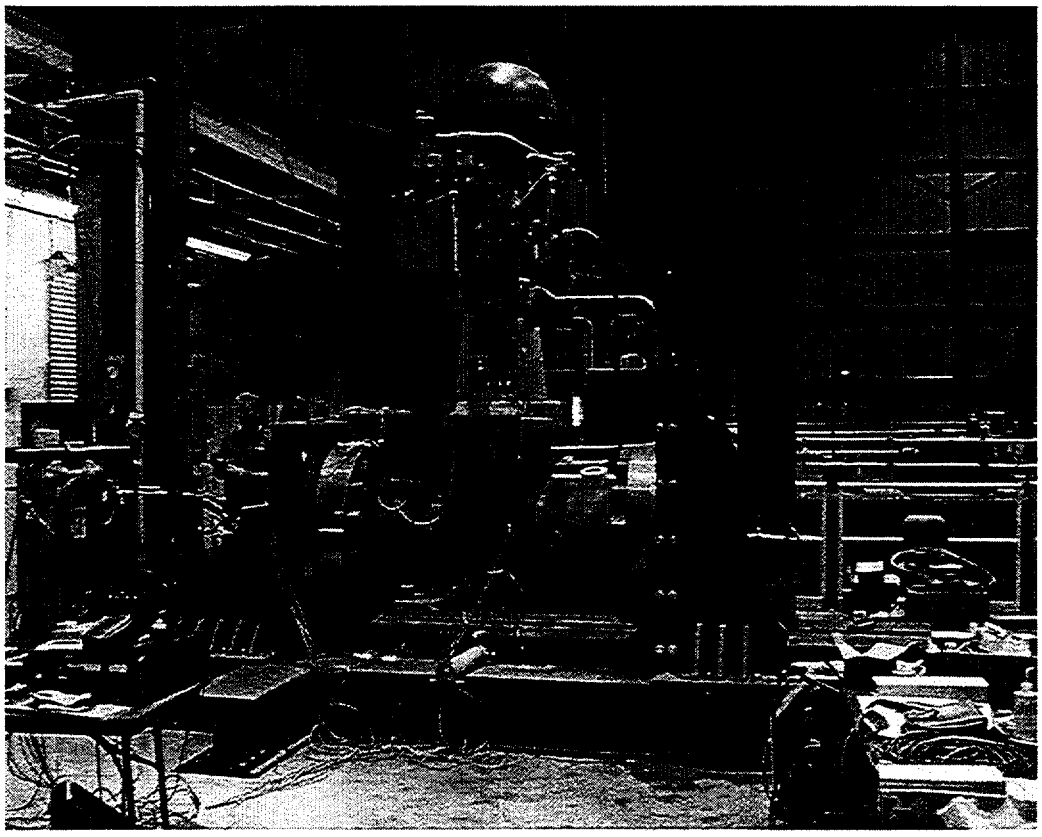

Figure 6 – Size 20 EMFIV Inspection Set up

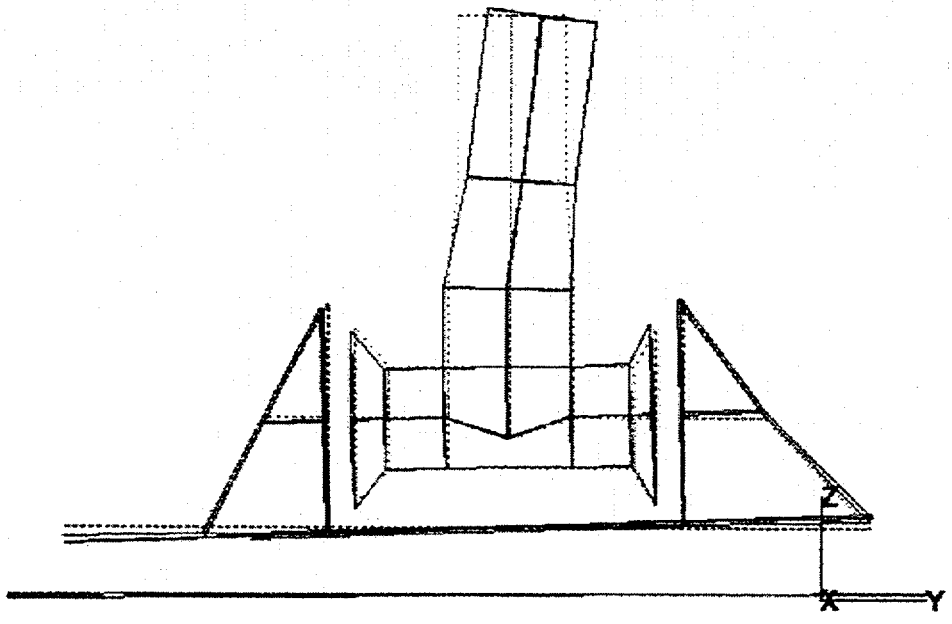

Figure 7 – Mode 6 (48.07 Hz) for the Size 20 EMFIV (closed) and Fixture

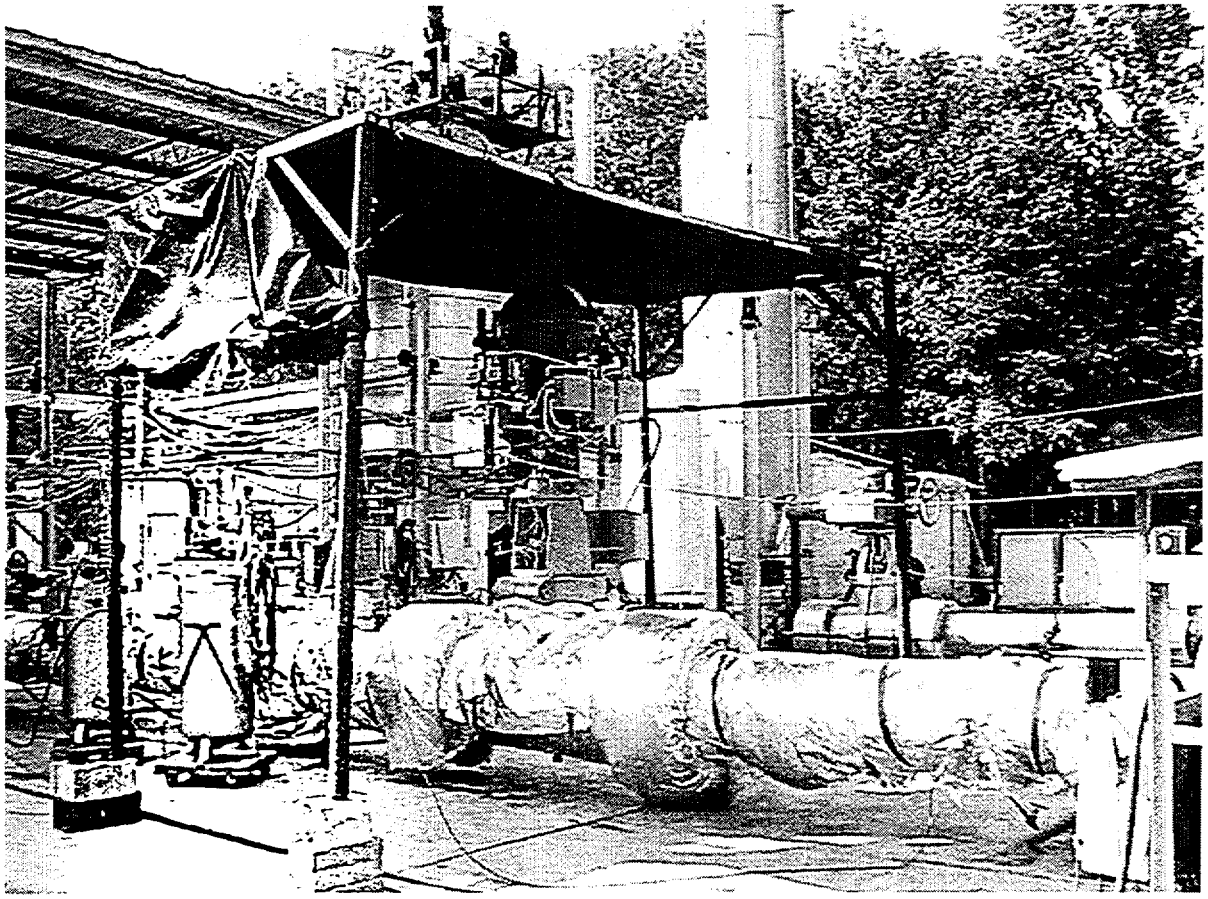

Figure 8 – Typical Test Set-up for the Cold and Hot Cycle Testing and the Flow Interruption Testing

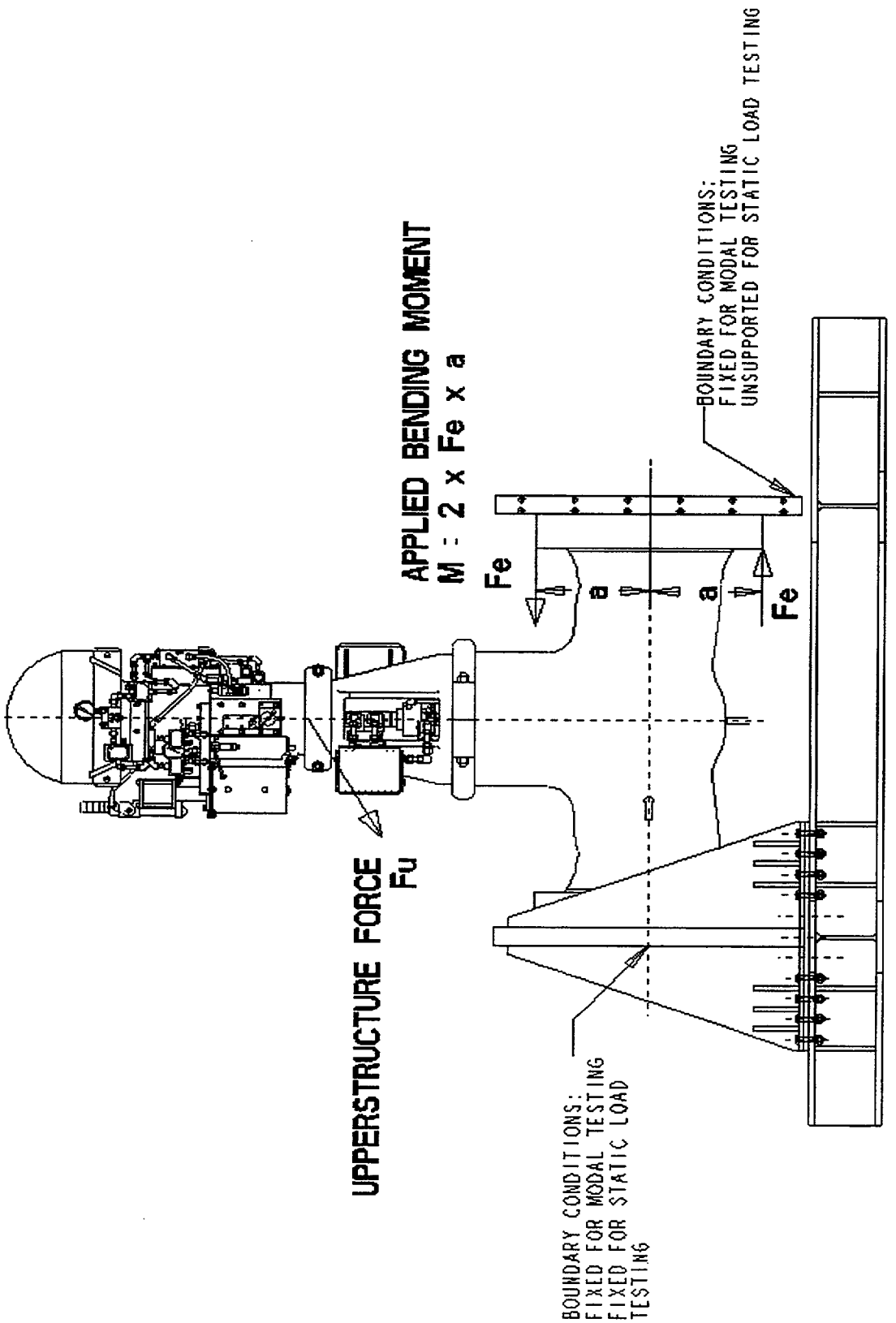

Figure 9 – Schematic of End Loading/Seismic Testing

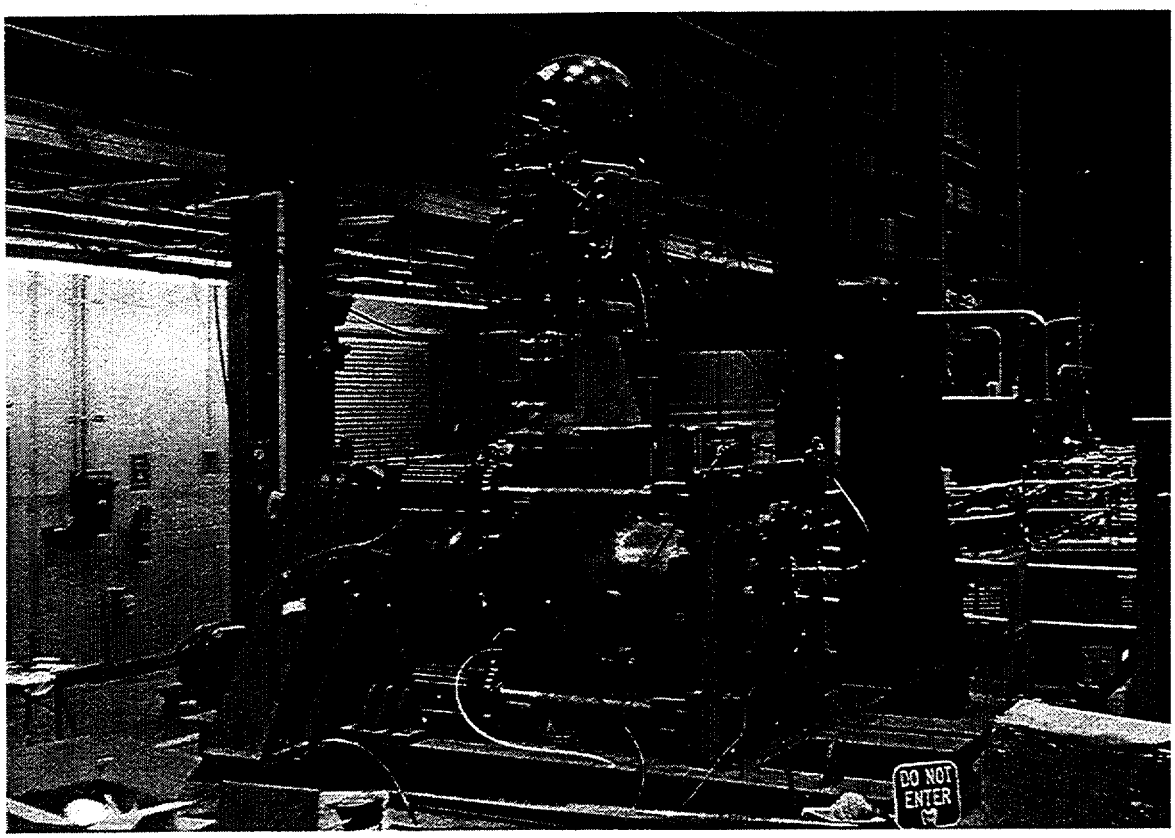

Figure 10 – Test Set-up for the End Loading and Seismic Loading Test

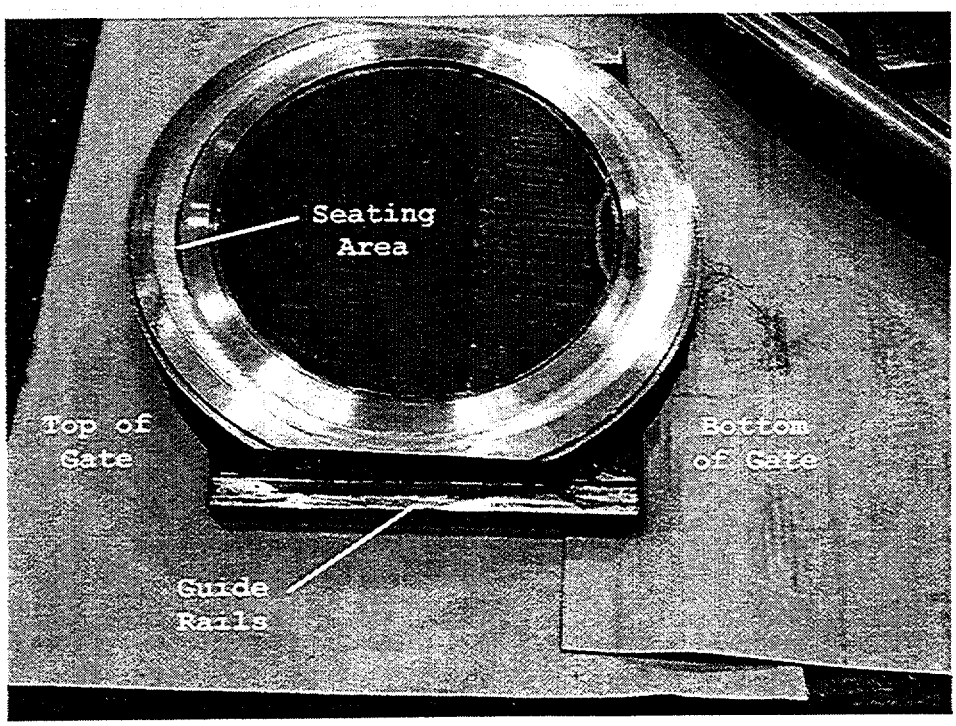

Figure 11 – Photograph of the Downstream Gate taken during the Post Test Inspection

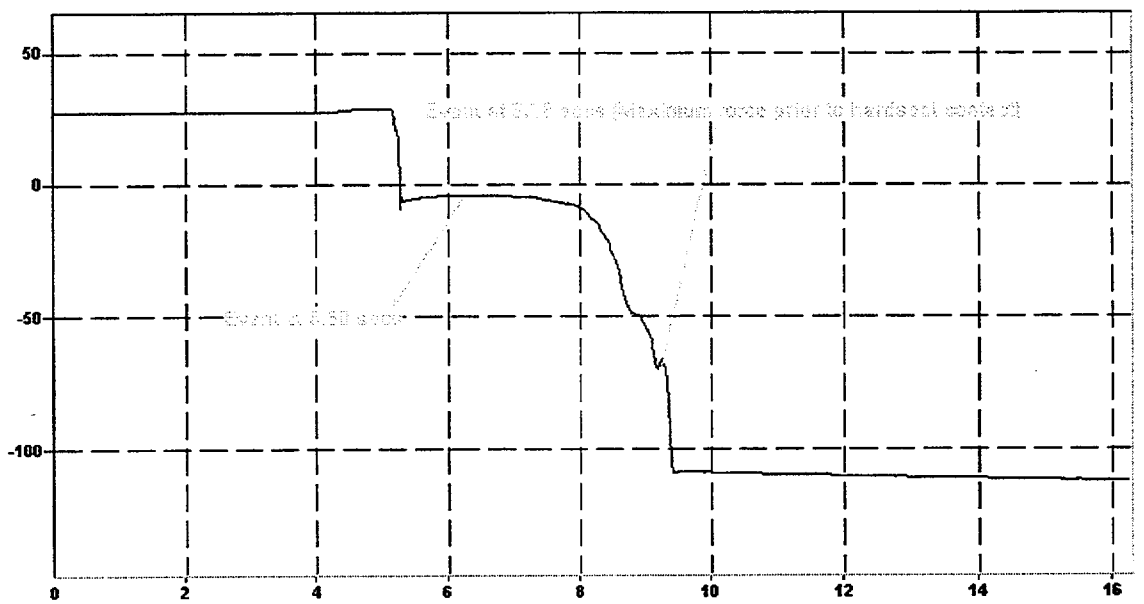

Figure 12 – Valve Force during the Flow Interruption Test at Minimum Motive Power

Use of Inductive Position Indicator to Verify Check Valve Position

David H. Peyvan, Pilgrim Nuclear Power Station, Entergy Corporation
Beat Buchmann, CCI AG, Winterthur, Switzerland

In the 1930s, the need for physical measurements in the chemical process industry caused various differential transformer designs. Since then, the Linear Variable Differential Transformer (LVDT) techniques have been improved and experienced as highly reliable and robust. The LVDT is an electromechanical device that produces an electrical output proportional to the displacement of a separate, moveable magnetic or ferritic core. It was not until the late 1960s that advances in electronic hybrid microcircuits eliminated several limitations of the early devices.

Pilgrim Station, a 670MWe Boiling Water Reactor (BWR) commissioned in 1972, undertook an investigation of methods for repeatable monitoring and accurate recording of disc position of swing-disc check valves. After reviewing available technologies, Pilgrim settled on an Inductive Position Indicating System (IPIS) incorporating recent technological improvements.

The Position Indicator is designed for measuring displacement at very high temperatures and high radiation exposures. Hence, it is made exclusively from inorganic materials, mainly metals and ceramics. The Position Indicator case is weld sealed to prevent any moisture accumulation and isolation leakage.

It is a common procedure to perform nonintrusive testing (NIT) methods of check valves. Most of the plants are using acoustic and magnetic monitoring techniques to verify the opening or closing capability of safety-related check valves. As a matter of fact, traditional NIT techniques do not provide accurate and repeatable results. So the NIT analysis may provide wrong results due to inadequate valve performance (see NRC Information Notice 2000-21).

The use of Position Indicators allows verification of any valve position at any operating condition in a harsh environment. Hence there are several benefits: Valve remote diagnoses can be performed in normal operation. Unneccessary valve disassembly and inspection can be avoided. This is also most important in high radiation fields where all service work means exposure of personnel to radiation dosage. To conclude, the IPIS cuts down costs and time. It is also not wise to rely on only one specialist who interpretes the analysis of traditional NIT results on safety-related valves.

As a result of the successful operation of the IPIS system at Pilgrim Station and operational experience in the U.S. and abroad, the IPIS is a proven technology for precision valve position indication.

Axial Flow Check Valve Dynamic Response Testing— Using Test Results to Select the Optimum Valve Design

Robert Gormley, Curtiss Wright Flow Control, Enertech Division
Ivan Michel, Curtiss Wright Flow Control, Enertech Division

Abstract

A comprehensive set of dynamic response curves is essential to selecting the optimum check valve design for applications susceptible to pressure surge. This paper illustrates the accuracy of these curves by calculating expected performance and comparing this to actual system response measured during transients. By using the dynamic test results and the analytical sizing methodology illustrated in this paper, design engineers can accurately predict the performance of various axial flow check valves before they are purchased and installed. Variables such as disc geometry, bearing design, spring selection, and internal component configuration contribute greatly to the dynamic performance of axial flow check valves. This paper analyses how dynamic performance can be controlled by proper selection of these variables.

Introduction

Steady State and Dynamic flow loop testing (Ref. 1,2,3,4,5) has been completed on a number of, axial flow check valves designed for use in nuclear plants. This testing offers the design engineer the ability to evaluate these designs as solutions for applications experiencing damage due to pressure surge. This paper will identify nuclear plant applications susceptible to pressure surge, describe the need for dynamic testing, summarize the test methodology and provide a step-by-step approach to using the curves, including examples of actual applications.

Check valves are utilized in numerous applications throughout nuclear power plants to prevent reverse flow of fluids. One of the most common uses for check valves is at the discharge of pumps to prevent reverse flow while a pump is in standby. This ensures that pumps do not rotate backwards and system inventory is not depleted when pumps are placed in standby with the discharge isolation valve left open.

In most cases, a swing check was the original valve design specified for Balance of Plant (BOP) and Safety Related pump discharge applications. During the design phase, consideration of a pump-discharge check valve's dynamic performance characteristic was rarely factored into the design specifications. Swing checks, and to a lesser extent, duo-disk check valves, were chosen for pump discharge applications based mainly on their price, flow capacity, seat leakage capability and conformance to ANSI B31.1 and ASME Section III design criteria. Steady state operating pressures are greatly exceeded

during severe pressure spikes resulting from rapid check valve closure during pump trips and gas expansion transients. Design specifications were typically written around steady state performance criteria, not the more limiting transient condition.

Transient surge pressures will evolve in a piping system when fluid velocity is changed rapidly. This can occur by rapid valve closure or opening or vapor pocket collapse. Resultant forces exerted by pressure surge have caused pipe movement damaging supports and anchors, fractured pipe, over-ranged gages and forced pumps/motors out of alignment. High transient pressures have also resulted in rupture of upstream and downstream piping.

All nuclear power plants have applications susceptible to pressure spikes, of varying degrees of severity, caused by the rapid closing of check valves. Some plants are fortunate to have system configurations that do not generate pressure surges high enough to cause damage or exceed design pressures. In many cases, pump start-up and shutdown procedures have been modified requiring an "Operator Work Around." Operations personnel are dispatched to the pump to close the manually operated discharge isolation valve on a pump being placed in standby. After the pump is secured, the discharge valve is typically reopened. Another option is to install accumulators at the discharge of pumps to absorb the pressure surge after a pump trip.

There are some sites that have replaced originally supplied check valves with similar or alternate designs in an effort to eliminate problems associated with pressure surge. For the nuclear plants in the process of implementing design changes to eliminate the potential for damage due to pressure surge or to remove the need for an Operator Work Around, having the data needed to accurately calculate the dynamic performance of a replacement check valve design is essential. As an example contrasting the performance of a swing check vs. an axial flow check valve, see Figure 1. Check valve "A" is an axial flow design, valve "B" is a swing check. The resultant pressure surge with an axial flow design is roughly ten times less due to the low mass disc, short stroke and fast closure time characteristic of axial flow check valve designs. How does an engineer determine the maximum pressure surge as a function of check valve performance?

The only way to accurately predict the dynamic performance of a check valve is to conduct testing that determines accurate reverse velocity (V_R) vs. system deceleration (dV/dT) curves. Although a check valve design may look similar, seemingly irrelevant differences can provide vastly different dynamic test results. Swing check valves with lever arms will react differently than standard swing checks. Axial flow check valves that are center guided with multiple bearing surfaces will react differently to rapid flow reversal than ring shaped, floating disc designs.

The design engineer or system engineer tasked with eliminating problems related to pressure surge must have access to dynamic test results in addition to the experience to know how to use them. They must also be familiar with the various check valve designs available and recognize the differences that affect dynamic performance. One important lesson learned in the nuclear industry is that valves of similar design may have exceedingly different performance characteristics. As an example, when the operating torque required for symmetric butterfly valves is used to size double or triple offset butterfly valve actuators, the result is an undersized

actuator. Although symmetric and high performance butterfly valves both contain very similar components, disc, shaft, bearings, the torque required for seating and unseating is vastly different. With all valve designs, the engineer must be careful not to assume valve performance characteristics based on generic valve types. As illustrated in this paper, seemingly similar axial flow designs will have different dynamic performance characteristics.

Systems Susceptible to Check Valve Induced Pressure Surge in Nuclear Power Plants

Systems at risk are those with multiple pumps discharging to a common discharge header and those with one or two pumps that discharge against a high head. There are also applications, such as Residual Heat Removal, that have experienced high pressure spikes generated as the result of gas expansion after the restart of pumps following a Loss of Offsite Power (LOOP).

Parallel pump configurations—Service Water, Heater Drain, Cooling Tower Makeup, Screen Wash & Component Cooling Water Systems

These systems are typically configured with multiple pumps in parallel, See Figure 2, with one pump in standby and either one or two pumps running, depending on the cooling load required. A loss of power to one running pump, or an intentional pump trip, can cause a damaging pressure transient. Once the tripped pump begins to coast down the standby pump starts automatically. The pressure between the tripped pump and the associated check valve drops below the header pressure. Provided other pumps continue to feed the common header or a high discharge head exists, flow will quickly reverse and run from the header to the pump discharge closing the check valve. The instant the check valve closes, the fluid momentum is transferred into a pressure wave that travels downstream causing a spike in downstream pressure. This scenario takes place in typically less than one second.

Generally, the worst case configuration is the trip of one pump while the other pumps continue to run discharging to the common header. Observed in some applications is a high transient pressure both upstream and downstream of the check valve. Upstream pressures are caused by column separation and may exceed the peaks measured on the downstream side.

High head—Main Feed System

High head applications, such as Main Feed, Main Feed Booster, and Condensate pumps are at risk of severe pressure surge transients if one or all of the running pumps were to trip. One nuclear plant designed with two 100% duty Main Feed pumps experienced severe pipe movement causing fractures and serious damage, but no pipe rupture (Ref. 11). When alternating pumps, this site started the shutdown pump and secured the previously running pump after the system became stable. This evolution was done at reduced power levels. When the pump was secured, a large pressure transient was initiated. The damage was due to the delayed closure of the installed swing check valves. When the check valves closed during high reverse velocity a large downstream pressure spike occurred. This was followed by the formation of a vapor cavity on the upstream side, which quickly collapsed causing additional pressure spikes. This incident was one of the precursors to further in-depth studies on the affect of various check valve designs and their ability to mitigate pressure surge.

Vapor bubble Recoil - RHR System

Residual Heat Removal Systems typically incorporate a vertical, U-tube heat exchanger where non-condensable gasses may accumulate. After a Loss of Offsite Power (LOOP) event, the RHR pumps lose power causing this gas bubble to expand. Once the Emergency Diesel Generators start and load the Essential Bus, the RHR pumps receive a start signal. During the pump start transient, there is a pressure surge due to the fluid momentum that compresses the gas bubble in the heat exchangers which subsequently expands once the pressure drops to steady state levels causing the check valves to slam closed.

In an effort to isolate the cause of high pressure transients associated with a specific RHR application, Enertech instrumented an RHR system as illustrated in Figure 3. The RHR pump was started after instrumenting the loop using instrumentation of a sampling rate of 2,500 to 50,000 samples per second (SPS). This was electronically reduced to either 250 SPS or 5,000 SPS depending on the resolution needed to analyze the specific event. This instrumentation included position indicators (pos.) and accelerometers (accl.) on pump suction, discharge and header check valves and pressure (press) transducers in various locations as indicated in Figure 3. During this transient, caused by the recoil of a vapor pocket trapped in the high point of the RHR heat exchanger, a pressure spike of over 500 psig was recorded in the pump suction line. This was due to column separation and subsequent collapse after the discharge swing check valve slammed closed.

Dynamic Testing

What tools will dynamic testing offer the Design Engineer?

When a check valve is being evaluated for purchase as a replacement for an existing design, a modification package and the issuance of design specifications control the process. Valve data sheets and a request for quotation to various vendors are issued that ideally, illustrate all service, testing and design conditions that the valve must meet. Critical check valve characteristics vary based on the application but generally contain some minimum requirements such as:

- Size and Pressure class
- Pressure Retaining Material specifications
- Trim Material Specifications
- Minimum Cv
- Vmin (the velocity required to maintain a check valve disc in full open position without oscillation).
- Hydro and seat leakage test criteria

Rarely, if ever, do nuclear plants request that a check valve manufacturer provide dynamic performance curves. In applications susceptible to water hammer, this information is as critical as minimum Cv, weight, or pressure/temperature limitations. Having access to dynamic response curves will allow the design engineer to accurately calculate the resulting pressure surge magnitude affected by installing the replacement valve. To use these curves will require either:

- The dynamic response curves of both the original and the replacement check valve and the magnitude of pressure surge experienced with the original valve installed, or

- The maximum fluid deceleration through the check valve determined by hand calculations for a simple system or via computer generated hydraulic model for more complex systems. In addition, the engineer must have dynamic response curves for the check valve being evaluated for purchase and installation.

By taking advantage of these available curves, the design engineer will have the data necessary to calculate the new, resultant pressure surge under various transient conditions. This information can be used to:

- evaluate the cost-effectiveness of the modification prior to approval
- provide data necessary to compare other options such as air vessels or other system modifications
- select the most economical check valve design that limits pressure below the level where damage may occur to system components
- improve the accuracy of hydraulic system models

By eliminating the uncertainty of how a new check valve design will mitigate transient pressures, the cost justification process is made much easier. It allows the engineer to determine which valve designs will meet the transient design criteria. Once the acceptable options are selected, regarding dynamic performance, a more detailed comparison can be made using other criteria important in selecting the best option. Cost, delivery, V_{min}, C_V, will likely play an important role in making the optimum selection of check valve design. This design information also allows plant management to assign the appropriate weight/value to a pressure surge reduction project if they know the final result prior to making an investment in a plant modification. These projects will be competing for limited budgets alongside other projects that can also increase plant efficiency and/or safety.

How is check valve dynamic performance modeled in a flow loop?

Valve manufacturers providing check valves to nuclear plants for critical applications, both safety related and Balance of Plant (BOP) should be responsible for conducting flow tests to determine steady state and dynamic performance of their product. Steady state testing will identify characteristics specific to the valve design such as flow capacity (Cv), the velocity required to fully open the check valve (V_0), V_{min} and the liquid pressure recovery factor (F_L). This information is useful in calculating pressure drops, cavitation, choke points and predicting degradation of the check valve internals. Dynamic testing provides information characterizing a check valve's ability to react to rapidly changing system conditions that generate a rapid deceleration of fluid.

Dynamic test loops are designed to generate variable rates of fluid deceleration through a check valve. This rapid deceleration closely resembles the conditions associated with a pump trip or the recoil of a gas bubble in downstream piping. The test loops are instrumented to record the ability of the specific check valve to react to the change in forces acting on the disc. A typical test will measure time, flow/velocity, valve position and upstream and downstream pressure. Figure 4 illustrates velocity, disc position, upstream pressure, downstream pressure and differential pressure as a function of time. The elapsed time is 1 second.

This data is used to calculate:

- average dv/dt at the start of the transient

- maximum reverse velocity at the instant of initial disc closure

The test is repeated at different decelerations until sufficient data points have been collected to allow a plot to be generated comparing V_R (The reverse velocity at the instant of check valve closure) to dv/dt.

$$V_{Rmax} = f(dv/dt)$$

This curve is referred to as the check valve's dynamic performance curve and can be used to determine the maximum reverse velocity based on a given system deceleration. For each one foot per second change of velocity a pressure change of approximately 50-60 psi occurs for metal pipes. Using the Joukowski equation, the maximum reverse velocity can be used to calculate the resulting pressure surge.

$$\Delta p = \pm \rho a v_r$$

ΔP = Pressure Surge and the instant of check valve closure

a = The wave speed (ft/sec)

ρ = The density of the fluid (lb/ft^3)

v_R = The reverse velocity at the instant of check valve closure (ft/sec)

Axial flow and duo-disc check valves, among others, utilize a spring to apply a force to the obturator in the closed direction. With the wide range of potential spring rates available for use in any one check valve design, it is impractical to perform dynamic testing for each potential spring selection. It is also not economically justified to test every size of a given check valve design. Fortunately, a method exists to incorporate these variables, valve size and spring force, into a dimensionless form of a dynamic response curve. These curves allow check valves that are geometrically similar, but of different sizes and spring forces, to be characterized by one performance dimensionless curve. A 32" valve of a specific design will have different dynamic characteristics than a 12" version of the same design. Most likely, little difference will be noticed between a 30", 32" or 36" valve of the same design. A discussion of the theory and derivation of dimensionless performance curves is beyond the scope of this paper.

How were the check valves tested?

Dynamic testing of various axial flow check valves was conducted at the Delft Hydraulics Lab in The Netherlands. The purpose of this testing was to validate both steady state and dynamic performance characteristics of different check valve designs. The steady state check valve characteristics collected during the testing include flow capacity, pressure recovery factor and critical velocity for check valves with different spring configurations. One unique aspect of the steady state testing was the measurement of disc position as a function of flow rate in both the stroke open direction and stroking closed evolution. Although the steady state testing results are important, this paper will focus on the results related to dynamic tests. The dynamic tests were conducted to generate dimensional and non-dimensional performance curves that plot reverse velocity as a function of system deceleration.

Two test loops were used, one for 12" valves and smaller, the other for valves between 12" and 32" NPS. The test loops are designed to generate variable deceleration rates of water in the reverse direction through the installed check valves after a constant flow rate is established in the forward flow direction. This deceleration is effectuated by means of rapidly increasing the pressure downstream of

the check valve. For small bore check valves the upstream pressure was rapidly decreased. Either method closely duplicates power plant conditions causing check valve slam during transients. This paper compares only the tests conducted using the large bore test loop on 32" valves.

Large Diameter Check Valve Dynamic Testing

Tests conducted on 32" and 24" axial flow check valves have been conducted using the large test loop as illustrated in Figure 5. This is an open loop with constant upstream pressure maintained by a head tank. The head tank level is maintained constant by an overflow line and eight centrifugal pumps taking a suction from a reservoir. Downstream of the check valve, mounted in the test section, is the High Pressure Tank, followed by a 24" throttle valve used to adjust flow to a point sufficient to fully open the check valve. Flow in the reverse direction is caused by rapidly pressuring the high-pressure tank via a fast acting (<0.5 seconds) air valve that is connected to an Air Reservoir. The rate of deceleration is controlled by varying the pressure in the Air Reservoir (2472 ft^3). During steady state testing, the Air Reservoir is isolated from the water filled High Pressure Tank (212 ft^3) by the fast acting air valve. From an initial steady state flowing condition, the fast-acting air valve is opened, rapidly reversing flow through the check valve. Fluid velocity and pressure are measured as a function of time. The capacity of this test rig is limited to a deceleration of 65 ft/sec^2. This dynamic test measures the following parameters as a function of time:

- flow rate
- disc position using a strain gauge
- upstream pressure (P1)
- downstream pressure (P2)

These parameters are used to calculate

- The fluid velocity gradient dv/dt (ft/sec^2)
- The maximum reverse velocity $V_{R\,max}$ (ft/sec)

The test is repeated for a variety of decelerations. The complete test is typically conducted once with the check valve fitted with relatively weak spring; then repeated using a stronger spring.

Dynamic Test Equipment

- Flow rate was measured with an electromagnetic flowmeter, accuracy +/- 5% of measured value.
- The check valve position was measured using a strain gauge mounted on one of the three radial guide assemblies. On axial flow designs that utilize a center guiding stem, instead of a radial guide assembly, valve position was not measured.
- Dynamic upstream and downstream pressures were measured using piezo-electric pressure transducers, 100 bar range, 40 kHz frequency and charge amplifiers with frequency range of 0-180 kHz, accuracy +/- 1%.

Presentation of Dynamic Test Results

When evaluating the performance of various automobiles, criteria such as 0-60 time, top speed and braking distance are normally provided corresponding to the specific model of car along with any performance enhancing options such as: turbo, larger engine displacement, body style etc. How valuable is performance data associated with only a generic car type such as sports car, sedan or pickup truck instead of the specific model? Would you assume that a Chevrolet Cavalier

offers the same performance as the Chevrolet Z06 Corvette? Of course not, any more than you should assume that all axial flow check valves offer the same dynamic performance characteristics. When using dynamic performance curves, the design engineer should ensure they are also provided with the exact configuration of valve tested and how the test was conducted. For each of the axial flow check valves tested, we have provided a standardized method to present the relevant data. Type, Manufacturer/Model, Size, V_0, Orientation, Test Medium, Test Method, Drawing of Valve, Description of Valve and Description of Test Specifics and provided for each test conducted.

Since different axial flow designs have different performance characteristics, we have tested multiple designs of the same 32" size, Model DRV-G, DRV-B and KRV-B. We have also tested 12" and 24" DRV-B's, see Figure 6. In addition to NozzleCheck valve test results we have included dynamic performance curves for Mokveld 32" Axial Flow designs (Ref. 7) in addition to swing check and Duo-Disc designs (Ref.6) . Although all of the relevant information was not available, the Mokveld check valve curves provide a comparison of different results for valves of the same type. The test results of swing checks and Duo-Discs are offered for use as comparison to axial flow check valve performance characteristics.

When testing spring loaded check valve designs it is critical to identify the specific spring design used during testing. The strength of the spring is one variable, within one valve's design, that significantly affects dynamic performance. One simple way to differentiate between spring designs is to categorize them by the associated V_{min} or V_0. The stronger the spring force, the higher velocity required to fully open the valve. In addition, the closing times are faster with stronger springs resulting in lower reverse velocities. In the testing conducted on the NozzleChecks at Delft Hydraulics, we identify the specific spring by the minimum flow required to fully open the valve, V_0. It is also important to compare the steady state velocity prior to the start of the dynamic test and compare it to the valve's V_0 value. The velocity must be higher than valve's V_0 to fully open the valve. Running the test at less than the fully open position results in lower reverse velocity values. Note that the 32" DRV-G tests were conducted with the valve slightly less than fully open. As a general description, you will sometimes see various springs identified as weak, medium or strong. This general categorization will vary between different valve manufactures and can introduce large errors in calculating pressure surge magnitudes; the actual V_0 values should be used when available.

Type: NozzleCheck
Manufacturer/Model: Entech/NozzleCheck Model DRV-B
Size: 32" NPS
V_0 -Strong Spring- 8.81 fps
V_0 -Weak Spring- 6.1 fps
Orientation: Horizontal
Test Medium: 66 °F Water
Test Loop: Large Bore Loop at Delft Hydraulics
Dynamic Response Curves and Drawing: Figure 7

Description of Valve

This test was conducted using the original style of DRV-B. The DRV-B has a single-piece body with a ring style disc that fits in a recessed area of the diffuser. The disc is acted on by a set of helical springs evenly spaced around the circumference of the disc. The DRV-B inlet geometry consists of inlet vanes

that straighten the flow stream equalizing uneven velocity gradients. A cone shaped section in the center of the inlet directs the flow into the vanes and gradually away from the center.

The ring shaped disc provides two fluid paths past the inner and outer seats. Relative to a circular disc of the same size valve, typical of swing checks or axial flow designs such as the DRV-Z, the DRV-B disc is smaller and lighter. The disc face remains perpendicular to the inlet flow direction throughout the full stroke. The DRV-B has a stroke length longer than both the DRV-G and KRV-B. There is no stem in this valve which minimizes the force needed to overcome the high friction typical of center-guided designs. With flow in the reverse direction and the valve fully open, the diffuser shields the disc from drag forces tending to close the valve.

Description of Test

This test was conducted twice, once with the strong spring and again with the weak spring. The initial steady-state velocity prior to introduction of the transient was 6.23 ft/sec with the weak spring and 8.86 ft/sec with the strong spring. Both tests began with the valve fully open. The dynamic characteristic with weak spring was measured up to a maximum deceleration of 27.13 ft//sec^2 corresponding to a backflow of 2.36 ft/sec. A maximum deceleration of 54.23 ft/sec^2 was generated with the strong springs installed, resulting in a maximum backflow of 3.12 ft/sec.

Type: Axial Flow
Manufacturer/Model: Entech/NozzleCheck Model KRV-B
Size: 32" NPS
V_o: 6.56 fps
Orientation: Horizontal
Test Medium: 66 °F Water

Test Loop: Large Bore Loop at Delft Hydraulics
Dynamic Response Curves and Drawing: Figure 8

Description of Valve

A ring shaped disc, short face-to-face, and center disc guide characterizes this axial flow design. The disc has two seating surfaces with flow being divided between inner and outer cavities. The ring shaped disc is connected to the concentric shaft via multiple vanes. In the fully open position, a single shaft/bearing interface carries the weight of the disc. The disc face remains perpendicular to inlet flow at all positions from fully closed to fully open applying maximum fluid force to the valve obturator. In the fully open position, the KRV-B disc area is exposed to maximum fluid drag forces when flow reverses. The stroke length is longer than the 32" DRV-G but shorter than the DRV-B.

A single helical spring is used to increase closure speed in addition to providing added seat load in the closed position. The minimum velocity required to fully open the valve is dependent on the spring design and will typically vary from a minimum of 3 ft/sec.

Description of Test

This testing was commissioned to determine both the resistance coefficient (C_v) and dynamic performance characteristic for a 32", ANSI 150 Model KRV-B. The valve was dynamically tested using a spring configuration related to a Vmin of 6.56 ft/sec with an initial velocity of 7.87 ft/sec. Testing was repeated 11 times varying deceleration from 9.3 ft/sec^2 to 56.13 ft/sec^2. The maximum backflow recorded was 2.0 ft/sec. Valve position was not measured.

Type: Axial Flow
Manufacturer/Model: Entech NozzleCheck Model DRV-G
Size: 32"
V_o -Strong Spring-8.92 fps
V_o -Weak Spring- 6.2 fps
Orientation: Horizontal
Test Medium: 66 °F Water
Test Loop: Large Bore Loop at Delft Hydraulics
Dynamic Response Curves and Drawing: Figure 9

Description of Valve

The model DRV-G is similar to the DRV-B. The main differences are the two piece body and larger flow area of the DRV-G, which results in a higher Cv. There are differences in the shape of inlet and outlet flow passages. As in the DRV-B design, downstream of the disc is a diffuser that shields the disc from drag force in the reverse flow direction when fully open. The DRV-G has the shortest stroke length compared to the DRV-B or KRV-B.

Description of Test

This test was conducted twice, once with the strong spring and again with the weak spring. The initial steady-state velocity prior to introduction of the transient was 8.27 ft/sec with the weak spring and 11.81 ft/sec with the strong spring. Both tests began with the valve nearly full open. The dynamic characteristic with weak spring was measured up to a maximum deceleration of 30.74 ft/sec^2 corresponding to a backflow of 2.59 ft/sec. A maximum deceleration of 51.1 ft/sec^2 was generated with the strong springs installed, resulting in a maximum backflow of 2.52 ft/sec.

Type: Axial Flow
Model: Mokveld Circular Disk- TKZ-E or similar.
Size: 32"
V_o - 6.9 fps
Orientation: Horizontal
Test Medium: Unknown
Test Loop: Unknown, Possibly Large Bore Loop at Delft Hydraulics
Figure 10

Description of Valve

This model uses a center guided, circular disc similar to the model DRV-Z design. The valve has a diffuser that shields the disc from drag forces in the reverse flow direction. The flow testing information comes from Koetzier, Kruisbrink & Lavooij (Ref. 7), which does not provide specific information regarding the exact configuration of valve tested. We have included these curves to illustrate the wide range of results obtainable when comparing axial flow check valves of the same size, but different types.

Type: Swing Check and Duo-Disc
Model: Unknown
Size: Various
V_o -Various
Orientation: Horizontal
Test Medium: Water
Test Loop: Analytically determined based on flow test data
Figures 11 and 12

Dynamic response curves, Figures 11 and 12, are provided using data from Ellis & Mualla (Ref. 8) and are based on numerical modeling used to extend the value of actual test data. The values of v_r as a function of dv / dt are optimistic and should provide the user with pressure surge magnitudes lower than actual. Specific information regarding the configuration of the tested swing check or duo-disc is not provided.

Discussion of Test Results

Test results are different for each type of axial flow check valve tested. An interesting point is the difference between the performance of the DRV-B compared to the DRV-G. Even though their designs seem nearly identical except for the center flange, the resulting reverse velocity is markedly less with the DRV-G resulting in a lower pressure surge. This is likely due to a number of factors related the test method and the valve design. The DRV-G dynamic test was conducted with the valve slightly less than fully open which, provides added drag force on the disc in the reverse direction in addition to a shorter stroke length. The DRV-G has a larger flow and a shorter stroke length than the DRV-B. This provides for faster closure. Both the DRV-G and DRV-B have similar disc geometry and weight.

The most interesting result of the testing is the performance of the model KRV-B. It has the longest stroke and heaviest disc but closes quicker under reverse flow than the DRV-B or DRV-G. The KRV-B also has to overcome the higher friction forces attributed to a heavier disc sliding along a center bushing. The KRV-B spring is slightly stronger than the weak springs used for the DRV-B and DRV-G but not enough to explain the difference in performance. The reason for the exemplary dynamic performance is likely due to the disc design. Since the disc protrudes from the back end of the valve and is fully exposed to the force of the reverse flow the drag force is much higher under reverse flow conditions. As a result the disc closes faster, and results in lower pressure surges than the other models.

Comparing the NozzleCheck flow testing to test results conveyed from (Ref. 7) illustrate a drastic difference in performance. The main difference between the DRV-B, DRV-G and KRV-B compared to the Mokveld design is the disc shape. The Mokveld design uses a disc and diffuser shape similar to the NozzleCheck Model DRV-Z. A circular, center-guided disc is attached to the stem and recessed in a diffuser as illustrated in Figure 10. The weight of this disc is higher than that of a ring style of the same size, there is also a large bearing surface that adds a frictional force component that is much higher than the DRV-B or DRV-G designs. During a reverse flow condition, flow is diverted away from the backside of the disc by the diffuser, similar to the DRV-B and DRV-G. There is effectively no drag force on the disc until it leaves the fully open position.

How to Calculate Pressure Surge Using Dynamic Response Curves

Nomenclature:

Δp = Transient pressure surge (psig)

a = Wave propagation speed (ft/s)

ρ = Fluid density (lb/ft^3)

p_1 = Operating line pressure (psig)

$p_{allowable}$ = Maximum allowable pressure in the line (psig)

v_r = Reverse velocity through the header at the instant of disc closure (ft/s)

g = Gravity (ft/s^2)

$p_{transient}$ = Downstream line pressure at valve closure (psig)

K = Bulk modulus $\left(\frac{\text{lbf}}{\text{ft}^2}\right)$

D = Pipe diameter (ft)

E = Young's modulus of elasticity $\left(\frac{\text{lbf}}{\text{ft}^2}\right)$

e = Pipe wall thickness (ft)

φ = Restraint factor (for simplicity, this parameter is assumed to be equal to 1)

When selecting a check valve for systems susceptible to water hammer the resulting pressure surge due to rapid valve closure should be predicted. Once predicted, it is combined with the line pressure to determine the maximum pressure that will occur during a transient. This resultant maximum pressure should be less that the maximum allowable system pressure to ensure safe operation.

There are two parameters that are required to determine the maximum transient pressure:

a) The deceleration of the flow dv / dt

b) The line pressure p_l

Deceleration, related to check valve dynamic performance, is typically defined as rate of change in velocity with time of the fluid at the check valve outlet. This is measured or calculate from the time velocity begins to decay after a pump trip until the initial check valve closure. This deceleration is nearly constant over the entire period. We calculated an average dv / dt value for each of the testing in (Ref 1,2,3,4.)

In simple systems, deceleration can be readily determined. For complex systems, a computer analysis is needed to determine the fluid deceleration.

There are two methods that can be used for check valve selection or evaluation. Method 1 is used if transient deceleration is known. Method two is used in lieu of having deceleration but requires the engineer to know maximum transient pressure as well as access to dynamic performance curves for the installed valve. The first would be used to select a valve based on the known parameters of the system prior to installing the valve.

Method 1

The resultant pressure surge due to valve closure can be calculated using the Joukowski Formula:

$$\Delta p = \pm \rho a v_r \qquad (1)$$

However, gravity and a unit conversion must be incorporated into the equation to make the units work. For application, the equation becomes:

$$\Delta p = \frac{\pm \rho a v_r}{144 g} \qquad (2)$$

Where:

Δp = Pressure change, surge (psig)

a = Wave propagation speed (ft/s)

ρ = Fluid density (lb/ft^3)

P_l = Operating line pressure (psig)

$p_{allowable}$ = Maximum allowable pressure in the line (psig)

v_r = Reverse velocity of the system (ft/s)

g = Gravity (ft/s^2)

$p_{transient}$ = Downstream line pressure at valve closure (psig)

The following steps can be used to assist in selecting a check valve for a particular system.

1) Determine either analytically or through computer simulation, the deceleration dv / dt, through the subject check valve as a result of a system transient causing the closure of the check valve. This can be calculated assuming no check valve in the line.

2) Determine what the wave propagation speed and fluid density are for the systems

particular media, a and p_f.

To assist with determining wave propagation speed, a, refer to the following basic formula for thin walled pipes:

$$a = \left(\rho \left(\frac{1}{K} + \frac{D}{Ee} \phi \right) \right)^{-1/2} \quad (3)$$

Refer to Figure 13 for reference:

3) Establish the maximum allowable pressure surge for the system based on the piping and component design limitations. Maximum allowable line pressure. $(p_1 + \Delta p) = p_{allowable}$

4) Calculate, using the Joukowski Formula, the maximum allowable reverse velocity of the system (υ_r).

$$v_r = \frac{\Delta p}{a\rho}$$

5) Evaluate check valve performance curves, such as those provided at the end of this report, to determine which meet the systems reverse velocity requirements. Locating the on the y-axis and tracing a horizontal line does this. Then, locate the dv/dt value and trace a vertical line. Any check valve performance curves that intercept the vertical line between the x-axis and the horizontal υ_r line will meet the requirements.

Example 1

In designing a new system, consider there are three pumps operating in parallel, discharging into a common header. A check valve is required immediately after each pump discharge. Assume an ANSI 150# 12" valve is required. The media being pumped is ambient temperature demineralized water, via stainless steel piping. The operating pressure is approximately 100 psig, with maximum allowable system pressure of 200 psig. The calculated deceleration of the system is 40 ft/s^2 during a single pump trip with the remaining two running. The System Engineer is in the process of evaluating the system for possible check valve options. Refer to Figure 13 for the wave propagation value.

Known:

$a = 4150$ ft/s

$\rho = 62.4$ lb/ft^3

$g = 32.2$ ft/s^2

$\Delta p = 100$ psig

(1) Determine maximum allowable υ_r using the Joukowski Formula:

$$v_r = \frac{(100)(144)(32.2)}{(62.4)(4150)}$$

$$v_r = 1.79\, ft/s$$

(2) Evaluate which check valves would meet this reverse velocity requirement based on a deceleration of 40 ft/s^2 during a pump trip. Compare the available dynamic performance curves of potential replacement check valves. Assume that the only check valve models evaluated as potential replacements are 12" DRV-B axial flow valves, standard swing checks and duo-disc valves.

a) Refer to Figure 14 in the reference section of this report. At 40 ft/s^2 the 12" DRV-B has a reverse velocity of approximately 0.9 ft/s with a weak spring and 0.24 ft/s with a strong spring. Both will meet the reverse velocity requirement of this system.

b) Refer to Figure 14 in the reference section of this report. At 40 ft/s^2, the 12" Swing Check Valve has a reverse velocity of approximately 8.8 ft/s. This valve will not meet the reverse velocity requirement.

c) Refer to Figure 14 in the Reference section of his report. At 40 ft/s^2, the 12" Duo-Check Valve has a reverse velocity of approximately 5.2 ft/s. This valve will not meet the reverse velocity requirement.

(3) Based on the system specifications, the calculations performed and the graphical evaluations, the DRV-B Check Valve is the only design suitable for this application.

Method 2

The second method is used when the deceleration of the system associated with a particular transient is not known. The dynamic performance curve of the installed valve and the maximum downstream pressure level during check valve closure must be known. This method allows the user to estimate the system deceleration based on how the installed check valve reacts to rapidly changing conditions compared to results from past dynamic flow testing. Although not as accurate as method 1, this will provide the engineer with a means to evaluate various check valve designs without having to build a hydraulic model of a complicated system. The following steps would be used.

(1) Once again, use the Joukowski Formula to calculate the reverse velocity associated with the installed valve at the subject transient.

(2) Using the performance curve for the installed check valve, the system's dv / dt associated with a specific check valve closure time can be determined. Draw a horizontal line from the v_r value on the y-axis to the point where it intersects the curve. Then, from the intersecting point on the curve, draw a vertical line to the x-axis. This will determine the dv / dt of the system.

(3) Continue with Step 2 of Method 1 described above.

Example 2

A pump discharge, swing check valve in the Low Pressure Safety Injection (LPSI) system (Ref. 10) is causing damage to system components when the pump is tripped. After pump trip, resulting pressure surge is exceeding the design limitation of system components upstream and downstream of the check valve. The Design Engineer is faced with the task of identifying a replacement valve that would prevent these surges from occurring. The existing Swing Check Valve has a diameter of 12". Based on measurements taken, the pressure surge experienced when the pump trips is 174 psig. The maximum allowable pressure surge based on system design is 100 psig

Known:

$a = 4150$ ft/s

$\rho = 62.4$ lb/ft^3

$g = 32.2$ ft/s^2

$\Delta p = 174$ psig

Desired $\Delta p = 100$ psi

$D_i = 12$"

(1) First determine what the reverse velocity is for the existing valve. Use the Joukowski Formula:

$$v_r = \frac{(174)(144)(32.2)}{(62.4)(4150)}$$

$$v_r = 3.12 ft/s$$

(2) The next step is to determine what the reverse velocity should be to achieve the desired pressure surge. Again, use the Joukowski Formula:

$$v_r = \frac{(20)(144)(32.2)}{(62.4)(4150)}$$

$$v_r = 0.36 ft/s$$

(3) Now that the required v_r is known, the next step is to review the performance curve for the installed check valve and determine what is the system's *dv / dt.*

(4) Refer again to Figure 14 provided in the Reference section for the performance curve for a Swing Check Valve. By using $v_r = 3.12 ft/s$ and the curve, it can be determined that the system's *dv / dt* is approximately 21 ft/s^2.

(5) The next step is to determine which check valve will produce the desired reverse velocity of $v_r = 0.36 ft/s$ at the system's *dv / dt* of 21 ft/s^2. Knowing the *dv / dt* of the system, and the size of the desired valve, it is only a matter of reviewing the different check valve curves.

(6) Refer again to Figure 14 for the performance curve for the Duo-Check valve. For a *dv / dt* of 21 ft/s^2, a 12" Duo-Check Valve will produce a reverse velocity of 2.5 ft/s.

(7) Refer again to Figure 14 provided in the Reference section for the performance curve for the DRV-B Check Valve. For a *dv / dt* of 21 ft/s^2, a 12" DRV-B Check Valve will produce a reverse velocity of 0.32 ft/s with a weak spring and 0.26 ft/s with a strong spring.

(8) Based on this evaluation, a 12" DRV-B Check Valve with a weak or strong spring would reduce the pressure surge to acceptable levels.

Conclusion

This extensive testing completed on the DRV-B, KRV-B and DRV-G axial flow designs should offer the Design Engineer a valuable tool when exploring methods to mitigate the adverse affects of pressure surge. It is apparent that dynamic performance curves as stand-alone documents, without a detailed description of both the valve and test methodology, tell only half the story. Within the family of axial flow check valves there are an assortment of designs available that offer various advantages to the end user. With regard to dynamic performance, each design reacts differently to rapid deceleration of fluid and produces pressure waves of varying magnitudes. Hopefully the information within this paper can be used as a tool to select the most economical design to mitigate pressure surge and improve the accuracy of system hydraulic analysis.

References

1. A.C.H Kruisbrink, Mannesmann Demag-High Dynamic Check Valve type KRV-B, size 800mm, Investigation into Dynamic Behavior, Delft Hydraulics, February 1998.

2. A.C.H Kruisbrink, Mannesmann Demag Nozzle Check Valve-DRV-B 32", Investigation into Dynamic Behavior, Delft Hydraulics, February 1986.

3. A.C.H Kruisbrink, Mannesmann Demag Nozzle Check Valve DRV-G NW 800, Investigation into Dynamic Behavior, Delft Hydraulics, February 1986

4. D.J. van Putten, Mannesmann Demag nozzle check valve-DRV-B 300/ANSI 300, Investigation into Dynamic Behavior, Delft Hydraulics, September 1982.

5. A.C.H Kruisbrink, Mannesmann Demag Nozzle Check Valve DN 600 Type DRV-B PN 10, Test Report, Delft Hydraulics, January 1999.

6. H.D Perko, *Check Valve Dynamics in Pressure Transient Analysis*, 5th International Conference on Pressure Surges, Hannover, F.R. Germany, 22-24 September 1986.

7. H. Koetzier, A.C.H Kruisbrink & C.S.W. Lavooij, *Dynamic Behavior of Large Non-Return Valves*, 5th International Conference on Pressure Surges, Hannover, F.R. Germany, 22-24 September 1986.

8. J. Ellis & W. Mualla, *Selection of Check Valves*, 5th International Conference on Pressure Surges, Hannover, F.R. Germany, 22-24 September, 1986.

9. Enertech RHR Water Hammer Testing Report, 1995.

10. Dr. B. Hannah, J. Sponsel, R. Gormley, M. Kostelnik, *Detailed Performance Comparisons Between Swing Type and In-Line Nozzle Check Valves to MitigateWaterhammer Effects,* EPRI Valve Technology Symposium, August 14-16, 2001.

11. A.R.D. Thorley, Fluid Transients in Pipeline Systems, D&L George LTD, 1991.

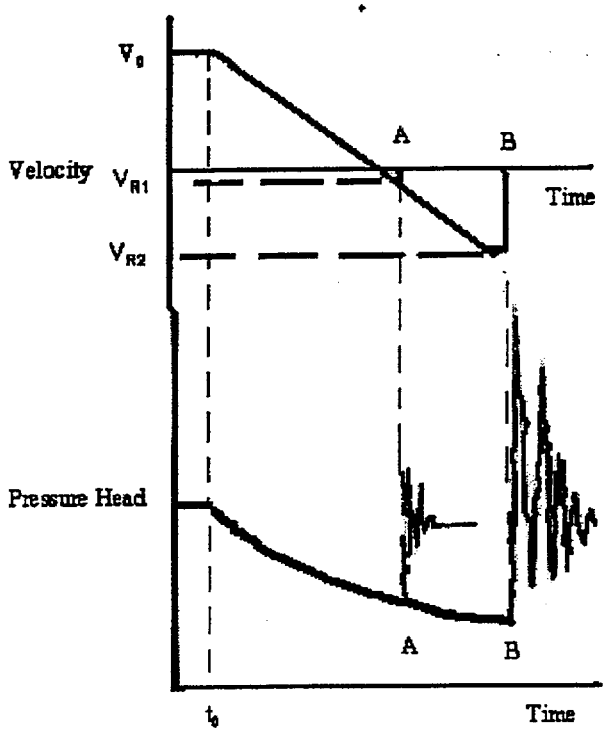

Velocity and Pressure History after a pump trip, downstream of the discharge check valve. The "A" check valve closes faster, with a lower V_{R1}, and much smaller pressure rise. The "B" check valve closer slower, with a higher V_{R2}, resulting in a higher pressure rise.

Figure 1

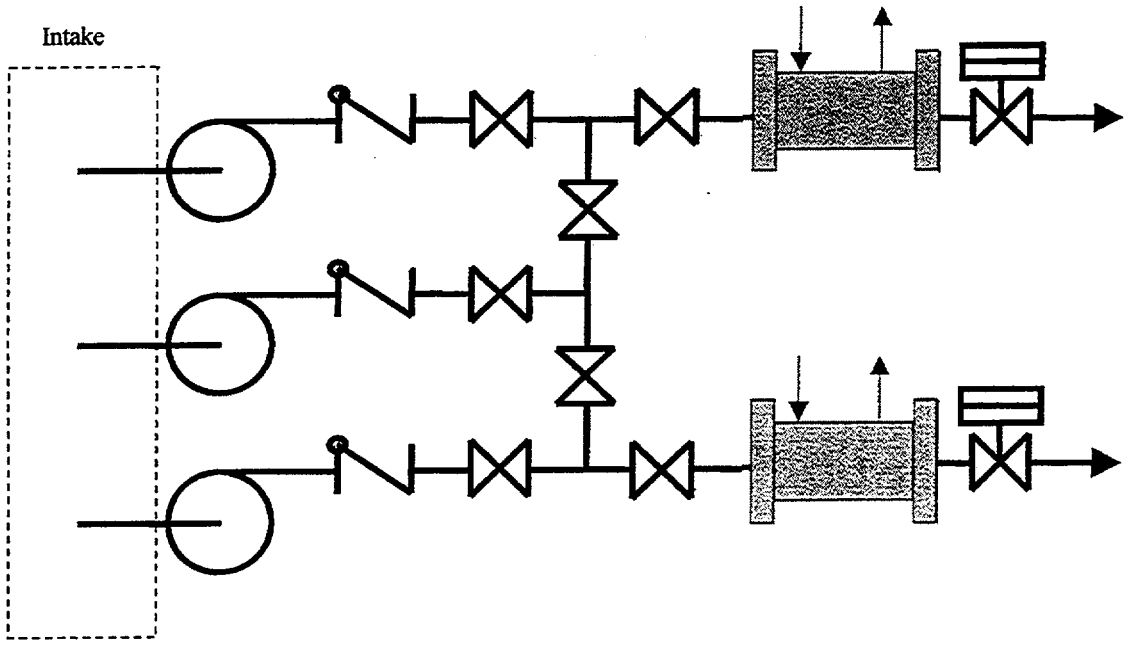

Figure 2. Typical Parallel Pump Cooling System

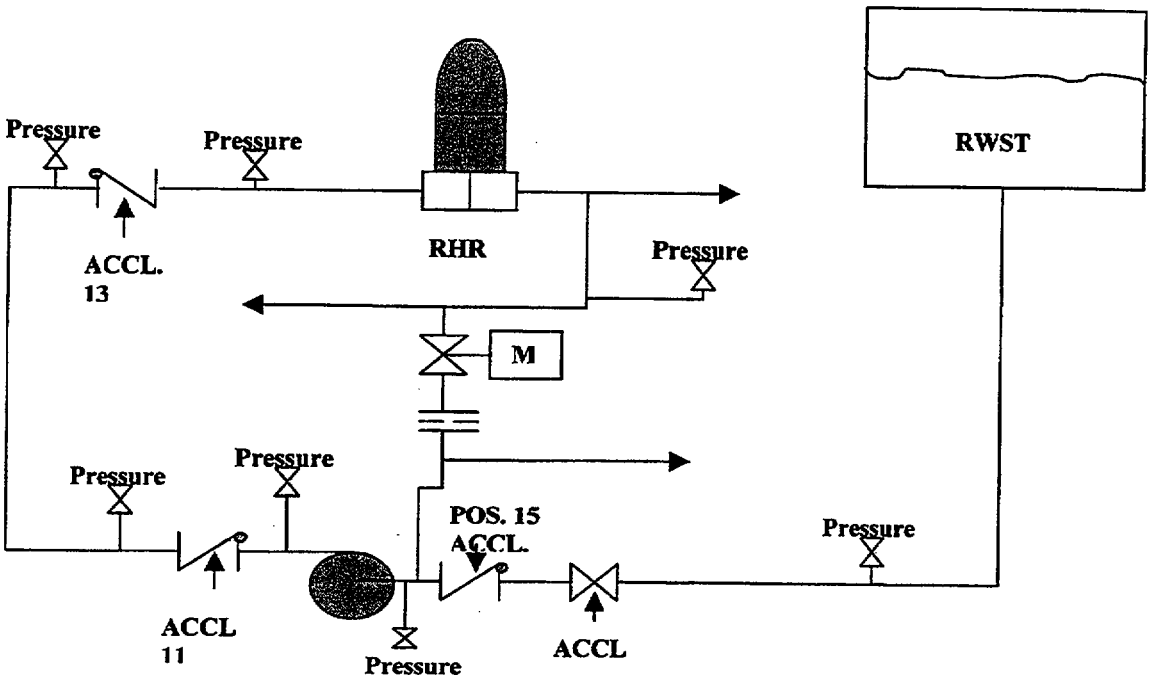

Figure 3. RHR Waterhammer Test Instrument

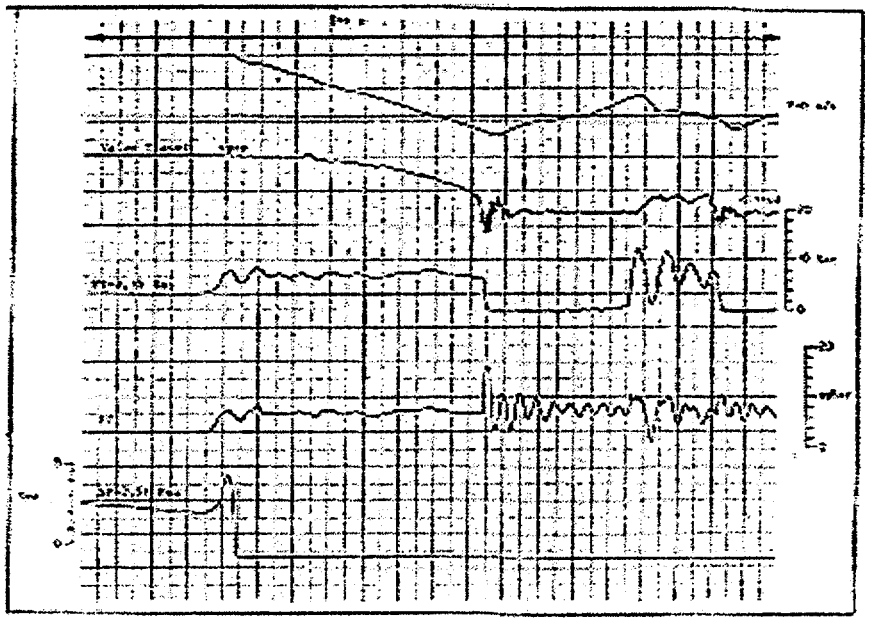

Figure 4. Recording of Dynamic Test Data for Axial Flow Check Valve

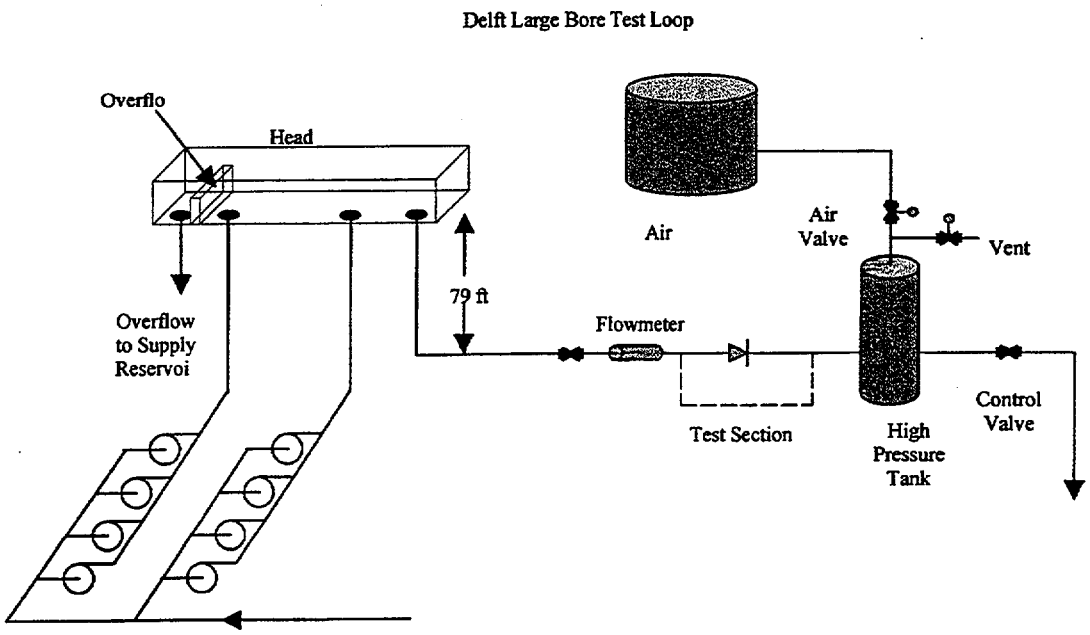

Figure 5

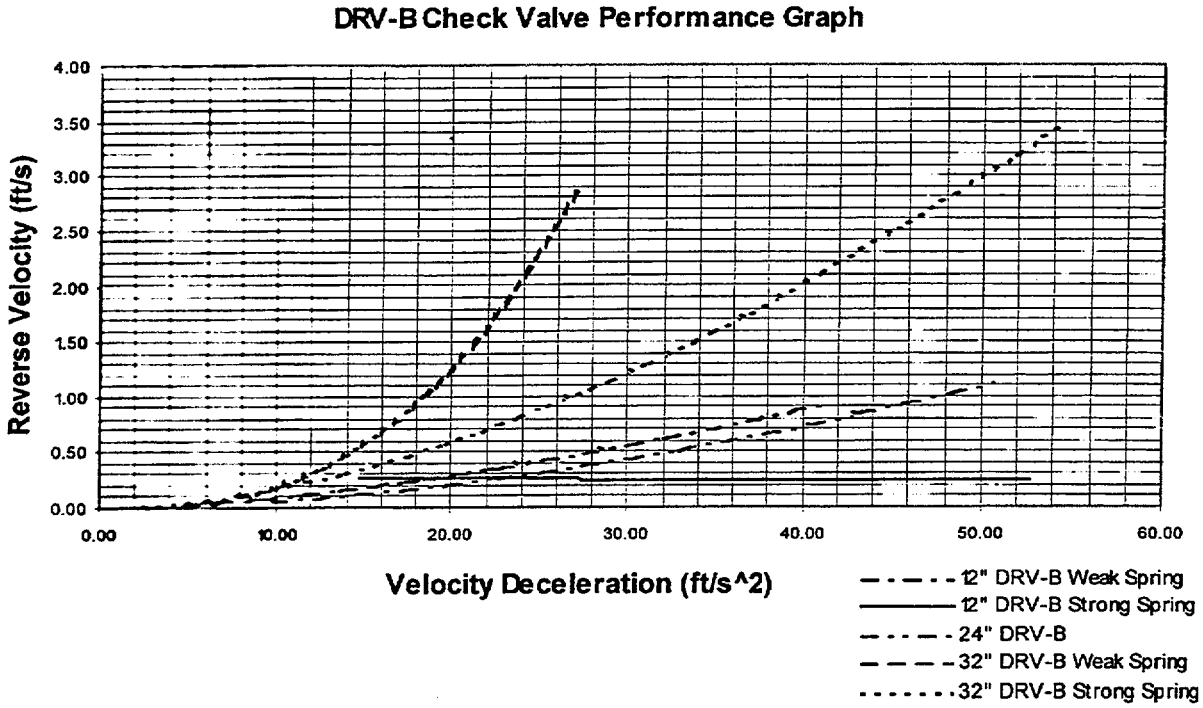

Figure 6

Type: NozzleCheck
Manufacturer/Model: Entech/NozzleCheck Model DRV-B
Size: 32" NPS
V_o -Strong Spring- 8.81 fps
V_o -Weak Spring- 6.1 fps
Orientation: Horizontal
Test Medium: 66 °F Water
Test Loop: Large Bore Loop at Delft Hydraulics

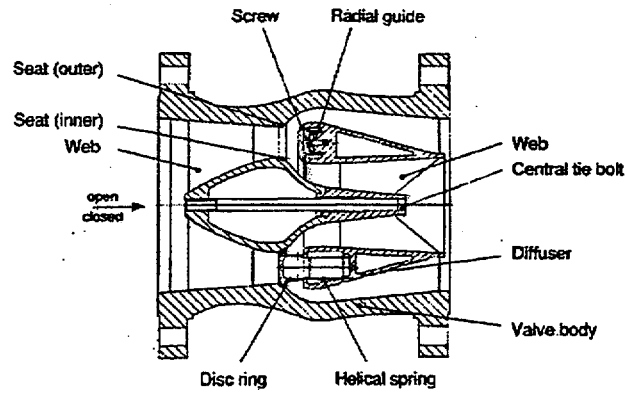

DRV-B Performance Graph for Weak and Str

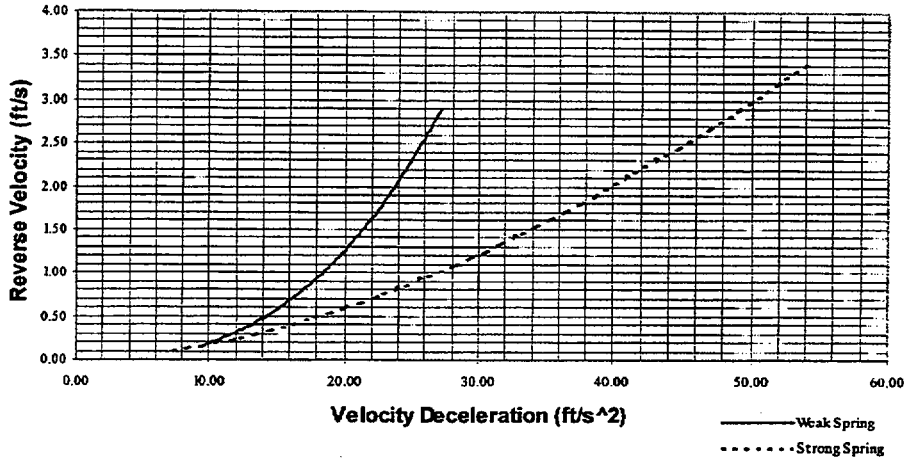

Figure 7

Type: Axial Flow
Manufacturer/Model: Entech/NozzleCheck Model KRV-B
Size: 32" NPS
V_o: 6.56 fps
Orientation: Horizontal
Test Medium: 66 °F Water
Test Loop: Large Bore Loop at Delft Hydraulics

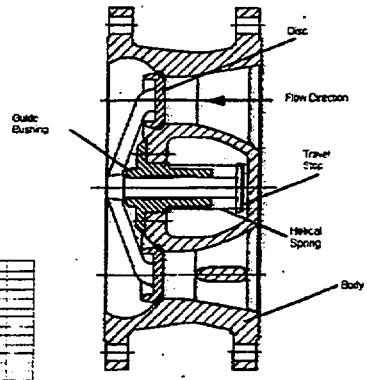

32" KRV-B Performance Graph

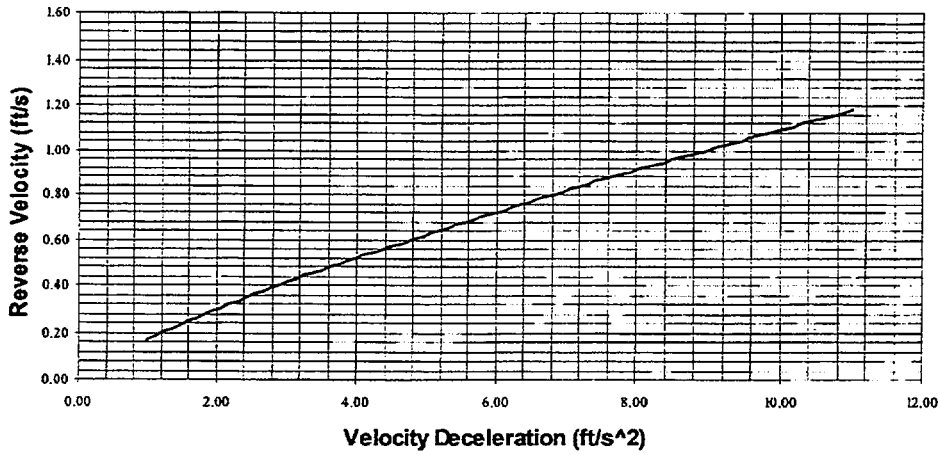

Figure 8

Type: Axial Flow
Manufacturer/Model: Entech NozzleCheck Model DRV-G
Size: 32" NPS
V_o -Strong Spring-8.92 fps
V_o -Weak Spring- 6.2 fps
Orientation: Horizontal
Test Medium: 66 °F Water
Test Loop: Large Bore Loop at Delft Hydraulics

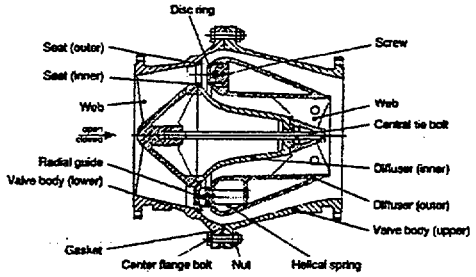

32" DRV-G Performance Graph for Weak and Strong Springs

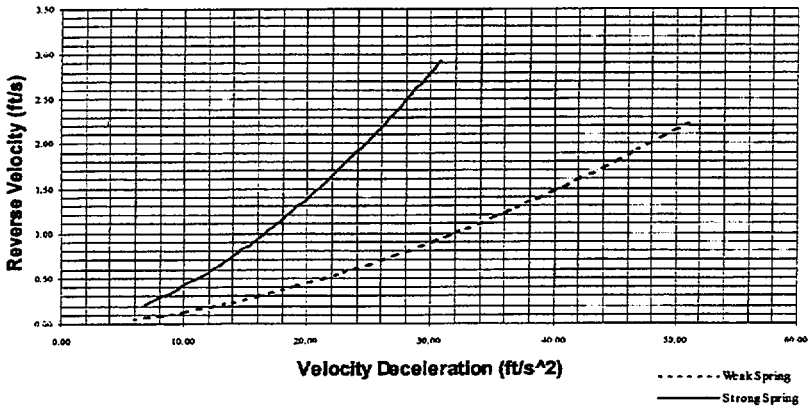

Figure 9

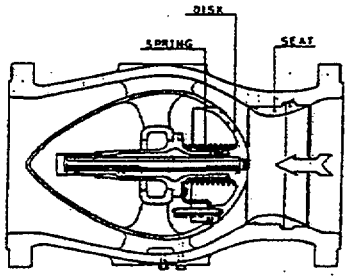

Type: Axial Flow
Model: Mokveld Circular Disk- TKZ-E or similar.
Size: 32" NPS
V_o - 6.9 fps
Orientation: Horizontal
Test Medium: Unknown
Test Loop: Unknown, Possibly Large Bore Loop at Delft Hydraulics

32" Mokveld Performance Graph

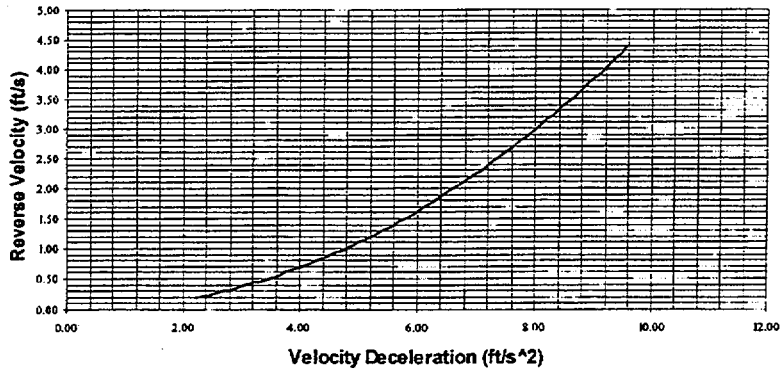

Figure 10

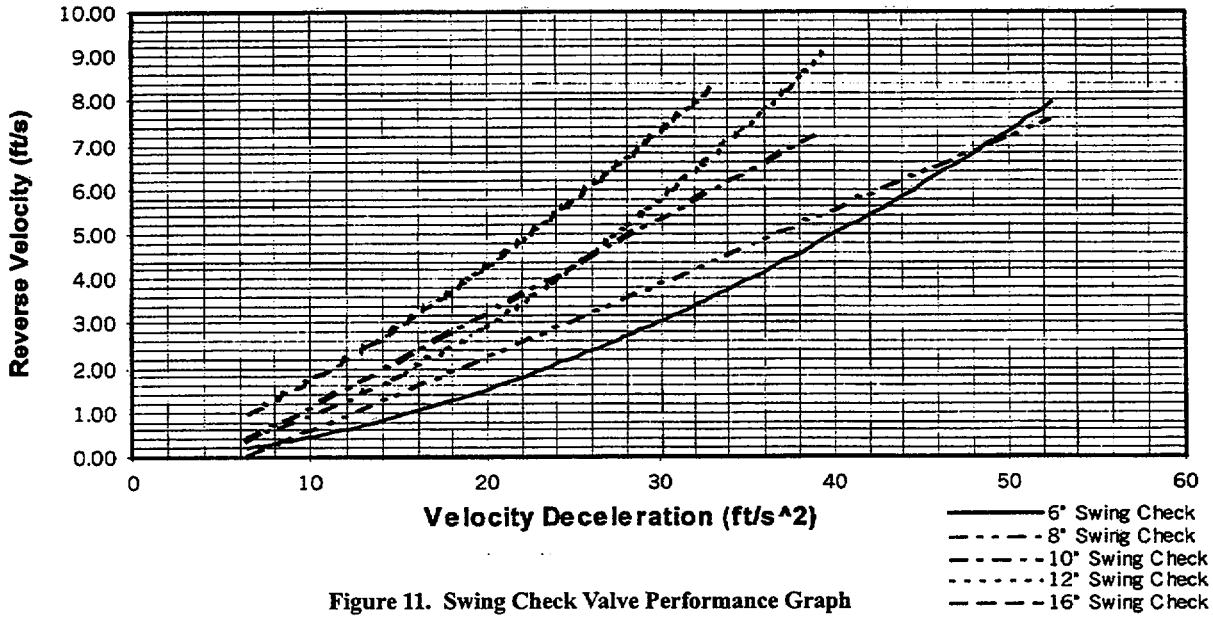

Figure 11. Swing Check Valve Performance Graph

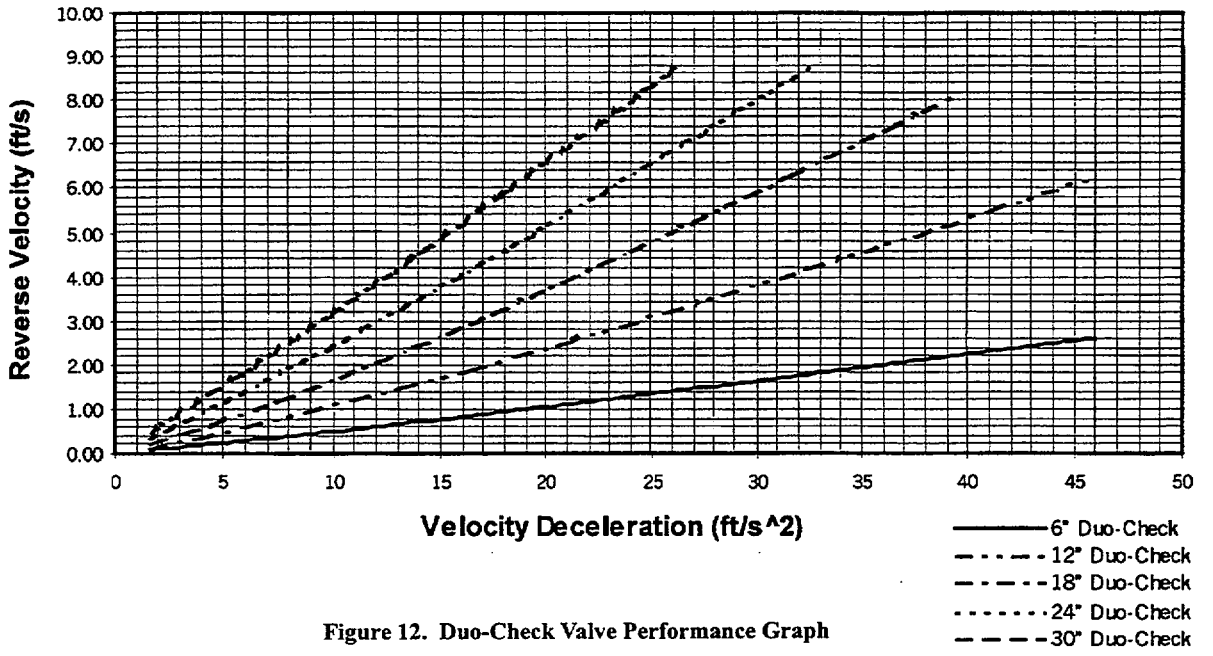

Figure 12. Duo-Check Valve Performance Graph

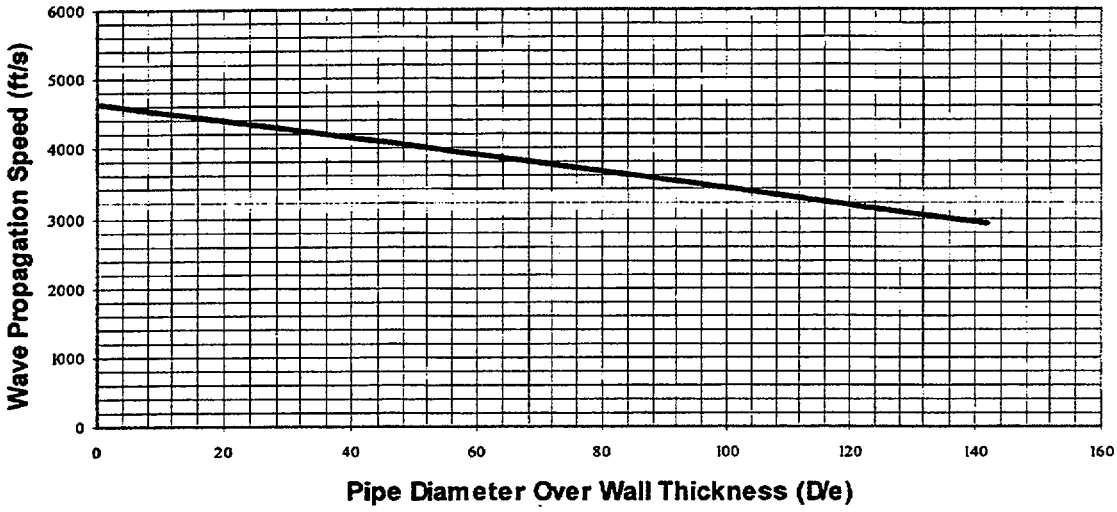

Figure 13. Wave Propagation Speed for Water in Stainless Steel Pipe

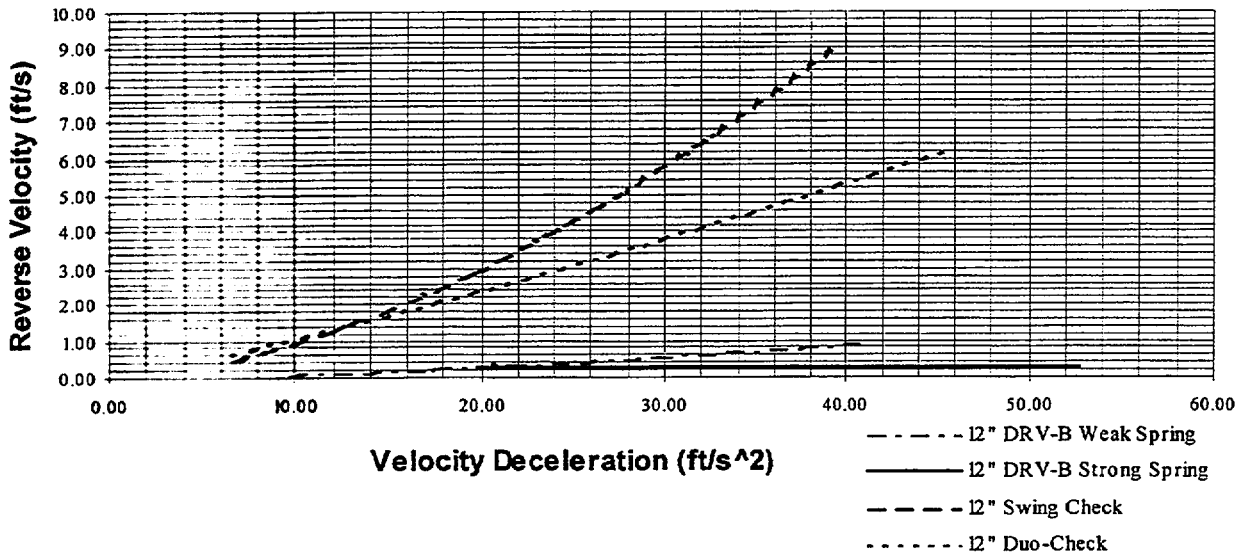

Figure 14. Overlap of Performance Curves for Multiple Check Valve Types

Session 2(b)

Motor-Operated Valves II

Session Chair

Artin Dermenjian
Sargent & Lundy Corporation

The Joint Owners' Group Program on MOV Periodic Verification

Tim Chan, TVA
Robert Doyle, Arizona Public Service
Chad Smith, Duke Energy
Glenn Warren, Southern Nuclear Operating Co.
Paul Damerell, MPR Associates
Todd Spears, MPR Associates

Abstract

To address long-term motor operated valve (MOV) performance, the Babcock & Wilcox, Boiling Water Reactor, Combustion Engineering and Westinghouse Owners' Groups (B&WOG, BWROG, CEOG and WOG) teamed in 1997 to form the Joint Owners' Group (JOG) MOV Periodic Verification (PV) Program. This program is nearing completion, with 98 of the 103 operating U.S. reactor units participating. The goal of the program is to provide a justified approach for periodically testing MOVs, that addresses potential degradation. The program defines an interim approach that specifies periodic tests without flow and differential pressure (DP), at a frequency determined by the MOV's risk significance and margin. To justify this approach, each participating plant is also DP testing 2 valves per unit. Each valve is tested three times over five years, with at least one year between tests. The data are evaluated jointly to confirm or adjust the initial guidance. The majority of the tests are complete and conclusions are coming into focus.

For gate valves, when the valve factor is initially low, increases can occur between one test and a later test. One common way that the valve factor becomes low is disassembling and reassembling the valve. The data show that, following valve disassembly and reassembly, the valve factor tends to be reduced, and it tends to increase in subsequent service. Outside of the valves disassembled and reassembled, some gate valves have low valve factors apparently because the valves are not stroked under DP conditions in service.

For butterfly valves, there have been no observations of degradation in bearing friction coefficient. A few valves with bronze bearings in raw (untreated) water service have shown significant variations in friction, but they tend to be a mixture of increases and decreases with no pattern of degradation.

Globe valves, both unbalanced and balanced, tend to show a constant valve factor with no indication of degradation.

Keywords: periodic verification motor operated valve degradation

Background

Ninety-five percent of the nuclear power plants in the U.S. are participating in the Joint Owners' Group (JOG) motor operated valve (MOV) Periodic Verification (PV)

Program. A previous paper (Reference 1) described the technical bases, content and approach of the JOG PV Program. Briefly, the program helps U.S. nuclear power plants address long-term MOV performance and periodic verification, to satisfy NRC Generic Letter 96-05. All four of the U.S. nuclear plant Owners' Groups (Boiling Water Reactor, Combustion Engineering, Westinghouse and Babcock & Wilcox Owners' Groups) are included. This united approach has key benefits for the participating plants and for the regulator. Importantly, it conserves resources. Cost effectiveness is achieved by sharing the burden of valve testing among the participating plants. Also, because the program provides a uniform approach for all participating plants, the regulator's burden to individually inspect and approve multiple programs is alleviated. Accordingly, the plants can operate under a predictable regulatory expectation with high certainty of acceptance. Finally, because the program has 98 participating units, an extensive set of MOV test data is being generated, collected and evaluated. These data, which are far more extensive than any single plant could expect to generate, provide the basis for a strong technical justification.

As mentioned above, a key element of the JOG PV Program is MOV testing at the participating plants. This testing is performed under conditions with flow and differential pressure (DP). Each participating unit is testing two valves under DP conditions. Each valve is tested three times over a spread of five years, with at least a one-year separation between tests. The test valves were selected so that, in aggregate, they cover the valve features and system conditions most commonly encountered in nuclear power plants.

Two previous papers (References 2 and 3) described the early experience with in-plant valve testing and showed results from early tests. Most of the test results in the first paper (Reference 2) were from the first (baseline) test of the planned three-test series. Accordingly, the insights on potential valve degradation were limited. In the more recent paper (Reference 3), some information from repeat tests was presented, and preliminary insights from these tests were discussed. At the time the present paper was prepared, the amount of data has increased considerably, and there are now an appreciable number of tests covering the second and third tests in the series. The purpose of this paper is to update the test results and insights gained in the program from these data.

In-Plant DP Testing

The DP test program includes 197 valves, subdivided into 149 gate valves, 28 butterfly valves, 12 unbalanced disk globe valves, and 8 balanced disk globe valves. Each valve is tested three times under nominally identical DP conditions. Consecutive tests are separated by at least one year.

To ensure that data obtained from in-plant tests are satisfactory for use in the JOG PV Program, a test specification is used, which includes requirements for:

- Test valve maintenance and material conditions
- Test conditions
- Test instrumentation
- Test sequence
- Test data evaluation
- Test documentation

The goal of the standard test specification is to ensure that all valves and testing are properly controlled to achieve adequate consistency

and quality from test results obtained from multiple plants. Importantly, the test specification requires that time-history data for stem thrust (or torque for butterfly valves) and DP be obtained. Further, the specification requires analyzing and summarizing the data in a prescribed manner. Finally, the specification requires a test sequence which includes both static and DP test strokes.

At the time this paper was prepared, about 440 test data packages had been submitted by the participating plants to the JOG Program, and about 355 of those packages had been reviewed and accepted. In general the experience with testing has been positive, and the data packages have provided a good source of information. In a few tests (baseline and subsequent) the instrumentation or test conditions have failed to meet the specification, and test data were rejected. At this time, the rejection rate of data submitted to the program is about 7%. The discussions below cover all of the data from valves that have repeat tests accepted into the program, which is about 60% of the valves.

Gate Valve Test Results

Each gate valve DP test is evaluated in a consistent manner so that the data from different valves can be meaningfully compared. During this evaluation, several key "stroke points" are identified, and the "valve factor" is calculated for each of these stroke points. Valve factor is defined as the ratio of the thrust required to move the valve disk (or "DP thrust") to the product of DP and the area based on the mean seat diameter ($Area_{ms}$).

$$Valve\ Factor = \frac{DP\ Thrust}{DP * Area_{ms}}$$

The stroke points identified and evaluated in gate valve tests include:

Closing Strokes

- Flow isolation
- Initial wedging
- Initial wedging – second point (if applicable)
- Maximum thrust up to the initial wedging point

Opening Strokes

- Just after unwedging
- Maximum thrust after unwedging
- Flow initiation

The gate valve results are analyzed to evaluate both disk-to-seat sliding and guide slot-to-rail sliding, by examining results from different portions of the strokes. After the subdivision, the data are further broken down to examine different materials pairs, fluid conditions and extent of valve stroking. Other factors, such as stem orientation, normal valve position, etc., can also be examined, but so far have not been found to be important.

One factor that is highly important is whether or not the valve was disassembled before the baseline tests, and data are typically segregated according to this criterion. Specifically, the test results from numerous gate valves show that when a gate valve is disassembled and reassembled, the valve factor tends to be reduced, and can then increase in subsequent service.

Figures 1 and 2 show two sets of results from similar types of gate valves. Both graphs show results from valves with Stellite disk

and seat faces, in systems with treated water less than 120°F, and that stroke under DP conditions from one to four times between tests. The results on these graphs cover disk-to-seat sliding.

On these graphs the terms B1 and B2 refer to the first and second DP closing strokes of the baseline tests; S1 and S2 refer to the first and second strokes of the second test; T1 and T2 refer to the first and second strokes of the third test. For each test (B, S and T), the DP strokes are typically preceded by a stroke without flow or DP. Recall that there is at least one year between B and S tests, and between S and T tests. Although Figures 1 and 2 cover closing strokes at the initial wedging stroke point, similar behavior is observed in the opening direction and at other stroke points. A heavy line on each figure shows the average valve factor in the first stroke of the baseline test and the first stroke of the second test. The change in this average (increase or decrease) reflects the overall behavior of the group. The third test results have not yet been included in the average because of the small amount of data. Each valve is identified by a program-unique number adjacent to the data curve (e.g., GXX.XX).

The first graph shows results for valves that were not disassembled before their baseline tests, and the second graph shows results for valves that were disassembled prior to their baseline tests. When the valves are not disassembled (Figure 1), the valve factors show some increases from low initial values and some decreases from high initial values, but overall are stable as reflected in the flat line displaying the average values. When the valves are disassembled (Figure 2), most of the baseline test valve factors are lower and there is an increasing trend in valve factor, with the lowest valve factors showing the largest increases. The positive slope of the average line shows the increasing trend. There is one exception in Figure 2 (valve G69.08) which is discussed below.

The results in Figures 1 and 2 are not surprising. Although significant data have not been published, plant personnel who work routinely with motor-operated gate valves have reported for many years that valve factors tend to be reduced following disassembly and reassembly of the valve. Most often this is first observed as a reduction in the valve's unwedging load. Others have also observed that low valve factors can tend to rise as the valve is stroked. For example, in the EPRI MOV program (Reference 4), valves that had not been previously DP stroked were observed to typically have low valve factors (~ 0.2), which increased as the valves were "preconditioned" (stroked under DP conditions). This behavior helps to explain the one valve with different behavior (G69.08) on Figure 2. Instead of testing the valve immediately after reassembly, valve G69.08 was stroked several times under DP conditions before its baseline test was performed. This stroking increased the valve factor, as reflected by the baseline test results.

Although the JOG program testing is not complete, results from several gate valves have confirmed the observations summarized above. These observations have been communicated to the program participants. The importance to individual plants is that when a gate valve is disassembled and reassembled, a test conducted afterward is likely to show a lower valve factor which may increase in service. Therefore, other information (e.g., pre-disassembly tests or tests of other similar valves) should be considered to justify the setup of the valve.

Although disk-to-seat sliding results can be subdivided according to different materials,

fluid conditions and stroking histories, all tend to show the dominant effect of disassembly/ reassembly discussed above.

- Figures 3 and 4 show results for valves with non-Stellite disk-to-seat materials, and Stellite-faced valves in raw water service, respectively. All of the test results are from water systems less than 120°F. Also all of the test data are from valves that were not disassembled, with one exception. The exception is the data labeled G92.01 on Figure 3. Because this (non-Stellite) valve shows a stable valve factor with no apparent impact of the disassembly, we have left it grouped with the other data on Figure 3. Although a mixture of valve factor increases and decreases are observed, increases tend to occur on valves with lower initial valve factors, and decreases occur on valves with higher initial valve factors. The largest increase occurs on one of the non-Stellite valves (G89.03) that started at a low valve factor. The higher valve factor in its second test is still below other typical valves. There is no average line on Figure 3 because these data cover several material combinations. The average line in Figure 4 shows that the average valve factor decreases slightly.

- Figures 5 and 6 show results from Stellite-faced valves in hot water (>120°F) or steam service. The first graph covers valves that were not disassembled and the second graph covers valves that were disassembled. Trends similar to those discussed previously are evident. The flat average line on Figure 5 shows that, as a group, the valve factor is not changing. One valve (G79.02) that appears to be an exception on Figure 5 was carefully evaluated. The evaluation showed that the increase on Figure 5 was the result of changes in measurements affected by actuator maintenance between the baseline and second tests, and not valve degradation.

- Figures 7 (valves not disassembled) and 8 (valves disassembled) show results from Stellite-faced valves in treated water service (<120°F), that are not DP-stroked except during these tests. Similar trends to the other results are observed. Specifically, the flat average line in Figure 7 shows that, as a group, the valve factor is not changing. However, the valve factor increases for the disassembled valves (Figure 8) tend to be not as large as other groups (e.g., Figures 2, 6 or 10). Apparently, the absence of DP stroking mitigates the valve factor increase for these valves.

- Figures 9 (valves not disassembled) and 10 (valves disassembled) show results from Stellite-faced valves in treated water service (<120°F), that are DP-stroked routinely (>4 times/year). The average line in Figure 9 is drawn out to the third test because there is a similar amount of data to the other tests. As can be seen, the valve factor is stable. The rises in valve factor from the baseline tests in disassembled valves (Figure 10) are sharper than in other data (e.g., Figure 8), indicating that the DP stroking contributes to this effect.

The trend of the data suggests that the most significant influence on potential increases in valve factor is the current value of the valve factor. Hence, a correlation between these parameters would be expected. Figure 11 shows all of the gate valve data for disk-to-seat sliding (self-mated Stellite; treated water <120°F) plotted in these terms. The y-axis is the observed change in value from one JOG test to the next one. The x-axis is the

"starting" value of valve factor. A correlation with a negative slope is clearly evident. Valves that show increases in valve factor tend to be those with low valve factors; valves with high valve factors tend not to show increases.

With regard to guide slot-to-rail sliding, Figures 12 and 13 show results for stainless steel and Stellite guides, respectively. Most of the data show stable valve factors. A couple of valves in Figure 12 show increases between the baseline and second tests. These valves were disassembled prior to their baseline tests indicating that disassembly and reassembly may affect guide friction similar to disk-to-seat friction.

Butterfly Valve Test Results

Butterfly valve tests results are evaluated to determine the bearing friction coefficient, which is proportional to the bearing torque component. Although other torque components affect the total required torque, the other components have been judged not to be susceptible to degradation (hydrodynamic torque) or are capable of being evaluated during normal static, or zero DP, testing (seat torque). Bearing torque is determined by examining the differences in required torque between static and DP test strokes.

Figures 14 and 15 show bearing friction coefficient results from butterfly valves with bronze bearings in treated water systems and raw water systems, respectively. All of the valves are tested near room temperature (<100° F). For the valves in treated water systems, the bearing friction coefficient tends to remain nearly constant or decrease (comparing first stroke to first stroke). For valves in raw water service, considerably more variation is observed, but there is no increasing or decreasing trend. Figure 16 shows results for valves with non-bronze bearings, in both treated and raw water systems. The bearings are typically composite materials. These valves show stable or decreasing bearing friction coefficients.

Balanced Disk Globe Valve Test Results

Balanced disk globe valves tend to exhibit low values of DP thrust, due to their design. Test results from the JOG PV Program have verified this expectation. The required thrust tends to be dominated by packing thrust and stem rejection load; the DP component is minor. The DP load in a balanced disk globe valve is attributed to the small amount of pressure imbalance present in the disk and to friction between the disk and its cage. Only the second of these mechanisms is susceptible to degradation.

Figure 17 shows the valve factor at unseating (opening stroke) for balanced disk globe valves. Two of the three highest curves (BG05.1 and BG07.1) are valves with an area imbalance that tends to make them self-closing. Hence, they show higher opening valve factors but do not have a positive required DP thrust in the closing direction. The third valve with a higher valve factor is affected by a non-uniform packing load that distorts the valve factor calculation (both opening and closing). As more data are obtained for this valve, we will attempt to correct this effect.

As shown in Figure 17, very little apparent degradation has occurred in the valves tested to date. Typically the valve factor remains constant, although minor changes have been observed. These changes are typically less than the uncertainty of the measurements. The decrease for BG06.1 was due to the disappearance of a small disk unwedging thrust in the second test series.

Unbalanced Disk Globe Valve Test Results

As part of the original basis of the program (Reference 1), no degradation mechanisms were identified for unbalanced disk globe valves. Repetitive tests of several unbalanced disk globe valves have been included in the JOG PV Program to confirm that the required thrust does not change while the valve is in service. Repeat tests from some of those globe valves have now been obtained. The results are shown in Figure 18. All of these results are from globe valves in water systems near room temperature (<100° F). As expected, the valve factor remains nearly constant throughout the tests.

Summary

1. The JOG PV Program is being used by the vast majority of U.S. nuclear power plants to implement their periodic verification testing and to determine the potential degradation in required thrust or torque for gate, globe and butterfly valves.

2. A key component of the JOG PV Program is in-plant valve testing. The testing is well under way, and an appreciable amount of data from repeat (second and third) tests have been obtained.

3. Gate valves that are disassembled and then reassembled tend to exhibit a reduced valve factor when they are tested after reassembly. The valve factor can subsequently increase while the valve is in service.

4. Some gate valves have low valve factors because they have not been stroked against DP conditions in their normal service. The valve factor can increase to an average value in successive DP tests, apparently due to the DP stroking.

5. Butterfly valves with non-bronze bearings or with bronze bearings in treated water systems tend to show a stable or decreasing bearing friction coefficient when they are repeat-tested, showing no degradation.

6. Butterfly valves with bronze bearings in untreated water systems show variations (increases and decreases) in bearing friction coefficient, but there is no trend of degradation.

7. Balanced disk globe valves exhibit low valve factors and low changes in valve factor. There is no degradation in required thrust.

8. Unbalanced disk globe valves exhibit stable valve factors, as expected. Repeat tests indicate that the valve factor remains nearly constant.

References

1. Warren, G., S. Loehlein, F. Winter and P. Damerell, *The Joint Owners' Group Program for Motor-Operated Valve Periodic Verification,* Proceedings of the Fifth NRC/ASME Symposium on Valve and Pump Testing, NUREG/CP-0152, Vol. 2, pp. 3A-23 to 3A-45 (1998).

2. Bunte, B., S. Loehlein, F. Winter, and P. Damerell, *Early Results from the Joint Owners' Group MOV Periodic Verification Program,* EPRI/NMAC Seventh Valve Technology Symposium, Incline Village, NV: May 26-28, 1999.

3. Bunte, B., S. Loehlein, C. Smith, and R. Doyle, *The Joint Owners' Group MOV*

Periodic Verification Program – Forging Ahead with Testing Learning, Proceedings of the Sixth NRC/ASME Symposium on Valve and Pump Testing, NUREG/CP-0152, Vol. 3, pp. 2B-85 to 2B-101.

4. Harrison, D., P. Damerell, J. K. Wang, M. Kalsi, and K. Wolfe, *Gate Valve Performance Prediction,* Third NRC/ASME Symposium on Valve and Pump Testing, NUREG/CP-0137, pp. 371-389.

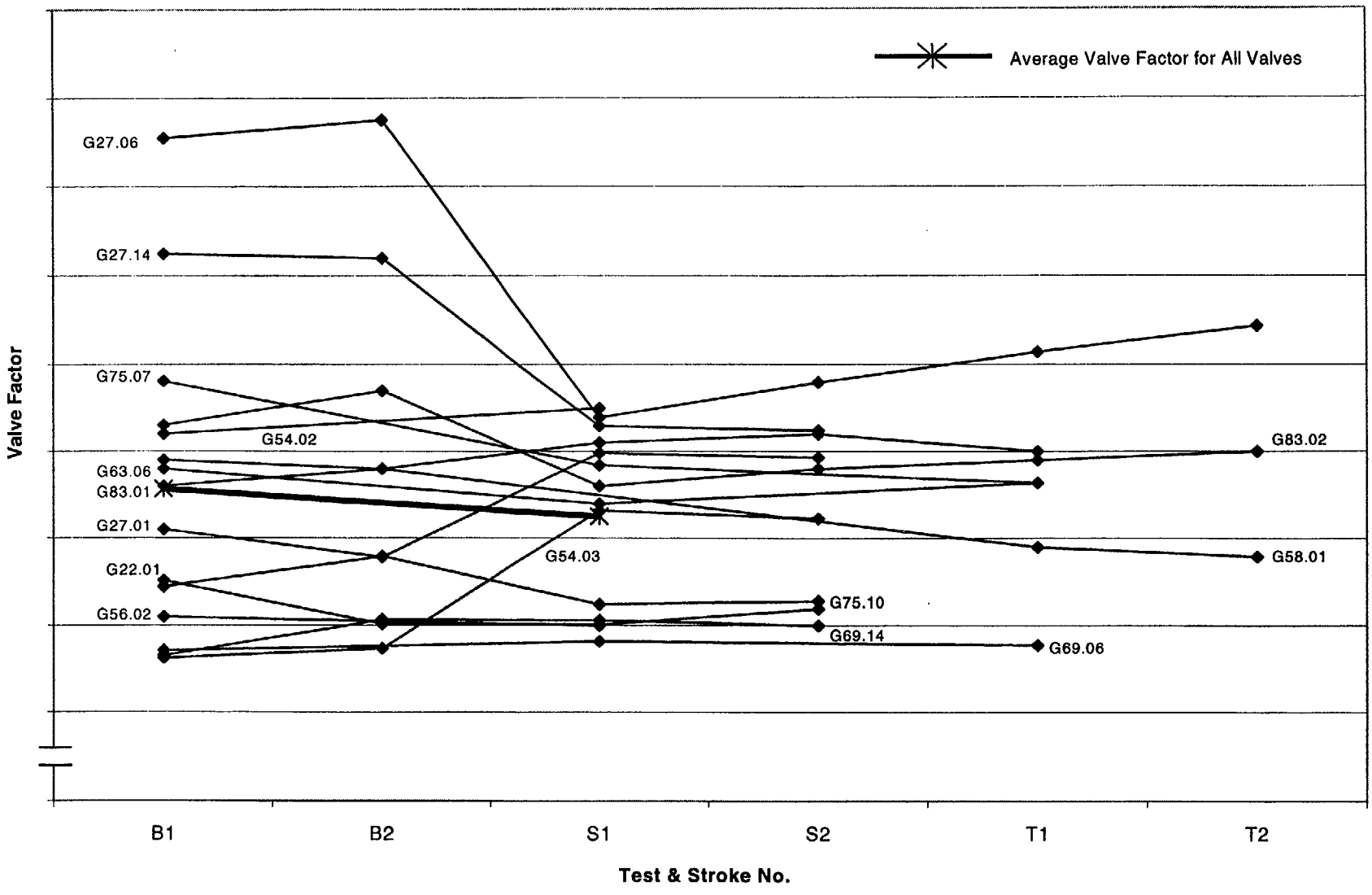

Figure 1. **Progression of Closing Valve Factor at Initial Wedging for Gate Valves in Treated Water Systems with 1 to 4 DP Strokes Between Tests (valves not disassembled).**

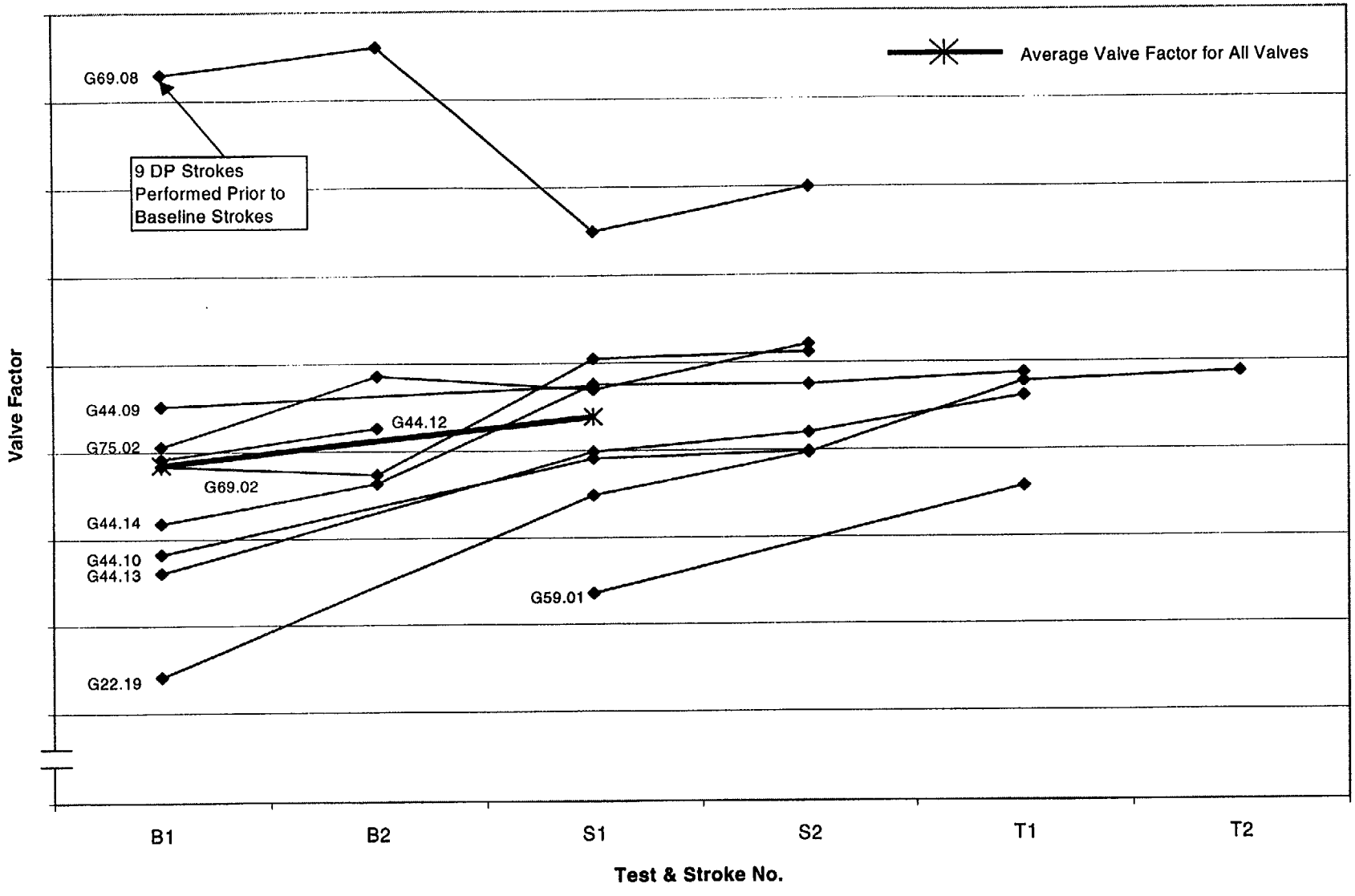

Figure 2. Progression of Closing Valve Factor at Initial Wedging for Gate Valves in Treated Water Systems with 1 to 4 DP Strokes Between Tests (valves disassembled and reassembled before baseline test).

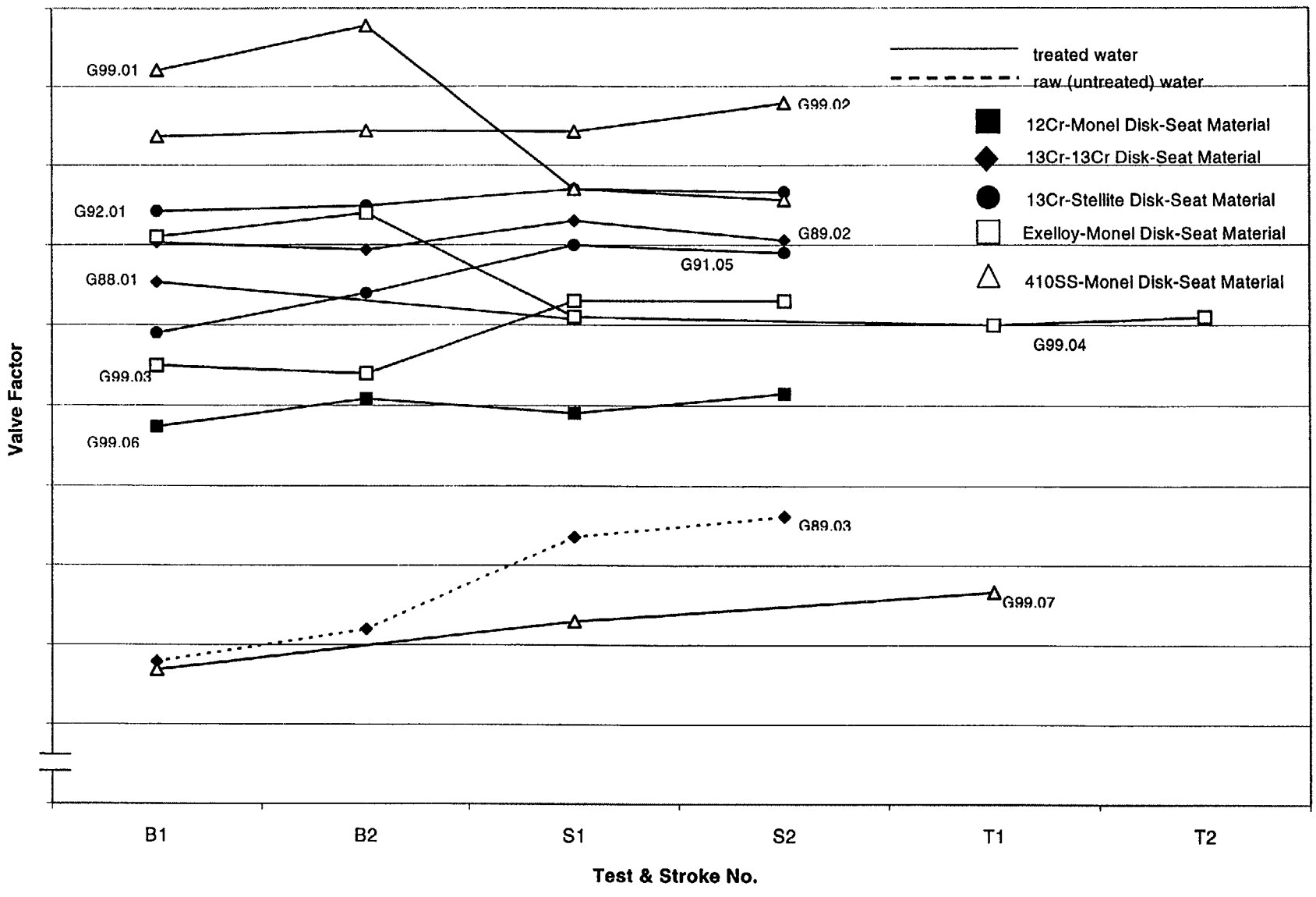

Figure 3. Progression of Closing Valve Factor at Initial Wedging for Gate Valves with Non-Stellite Disk and Seat Materials.

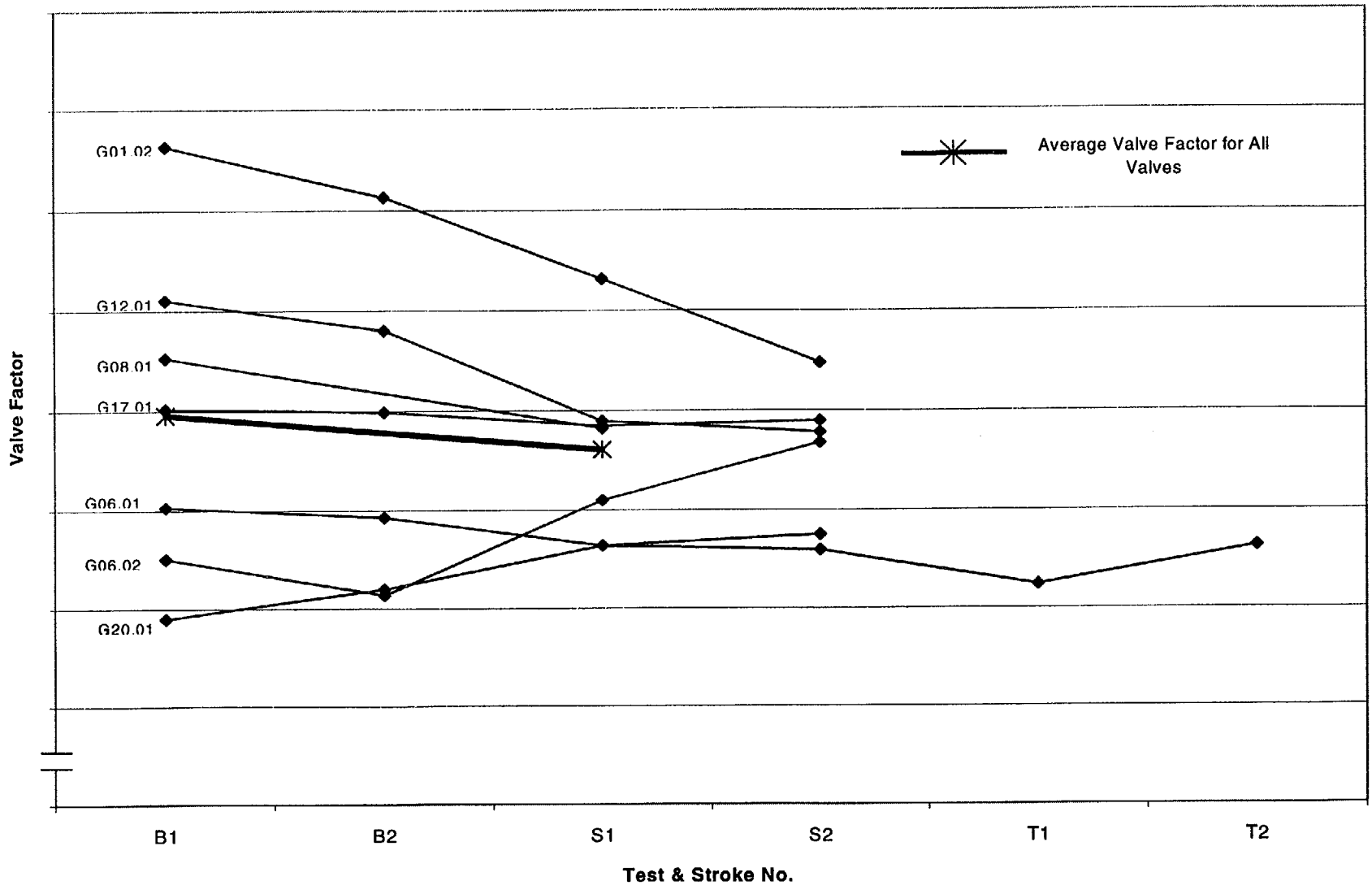

Figure 4. Progression of Closing Valve Factor at Initial Wedging for Gate Valves with Stellite Disks and Seats in Untreated Water Systems.

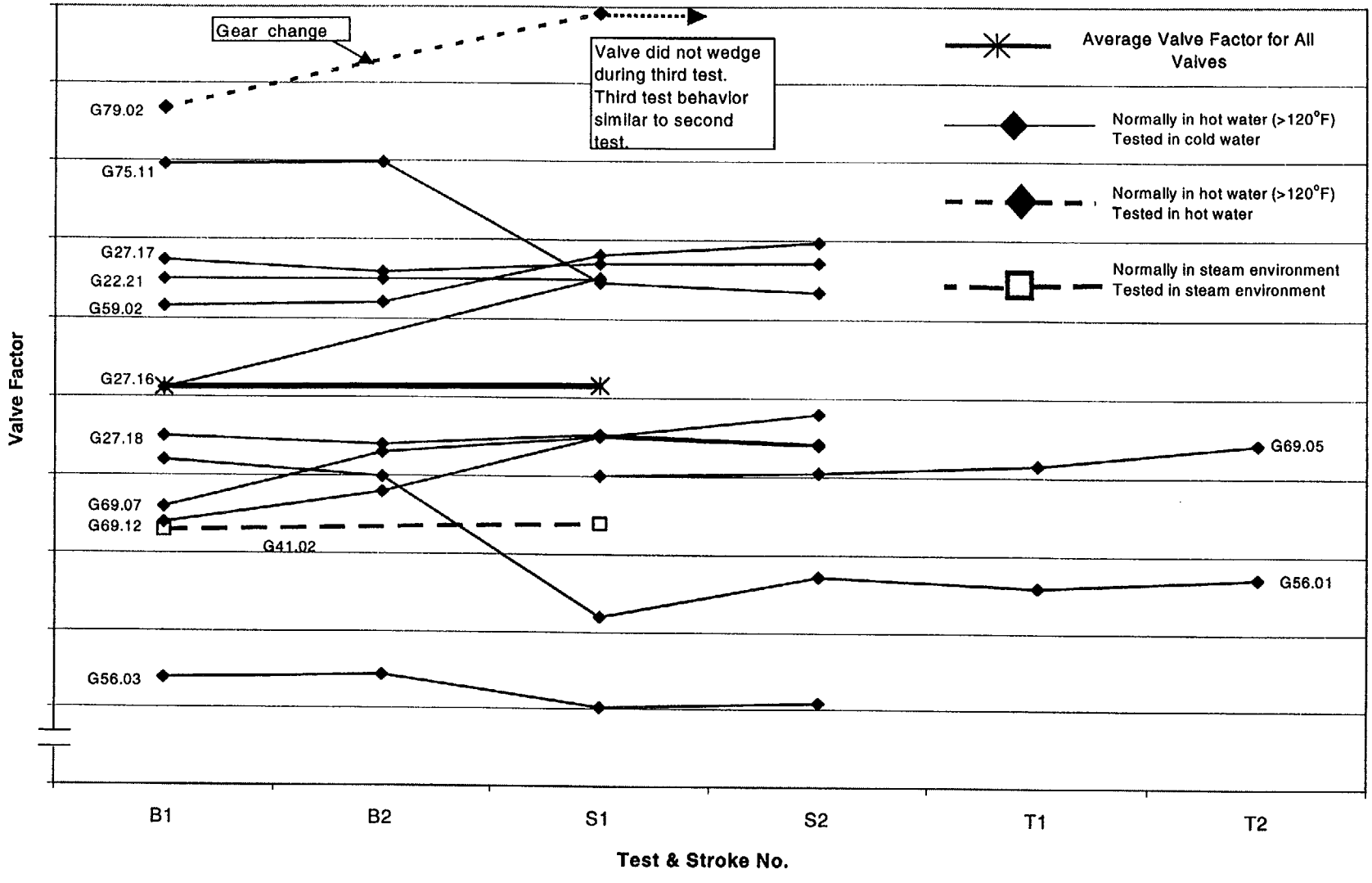

Figure 5. Progression of Closing Valve Factor at Initial Wedging for Gate Valves in Hot Water or Steam Systems (valves not disassembled).

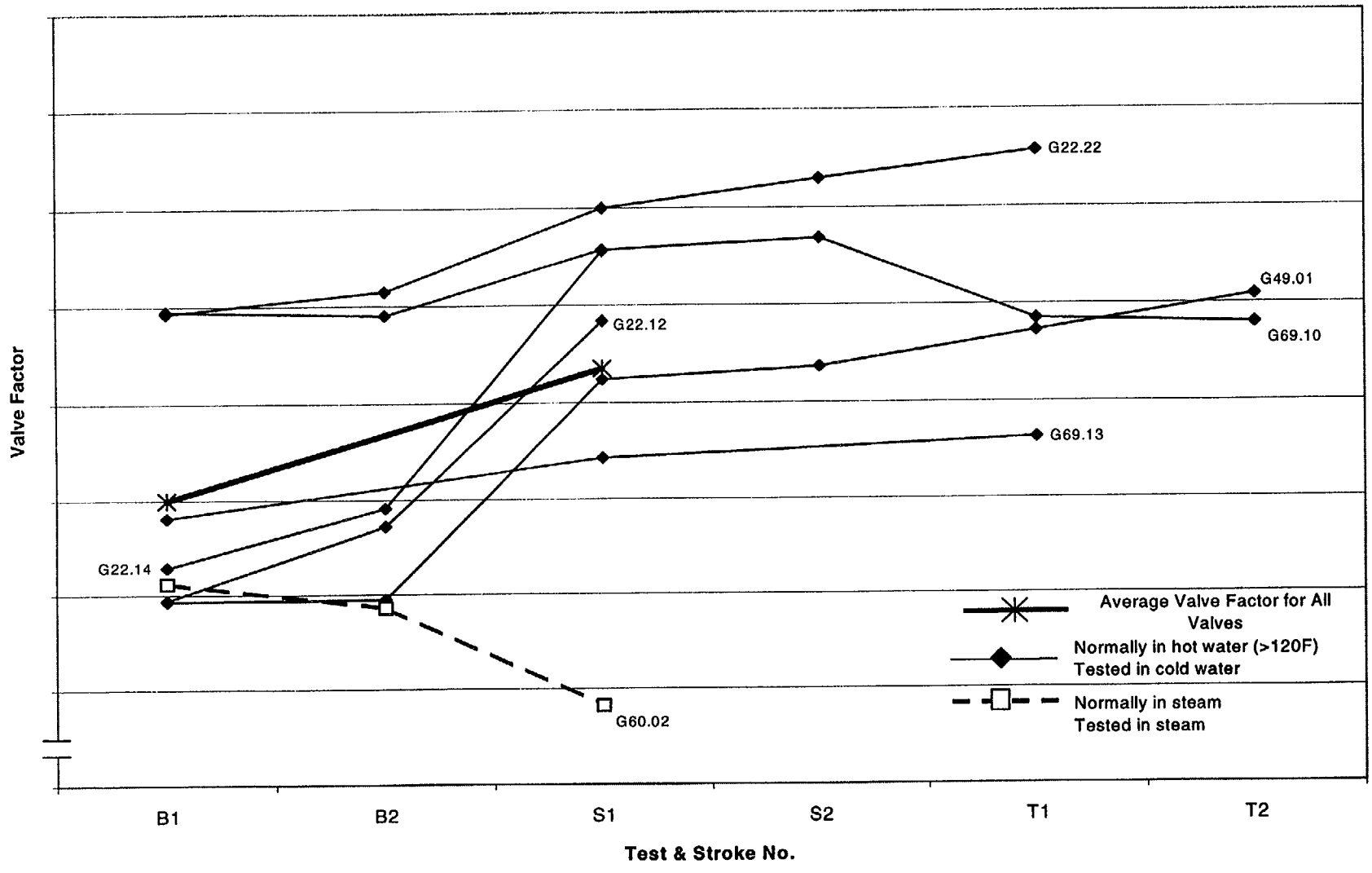

Figure 6. **Progression of Closing Valve Factor at Initial Wedging for Gate Valves in Hot Water or Steam Systems (valves disassembled and reassembled before baseline test).**

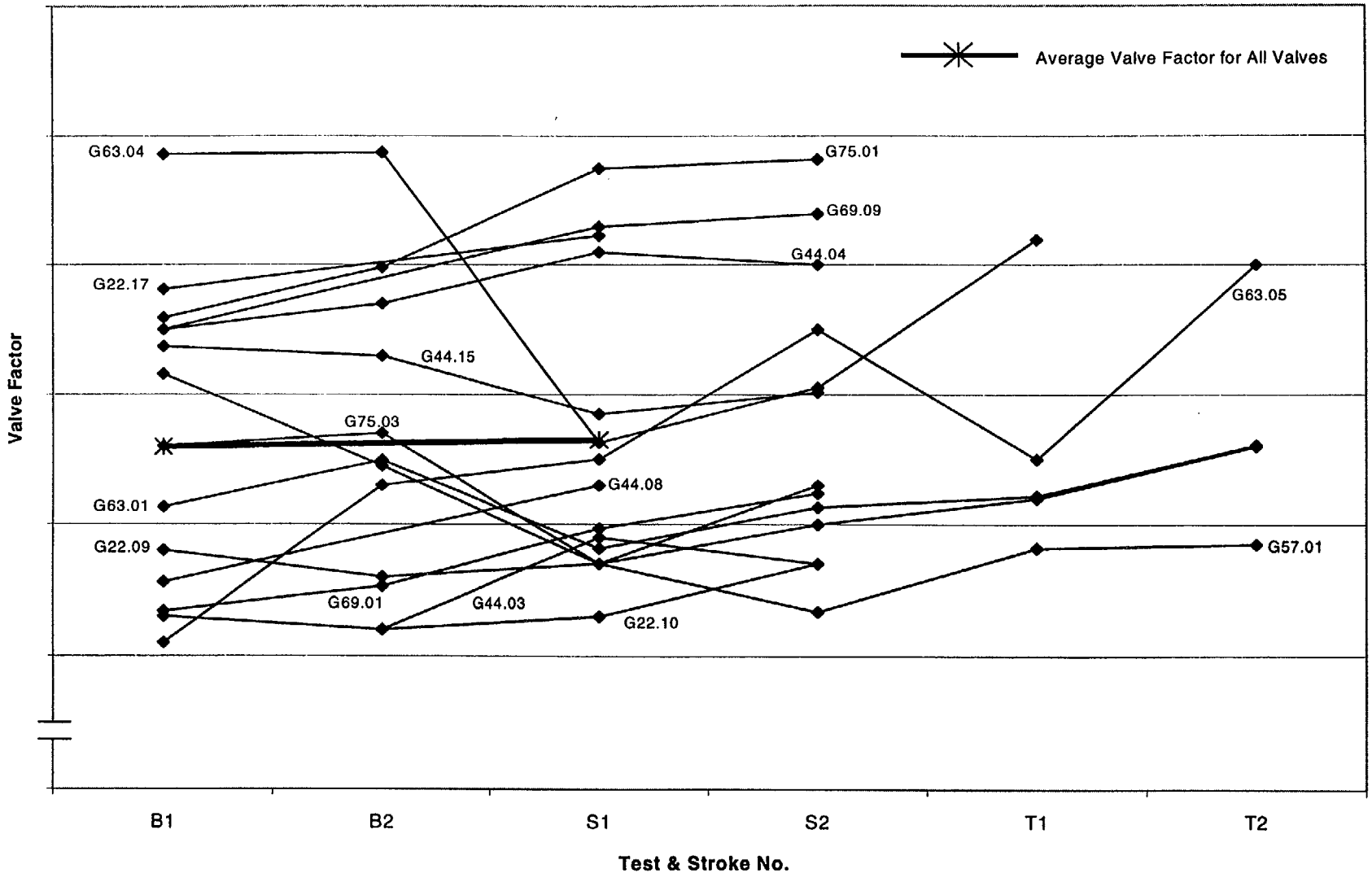

Figure 7. **Progression of Closing Valve Factor at Initial Wedging for Gate Valves in Treated Water Systems that are not Stroked Under DP Conditions (valves not disassembled).**

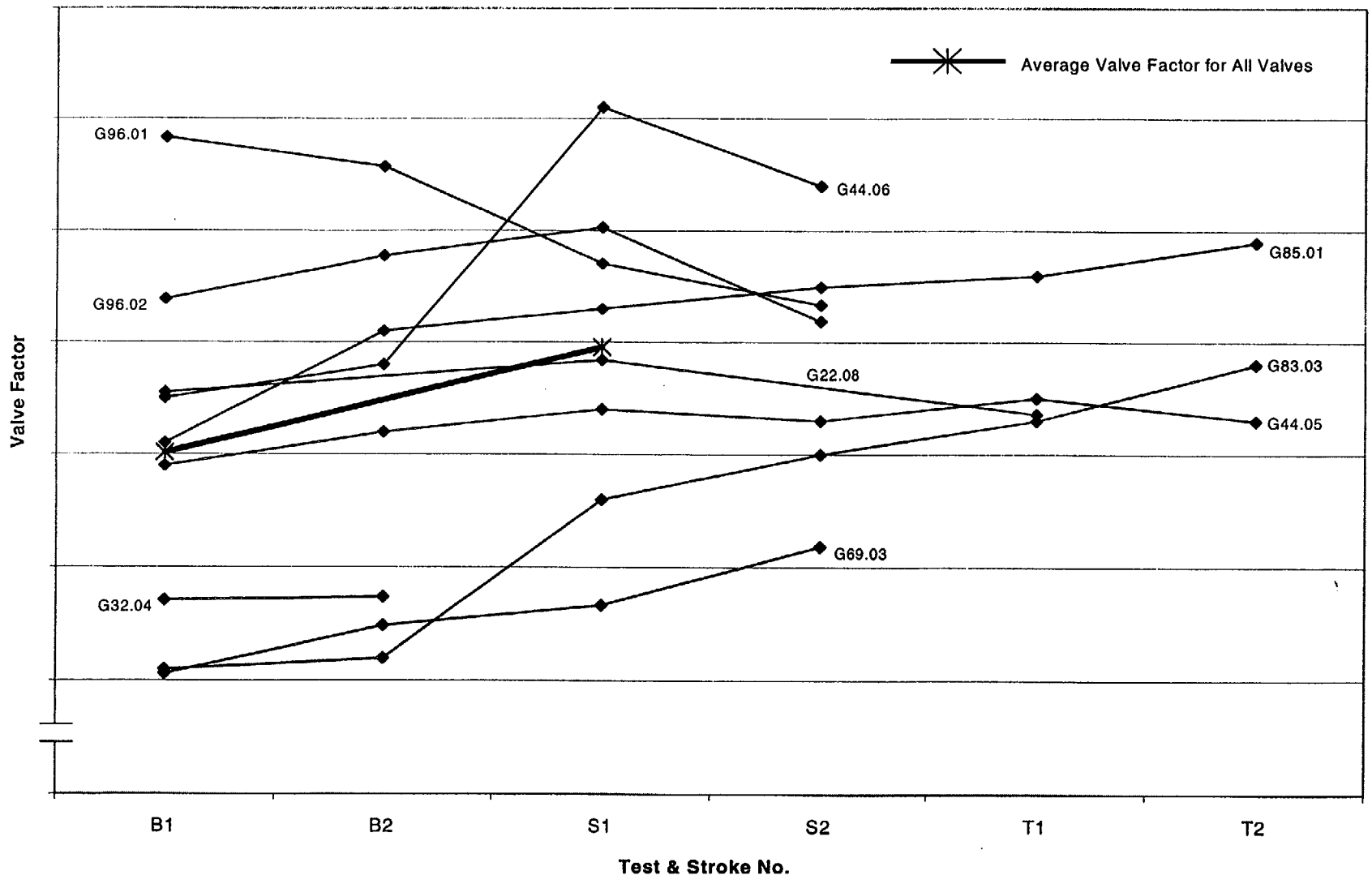

Figure 8. **Progression of Closing Valve Factor at Initial Wedging for Gate Valves in Treated Water Systems that are not Stroked Under DP Conditions (valves disassembled and reassembled before baseline test.).**

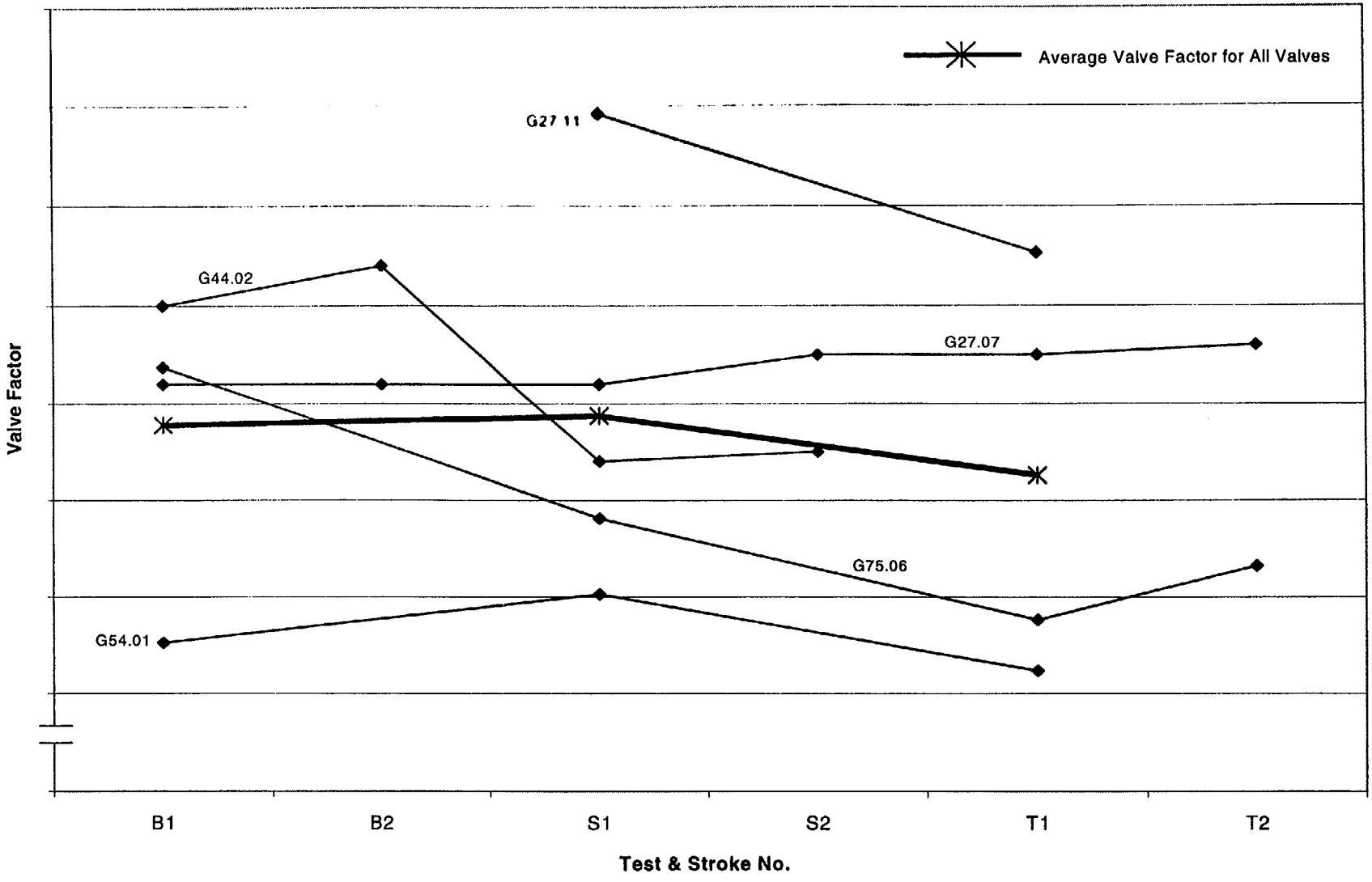

Figure 9. **Progression of Closing Valve Factor at Initial Wedging for Gate Valves in Treated Water Systems with >4 DP Strokes Between Tests (valves not disassembled).**

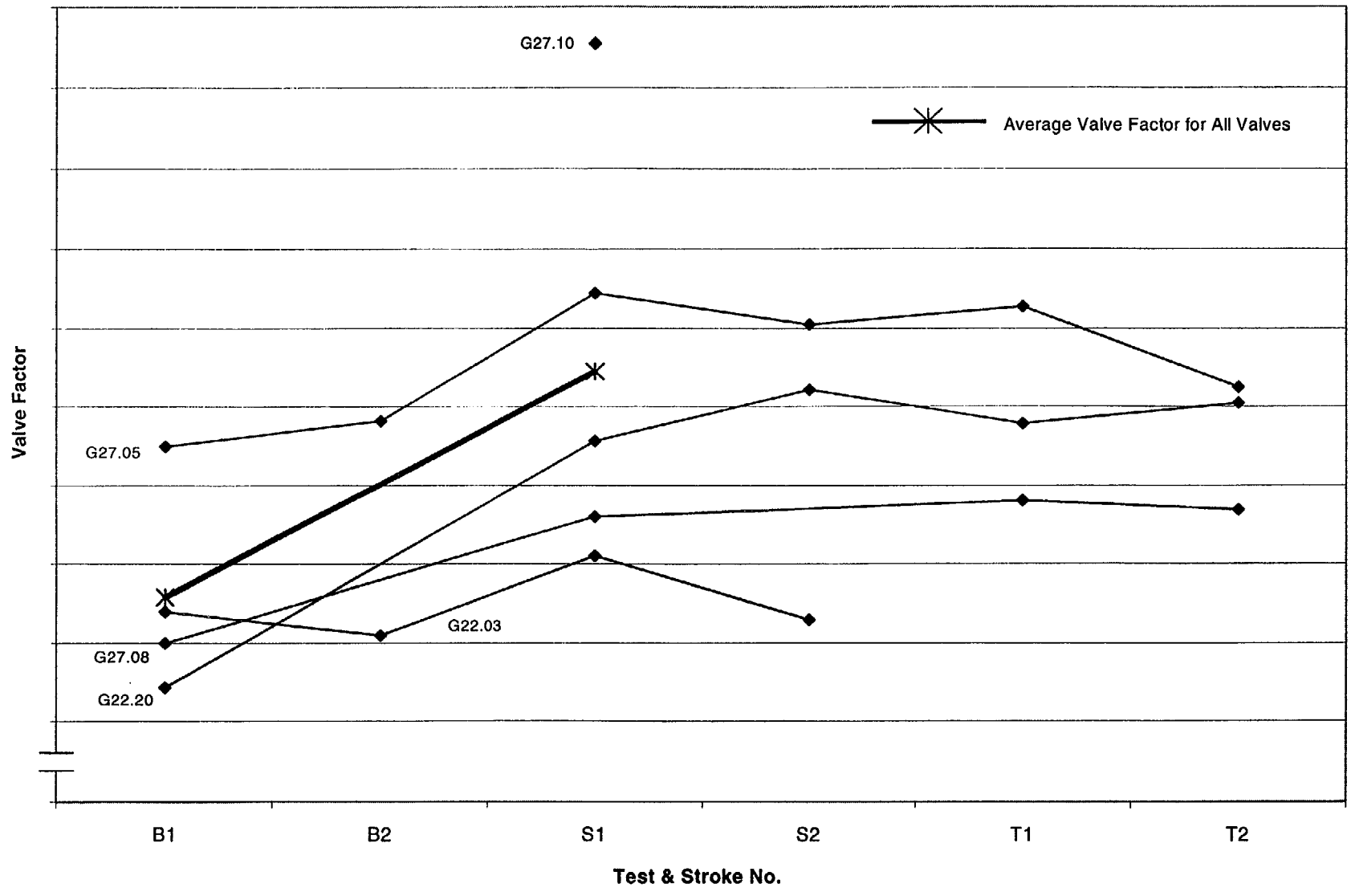

Figure 10. Progression of Closing Valve Factor at Initial Wedging for Gate Valves in Treated Water Systems with >4 DP Strokes Between Tests (valves disassembled and reassembled before baseline test).

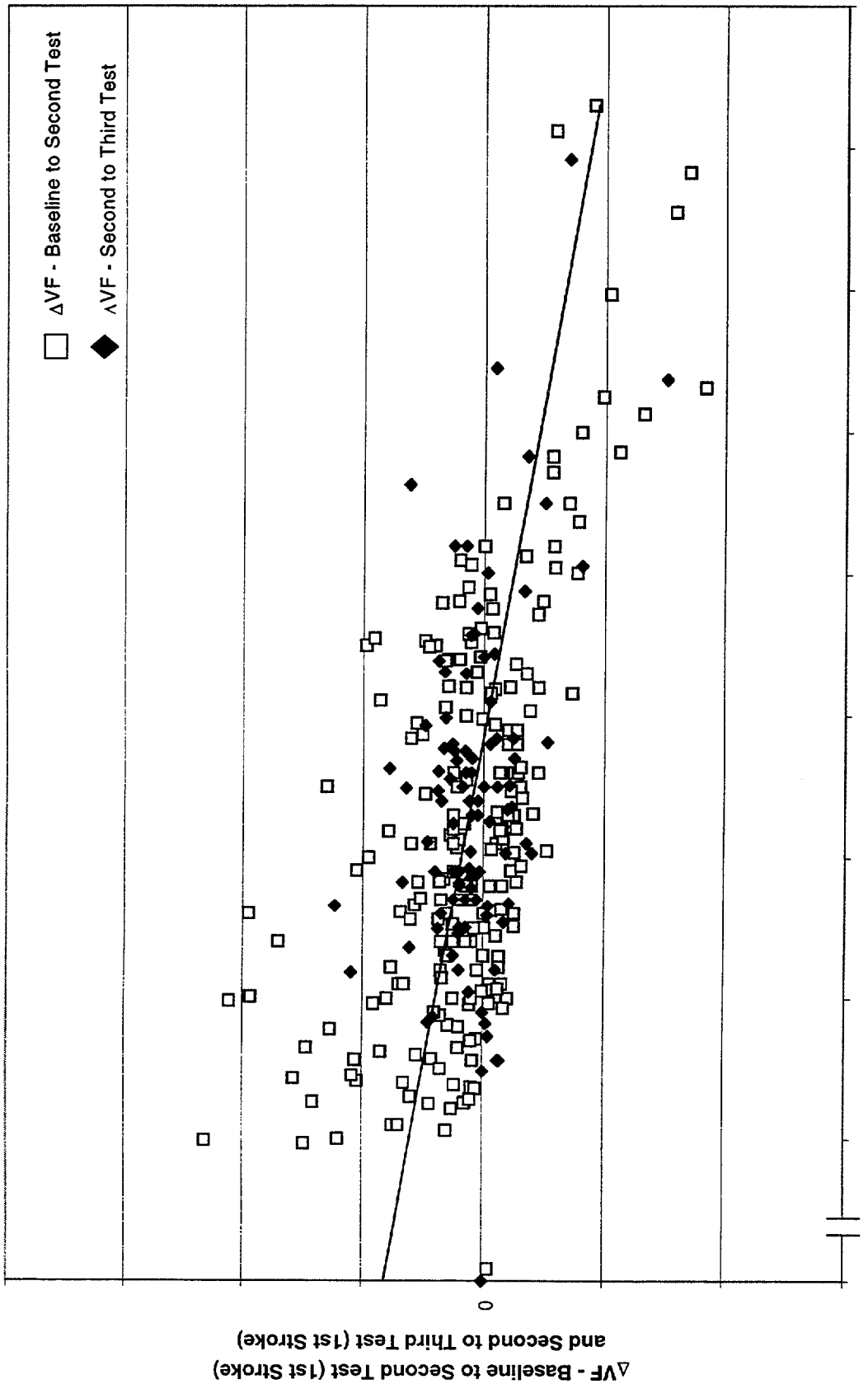

Figure 11. Effect of Initial Valve Factor on Change in Valve Factor to Subsequent Test.

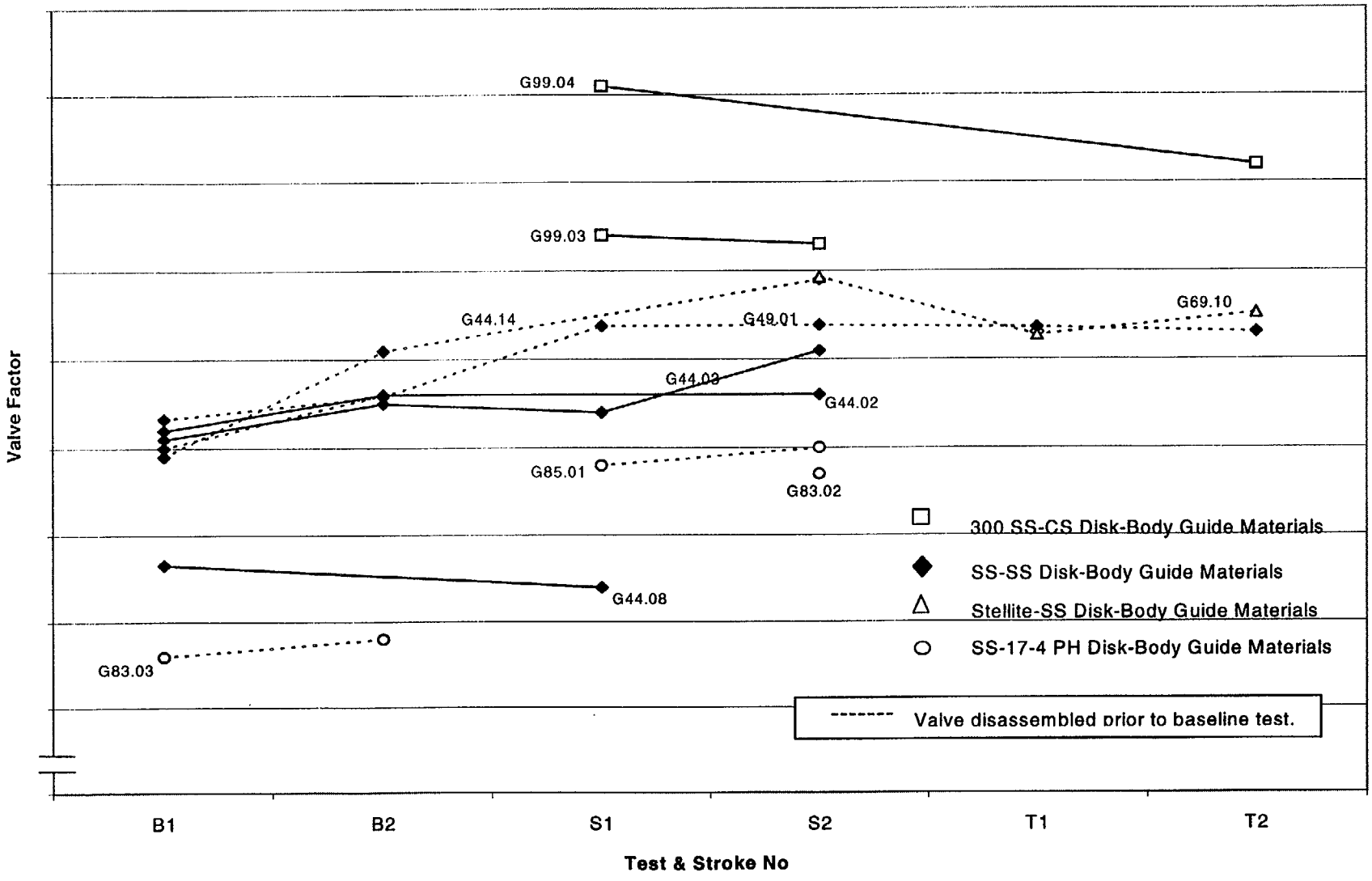

Figure 12. Valve Factor for Guide-Controlled Thrust in Gate Valves with Non-Stellite Guide Materials.

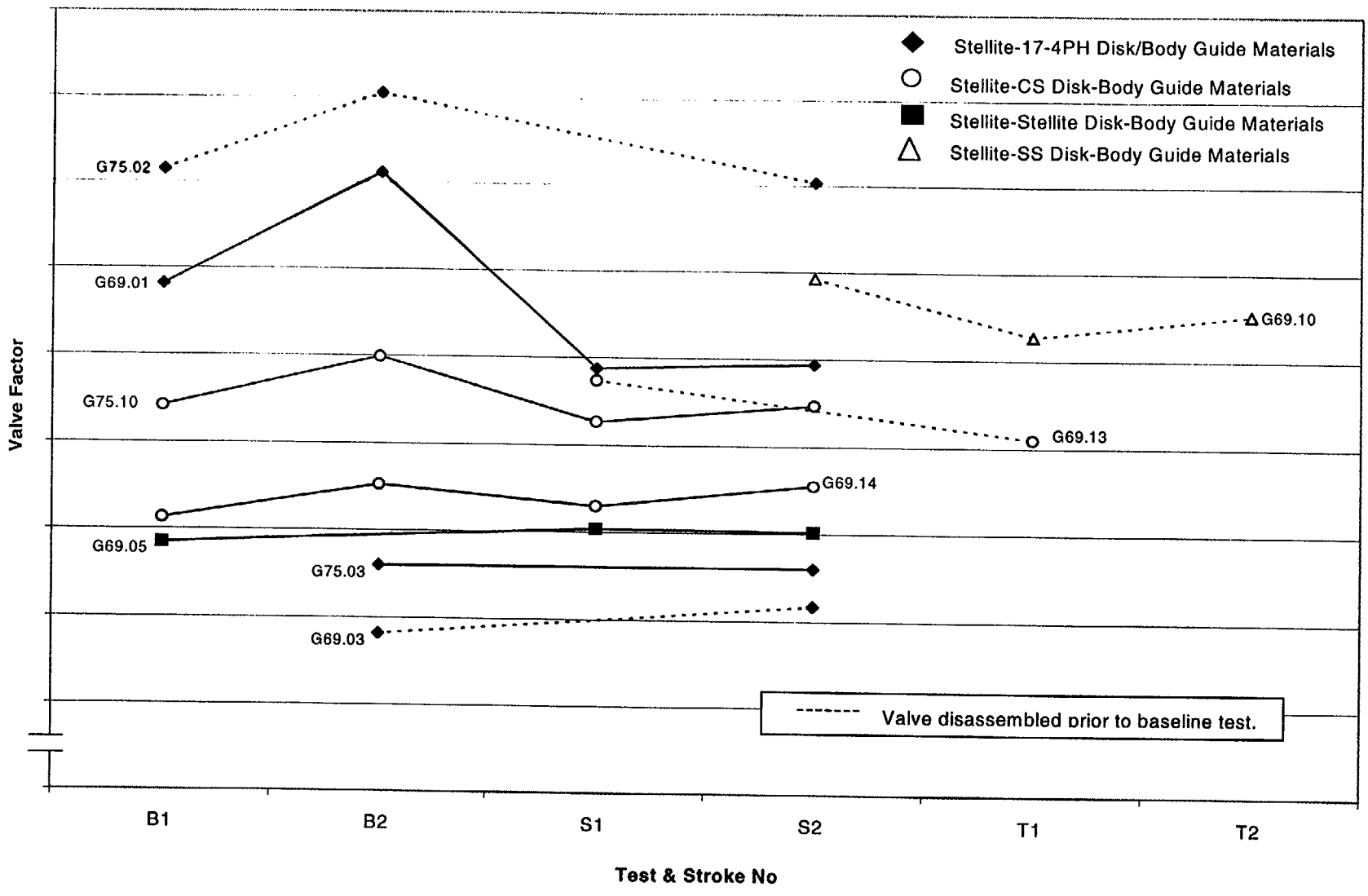

Figure 13. Valve Factor Guide-Controlled Thrust in Gate Valves with Stellite Guide Materials.

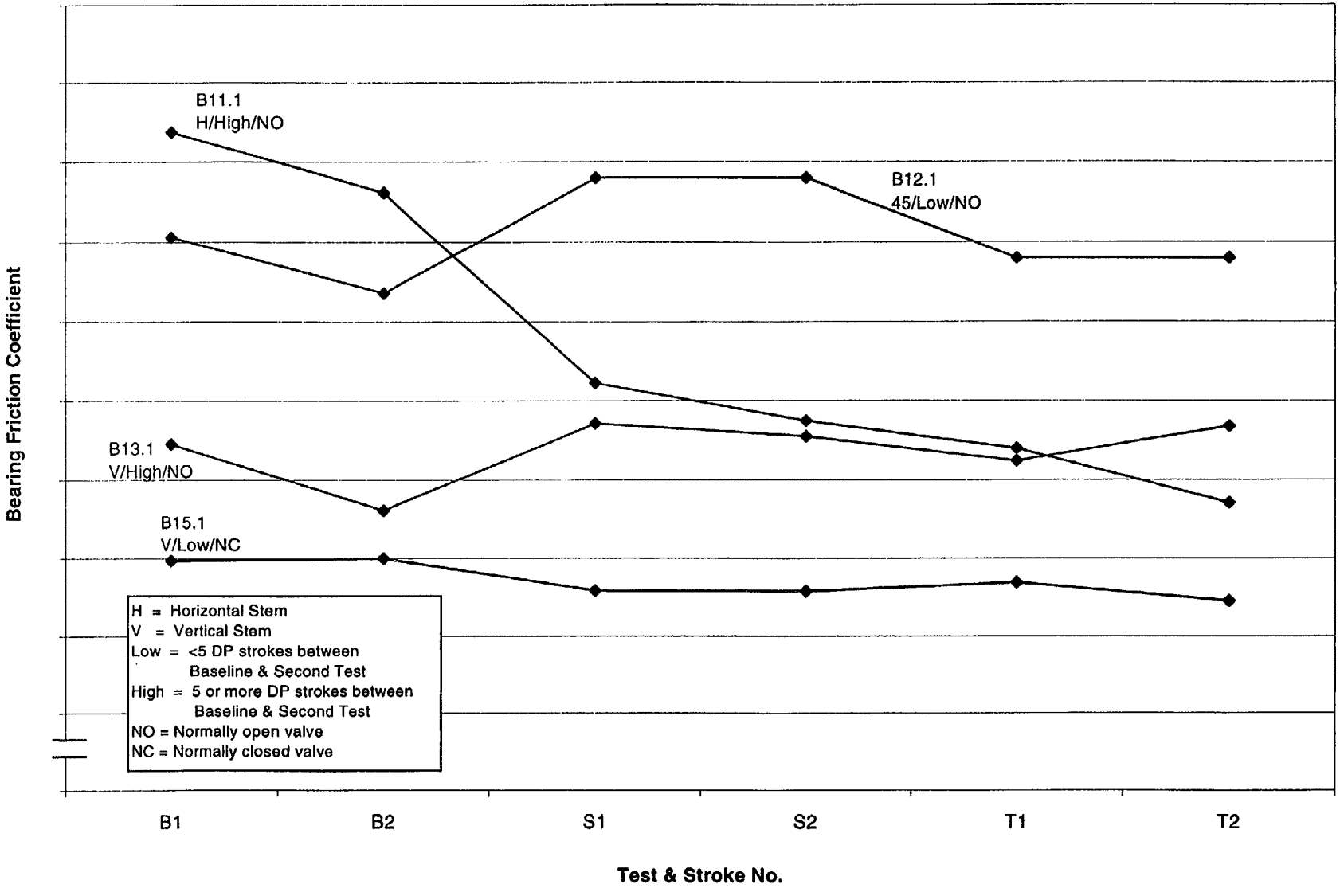

Figure 14. Progression of Bearing Friction Coefficient in Butterfly Valves with Bronze Bearings in Treated Water Systems.

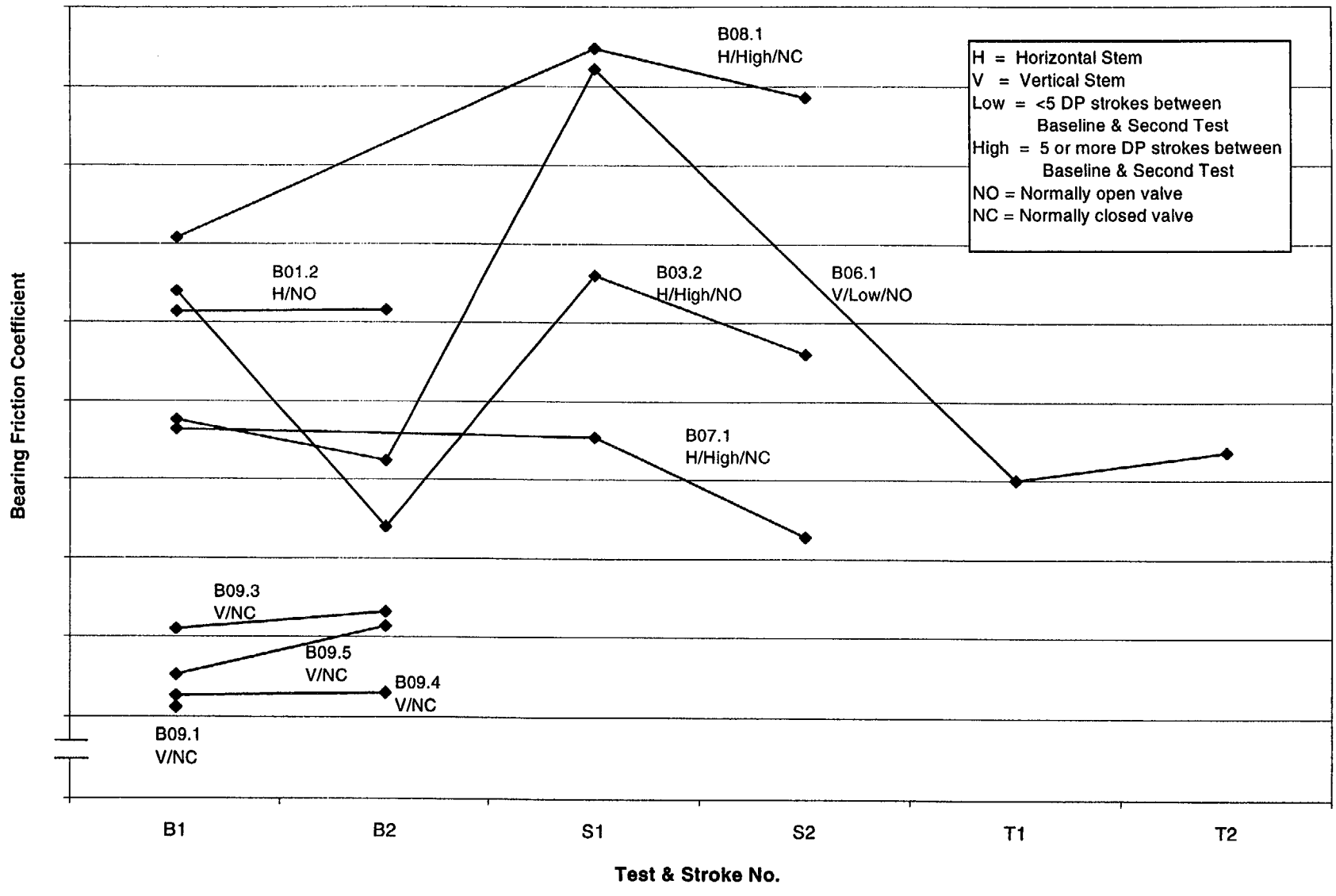

Figure 15. Progression of Bearing Friction Coefficient in Butterfly Valves with Bronze Bearings in Untreated Water Systems.

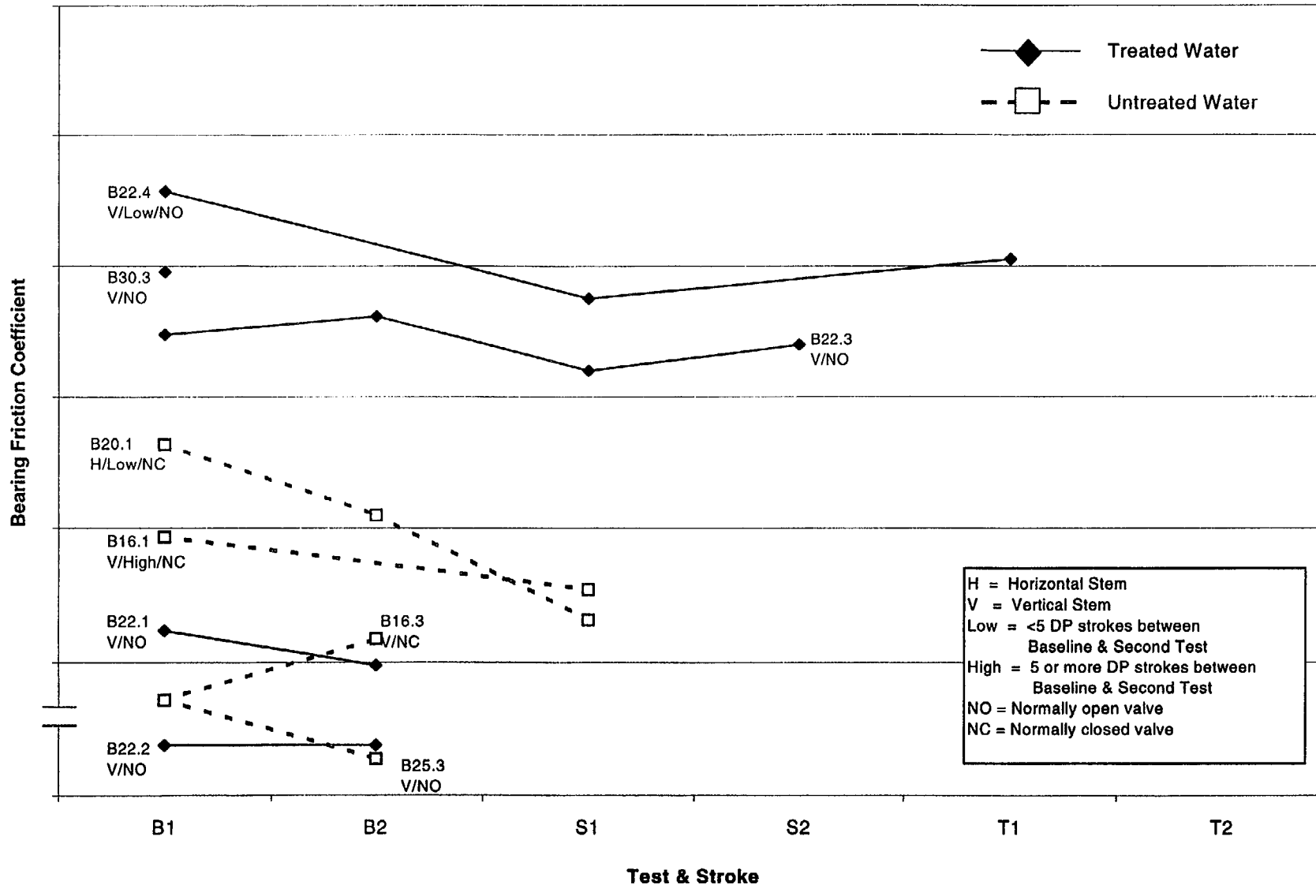

Figure 16. Progression of Bearing Friction Coefficient in Butterfly Valves with Non-Bronze Bearings.

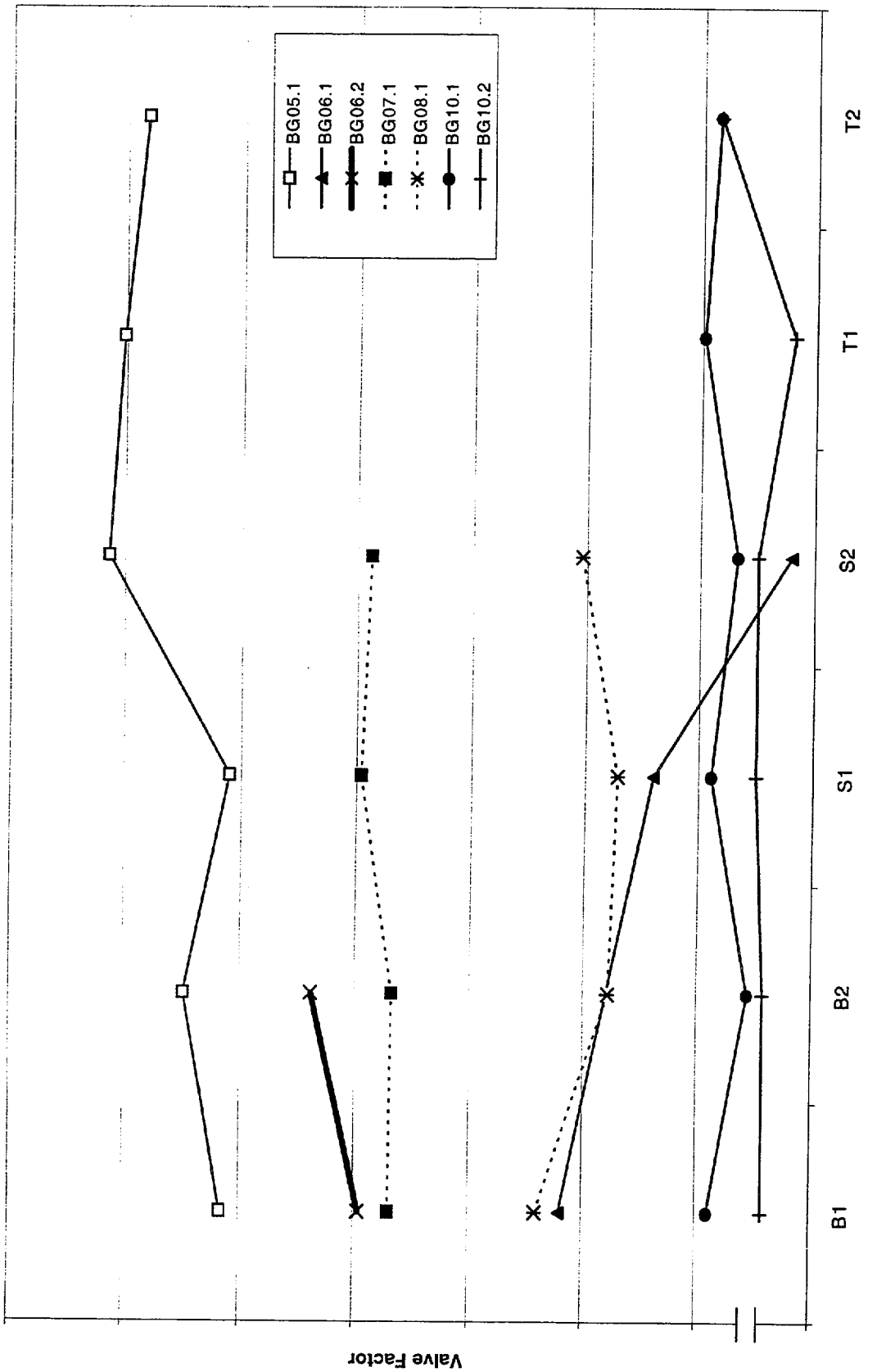

Figure 17. Progression of Opening Valve Factor at Unseating for Balanced Disk Globe Valves.

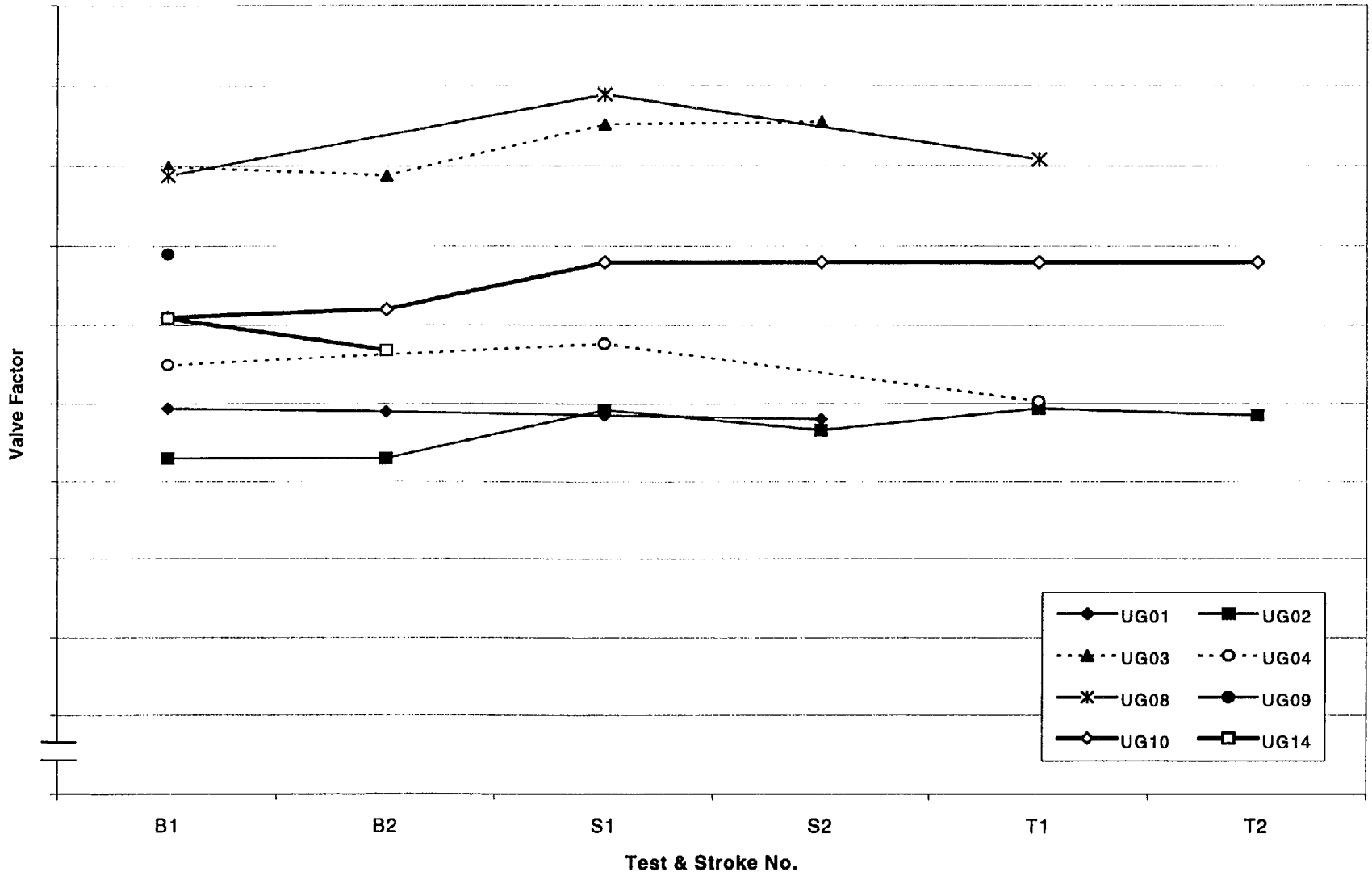

Figure 18. Progression of Closing Valve Factor for Unbalanced Disk Globe Valves with Underseat Flow.

Application of the TREMOLO Computer Program to Address Valve Operability and Fluid Transient Issues in the Republic of Korea

Tom Elicson, Fauske & Associates, Inc. (FAI)
Yang-Seok Kim, KEPRI
Thomas F. Hoyle, Energy Northwest

Purpose

Valve operability and condensation-induced water hammer in cooling water systems are issues of ongoing concern in the nuclear power industry. Many of the pipe flow transients challenging valve operability and potentially leading to two-phase flow conditions in piping systems are one-dimensional. As such, these fluid transients can be analyzed by an appropriate one-dimensional, transient computer program, such as TREMOLO.

TREMOLO is a transient thermal hydraulic code developed specifically to analyze single- and two-phase flow conditions in power plant piping systems. TREMOLO —Thermal hydraulic REsponse of a Motor-Operated valve Line—was so named since it was originally developed in response to NRC Generic Letter 89-10 (USNRC, 1989) to evaluate pressure oscillations associated with valve closures and openings in piping segments that could be exposed to two-phase flow conditions.

Over the past eight years, transient methods, such as those embodied in the TREMOLO computer program (Elicson, et al., 1999, Elicson, et al., 2000) have been used to analyze valve operability issues and valve line transients at numerous nuclear power plants in the United States in response to NRC Generic Letters 89-10 (USNRC, 1989) and 96-06 (USNRC, 1996). These analyses were performed in house by experienced staff, and computer models were typically developed and analyzed over a period of weeks.

Based on this experience, a TREMOLO code version has recently been developed which runs on a personal computer with an advanced point-and-click graphical interface. The design philosophy of the interface is to allow valve and system engineers (as opposed to computer analysts) to rapidly and accurately develop and analyze pipeline models. The time required to develop and analyze pipeline models has been reduced from a period of weeks to hours or days, depending on the model complexity.

The interface focuses on minimizing time spent developing code input and processing code output. This is accomplished with point-and-click interfaces to process code input as well as code output. Also, an advanced feature, termed "Report-Ready Output", has been developed to allow engineers to rapidly document results of their analyses.

With these innovations, KEPRI selected TREMOLO to be used by their own analysts throughout the KEPRI motor-operated valve (MOV) program in the Republic of Korea. Potential applications in the KEPRI program include determination of valve design basis closing differential pressure, design of dynamic stroke testing to minimize potential for waterhammer, interpretation of test results and operational transients, analysis of steam or accidental steam/water flow to the auxiliary feedwater pump turbine, and flow simulation for proposed design changes of piping systems.

This paper will discuss TREMOLO applications in the KEPRI MOV program, present results of code benchmarks against dynamic differential pressure (DP) testing data, present detailed results of an analysis performed by KEPRI for a reactor coolant pump thermal barrier heat exchanger isolation valve, and discuss valve line geometries for which transient analysis can yield lower closing DPs.

Introduction

Under postulated accident conditions the developed differential pressure an MOV must overcome is strongly dependent on the pipe geometry and dynamic effects of valve closure. In cases where the original design basis evaluation relied on static analysis and did not consider transient effects, the results may have significantly over stated the actual MOV DP. Typically, design basis analyses that have used static methods simply assume the closing DP is equivalent to the full system pressure, where the system pressure would be the shutoff head of a safety-related pump or the nominal reactor coolant system (RCS) pressure.

As plant equipment has aged, valve factors have increased, implying that the valve operators may no longer deliver the required thrust to ensure valve operability against the full system pressure. When valve operability is brought into question, three general options exist to resolve the operability issue: additional testing, equipment modification, or analysis. Typical equipment modification might include replacement of the valve operator which would require:

1. Design analysis and vendor support to properly size the new valve actuator.
2. Hardware purchase for valve actuator and valve.
3. Additional outage management

The estimated cost for such an approach typically exceeds $100,000.

In light of this cost of complying with Generic Letter 89-10, *Safety-Related Motor-Operated Valve Testing and Surveillance*, a more accurate assessment of the MOV closing differential pressure has proved to be a reasonable approach compared to valve replacement.

For many valve line geometries a transient analysis approach has proven effective, often times yielding closing differential pressures much lower than indicated by the original, static design basis analysis. Such is the case for the isolation valve located on component cooling water return piping of reactor coolant pump thermal barrier heat exchangers in some pressurized water reactors. A review of the valves considered in the KEPRI MOV program indicated that a number of thermal barrier heat exchanger isolation valves were present that could benefit from transient analysis.

The remainder of this paper will provide details of the KEPRI analysis that yielded a closing differential pressure of about one-half of the full RCS pressure for this particular valve. This paper will also describe the capabilities and validation of the TREMOLO code used in the KEPRI analysis.

Finally, information will be provided to allow valve engineers to review the valves in their program and identify those valves for which transient analysis could yield MOV DPs much lower than stated in the original, static design basis evaluations.

TREMOLO Code Capabilities

TREMOLO is a transient thermal hydraulic code developed to analyze single- and two-phase flow conditions in plant piping systems. TREMOLO—Thermal hydraulic REsponse of a Motor-Operated valve Line—was so named since it was originally developed in response to NRC Generic Letter 89-10 to evaluate pressure oscillations associated with valve closures and openings in piping segments that could be exposed to two-phase flow conditions. Incidentally, a rapid fluctuation of a musical tone caused by the reiteration of pressure waves is also known as a tremolo.

Principally, TREMOLO is a node and junction code that uses a one-dimensional, "one and a half" fluid model which implies separate mass and energy equations for each of the two fluid phases and a single momentum equation to describe the fluid mixture. TREMOLO considers two fluid phases (liquid and vapor), which may exist in a non-equilibrium state. To provide closure to this system of equations, fluid transport between the phases is defined and an equation of state is used.

The TREMOLO code contains models of the phenomena relevant to the study of transient two-phase flow and condensation-induced water hammer events that could occur in process piping systems. These models were selected and developed based on an understanding of the dominant physical processes expected during accident conditions postulated to occur in service water cooling systems of nuclear power plants. Namely, based on in-house scaled experiments, and a review of the open literature, the dominant phenomena modeled in TREMOLO include:

- One-dimensional, non-equilibrium, two-phase fluid flow.
- The presence and influence of residual gas bubbles in the fluid following large scale void collapse.
- Steam condensation on cold pipe walls.
- Steam condensation on the cold liquid phase.
- Non-condensible gas coming out of solution at pressures higher than the vapor pressure corresponding to the liquid temperature.
- Fan coil heat transfer.
- Changes in the valve flow coefficient (Cv) throughout the valve opening and closing strokes.

User Interface

The TREMOLO graphical interface was designed after reviewing the process required for an engineer to fully analyze a valve line and document the results in a qualified design report. This process engineering identified four general steps for valve line analysis:

1. **Identification of a valve line for analysis and data collection.** Data collection typically consists of assembling plant piping isometrics and valve design data as

well as defining the design basis accident and sensitivity parameters. Data collection may also consist of a system walkdown when feasible.

2. **Model development.** Traditionally, model development required hand calculations to convert the piping isometrics into code inputs. Hand calculations are documented in a verified calculational note.

3. **Analysis.** During the analysis phase, multiple code runs are performed and results are reviewed and cataloged to investigate the base case and sensitivity accident sequences.

4. **Documentation.** The methods and results are compiled in a verified design report.

The TREMOLO graphical interface is designed to reduce the time required to address each of these four steps. This is accomplished allowing engineers to use point-and-click operations to quickly and accurately create working pipeline model schematic from pipeline isometrics and other commonly available design documents. The same model schematic is then used for running the computer program and reviewing calculations of pressures, temperature and reaction forces at any point in the pipeline (see Figure 1). On screen results and calculations can quickly be added to design reports with the Report-Ready Output features of the interface. In essence, the interface minimizes the time engineers must spend performing routine tasks and allows the engineer to focus more time and energy on the actual engineering analysis.

Background of the KEPRI MOV Program

The Ministry of Science and Technology (MOST) has issued regulatory recommendations to provide the general guideline, which has been basically derived from the U.S. Generic Letter 89-10. These recommendations were issued on June 13, 1997. According to these recommendations, Korea Electric Power Corporation (KEPCO) has developed a program to evaluate the operability of safety-related MOVs. This program basically consists of engineering and diagnostic analyses.

In preparation for an effective MOV program, twelve MOVs in Yonggwang (YGN) unit 1 had been selected and tested in 1999. From the implementation results of YGN unit 1 pilot program and experiences in 2000, a formalized Korean MOV program was established in early 2001. In this connection, KEPCO and KHNP (Korea Hydro & Nuclear Power) have performed the following: the operability evaluation under the design basis conditions of the safety related MOVs for the units in operation (18 units, including 2 units in pre-operation); development and upgrade of the computer program, called MOVIDIK (Motor Operator Valve Integrated Database Information of KEPCO), to enhance evaluation reliability and to reduce man-hours; and development of the periodic verification technology.

For valve operability evaluations, the initial work is to review the design basis scenarios and to calculate the DP when the MOV is actuated under the design basis conditions. The simple Bernoulli equation or EPRI SFM (System Flow Model) is used to calculate the design basis DP for most MOVs, but other commercial flow analysis codes, such as TREMOLO, are used for the optimum calculation to improve the margin.

Additional details of the KEPRI MOV program are provided by B. N. Kim, et al.,

2000a, B. N. Kim et al., 2000b, and W. Kim, et al., 2000.

Validation of TREMOLO Models for MOV DP Calculations

As part of their MOV program, engineers at Energy Northwest's Columbia Generating Station performed DP testing of the reactor core isolation cooling (RCIC) return line isolation valve, RCIC-V-59. The following paragraphs summarize dynamic benchmarking of the TREMOLO 3.0 code against both the opening and closing stroke of the Columbia Generating Station RCIC-V-59 DP test performed in January, 2000. These benchmarks are relevant to GL 89-10 applications of TREMOLO because the very essence of the GL 89-10 analyses is the determination of the differential pressure across motor-operated valves during their closing or opening strokes.

RCIC test initial test conditions are achieved by closing RCIC-V-59 and then pressurizing the line upstream of the valve by operation of the RCIC pump. For the test analyzed here, the initial line pressure is 8.96 MPa (1300 psia) at the location of RCIC-V-59. Once RCIC-V-59 is opened, the increased flow through the system results in a lower RCIC pump discharge pressure. A flow control valve and pressure reducing orifice were used to limit the full system flow to 0.0442 m^3/s (700 gpm) for this test. The RCIC discharge pressure decreases to 7.56 MPa (1097 psia) once full flow, equilibrium conditions are achieved. The dynamic effects of the RCIC pump are modeled as the upstream pressure boundary condition in the benchmark calculation.

Once the initial test conditions are established, the test is performed by stroking open RCIC-V-59 to initiate flow, allowing the flow to reach a steady state condition, and then stroking closed RCIC-V-59. The opening stroke and the closing stroke times are both 12 seconds. Test measurements were taken to determine the pressure and stem thrust force of RCIC-V-59 throughout the test.

In all, 50 seconds of test data were provided by Energy Northwest. The complete test includes stroking valve V-59 from closed to open, holding V-59 fully open until steady state flow conditions are achieved, and then stroking the valve closed. Results presented in Figure 2 address the opening stroke portion of the test, while Figure 3 addresses the closing stroke portion of the test.

Figure 2 compares the TREMOLO 3.0 pressure calculation at the inlet of valve V-59 to the test data. In this portion of the test, V-59 is initially closed and the pipe upstream of the closed valve is pressurized to the RCIC pump shutoff head. Then, the valve is stroked open over 12 seconds. In this figure, the valve opening stroke begins at time zero, and even though the opening stroke is not completed until 12 seconds, the calculation is terminated once steady state flow conditions are achieved at 5 seconds.

Since the RCIC pump was the pressure source for the test, the upstream boundary pressure varied during the test according to the RCIC pump head curve. Pump discharge pressure measurements were provided by Energy Northwest and these measurements are used in the dynamic benchmark subroutine to model the upstream boundary pressure as a function of time.

Figure 3 compares TREMOLO 3.0 calculations against test data for the closing stroke of gate valve RCIC-V-59. In Figure 3, the closing stroke begins at time zero and ends 12 seconds. Overall, the TREMOLO calculations closely follow the Columbia

Generating Station test data. Predictions of the peak pressure are within 2% of the test data (test data peak pressure: 9.95 MPa / 1443 psia vs. TREMOLO peak pressure: 9.97 MPa / 1417 psia).

The test data also indicates pressure "ringing" of ±0.17 MPa (±25 psi) after valve closure (i.e., at times greater than 12 seconds in Figure 3). The TREMOLO calculations indicate the pressure ringing with smaller amplitudes of ±0.14 MPa (±20 psi) that dampen to ±0.034 MPa (±5 psi) by the end of the calculation. The amplitudes of the pressure waves may be influenced by the dynamic behavior of the RCIC pump. Test data indicate an oscillating pump discharge following valve closure. This behavior is not modeled in the benchmark calculation.

This benchmark against actual plant data collected during a valve DP test is the most relevant test of the TREMOLO code capability to predict valve closing DP. The good agreement between the TREMOLO calculations and the test data indicate that the TREMOLO code models are quite capable of providing reliable valve DP calculations for both the opening and closing stroke of the valve. For additional benchmark results, see Elicson et al., 1999, and Hammersley and Elicson, 2000.

KEPRI MOV DP Analysis of Isolation Valve EHGV337

Recently, as part of their on-going MOV program, KEPRI performed a two-phase flow transient analysis using the TREMOLO 3 computer program to determine the design basis closing DP for a thermal barrier heat exchanger isolation valve, EGHV337. The isolation valve is located on the cooling water return piping approximately 42 m (137 ft) downstream from the thermal barrier heat exchanger. The heat exchanger, itself, provides cooling to the reactor coolant pump seals and the heat exchanger tubes act as a pressure boundary to the RCS. The safety function of the isolation valve is to close upon receipt of a high flow signal to isolate the cooling water return line in the event of a rupture of a thermal barrier heat exchanger tube.

As shown in Table 1, the normal operating pressure and temperature of the component cooling water line to the thermal barrier of the reactor coolant pump are 0.7929 MPa [115 psia] and 310 K [98 F], respectively. However, in the event of a thermal barrier rupture, primary coolant from the reactor coolant system can leak into the component cooling water system (CCWS). A flow switch is mounted in each thermal barrier return line,which will isolate the thermal barrier when the flow increases to .00379 m^3/sec [60 gpm]. A backup high flow transmitter in the common CCWS return line from the three thermal barriers (one each for the reactor coolant pumps) will close a containment isolation valve (EG HV-337) inside the containment when the flow reaches 0.0136 m^3/sec [215 gpm]. The closure of the isolation valve (EG HV-337) and the two check valves in each supply line to each thermal barrier will isolate the thermal barrier lines from the rest of the CCWS. The component cooling water piping to the thermal barrier, which is isolated from the rest of the CCWS, may be subjected to the reactor coolant system operating pressure and temperature; hence, it is designed for 17.24 MPa [2500 psia] at 566 K [560 F]. A thermal relief valve (PSV-436) is provided in the line feeding the thermal barriers to prevent overpressure.

Under these scenarios, the design basis differential pressure was assumed to be the

difference between the full RCS pressure and the component cooling water system pressure: 16.44 MPa differential (2385 psid). An evaluation of the valve actuator determined that the actuator did not have enough capacity to close the valve against this differential pressure, i.e., the actuator would need to be replaced if the required thrust to close the valve could not be reduced. Before declaring the valve inoperable, it was decided to use transient two-phase flow methods to re-calculate more realistic valve closing DP. Results of the transient calculations, performed with the TREMOLO 3 computer program are presented, below.

The transient DP analysis for the thermal barrier isolation valve postulates the guillotine rupture of a single a 0.019 m [0.75-inch] diameter thermal barrier heat exchanger tube. High energy RCS fluid flows through the heat exchanger tubes, while component cooling water flows outside the tubes through a heat exchanger header and into the CCWS return piping. Immediately after the tube rupture, the fluid in the CCWS piping accelerates in response to the high pressure source at the site of the tube rupture. As the cooling water flow increases, a close signal is received by isolation valve EGHV337. In the current calculation, the valve begins to close at 1.3 seconds and has a 19 second stroke time. The complete set of initial and boundary conditions for this accident scenario are listed in Table 1.

Immediately following the heat exchanger tube rupture, high energy coolant enters the lower pressure CCWS piping and begins to flash, creating a steam void in the piping in the vicinity of the heat exchanger. The expanding steam volume pushes the cold water down the pipe creating strong pressure and flow transients during the first few seconds following the tube rupture. The expanding steam volume can be seen in Figure 4 which presents the calculated axial void profile 1 second and 2 seconds after the tube rupture and at the instant of full valve closure (i.e., 20.3 seconds). The pressure and flow transients are presented in the temporal plots presented in Figures 5 and 6.

Eventually, because of the long stroke time (19 seconds), an equilibrium flow condition is obtained which is controlled by the critical flow of slightly subcooled liquid through the ruptured tube. In addition, the entire length of CCWS return piping out to the isolation valve is voided (see Figure 7) and the pipeline components in the vicinity of the isolation valve have heated up (see Figure 8) prior to valve closure.

As the isolation valve strokes closed, the hydraulic resistance across the valve increases, leading to an increased DP across the valve, as shown in Figure 5. The increased resistance also results in a decrease in flow through the valve as indicated in Figure 6 and a collapse of the steam voids, as shown in Figure 7.

Since the valve closing stroke is initiated at 1.3 seconds and the total stroke time is 19 seconds, the valve is fully closed at 20.3 seconds. At this time, the MOV inlet and outlet pressures are 5.92 MPa [856 psia] and 0.79 MPa [115 psia], respectively, resulting in a maximum value of the MOV DP of 5.13 MPa [741 psid]. Also, as shown in Figure 4, there is still significant voiding in the pipe at the time of valve closure. A closer examination of results indicates that more than 20% of the total pipe volume is voided at the time of valve closure.

Since the presence of steam voids provides a cushioning effect that prevents a rapid rise in line pressure, the total void volume can be used as a measure of the margin of success for this calculation. The 20% void reported

here indicates that significant margin exists in this calculation. In other words, closing DPs in the range of 5.13 MPa [741 psid] can be expected until the void collapses completely. This is evident by comparing results presented in Figures 7 and 5. Figure 7 shows that the final void collapses at 24.8 seconds. Figure 5 shows that the MOV inlet pressure remains below 8 MPa [1160 psia] until 24.8 seconds, and then rapidly increases to the full system pressure of 17.2 MPa [2500 psia].

Identification of Valve Line Geometries Yielding Lower Closing DP

Transient analyses like that presented above may not always yield lower closing DPs. Therefore, prior to embarking on a detailed analysis of a safety-related isolation valve, it is worthwhile to review the physics at work to develop general guidelines for identifying valve line geometries most likely to benefit from transient analysis.

Consider, first, the amount of liquid that is compressed in a "solid water" system. For the case of sudden valve closure, the water hammer pressure rise can be calculated by the well known Joukosky equation,

$$\Delta P = \rho u A_w \qquad (1)$$

where,

ΔP = pressure rise
ρ = fluid density
u = fluid velocity
A_w = sonic velocity

For a typical water-solid cooling water line (density: 990 kg/m^3; velocity: 1 m/s; sonic velocity: 1400 m/s) that experiences a sudden valve closure, the pressure rise predicted by Equation 1 is 990 x 1 x 1400 = 1.39 MPa [200 psi].

This pressure rise is also related to the fluid compressibility through the sonic velocity,

$$\Delta P / \Delta \rho = (A_w)^2 \qquad (2)$$

where, $\Delta\rho$ is the change in the liquid density.

For the preceding water hammer pressure rise of 1.39 MPa, the liquid density would increase by 1.39E6/(1400)^2 = 0.71 kg/m^3 [0.044 lb/ft^3].

This density increase implies that there can be no pressure rise in a water solid pipe at constant temperature unless the fluid addition to the pipe exceeds the water discharge through the closing isolation valve.

For a valve line, the competing effects of pressure rise and valve closure can be resolved with transient methods. In most cases, a water solid system will pressurize to the full system pressure prior to closure of the isolation valve. However, if a significant restriction or a small leak is present between the valve and the high pressure source, such as a back-leaking check valve, or a pump seal leak, then transient methods can yield lower closing DP even for a water solid system.

For boiling water reactor (BWR) systems, the safety injection lines for high pressure coolant injection (HPCI) and reactor core isolation cooling (RCIC) pumps have been successfully analyzed with transient methods. The HPCI and RCIC injection lines are typically designed with check valves between the isolation valve and the reactor pressure vessel, as shown in Figure 9 and back leakage through the check valves is credited. BWR recirculation isolation valves and pressurized water reactor (PWR) residual heat removal (RHR) injection lines with postulated pump seal leaks can also benefit from transient analysis (see Figure 10). In these scenarios, the effective seal leak area is determined based

on the design basis allowable leakage, while the actual leak rate is calculated from the leak area, pressure drop, and critical flow limits.

Regarding back leakage through a check valve, if the maximum allowable closing DP is known, then the transient analysis can be turned around to determine the maximum back leakage that can be tolerated while staying below the maximum DP limit.

In many cases, such as with the thermal barrier heat exchanger isolation valve, two-phase flow may be present in the system. Whenever high energy fluid is discharged into lower pressure piping, steam voiding can be anticipated. As long as the steam is present, the line pressure is controlled by the steam saturation pressure. Even though the steam void reduces the pressurization rate, the line may still reach the full system pressure prior to valve closure unless a flow restriction is present between the valve and the high pressure boundary. For example, the thermal barrier heat exchanger analysis considered discharge through a 0.019 m diameter tube into a 0.1 m diameter pipe.

For high energy valve lines without significant flow restrictions, a transient calculation would indicate that the line would reach the full system pressure prior to valve closure. However, the transient calculation may still be beneficial. Often times, as with the thermal barrier heat exchanger scenario, transient calculations can demonstrate that the hot water has heated up the isolation valve components (see Figure 8). By crediting the reductions in the valve factor due to the higher fluid and component temperatures, significant margin improvements can still be obtained.

Conclusion

Single and two-phase flow transient methods can be beneficial in determining design basis MOV DP and are being used in the KEPRI MOV program. KEPRI calculations performed with the TREMOLO 3 computer program have already yielded significant improvements in margin by reducing the design basis closing DP from 17 MPa (2500 psia) to less than 7 MPa (1000 psia) for the thermal barrier heat exchanger isolation valve.

Transient calculations have also proven to be effective for water solid valve lines when crediting check valve back leakage or pump seal leaks. Finally, transient methods can be used to provide a realistic assessment of pipe component temperatures for cases where high energy fluid enters the pipe line. Increased component temperatures can then be used to justify reduced valve factors, hence improving the isolation valve margin.

References

Elicson, G.T., Reeves, R.W., Fauske & Associates, Inc., Turner, M. Carolina Power & Light, "TREMOLO: Computer Methodology Which Yields Lower Closing DP's for MOVs/ AOVs," Proceedings of the Third AUG/MUG Combined Meeting, Clearwater, Florida (January, 2000).

Elicson, G.T., Henry, R.E., Hammersley, R.J., and Burelbach J.P., Fauske & Associates, Inc., "Dynamic Benchmarking Of TREMOLO—A Program For Pipeline Two-Phase Flow Transient Analysis," Ninth International Topical Meeting on Nuclear Reactor Thermal Hydraulics (NURETH-9), San Francisco, California, (October 3–8, 1999).

Hammersley R.E. and Elicson, G.T., "Two-Phase Flow and Waterhammer Transient Assessments with the TREMOLO Computer Code," International Meeting on "Best-Estimate" *Methods in Nuclear Installation*

Safety Analysis (BE-2000), Washington, DC (November, 2000).

Kim, B. N., D. H. Lee, Y. G. Park and P. T. Park, "MOV Issues in Korea: Industrial Implementation," AOV/MOV Users Group Combined Meeting, Clearwater Beach, Florida (Jan. 17-21, 2000).

Kim, B. N., et al., "Implementation Program of and Technical Approach to the Regulatory Recommendation on Safety-Related MOVs in Korea," Proceedings of the Sixth NRC/ASME Symposium on Valve and Pump Testing, Washington, DC (July 17–20, 2000).

Kim, W., O-Hyun Keum, and Key-Yong Sung, "MOV Issues in Korea: Regulatory Perspective," AOV/MOV Users Group Combined Meeting, Clearwater Beach, Florida (Jan. 17–21, 2000).

USNRC, 1989, Generic Letter 89-10: Safety-Related Motor-Operated Valve Testing and Surveillance.

USNRC, 1996, Generic Letter 96-06: Assurance of Equipment Operability and Containment Integrity During Design Basis Accident Conditions.

TABLE 1 Initial and Boundary Conditions for Analysis of Isolation valve EGHV337 Closing DP

Upstream boundary pressure and temperature	17.24 MPa, 566 K (2500 psia, 560 F)
Initial pipe pressure and temperature	0.7929 MPa, 310 K (115 psia, 98 F)
Downstream boundary pressure and temperature	0.7929 MPa, 310 K (115 psia, 98 F)
Tube break area	.000285 m^2 (.003066 ft^2)
Time to initiate valve closing	1.3 seconds
Valve stroke time	19 seconds
Valve Cv	.000323 $m^3/s/Pa^{0.5}$ (425 $gpm/psi^{0.5}$)

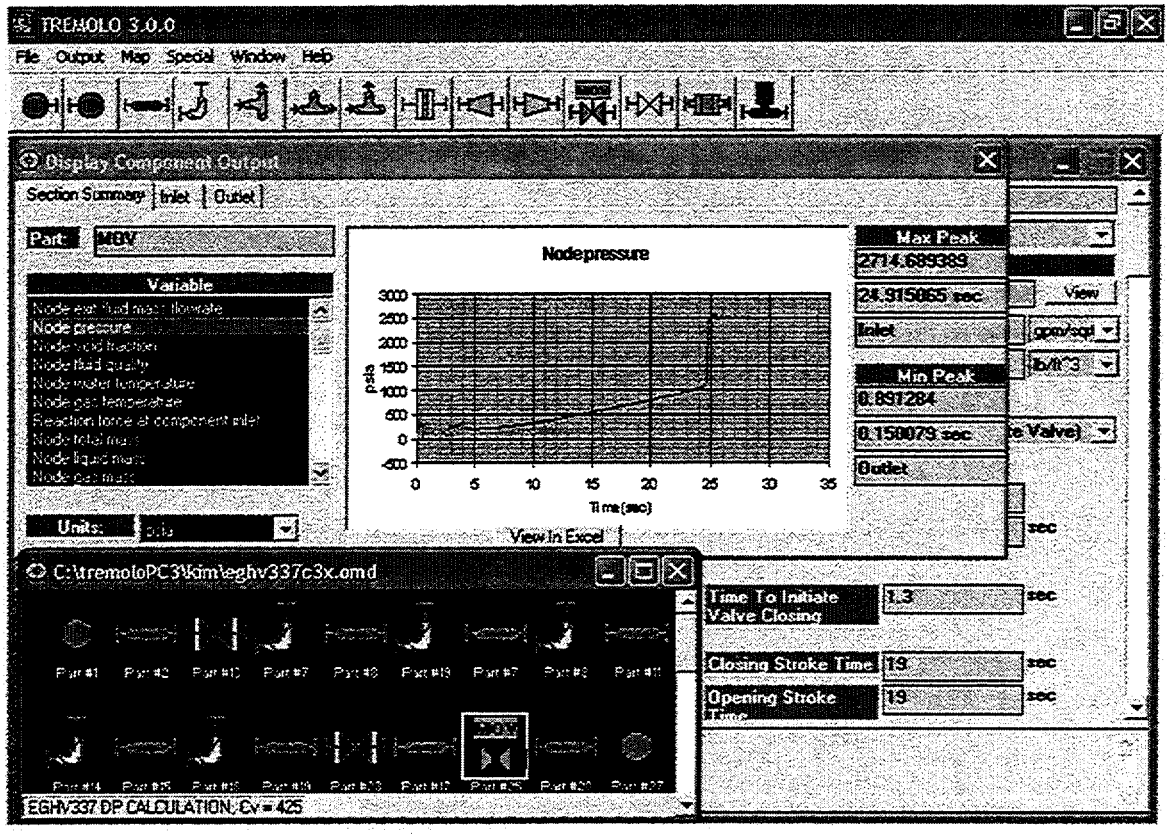

Figure 1. TREMOLO PC 3 Output Model for KEPRI MOV EGHV-337.

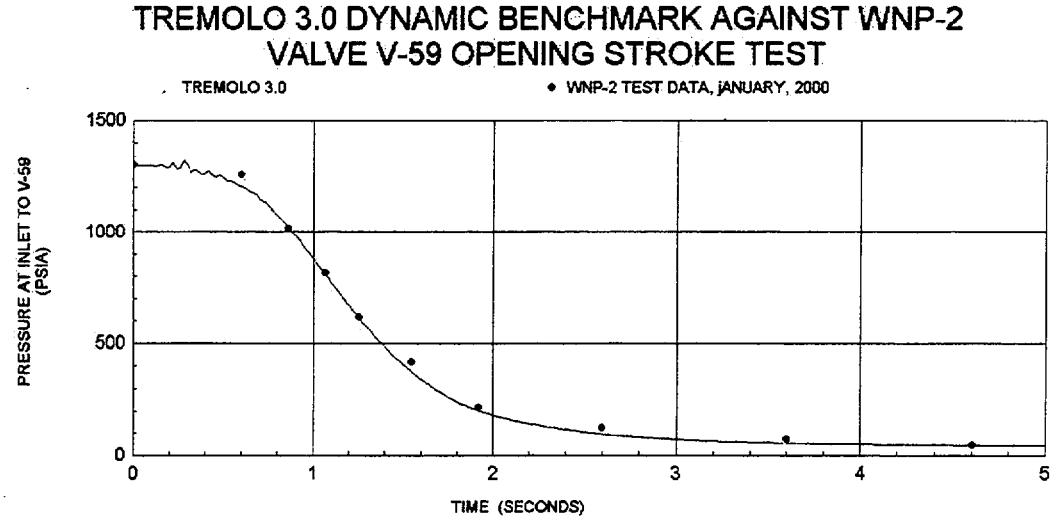

Figure 2. ***RCIC-V-59 Opening Stroke Benchmark.*** **Comparison of TREMOLO 3.0 calculations against DP test data collected in January 2000 for the Columbia Generating Station RCIC return line gate valve V-59. Valve stroke time is 12 seconds and opening stroke begins at time zero.**

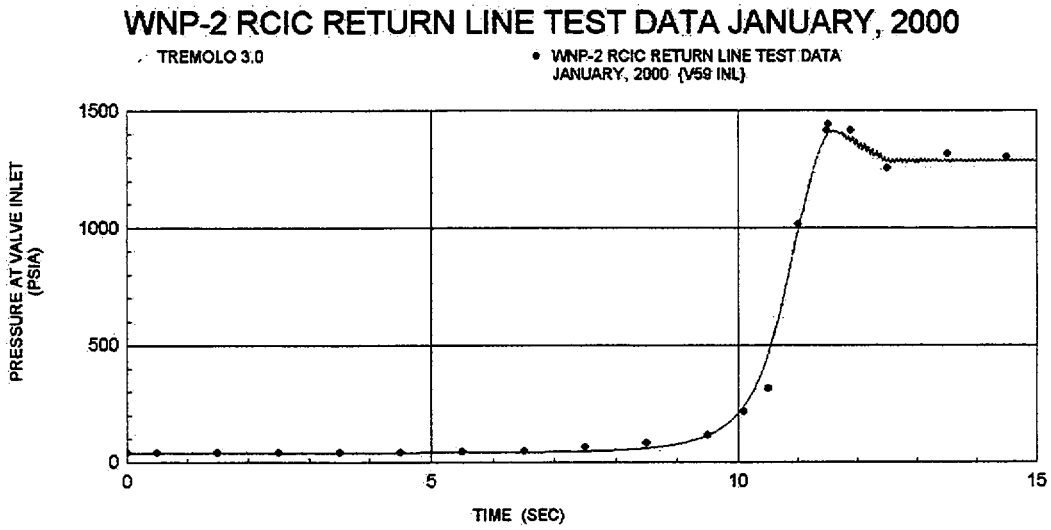

Figure 3. ***RCIC-V-59 Closing Stroke Benchmark.*** **Comparison of TREMOLO 3.0 calculations against DP test data collected in January 2000 for the Columbia Generating Station RCIC return line gate valve V-59. Valve stroke time is 12 seconds.**

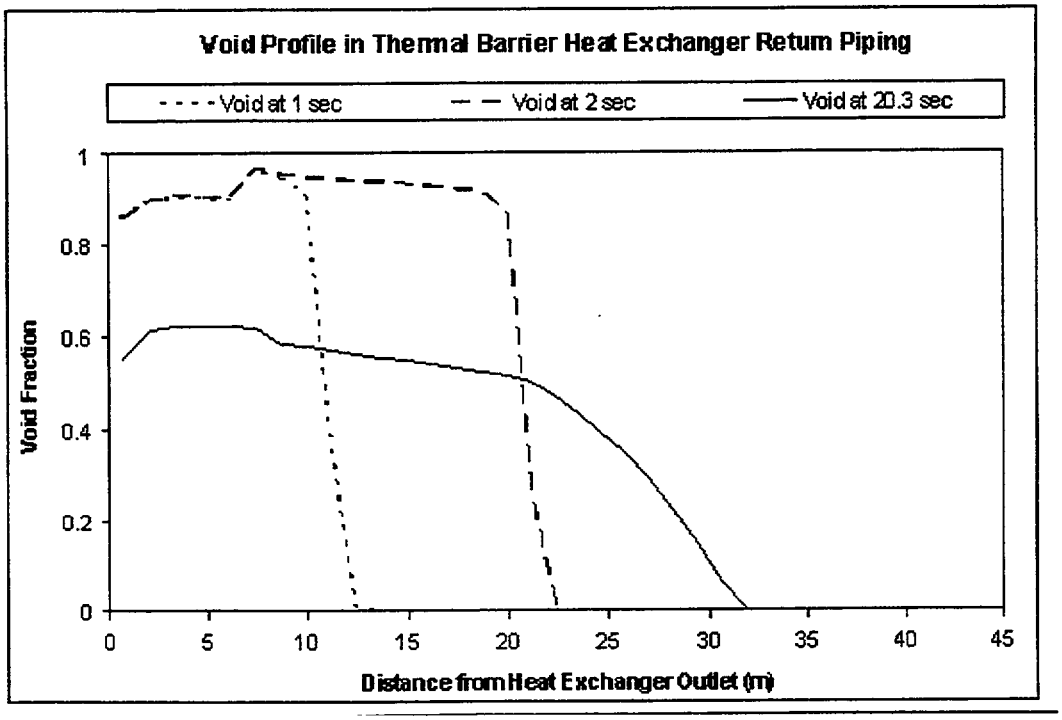

Figure 4. **EGHV337 Isolation Valve Axial Void profile at 1 sec, 2 sec, and 20.3 sec (time of valve closure). MOV is located 42 m from heat exchanger outlet.**

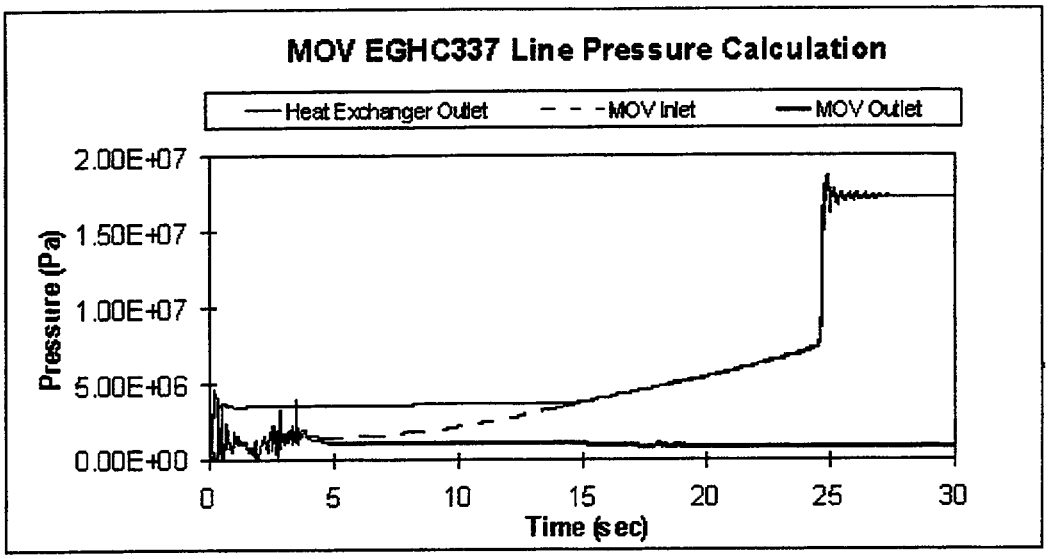

Figure 5. **EGHV337 Closing DP. MOV is closed at 21.3 seconds. MOV inlet pressure at time of valve closure: 5.92 MPa (856 psia). MOV outlet pressure at time of valve closure: 0.793 MPa (115 psia).**

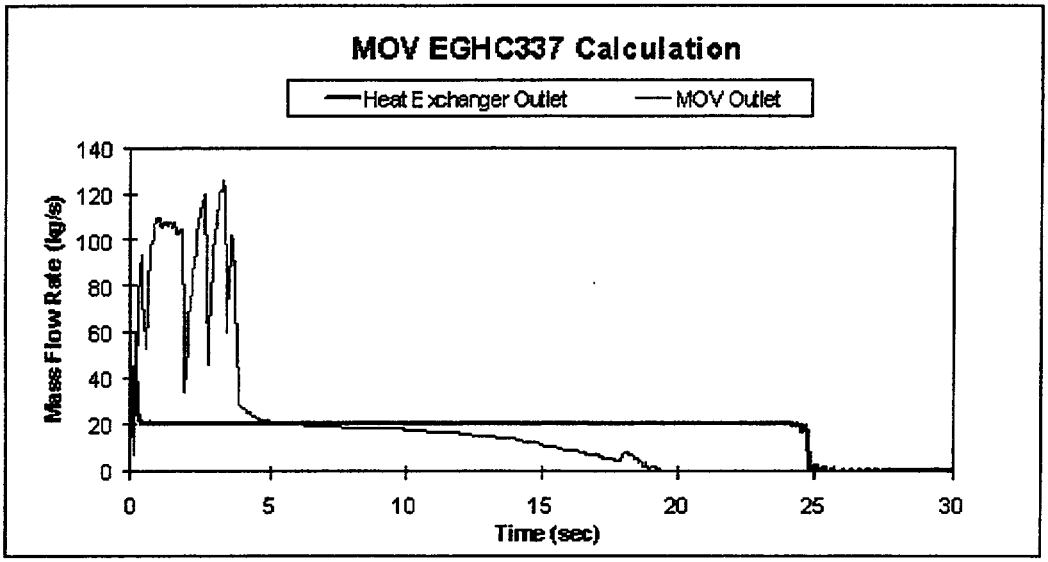

Figure 6. EGHV337 Mass flow rate. MOV is closed at 21.3 seconds.

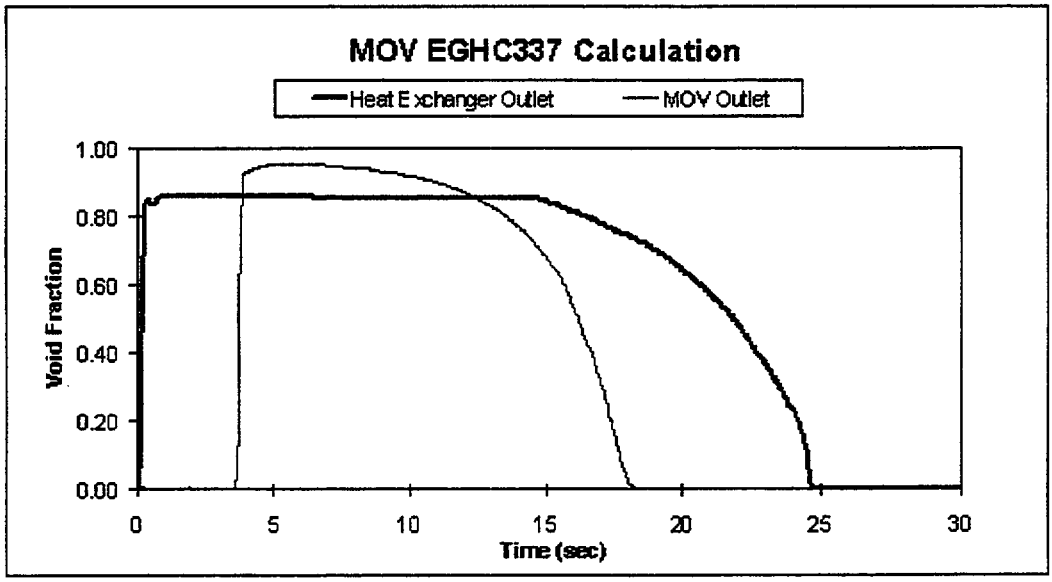

Figure 7. EGHV337 Void fraction rate. MOV is closed at 21.3 seconds.

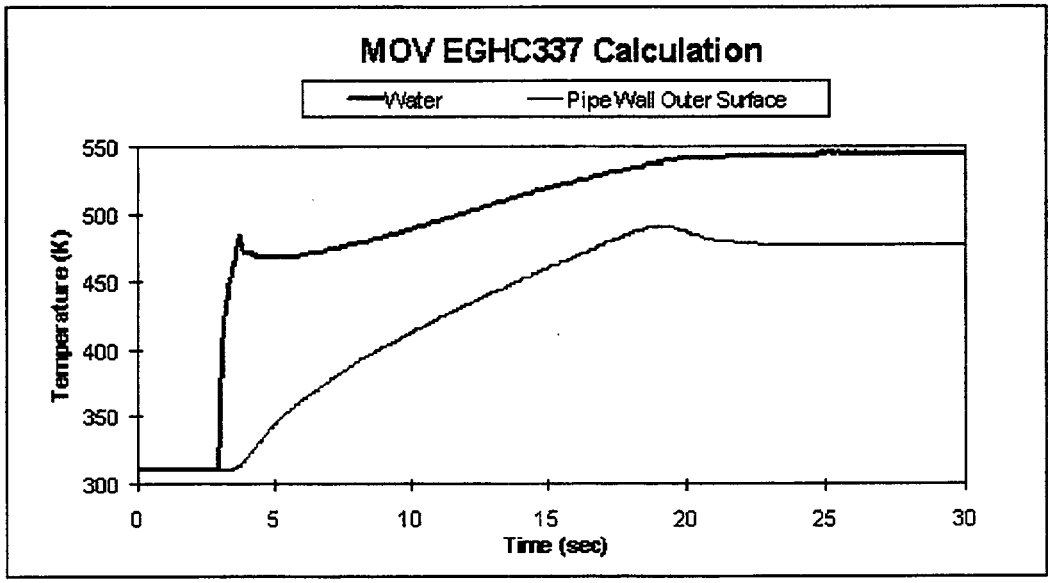

Figure 8. EGHV337 Water and pipe wall temperatures at MOV inlet. MOV is closed at 21.3 seconds.

MOV Configuration No. 1
BWR - RCIC Isolation Valve

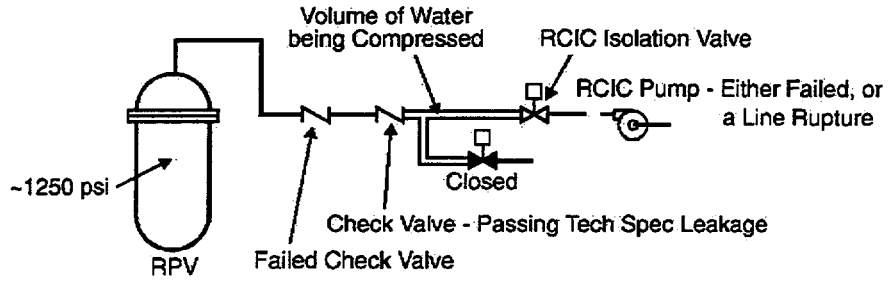

- MOV is required to close when RCIC pump fails
- Static analysis gave required $\Delta P_{CL} \approx 1250$ psi
- Dynamic calculation gave $\Delta P_{CL} < 200$ psi

Main Features

- Check Valve Leakage
- Water Compressibility
- Time Dependent MOV Hydraulic Resistance

TE946021.CDR 8-10-94

Figure 9. HPCI injection line transient analysis.

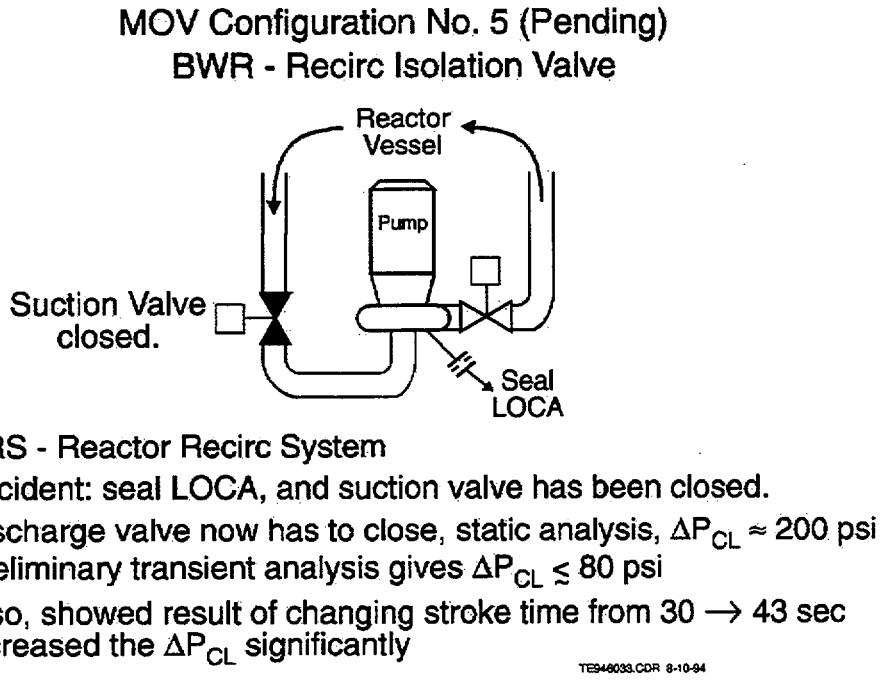

Figure 10. Reactor recirculation system isolation valve transient analysis following a pump seal leak.

Performance of MOV Stem Lubricants at Elevated Temperature

Kevin G. DeWall, John C. Watkins, and Michael E. Nitzel
Idaho National Engineering and Environmental Laboratory

Abstract

This paper documents the results of recent tests sponsored by the U.S. Nuclear Regulatory Commission (NRC) and performed by the Idaho National Engineering and Environmental Laboratory (INEEL). These tests address the effectiveness of the lubricant used on the threaded portion of the valve stem, where the stem nut turns on the stem. Recent testing indicates that an elevated temperature environment can lead to significant increases in the friction coefficient at the stem/stem-nut interface. Most valve actuator qualification tests are performed at room temperature. Similarly, in-service tests are run at ambient plant temperatures, usually in the 70 to 100°F range. Since design conditions can lead to valve operating temperatures in the 200 to 300°F range, it is important to know whether a temperature-induced increase in friction at the stem/stem-nut interface will prevent the operation of critical valves.

To evaluate elevated temperature performance, five different lubricants on four different valve stems and stem nuts were tested. The test series included collection of baseline data at room temperature, single step temperature tests where the temperature of the test setup was elevated directly to 250°F, and step testing where the temperature was elevated in steps to 130, 190, and 250°F, then returned to 70°F. This research produced the following conclusions:

- The physical characteristics of each lubricant change with increasing temperature, changing the frictional performance of each stem and stem nut.
- The consistency of the stem/stem nut coefficient of friction from one stroke to another changes significantly with increasing temperature.
- The stem/stem nut coefficient of friction can increase significantly at elevated temperature.
- The end of stroke friction behavior is highly dependent on the unique stem/stem nut tested, the lubricant, and temperature.
- Each individual stem and stem nut combination has unique characteristics with regard to variation between strokes, elevated temperature performance, and end of stroke friction behavior.

Introduction

During the past several years, the U.S. Nuclear Regulatory Commission (NRC) has supported research addressing the performance of motor-operated valves (MOVs) installed in nuclear power plants. This research included tests and analysis to determine the capability of safety-related MOVs to close (or open) when subjected to the conditions specified in the

plants' design documents. For some safety-related MOVs, these design basis conditions include high flow and pressure loads, high temperatures, and degraded voltage. This paper documents the results of recent tests sponsored by the NRC and performed by the Idaho National Engineering and Environmental Laboratory (INEEL) to address the effectiveness of the lubricant used on the threaded portion of the valve stem, where the stem nut turns on the stem. The effectiveness of this lubricant can impact the thrust output of the valve actuator and reduce the margin for ensuring the performance of the MOV. The research has recently been published in NUREG/CR-6750, "Performance of MOV Stem Lubricants At Elevated Temperatures," (Reference 1).

Background

In rising stem MOVs, the conversion of actuator output torque to a stem thrust load occurs at the stem nut, as shown in Figure 1. The ratio of actuator torque to stem thrust is generally referred to as the stem factor. For a specific valve stem and stem nut, the only variable in the conversion of torque to thrust is the coefficient of friction, as shown in the following power screw equation.

$$\frac{T_{output}}{Th_{stem}} = \frac{d\,(0.96815 \tan a + \mu)}{24\,(0.96815 - \mu \tan a)} \qquad (1)$$

where

T_{output} = The output torque of the valve actuator

Th_{stem} = The valve stem thrust

d = OD_{stem} - ½ Pitch

$\tan a$ = Lead/(πd)

μ = The stem/stem-nut coefficient of friction

OD_{stem} = The outside diameter of the stem

Pitch = The distance from the peak of one thread to the peak of an adjacent thread (inches/thread)

Lead = The distance the stem travels in one revolution of the stem nut (inches/stem revolution)

This equation is written for U.S. Customary units, where torque is in foot-pounds, thrust is in pounds force, and stem diameter and thread pitch and lead are in inches. The pitch is the distance from the peak of one thread to the peak of an adjacent thread (inches/thread). The lead is the distance the stem travels in one revolution of the stem nut (inches/stem revolution). As an example, if the configuration consists of two threads spiraling the stem instead of one, the lead is different from the pitch. (If only one thread spirals the stem, the pitch and the lead are the same.) The output torque consists of the torque delivered to the stem nut. The stem thrust is the thrust applied to the valve stem to move the stem and valve disc. The ratio of torque to thrust, shown in Equation (1), is the stem factor. The term *d* represents the mean diameter of the stem in terms of the thread contact area, treated as the midpoint of the depth of the thread. The design of Acme power threads is such that the depth of a single thread is equal to half the pitch, so *d* is equal to the outside diameter of the stem minus ½ the pitch (¼ the pitch on one side, and ¼ the pitch on the other side). The term tan *a* is the slope of the thread. The term *0.96815* is a constant in the Acme power thread equation, representing the cosine of half the thread angle (14.5 degrees for Acme threads). The value *24* (2 × 12) in the numerator represents the *d/2* calculation that provides the mean radius of the stem, combined with the conversion from inches to feet; stem measurements are in inches but torque values are in ft-lb.

TEST DESIGN

Test Equipment

The tests were conducted at the INEEL on the motor-operated valve load simulator (MOVLS), shown in Figure 2. The MOVLS is an instrumented test stand that provides dynamometer-type testing of valve actuators using load profiles that are very similar to the load profile a valve actuator would experience when closing a valve against a flow load. For elevated temperature testing and accelerated aging of the stem lubricant, the valve actuator was wrapped in heat tape and insulated so as to control the actuator, valve stem threads, and stem nut at the temperature required for testing of the stem nut lubricant. The design configuration allowed operation of the valve actuator without disturbing the heater or insulation. The following is a list of the major equipment used in the performance of this research.

- Limitorque SMB-0 actuator equipped with a Reliance 25 ft-lb 480V ac motor
- Limitorque SMB-1 actuator equipped with a Reliance 60 ft-lb 480V ac motor
- Stem 2, 1.750-inch-diameter, 1/4-pitch, 1/4-lead valve stem and stem nut
- Stem 3, 1.250-inch-diameter, 1/4-pitch, 1/2-lead valve stem and stem nut
- Stem 4, 2.000-inch-diameter, 1/3-pitch, 3/3-lead valve stem and stem nut
- Stem 5, 2.125-inch-diameter, 1/4-pitch, 1/2-lead valve stem and stem nut.

Instrumentation

During the testing of each stem/stem-nut combination, the temperature of the MOVLS components were monitored using eight thermocouples, strategically placed to allow monitoring of temperatures at various locations throughout the MOVLS. Each of the measurements was recorded at a rate of 600 samples per second by the data acquisition system whenever the actuator was operated. In addition, a chart recorder was used to track two of the temperature measurements throughout the test period.

Electrical measurements for the ac motors included the ac line current and voltage for each phase. Motor output torque and speed were measured using a torque cell and tachometer mounted between the motor and the gearbox. A torque arm attached to the valve stem measured the output torque of the gearbox, and an in-line load cell measured valve stem thrust. Other measurements included actuator torque switch trip, torque spring thrust and deflection, and valve stem position. Each of these measurements was recorded at a rate of 600 samples per second by the data acquisition system whenever the actuator was operated. Calibration of the load cells allows a measurement error ±60 lb. Calibration of the torque arm allows a measurement error of ±4 ft-lb for the small torque arm (Stems 2 and 3) and ±6 ft-lb for the large torque arm (Stems 4 and 5).

Lubricants Tested

Prior to each series of tests, the stem and stem nut were removed from the MOVLS and cleaned using a multi-step procedure to remove all traces of the prior lubricant. A fresh application of the next lubricant to be tested was then applied and the stem and stem nut were reinstalled into the MOVLS. Five lubricants commonly used in nuclear power plant MOVs were selected for testing. The lubricants tested were:

- Nebula EP1
- Chevron SRI

- Mobilgrease 28
- SWEPCO Moly 101
- LOCTITE High Performance N-5000 anti-seize

Test Matrix

Baseline tests were performed to provide data from MOVLS setup strokes and test strokes with the lubricant at ambient temperature. The tests were performed with the actuator torque switch set to produce a final stem force near the maximum allowed for the valve stem, the actuator, or the stem thrust and torque instrumentation, whichever was the limiting case. The level and pressure in the MOVLS accumulator was determined during the initial setup so that the running load was sufficient to produce a stem thread pressure that exceeded 10,000 pounds per square inch (psi) by the end of the stroke.

The elevated temperature tests consisted of two groups of tests. In the first group of tests, data at elevated temperature conditions of 250°F were collected for comparison with the baseline data. Following the 250°F tests, the actuator was allowed to cool down, and a final set of tests was performed at ambient temperature (70°F). The second group of elevated temperature tests was performed to investigate the temperature sensitivity of each lubricant by roughly identifying the temperature threshold at which the coefficient of friction departs from the baseline. This second group of tests was conducted by raising the valve actuator temperature in steps (130, 190, and 250°F) and performing five loaded strokes to acquire data at each step. Following the 250°F tests, the actuator was allowed to cool down, and a final set of tests was performed at ambient temperature (70°F).

RESULTS

Physical Observations

A number of photographs were taken to document the testing and the physical condition of the lubricants during the testing. These photographs are included in NUREG/CR-6750 (Reference 1). The following paragraphs provide general observations made during the testing and documented in these photographs.

Exxon Nebula EP1—We used new EP1 for these tests, rather than the old lubricant (shelf aged approximately 10 years) that had been in storage. As mentioned earlier, the old EP1 was the supply that provided the sample used in the earlier accelerated aging tests. With this grease and with the other greases, we applied a thick layer of the grease to the stem and then rotated the stem nut about the stem by hand to produce a thin uniform layer. A small bead of lubricant was allowed to remain on each end of the stem nut to ensure adequate supply was present to allow the stem to re-lubricate itself during valve strokes. (This is consistent with typical industry practices for stem lubrication.) After the testing was completed, the stem and stem nut were removed and the lubricant was inspected.

As a result of the testing, the Nebula EP1 lubricant had changed from a light tan color to brown and appeared to have hardened inside the stem nut. The grease returned to its original consistency by gently working the grease (rubbing a sample between our fingers). The test results show no change in the lubrication characteristics of this grease as a result of the testing.

Chevron SRI—As a result of the elevated temperature testing, the Chevron SRI grease changed from the original green to dark brown. The lubricant bead above the stem nut

and on the stem threads not worked during testing appeared to have hardened. The smear comparison, before and after testing, showed a change in color and consistency. A few days later, the oils in the grease had absorbed into the paper, approximately the same for each sample, indicating that the oil content remained consistent through the heat up and cool down.

Mobil Mobilgrease 28—This lubricant changed from a bright red color to almost black. Here again, the lubricant bead above the stem nut and on the stem threads not worked during the testing appeared to have thickened and hardened. The smear comparison, before and after testing, showed a change in color and consistency. A few days later, the absorption into the paper identified a changed after elevated temperature testing. The radius of absorption for the heated grease was about one half of that for the untested grease. The color of the oils being absorbed into the paper had also changed.

SWEPCO Moly 101—The Moly 101 did not appear to change as a result of the elevated temperature testing. A slight thickening of the grease was observed in the stem threads above and below the normal travel of the stem through the stem nut. We observed no difference in the before and after smear sample color, consistency, or absorption into the paper. No difference in the two samples was evident.

LOCTITE N-5000 Anti-Seize —The LOCTITE N-5000 anti-seize was also applied to the valve stem in an even, thin coat. After testing, the anti-seize had moved away from the threaded area, running down the stem. The N-5000 also separated, with the silver component running down the stem in a separate stream from the clear component. A very clear difference was observed in the lubrication layer on the bottom of the stem, which is the section being cycled during the test, and the layer on the top of the stem that had not been worked. Above the stem nut, the N-5000 looked the same as it did when it was originally applied. The anti-seize had also dripped from the stem nut onto the torque arm, again showing separation of the clear and silver components. This separation was clearly shown in the smear test.

Consistency Among Strokes

In order to make a consistent evaluation of the effects of different stems, lubricants, and temperatures on the friction coefficient, we chose to make this evaluation based on the performance observed at the end of the valve stroke, just prior to full seat contact. For a gate valve, this position is sometimes referred to as "at wedging." This analysis will take a single value for the stem nut coefficient of friction calculated from the average stem thrust and average stem torque based on the 200 data points (about 1/3 second) just prior to full seat contact. The figures discussed in the following sections will contain groups of five of these average stem nut friction values, one for each of the five valve strokes run at each test temperature.

Exxon Nebula EP1—Figure 3 contains the stem-nut coefficient of friction performance for the single step tests (70°F to 250°F and then back to 70°F) and includes data for each of the four stems tested. For both Stem 2 and Stem 3, the initial cold test data show a lower stem nut friction (4% and 8% respectively) in the first stroke than in subsequent strokes. The other four strokes operated at essentially the same stem nut friction value. This low first stroke characteristic did not appear on the hot tests (middle data sets); however, Stem 2 appeared to have greater scatter among the hot strokes. The Stem 2 coefficient of friction

increased for the final cold tests while Stem 3 returned to earlier cold performance, repeating the lower first stroke behavior. Stem 5 exhibited behavior similar to that of Stem 3.

Stem 4 is also shown in Figure 3 and shows very unique behavior. The coefficient of friction for the initial cold test starts very low at 0.086 and increases with each stroke to 0.124. The hot tests are stable, showing no increasing with stroke but running at values similar to the fifth stroke of the initial cold test. The final cold tests begin at the hot test value and increase dramatically with each stroke, ending at a very high value of 0.159. Figure 4 shows similar data for the incremental temperature step tests (70°F to 130°F to 190°F to 250°F and then back to 70°F). The performance of each of the four stems is similar to that shown in Figure 3. Stem 4 continues to exhibit large increases in stem nut coefficient of friction in the cold tests, but stable values in the each hot test. Similarly, Stem 2 shows greater scatter in the hot tests.

Chevron SRI—The Chevron SRI cold baseline test shows good repeatability among the five strokes, as shown in Figure 5. As the temperatures increase, more variability is evident among the five strokes, with the first being the lowest and increasing with each additional stroke. This trend reverses after cool down, where the first stroke can be 5 to 10% higher.

As with the Nebula EP1, Stem 2 with Chevron SRI has more scatter between tests at high temperature. Figure 5 contains two data sets for Stem 2, the first being the aging test series and the second being the single step elevated temperature test. During the 250°F tests, the Stem 2 coefficient of friction was basically the same for the first three strokes.

Figure 6 shows data for the incremental temperature step tests with Chevron SRI. The data shows good repeatability among each set of five strokes and more variability at elevated temperature. The coefficient of friction increases with each stroke at 130°F and 190°F. At 250°F, Stem 5 continues to increase with each stroke, but Stems 3 and 4 exhibit a higher first stroke with stable and slightly lower values for the second through the fifth strokes. Once again, the trend reverses after cool down, where the first stroke was 5% to 10% higher.

Mobil Mobilgrease 28—The Mobil Mobilgrease 28 cold baseline test shows good repeatability among the five strokes, as shown in Figure 7, with the exception of the first test series using Stem 4. The first cold baseline tests with Stem 4 and Mobilgrease 28 saw a significant increase in the stem nut coefficient of friction over the five strokes; however, we also observed that the actual values were extremely low (running from 0.03 to 0.05). Because the values were so low, the tests were repeated with a new coating of the Mobilgrease. This second set of tests (identified as Stem 4B) performed similarly to the other stems and the increase observed earlier had disappeared. Once again, Stem 2 has more scatter between tests at high temperature. Figure 7 shows that the stem nut coefficient of friction for Stem 2 at 250°F exhibits wide and random variations between 0.128 and 0.144. All stems show good repeatability during the final cold tests.

Figure 8 shows data for the incremental temperature step tests with Mobilgrease 28. Once again, we see the first cold baseline tests beginning at very low values for the stem nut coefficient of friction, while the second cold baseline tests are closer to that observed for the other stems. Figure 8 also shows that Stem 2 is very repeatable until the 190°F test.

SWEPCO Moly 101— Figure 9 contains the stem-nut coefficient of friction performance for the single step tests for SWEPCO Moly 101. Stems 2, 3, and 5 show very good repeatability over the five initial cold strokes, but Stem 4 begins very low and increases with each stroke, from 0.075 to 0.099. At 250°F, Stem 4 becomes stable over five strokes but Stems 2 and 5 show wide variations, 0.149 to 0.173 and 0.141 to 0.180 respectively. In the final cold tests, all four stems returned to earlier cold performance, repeating the lower first stroke behavior. Stem 4 exhibited a slight increase with each of the five strokes, but much less variation than in the initial cold tests.

Figure 10 shows similar data for the incremental temperature step tests. The performance of each of the four stems is similar to that shown in Figure 9, except that the Stem 4 strokes began at a higher stem nut coefficient of friction and were stable during the five initial cold strokes.

LOCTITE N-5000 Anti-Seize—The LOCTITE N-5000 Anti-Seize cold baseline tests show large variations among the five strokes, as shown in Figure 11. As the temperatures increase, more variability is evident among the five strokes for some stems (Stem 3 and Stem 5) but others show more stability (Stem 2 and Stem 4). After cooldown, the performance of each stem is similar to its cold baseline performance.

Once again, Stem 4 exhibits unique behavior. In both the initial cold baseline test and the final cold test, the stem nut coefficient of friction increases dramatically from the first stroke to the second stroke. From the first stroke to the second stroke in the final cold test, the coefficient of friction increased from 0.138 to 0.183, or a 33% increase. Values continue to increase with the third stroke to very high values (0.191 in the third final cold stroke) then decrease with the fourth and fifth strokes.

Figure 12 shows data for the incremental temperature step tests with LOCTITE N-5000. The performance of all four stems is similar to that shown in Figure 11. The data show large variations among the five strokes for many tests. Often the first stroke is very low when compared with subsequent strokes, as seen in the Stem 5 data and several tests with Stems 3 and 4. In contrast, the Stem 2 coefficient of friction begins high in many cases, as does Stem 3 in the 130°F test.

Change With Temperature

The figures in the preceding section of this paper also provide insights into the overall effect that elevated temperature has on each stem and lubricant. However, the variations from stroke to stroke for each test sometimes makes it difficult to clearly see the real temperature effect. This section of the paper provides an evaluation of the relationship between temperature and stem nut coefficient of friction using single values for each test. The single values are obtained by simply averaging each set of five strokes from Figures 3 through 12. The figures found in the following discussion show this average stem nut coefficient of friction plotted as a function of temperature for Stem 2. The figures also include a linear fit through those data points to help visualize the relationship. These figures are typical of the performance of the full data set of four stems and five lubricants. A complete set of figures for each stem and lubricant combination tested can be found in Reference 1.

Table 1 contains a summary of this analysis, and provides the 70°F and 250°F coefficient of friction values based on this linear fit. It also provides the percent change over the

Table 1. Change in stem/stem-nut coefficient of friction with temperature.

		Exxon Nebula EP1	Chevron SRI	Mobil Mobilgrease 28	SWEPCO Moly 101	LOCTITE N-5000
Stem 2	Stem μ - 70°F	0.128	0.118	0.112	0.116	0.133
	Stem μ - 250°F	0.127	0.149	0.142	0.164	0.162
	Percent Δμ	-0.6%	26.6%	26.8%	41.6%	21.9%
Stem 3	Stem μ - 70°F	0.105	0.103	0.097	0.103	0.111
	Stem μ - 250°F	0.102	0.120	0.100	0.120	0.099
	Percent Δμ	-2.8%	16.5%	3.1%	16.5%	-10.8%
Stem 4	Stem μ - 70°F	0.123	0.098	0.085	0.102	0.163
	Stem μ - 250°F	0.116	0.129	0.103	0.127	0.120
	Percent Δμ	-5.9%	32.1%	19.3%	24.7%	-35.4%
Stem 5	Stem μ - 70°F	0.120	0.109	0.106	0.103	0.128
	Stem μ - 250°F	0.113	0.135	0.122	0.137	0.140
	Percent Δμ	-7.2%	24.7%	15.0%	32.7%	9.4%

same temperature range. The negative values for percent change for all stems with the Nebula EP1 and for Stems 3 and 4 with the N-5000 indicate cases where the stem nut coefficient of friction decreased at elevated temperatures.

Exxon Nebula EP1—An overview of the data shown previously in Figures 3 and 4 show no general increase in stem nut friction at elevated temperature. Figure 13 shows the relationship between temperature and stem nut coefficient of friction using single values for each test of Stem 2 with Nebula EP1. The linear fit through the data points indicates a decrease in stem nut friction as temperatures increase. This was also true for Stems 3, 4, and 5 as well, as seen in Table 1. Recall from the previous section that the Nebula EP1 grease was also more stable with less data scatter and less influence of multiple strokes at elevated temperature than it was at cold conditions.

Chevron SRI—The data shown previously in Figures 5 and 6 indicated that temperature has a strong influence on stem nut friction for Chevron SRI. Figure 14 shows this increase for Stem 2. The linear fit through the data points shows a significant increase from 70°F to 250°F of 26.6% for Stem 2. Stem 4 saw the largest increase at 32.1%.

Mobil Mobilgrease 28—Figures 7 and 8 show that elevated temperature has a strong influence on the stem nut coefficient of friction for the Mobilgrease 28 for some stems and under some conditions. All stems show increases in friction during the single step tests. But during incremental step tests, Stem 2, the first Stem 4, and Stem 5 have increasing coefficients of friction. (Recall that Stem 4 testing was repeated due to the unusual performance in the first test series.) Stem 3 and the second Stem 4 show essentially no change with temperature. Stem 2 saw the largest increase with Mobilgrease 28, increasing 26.8% from 70 to 250°F.

SWEPCO Moly 101—The data shown previously in Figures 9 and 10 show that the SWEPCO Moly 101 has a strong stem nut coefficient of friction increase with temperature for all stems tested. The linear fit through the data points shows a significant increase from 70° F to 250°F for Stem 2 of 41.6%. Stems 5, 4, and 3 followed at 32.7%, 24.7%, and 16.5% increase, respectively.

LOCTITE N-5000 Anti-Seize—The data in Figures 11 and 12 show that temperature has a strong influence on the stem nut coefficient of friction for the LOCTITE N-5000 Anti-Seize for some stems and under some conditions. Stem 2 and Stem 5 show increases in friction during the single step tests, but Stem 3 and Stem 4 show decreases. During incremental step tests, Stem 3 and Stem 5 coefficients of friction do not change with temperature, while Stem 2 increases as temperature increases and Stem 4 decreases. As shown in Figure 12, Stem 2 with the N-5000 Anti-Seize experienced a strong coefficient of friction increase from 70 to 250°F, but with large variations during intermediate temperature steps. The friction actually became lower with the first step to 130°F.

Change In End of Stroke Friction Behavior (ESFB)

Our evaluation of the change in stem nut friction at the end of valve travel will look at the total change from full seat contact to the final stem position. To differentiate between this type of analysis and the more common rate-of-loading analysis, we shall refer to the MOV's end of stroke friction behavior (ESFB). In the following discussion we will compare the ESFB observed in the baseline cold tests with the ESFB observed at elevated conditions. This analysis will use a single value for the stem nut coefficient of friction, based on the last 200 data points (about 1/3 second) prior to full seat contact, and compare that to the average coefficient of friction based on the final loads (after torque switch trip).

A change in ESFB performance is not of great concern for closing an MOV since it occurs after the valve has seated. Recall that rate-of-loading or load-sensitive behavior deals with the same phenomena but focuses on torque switch setting under low load, ambient temperature conditions. An increase in ESFB means lower stem nut friction at the end of stroke and higher final stem thrusts. This could challenge MOV structural limits and greatly increase the unwedging thrust required to open an MOV. A decrease in ESFB reduces the final stem thrust, but might also reduce the thrust available to unwedge the MOV in the opening direction.

Table 2 provides a summary of this analysis and provides the average ESFB for the single step elevated temperature tests. It also provides the ESFB as a percent change based on the coefficient of friction prior to full seat contact.

Exxon Nebula EP1—Each of the four stems exhibited a drop in the ESFB from the initial cold test to the hot test, and then a return to the higher value after cooldown. The stems with more extreme ESFB also show the largest change in ESFB with elevated temperature. Stem 4 had the highest ESFB, beginning at 68%, meaning that the final friction was 68% lower than the running friction. At hot conditions, the ESFB dropped to 51%. Stem 3 was also high at a cold value of 51% and 25% hot. Stems 2 and 5 have lower initial ESFB at 28% and 31%, respectively. At 250°F, the ESFB for Stems 2 and 5 drops to 17% and 23%, respectively.

Chevron SRI—The ESFB performance of the four stems is quite different with Chevron

Table 2. Change in end of stroke friction behavior (ESFB) with temperature.

		Exxon Nebula EP1		Chevron SRI		Mobil Mobilgrease 28		SWEPCO Moly 101		LOCTITE N-5000	
		ESFB	% ESFB	ESFB	% ESFB	ESFB	% ESFB	ESFB	% ESFB	ESFB	% ESFB
Stem 2	**Initial Cold, 70°F**	0.037	28%	-0.002	-2%	0.004	4%	0.009	7%	0.029	21%
	Hot Test, 250°F	0.021	17%	0.030	18%	0.039	28%	0.028	17%	0.009	5%
	Final Cold, 70°F	0.039	30%	0.004	4%	0.009	8%	0.006	5%	0.037	25%
Stem 3	**Initial Cold, 70°F**	0.056	51%	0.022	20%	0.018	17%	0.022	20%	0.042	34%
	Hot Test, 250°F	0.030	25%	0.017	12%	0.002	2%	0.011	9%	0.024	20%
	Final Cold, 70°F	0.062	52%	0.024	22%	0.022	21%	0.021	19%	0.051	38%
Stem 4	**Initial Cold, 70°F**	0.071	68%	0.056	71%	0.023	22%	0.073	83%	0.067	40%
	Hot Test, 250°F	0.062	51%	0.053	46%	0.017	15%	0.059	50%	0.026	23%
	Final Cold, 70°F	0.083	59%	0.061	62%	0.027	27%	0.075	73%	0.052	30%
Stem 5	**Initial Cold, 70°F**	0.036	31%	0.020	19%	0.032	32%	0.031	31%	0.023	20%
	Hot Test, 250°F	0.027	23%	0.009	7%	0.024	19%	0.028	19%	0.020	14%
	Final Cold, 70°F	0.037	31%	0.021	19%	0.033	32%	0.028	26%	0.021	16%

SRI. Once again Stem 4 is very high during the cold tests with 71% ESFB in the initial cold test and 62% in the final. The hot test ESFB drops to 46%. Stem 3 is no longer high but instead performs very close to Stem 5. The ESFB performance of both Stems 3 and 5 drops during the hot tests. Stem 2 exhibits ESFB performance where the temperature influence is reversed. Stem 2 begins with a slightly negative ESFB and increased with elevated temperature.

Mobil Mobilgrease 28—The ESFB performance of the four stems is once again unique when tested with the Mobilgrease 28 lubricant. Stem 4 no longer has the highest ESFB performance, dropping from 68% and 71% for Nebula EP1 and Chevron SRI to 22% in the initial cold tests. Stem 5 is now the highest stem at 32% and drops to 19% at elevated temperature. Stem 3 has also moved to a much lower position, beginning at 17% in the cold test and dropping to almost zero in the hot test. Once again, Stem 2 exhibits ESFB performance where the temperature influence is reversed. Stem 2 begins with only 4% ESFB and increases dramatically to 28% with elevated temperature.

SWEPCO Moly 101—The performance of the four stems with Moly 101 is very similar to the performance of each stem with Chevron SRI except that Stem 5 is now a little higher than Stem 3. Once again Stem 4 is very high

during the cold tests with 83% ESFB in the initial cold test and 73% in the final. The hot test ESFB drops to 50%. Stem 3 is no longer high but instead performs very close to Stem 5. The ESFB performance of both Stems 3 and 5 drops during the hot tests. Stem 2 exhibits ESFB performance where the temperature influence is reversed. Stem 2 begins with a low ESFB and increased with elevated temperature.

LOCTITE N-5000 Anti-Seize—The ESFB performance of the four stems is much more consistent when tested with the N-5000 Anti-Seize. Stem 4 no longer has extremely high ESFB performance, dropping values very similar to Stem 3. Stem 4 remains highest stem at 40% and drops to 23% at elevated temperature. Stem 3 exhibits similar performance, beginning at 34% in the cold test and dropping to 20% in the hot test.

Stem 5 shows little change in its ESFB. It ranges from 20% to 14% for the initial cold test and the hot test, and returns to 16% in the final cold test. The Stem 2 ESFB performance is no longer opposite to that of the other stems. It begins at 21% ESFB and drops to almost zero with elevated temperature.

CONCLUSIONS

This research effort was performed to address the effectiveness of the lubricant used on the threaded portion of the valve stem. The effectiveness of this lubricant can greatly impact the thrust output of the valve actuator and reduce the margin for ensuring MOV performance at design basis. Our analysis looked at the performance of five lubricants on four stem and stem nut combinations. The following conclusions are based on this work.

- The physical characteristics of each lubricant change at elevated temperature. Some lubricants thicken while others thin, allowing the lubricant to move away from loaded surfaces. Some lubricants lose their oily components.
- The repeatability of the stem friction coefficient over multiple strokes depends upon the unique stem/stem nut and lubricant combination. Large variations in stem friction can occur between strokes. Complete breakdown of the stem lubrication can occur.
- Operation at elevated temperature can have a significant effect on the stem coefficient of friction. For many of the stem, stem nut, and lubricants, large increases in stem nut friction occurred. Some lubricants showed no effect and some stem/stem nut combinations produced decreasing friction.
- The value and the direction of change in the end of stroke friction behavior (ESFB) is highly dependent on the stem/stem nut and lubricant being tested.
- Each individual stem and stem/nut combination has unique characteristics with regard to the repeatability of the stem friction coefficient over multiple strokes, the elevated temperature performance, and the ESFB.
- Lubricant aging can cause the stem/stem nut coefficient of friction to increase.

REFERENCES

1. K. G. DeWall, et al, "Performance of MOV Stem Lubricants at Elevated Temperature," NUREG/CR-6750, INEEL/EXT-01-00816, United States Nuclear Regulatory Commission, October 2001.

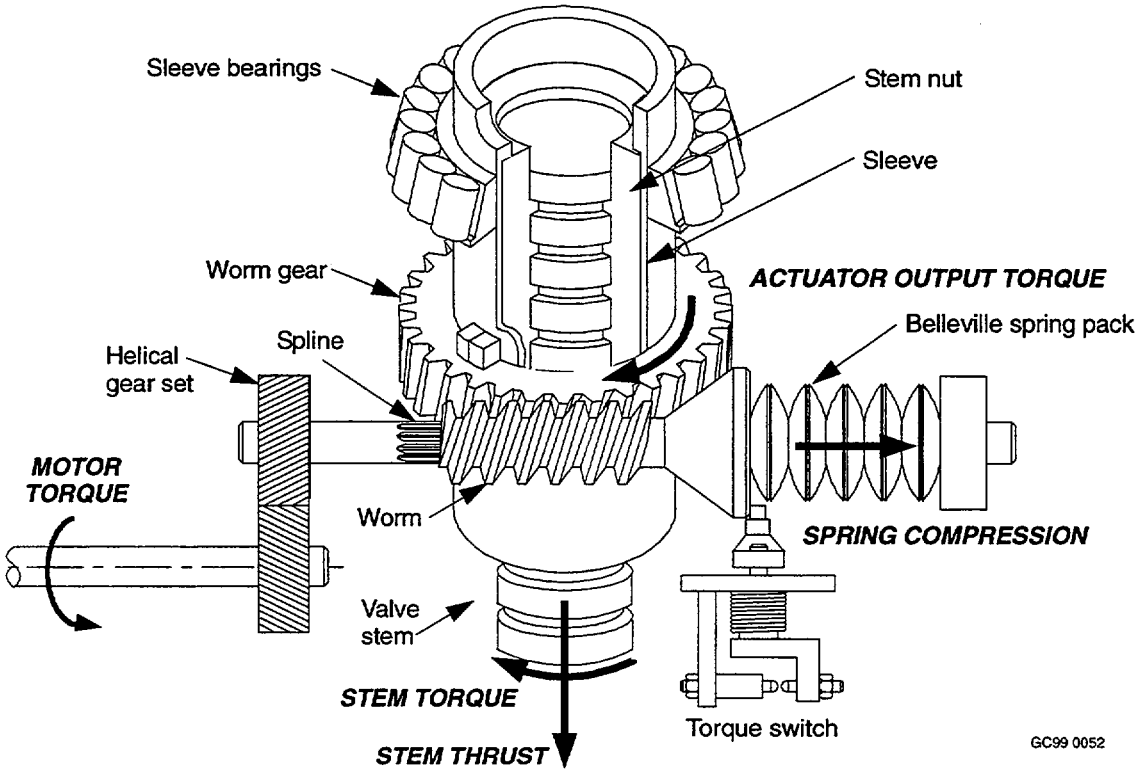

Figure 1. MOV actuator gearbox diagram.

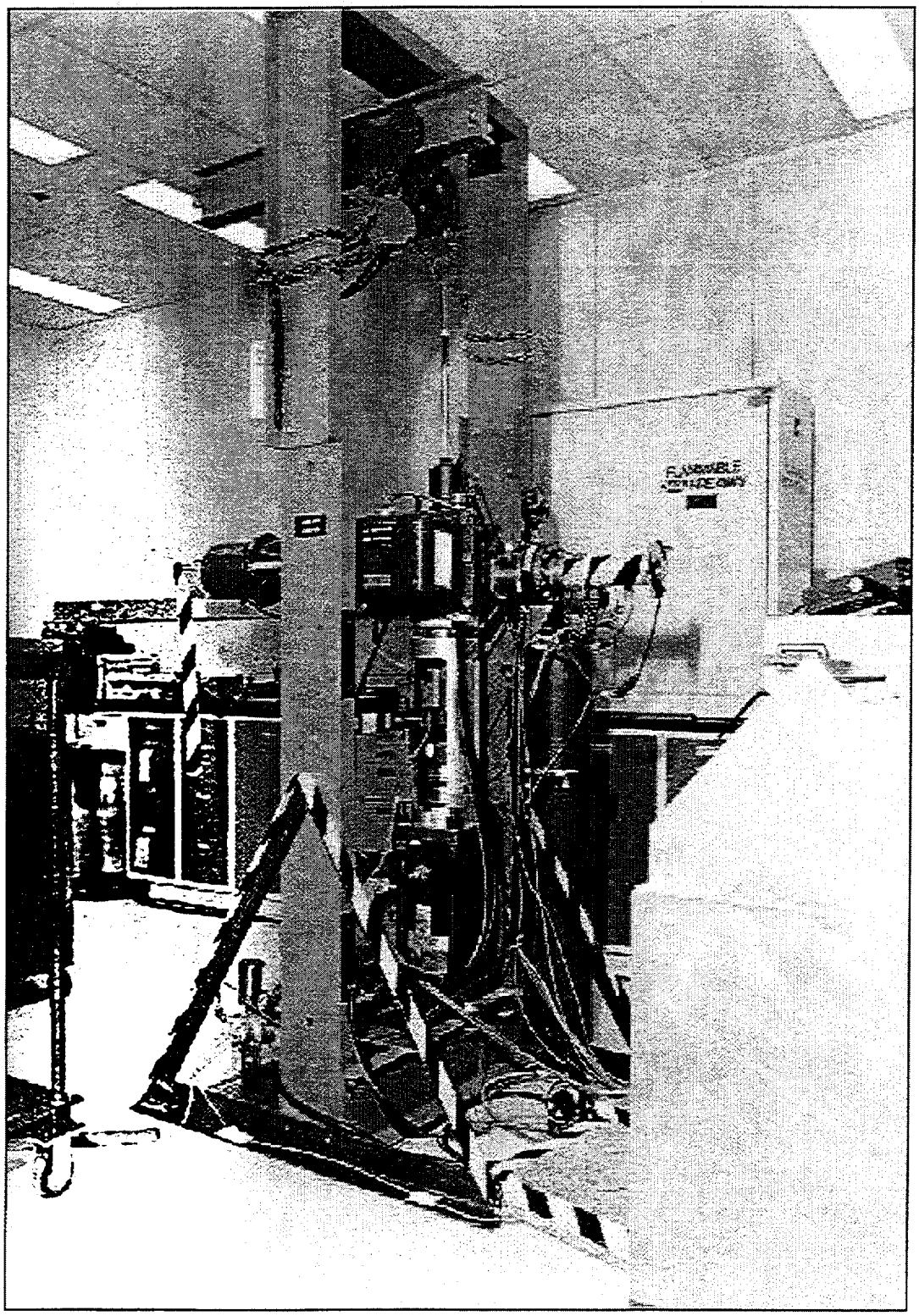

Figure 2. INEEL motor operated valve load simulator (MOVLS).

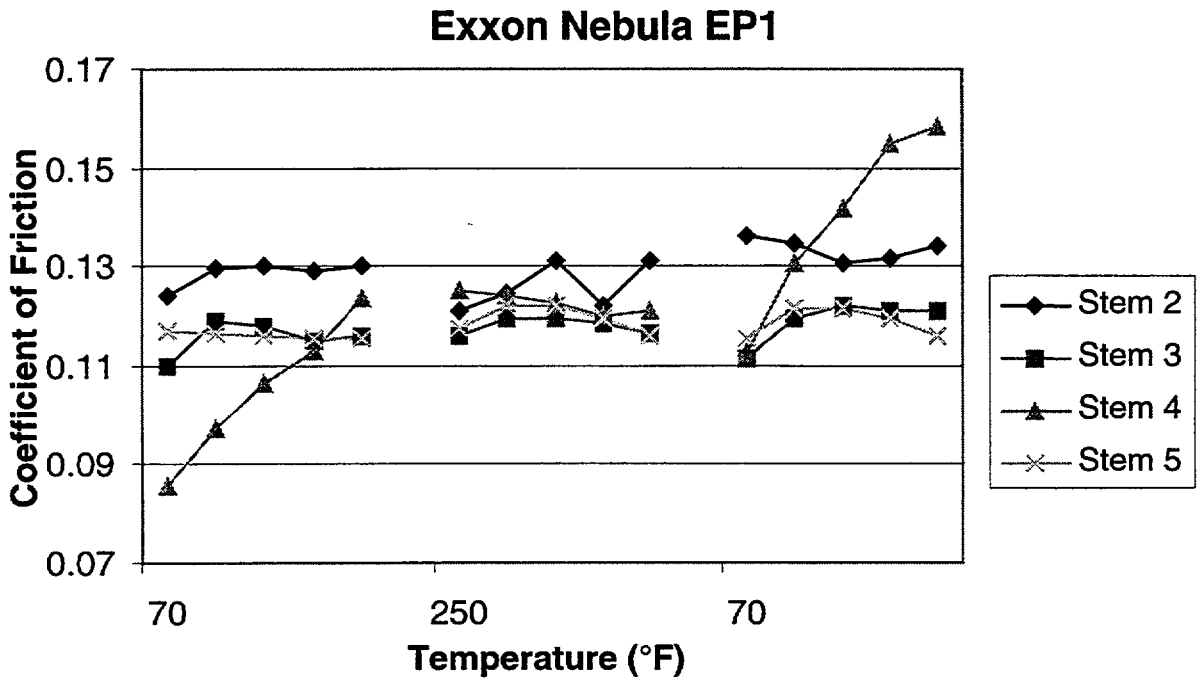

Figure 3. Stem nut coefficient of friction for each stroke of the single step tests with EP1.

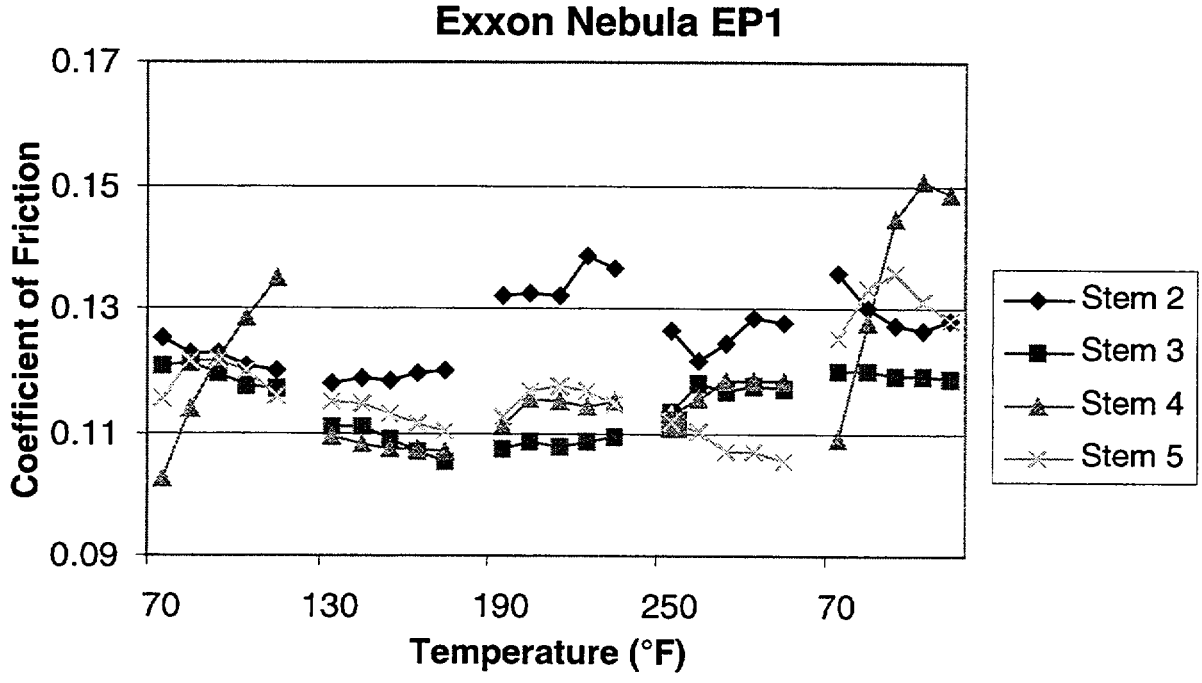

Figure 4. Stem nut coefficient of friction for each stroke of the multiple step tests with EP1.

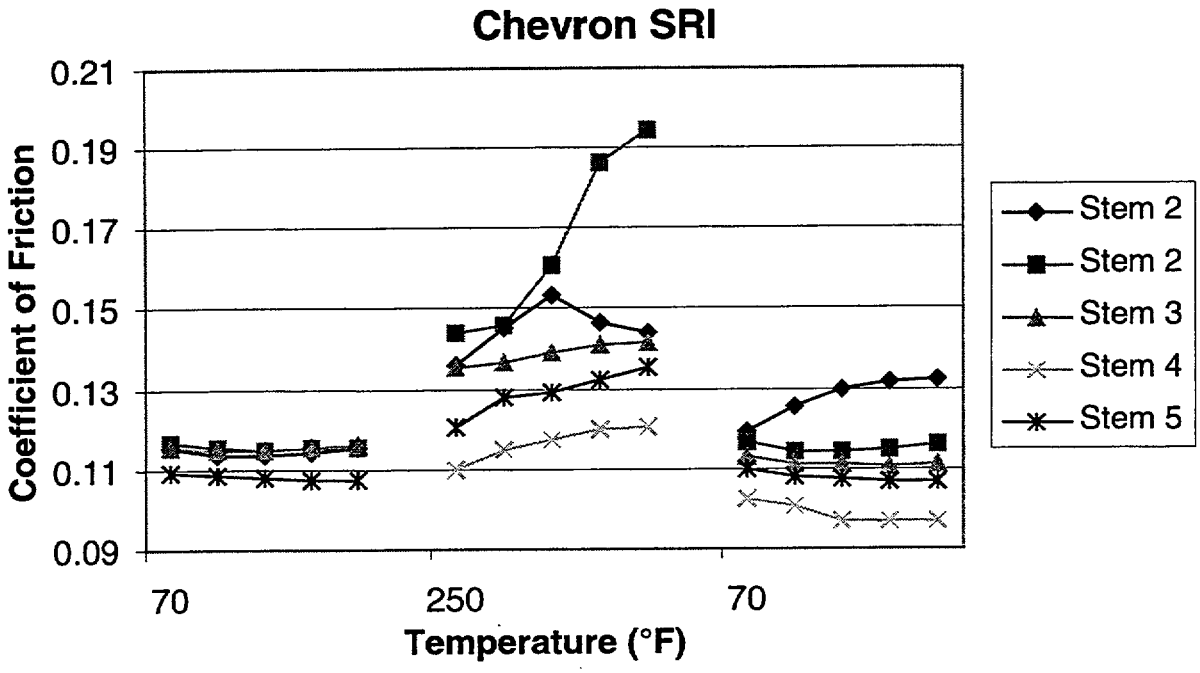

Figure 5. Stem nut coefficient of friction for each stroke of the single step tests with SRI.

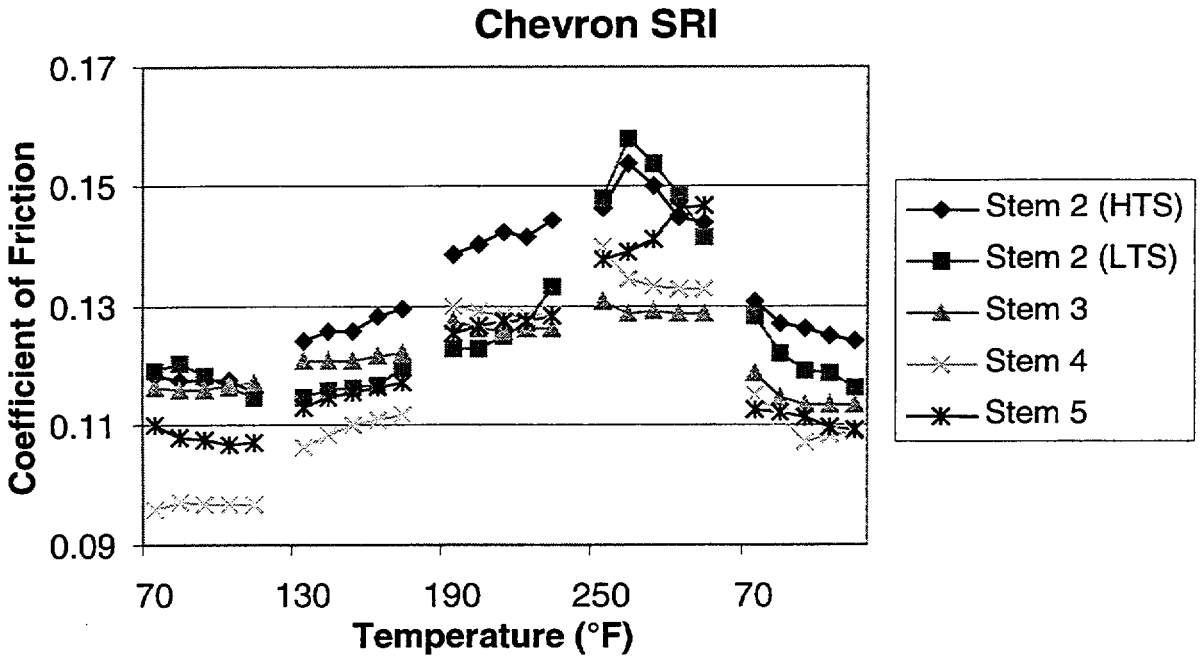

Figure 6. Stem nut coefficient of friction for each stroke of the multiple step tests with SRI.

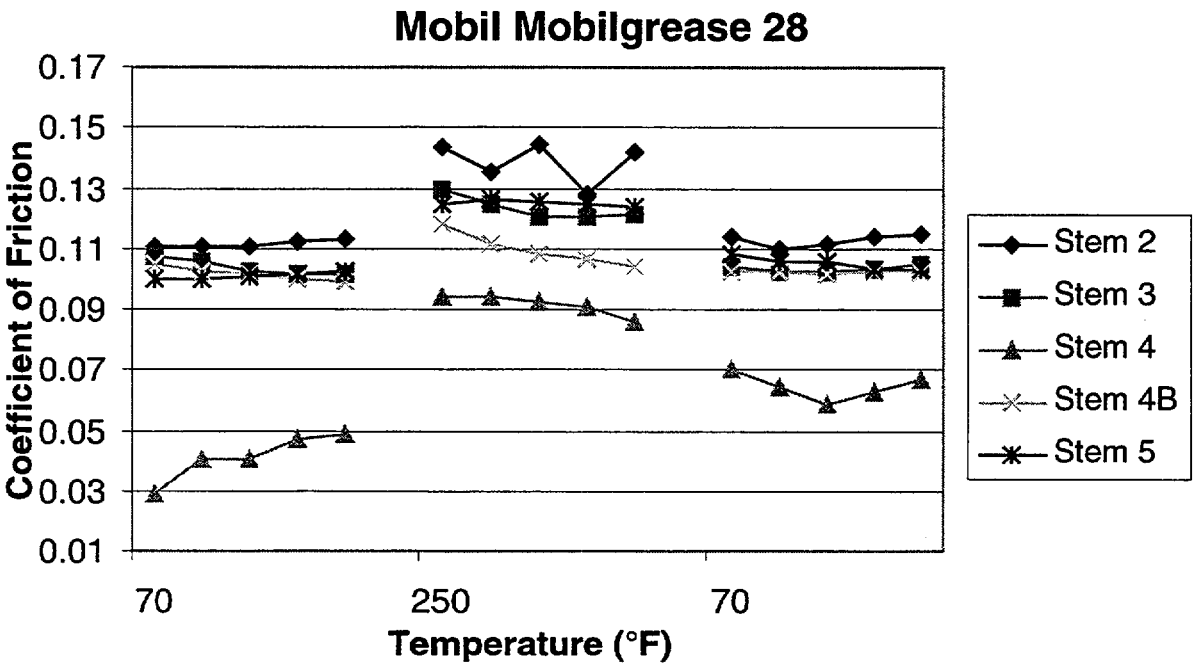

Figure 7. Stem nut coefficient of friction for each stroke of the single step tests with Mobil 28.

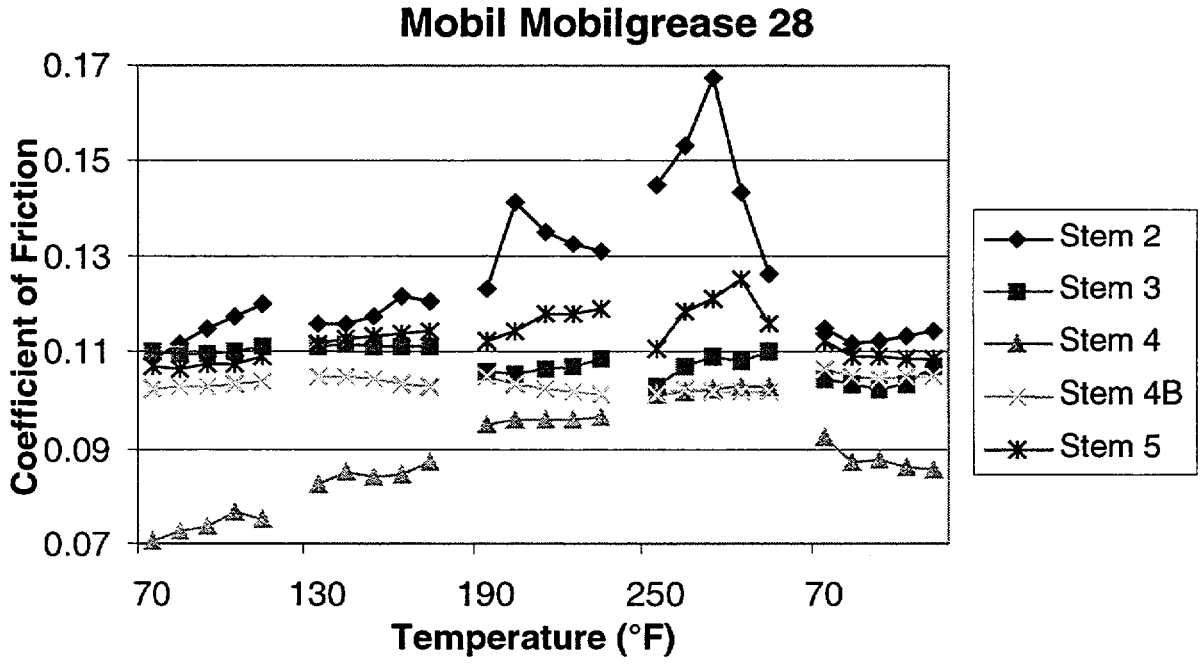

Figure 8. Stem nut coefficient of friction for each stroke of the multiple step tests with Mobil 28.

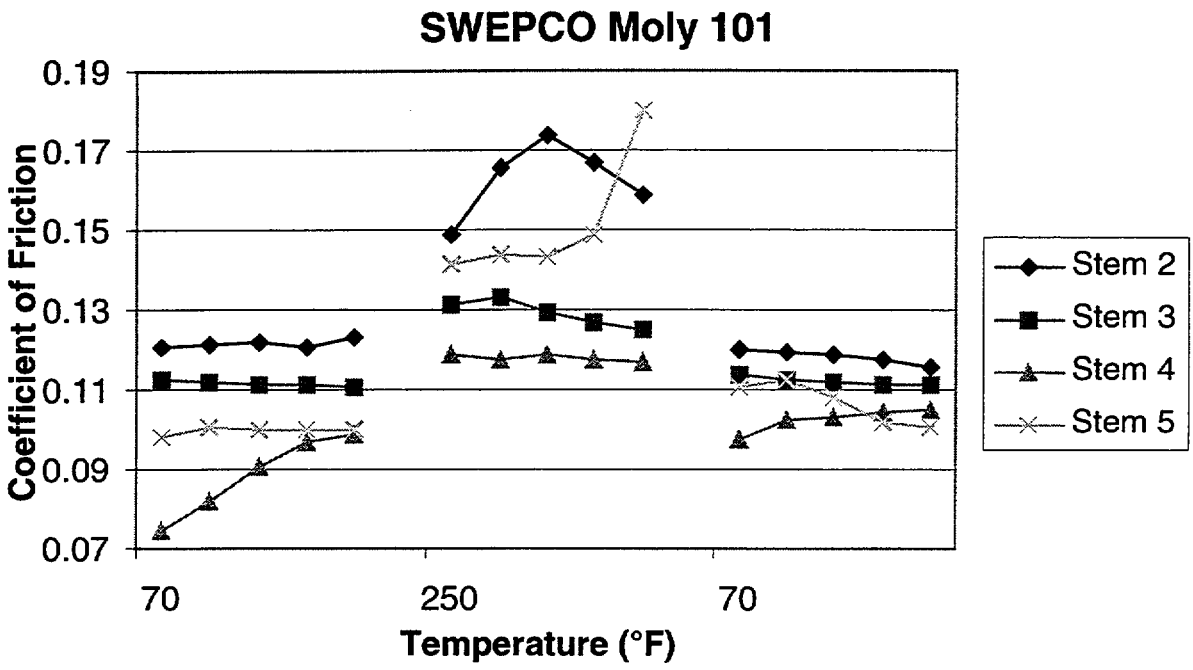

Figure 9. Stem nut coefficient of friction for each stroke of the single step tests with Moly 101.

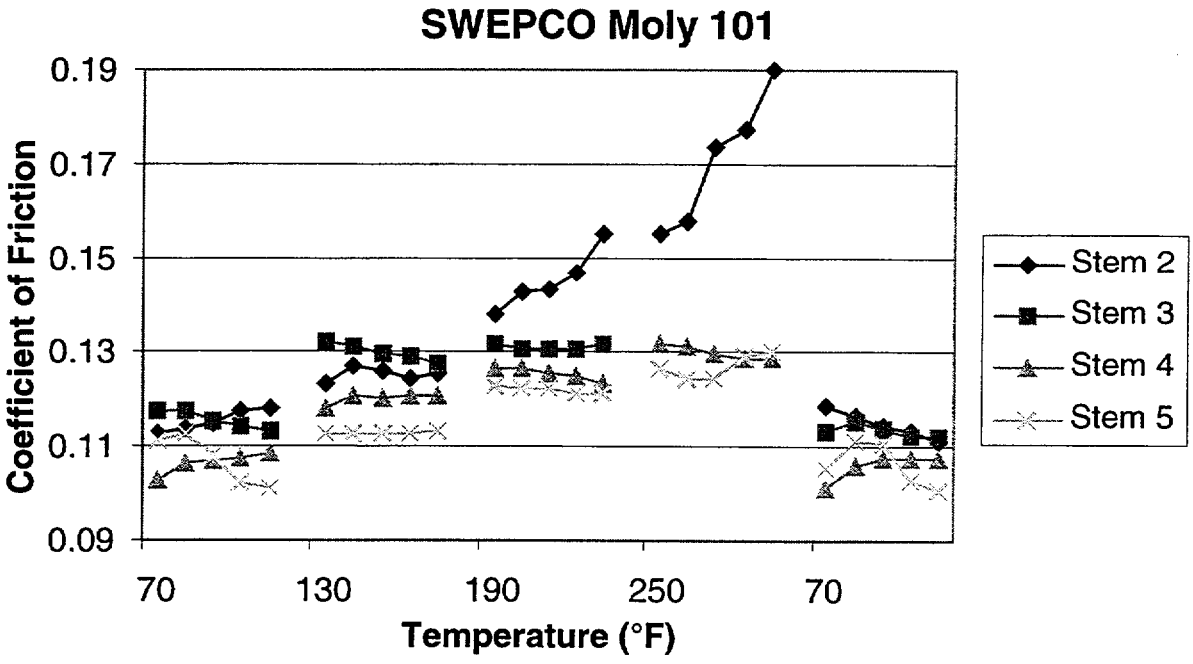

Figure 10. Stem nut coefficient of friction for each stroke of the multiple step tests with Moly 101.

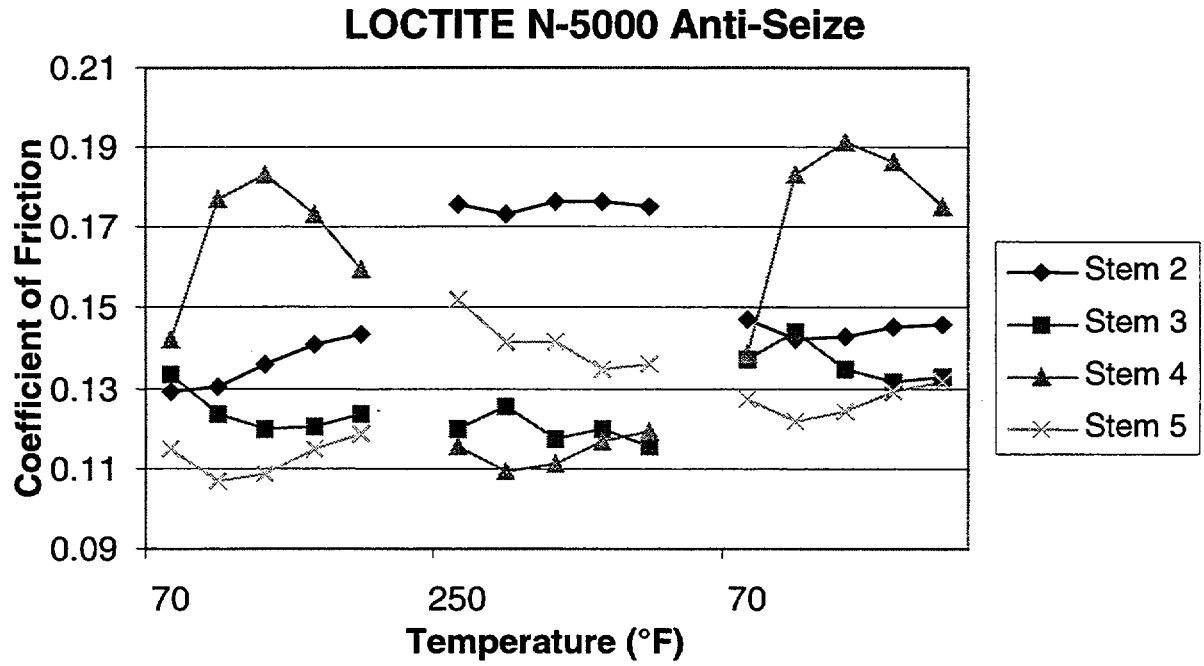

Figure 11. Stem nut coefficient of friction for each stroke of the single step tests with N-5000.

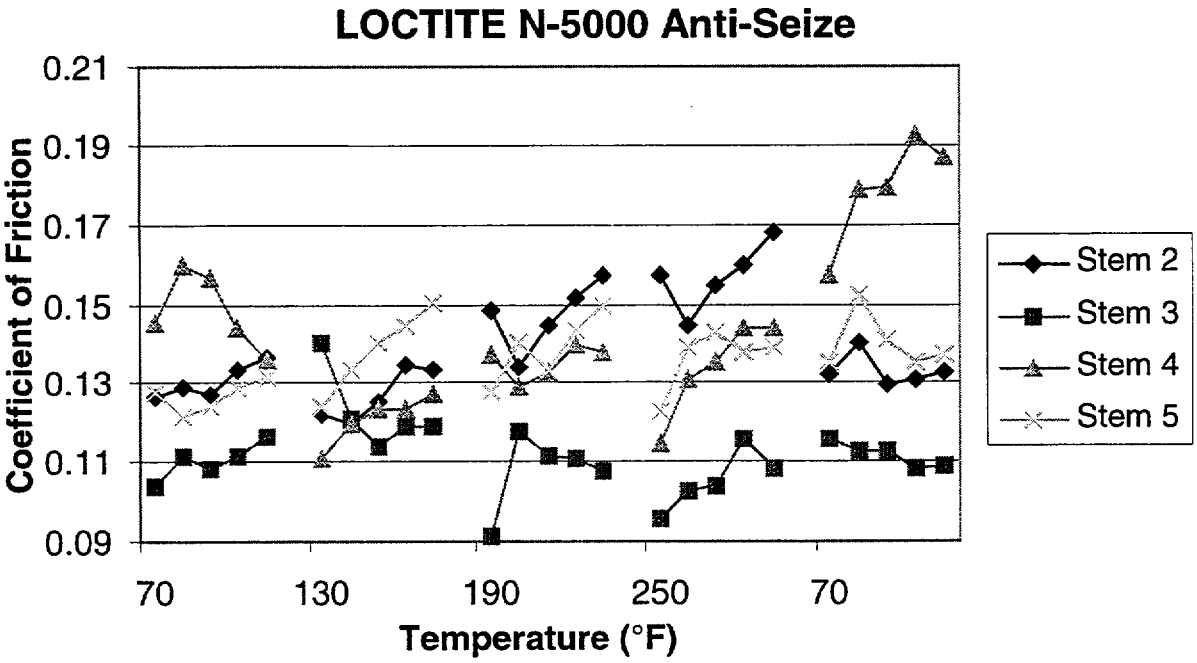

Figure 12. Stem nut coefficient of friction for each stroke of the multiple step tests with N-5000.

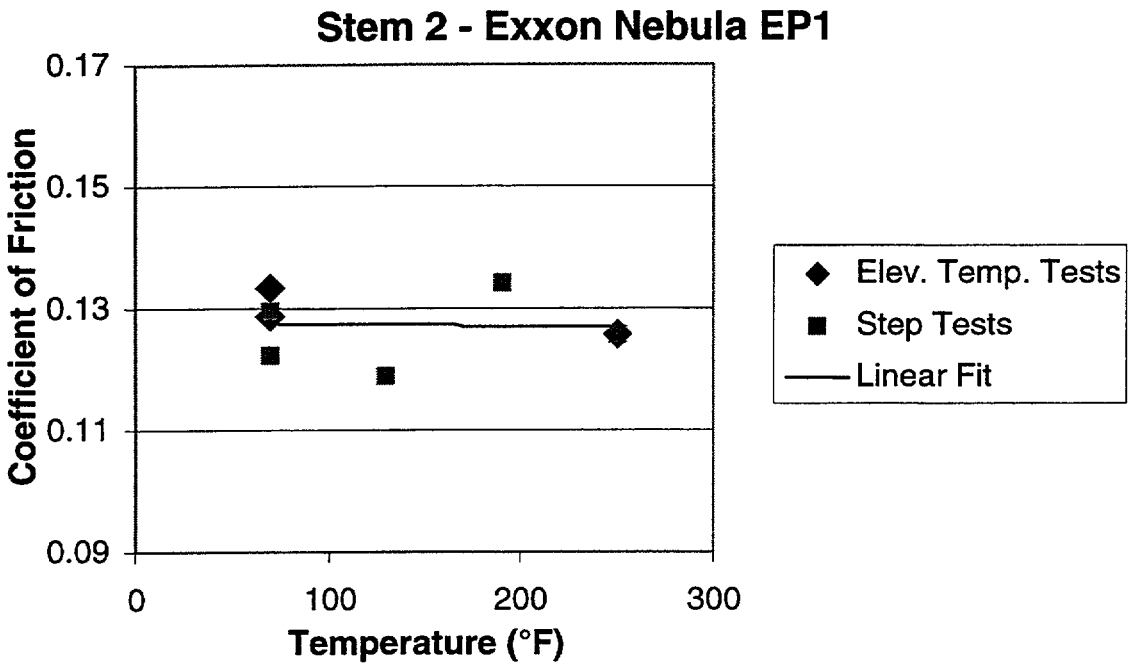

Figure 13. Typical flat or decreasing change in stem nut friction at elevated temperature.

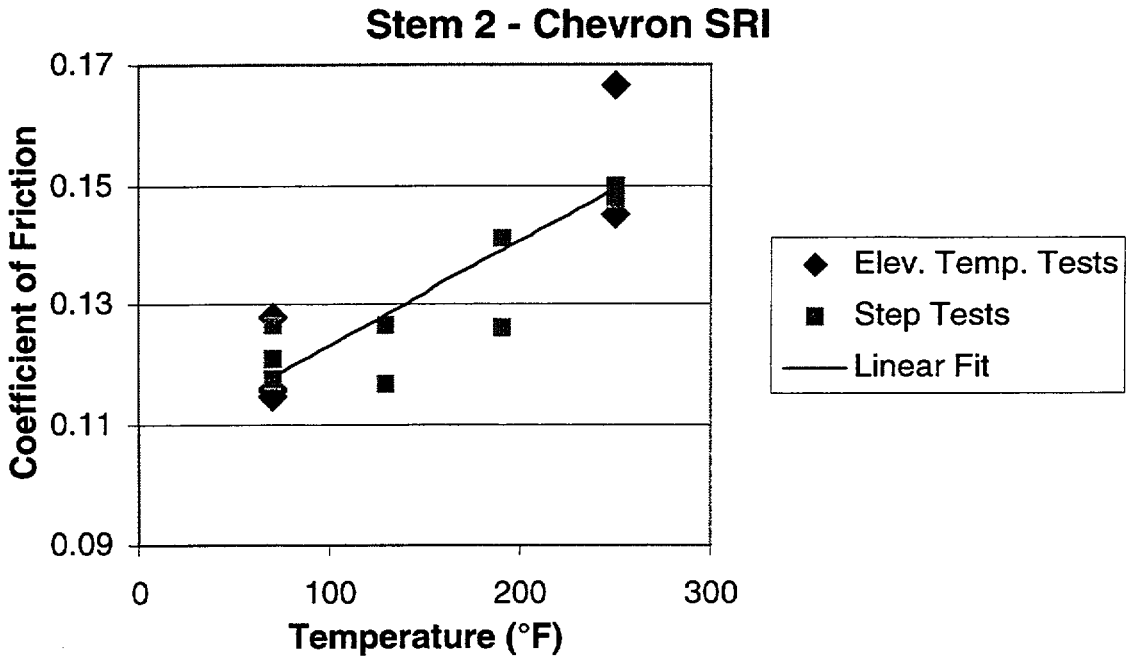

Figure 14. Typical increasing change in stem nut friction at elevated temperature.

Stellite 6 Friction Changes Due to Aging and In-Service Testing

John C. Watkins and Kevin G. DeWall
Idaho National Engineering and Environmental Laboratory

Abstract

For the past several years, researchers at the Idaho National Engineering and Environmental Laboratory, under the sponsorship of the U.S. Nuclear Regulatory Commission, have been investigating the ability of motor-operated valves to close or open when subjected to design basis flow and pressure loads. Part of this research addresses the friction that occurs at the interface between the valve disc and the valve body seats during operation of a gate valve. In most gate valves, these surfaces are hardfaced with Stellite 6, a cobalt-based alloy.

The nuclear industry has developed methods to analytically predict the thrust needed to operate these valves at specific pressure conditions. To produce accurate valve thrust predictions, the analyst must have a reasonably accurate, though conservative, estimate of the coefficient of friction at the disc-to-seat interface. One of the questions that remains to be answered is whether, and to what extent, aging of the disc and seat surfaces affects the disc-to-seat coefficient of friction. Specifically, does the accumulation of a surface film due to aging of these surfaces increase the coefficient of friction and if so, how much?

This paper presents results of specimen tests addressing this issue with emphasis on the following:

- The increase in the friction coefficient of Stellite 6 as it ages and whether the friction stabilizes.
- The effect periodic gate valve cycling due to in-service testing has on the friction coefficient.
- The results of an independent review of the test methods, processes, and the results of the research to date.
- The status of ongoing aging and friction testing.

Introduction

The Idaho National Engineering and Environmental Laboratory (INEEL) has been investigating the ability of motor-operated valves (MOVs) to function when subjected to design basis loads. Methods exist to analytically predict the thrust needed to operate these valves at specific fluid conditions; however, the analyst must have a reasonably accurate, though conservative, estimate of the coefficient of friction at the disc-to-seat interface (see Fig. 1). In most gate valves, these surfaces are hardfaced

with Stellite 6, a cobalt-based alloy. One of the questions that has not been addressed is whether, and to what extent, aging of the disc and seat surfaces affects the disc-to-seat coefficient of friction. Specifically, does the accumulation of a corrosion film on these surfaces during long term operation in harsh environments increase the coefficient of friction; and if so, how much?

This paper presents the latest results from an ongoing INEEL research project addressing this issue. The purpose of this project is to determine how aging degradation mechanisms can affect the performance requirements of MOVs over the long term. The results of this project will provide information on the coefficient of friction expected of a fully aged valve, including the effect of periodic valve cycling typical of in-service tests.

The project consists of subjecting Stellite 6 specimens to an environment simulating boiling water reactor (BWR) coolant conditions, representing the conditions a typical reactor water clean-up (RWCU) isolation valve would experience, and inducing the accumulation of a corrosion film. The project included analysis of the resulting corrosion film and testing of the specimens to determine the coefficient of friction. The Battelle Memorial Institute in Columbus, Ohio, performed the testing under a contract with the INEEL. The National Institute of Standards and Technology (NIST) has performed a critical review of the test methods, processes, and the results of the research to date.

Test Program

This paper describes two test programs dealing with the aging of Stellite 6 and the effect this aging has on friction. The first test program, or Phase I testing, has already been performed and details of this testing are presented in this section of the paper. The second, or Phase II testing, is currently underway and will be described in more detail later in this paper. The Phase I testing consisted of two types of aging tests.

- The first investigated natural aging at simulated BWR conditions. For these tests, we determined the corrosion film thickness and composition following 2-, 10-, 20-, 25-, 40-, 50-, and 78-day exposure periods to BWR conditions simulated in a corrosion autoclave. We performed friction testing on specimens after 2, 10, 20, 40, and 78-days exposure.
- The second also investigated natural aging but included the effect of periodic cycling on the valve corrosion films. The purpose of these later tests was to determine whether the film composition and friction coefficient are influenced by the periodic disc wedging encountered during in-service testing (IST). For these tests, we determined the composition of the corrosion film both before and after the simulated valve wedging which was performed after 25 days and again after 50 days in the corrosion autoclave. Friction testing was performed after 78 days in the corrosion autoclave.

The Phase I specimens were naturally aged at simulated BWR coolant conditions in a corrosion autoclave. To simulate BWR coolant conditions, the autoclave was attached to a reservoir of water in which the oxygen was controlled in the range of 100 to 200 parts per billion (ppb). Water from the reservoir was continuously supplied to the autoclave, with the temperature in the autoclave maintained at 550°F and the pressure at 1050 psi, slightly above the saturated steam pressure, such that the water was slightly subcooled.

We used a separate friction autoclave to perform the friction tests. The friction autoclave, like the corrosion autoclave, was attached to a reservoir of water in which the oxygen was controlled in the range of 100 to 200 ppb. Testing was performed with the autoclave heated to 550°F and pressurized to about 1050 psi. During each test, a specimen assembly consisting of two smaller 0.25-in. x 1.10-in. outer specimens and two larger 0.5-in. x 3.0-in. inner specimens was tested (see Fig. 2). The outer specimens were held in a stationary fixture, and the inner specimens were attached to a carrier bar connected to a movable pull rod. Actuation of the pull rod caused the inner specimens to slide along the outer specimens at a relative velocity of approximately 16 in./min, a rate within the range expected for typical gate valve operation.

The friction autoclave is equipped with a bellows that can exert a force on one side of the specimen assembly. Pressurizing the bellows imposes a normal force on the specimens to produce the specified nominal contact stress of 10 kips per square inch (ksi). The normal force required to achieve a 10-ksi nominal contact stress on the 0.25-in. x 1.10-in. contact zone is 2750 lb. This value was selected to approximate the stress level occurring during operation of typical RWCU system valves. (Assuming uniform load distribution, the calculated contact stresses at the seats for typical 4 and 6-in. valves under a differential pressure of 1,050 psi are 7.8 and 12.6 ksi, respectively.)

For the simulated valve wedging representing IST cycling, we used an in-service testing simulation rig. Unlike conditions in both the corrosion autoclave and the friction autoclave, conditions in the in-service testing simulation rig consisted of a water bath at room temperature and atmospheric pressure rather than simulated BWR coolant conditions. To subject the entire surface of each specimen to a simulated valve wedging, we placed like sized specimens with their Stellite 6 surfaces face to face, applied a normal load of 20 ksi, and moved the specimens 0.040-in. relative to each other. We selected a stress level of 20 ksi to approximate the bearing stress occurring during a valve wedging cycle of a typical RWCU system valve. The 0.040 in. displacement is based on the approximate distance the Stellite 6 surfaces on the disc and the seat would move relative to each other during valve wedging for a typical RWCU system valve. We considered using the high temperature friction autoclave for the simulated cycling, but it could not achieve the required contact stress on the larger 0.5-in. x 3.0-in. specimens. A normal load of 30,000 lb was required, well in excess of the capabilities of the friction autoclave.

Film Characterization

The chemical composition of the corrosion films was analyzed by Auger electron spectroscopy (AES) for some specimens and by X-ray photoelectron spectroscopy (XPS) for others (and both methods for a few specimens). With AES and XPS, the film is incrementally sputtered away, and the elemental compositions of planes in the corrosion film are measured. The results of these analyses are then plotted versus time (or depth, assuming a sputtering rate) to provide a depth profile so that the relative elemental concentrations can be evaluated. Fig. 3 shows a typical AES depth profile for Stellite 6 after exposure to natural aging conditions. As can be seen from the plot, the chromium concentration is almost constant through the corrosion film, whereas the cobalt is lean at the surface and rapidly rises between 1000 and 2000 Å. [One Angstrom (Å) equals one ten-millionth of a millimeter.]

The composition of the corrosion file was similar to that observed by other researchers [1, 2] for Stellite 6 specimens exposed to lithiated high temperature water. The results show that the surface of the corrosion film is rich in chromium and lean in cobalt.

As part of the critical review of this research, NIST also analyzed the corrosion film of 10-day and 50-day specimens using Atomic Force Microscope (AFM) and X-ray diffraction. NIST concluded that the corrosion film contains crystalline solids within an amorphous substrate. These crystalline solids could be chromium oxides, cobalt oxides, and/or carbides. Crystalline solids are, in general, very abrasive and can result in high friction between moving surfaces.

Friction Testing

Five sets of naturally aged specimens underwent friction tests. The aging times for these specimen sets were 2, 10, 20, 40, and 78 days. This testing showed that the coefficient of friction continually increased as the specimens aged and as the film thickness increased. In fact, Fig. 4 indicates that the friction not only increases as the specimens age, but that it does not appear to stabilize, or reach a plateau. These results question whether the friction coefficient will reach a stable value as the specimens continue to age. This information is important, because as the friction increases, the thrust demands of a valve will increase and influence the available operating margin of the MOV. The friction tests were performed with the specimens in an autoclave at 550°F and 1050 psi. As such, the continuously increasing friction is the result of the corrosion film and is not due to the preconditioning phenomenon that is encountered when friction testing is performed on specimens at ambient temperature.

Fig. 5 presents the same friction information in a different format to show how the coefficient of friction responds to continued stroking of the same specimen. The results show that the friction is highest during the first stroke and decreases with each subsequent stroke. Even though additional stroking of the specimens decreases the friction, the friction generally increased as the specimen aged. This continual increase in friction over time indicates the importance of trending the valve friction over time. The data also shows that the highest friction occurs during the first stroke and decreases with each subsequent stroke. The first stroke a valve experiences after it has been allowed to age and establish a corrosion film will result in the highest coefficient of friction and therefore require the highest stem thrust to overcome these friction forces.

The increase in friction as the specimen ages is due to the mechanical properties of the films (oxides and hydroxides) developed during aging. As the corrosion film develops, the friction coefficient would be expected to approach that which might be measured using specimens with the same composition as the corrosion film, i.e., solid oxide specimens. Oxides typically have higher friction coefficients than their metal counterparts. However, for the natural aging cases investigated thus far, the corrosion films were extremely thin. It is most likely that under the relatively high contact stresses of the experiments (10 ksi), these corrosion films were immediately ruptured upon the onset of sliding and subsequently were mixed into the substrate surface. This is typical behavior of a thin hard coating (such as the corrosion film of Stellite 6) on a relatively softer substrate. As such, the friction coefficient represents a mixture of the friction of the bulk Stellite 6 material and the friction of the corrosion film.

NIST has reviewed the friction testing to ensure that the testing simulated the actual operation of a valve. As tested, the full surface is initially in contact and the hard corrosion products are trapped between the surfaces. NIST noted that this was one possible contact mode. They also noted that another contact mode could occur with a disc tipped such that the moving surfaces come into contact and push the corrosion products out of the way without being trapped. To investigate this concern, selected Stellite 6 specimens were friction tested at NIST. Ten day and 50 day specimens were tested but the testing was performed at ambient temperature and pressure. Two types of friction tests were performed. One test configuration pushed the corrosion products out of the way and a friction between 0.15 and 0.17 was observed. The other test configuration trapped the corrosion products and a friction between 0.30 and 0.35 was observed. The latter configuration was comparable to the results of friction testing similar specimens in the autoclave, 0.35 to 0.40.

One set of specimens subject to natural aging conditions and simulated IST valve wedging cycles also underwent friction tests. The aging time for these specimens was 78 days, with simulated valve wedging cycles after 25 days and again after 50 days. Fig. 6 presents the results of this testing and shows that specimens that were subjected to simulated valve wedging cycles had a lower coefficient of friction, although it is not clear whether this trend will continue as the specimens age. During subsequent strokes, the effect of the simulated valve wedging on the resulting friction coefficient was either negligible or varied from stroke to stroke. This frictional behavior is influenced by changes in the condition of the surface due to previous strokes. As such, only the first stroke would be strongly influenced by the simulated valve wedging.

Revised Friction Testing Based on Recommendations From NIST

Based on a review of our previous Stellite 6 corrosion and friction testing, NIST recommended that additional friction testing should start from a non-contacting position similar to one of the contact modes of a valve and that further studies should be performed with more samples to verify the results. Based on these recommendations, we have redesigned the friction testing specimens for our Phase II testing and are in the process of aging these specimens at simulated BWR conditions for 0, 30, 60, 90, and 120 days. After each aging period, previously untested specimens will be friction tested. The redesigned specimens will be able to simulate two contact modes during the friction testing. The first is full surface contact with the corrosion products trapped between the surfaces. This mode is similar to the previous testing and will be used to baseline the performance of the new specimens with the performance of earlier specimens. The second simulates two moving surfaces coming into contact with each other and allowing the corrosion products to be pushed out of the way without being trapped.

Fig. 7 is a photograph of the redesigned inner and outer friction specimens. The smaller outer specimen (the right side of the figure) is initially positioned at the end of the larger inner specimen (the left side of the figure) that has the two riding surfaces, allowing the corrosion products to be trapped between the surfaces. As the inner and outer specimens move relative to each other, the outer specimen transitions onto the single riding surface of the inner specimen. The transition from the two-surfaced region to the single

surfaced region is flat so that the corrosion products can be pushed out of the way. The small specimens that are located between the inner and the outer specimens will be used to characterize the corrosion film.

The testing is currently in process. The testing and data evaluation are scheduled for completion during 2002. Because the testing is still ongoing, additional details are not available at this time. However, results of the testing will be presented during the Symposium.

Conclusions

This paper presents the latest results of an ongoing INEEL research project addressing the aging of Stellite 6 specimens at simulated BWR conditions. This project identified a number of trends in the frictional characteristics of Stellite 6 that may influence the available operator margin of an MOV as it ages. These trends are summarized below.

The friction of the naturally aged specimens shows a continual increase as the aging time increases, with no evidence of stabilizing, or reaching a plateau, after 78 days of aging. This continual increase in friction over time indicates the importance of trending the valve friction over time. This is because, as the friction increases, the thrust demands of a valve will also increase and influence the available operating margin of the MOV.

The data also show that the highest friction occurs during the first stroke and decreases with each subsequent stroke. The first stroke a valve experiences after it has been allowed to age and establish a corrosion film will result in the highest coefficient of friction and therefore will require the highest stem thrust to successfully operate the valve.

The single data point for the periodic valve wedging test suggests that periodic disc wedging will decrease the expected friction compared to a valve that is less frequently cycled. Although there is only a single data point and the effects of the IST cycle may be small for this case, the data suggest that increasing the time between IST cycling may allow the friction to increase enough to impact the available operating margin of an MOV.

Additional testing is underway. We are currently aging and friction testing the new specimens that address the concerns raised by NIST. This testing is scheduled for completion during 2002.

References

Hocking, W. H. and Lister, D. H., Corrosion of Stellite-6 in Lithiated and Borated High-temperature Water, Surface and Interface Analysis, 1988.

Hocking, W. H., et al., Mechanisms of Corrosion of Stellite-6 in Lithiated High Temperature Water, Corrosion Science, Vol. 25, No. 7, pp 531-557, 1985.

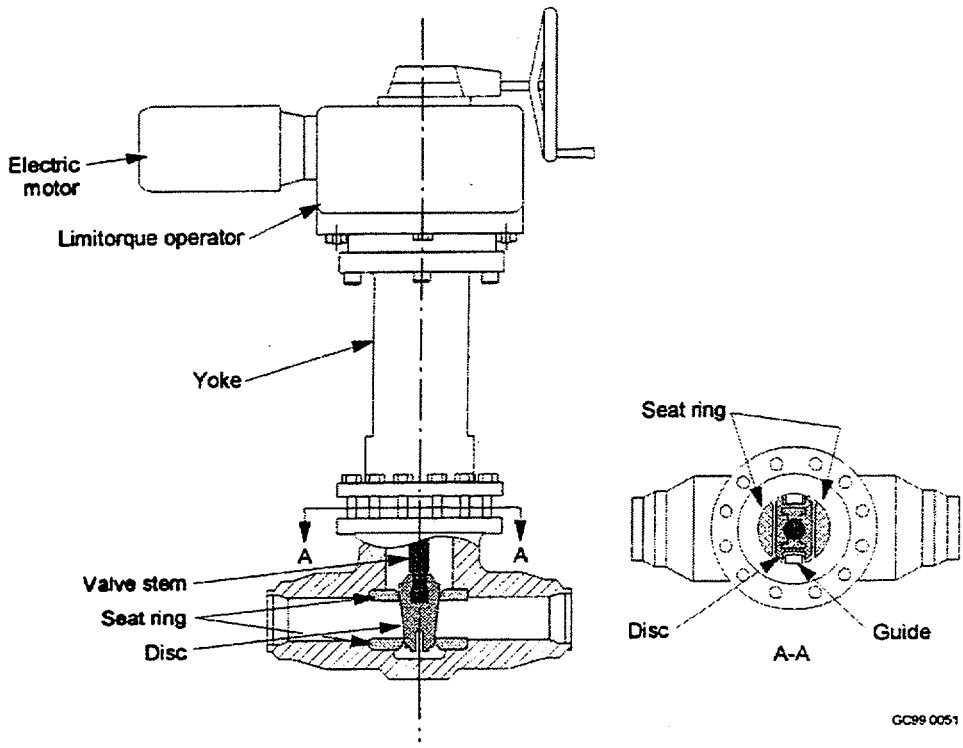

Figure 1. Diagram of a typical motor-operated gate valve showing the main components.

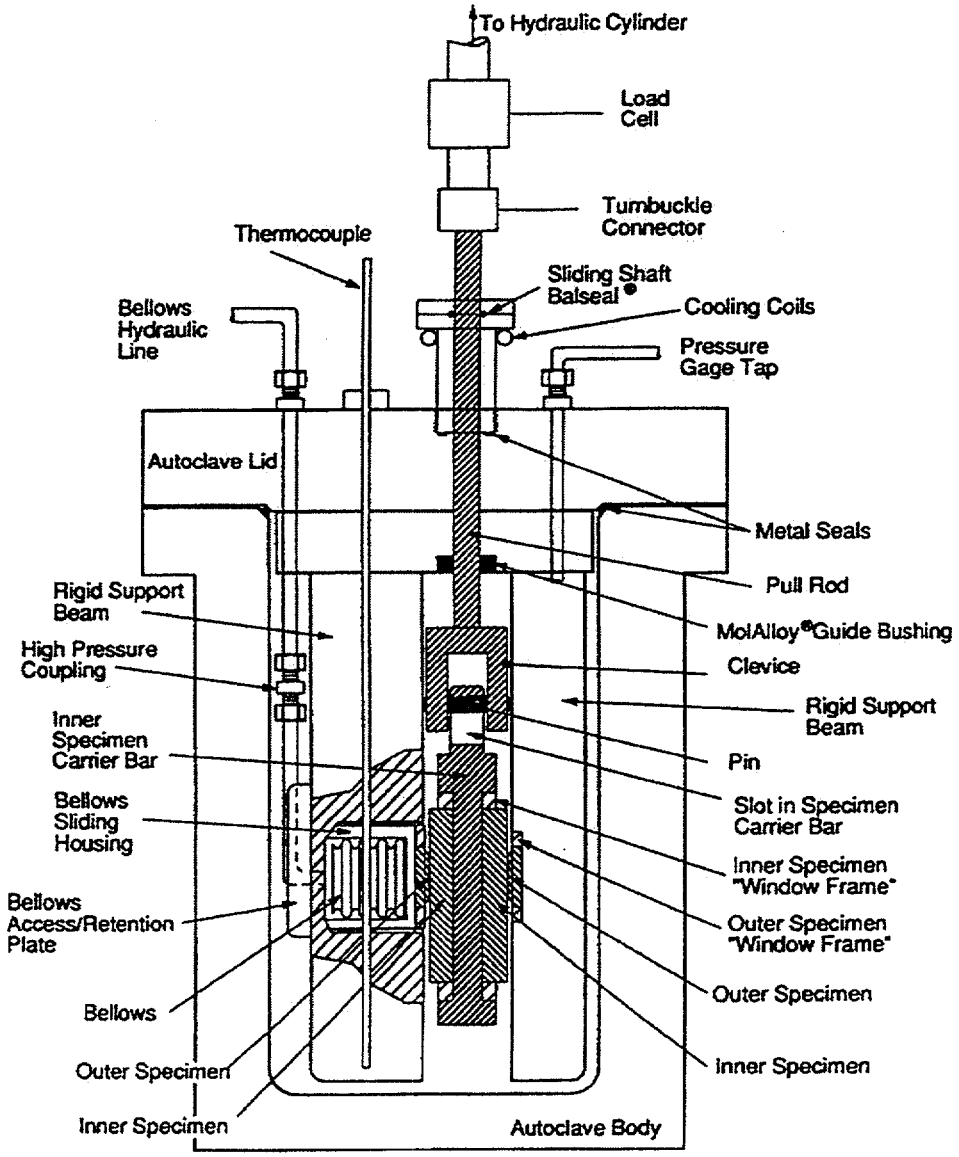

Figure 2. Diagram of the friction autoclave.

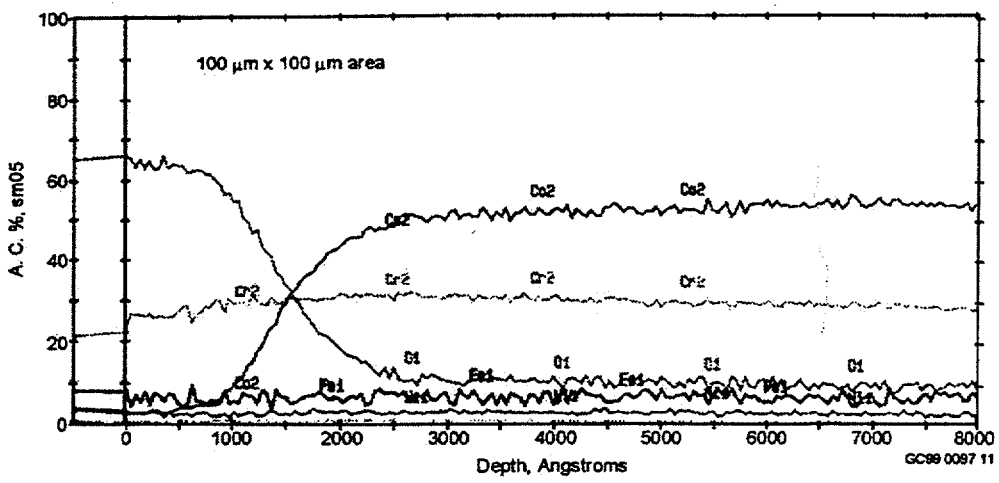

Figure 3. AES depth profile for Stellite 6 after 20 days exposure to natural aging conditions.

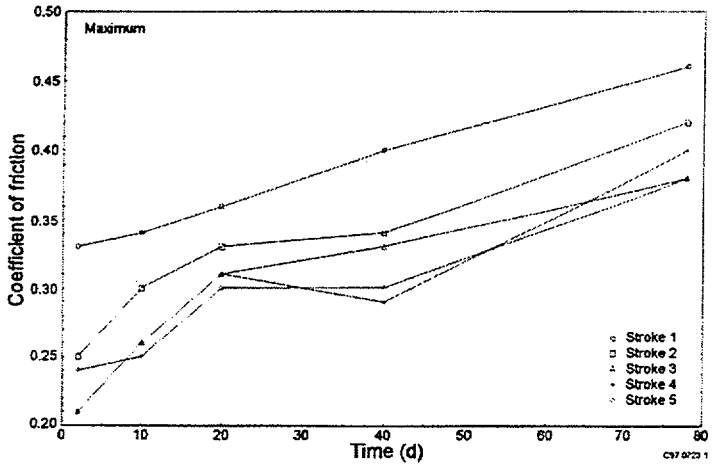

Figure 4. Coefficient of friction versus time for naturally aged Stellite 6 specimens; maximum values (top) and nominal values (bottom).

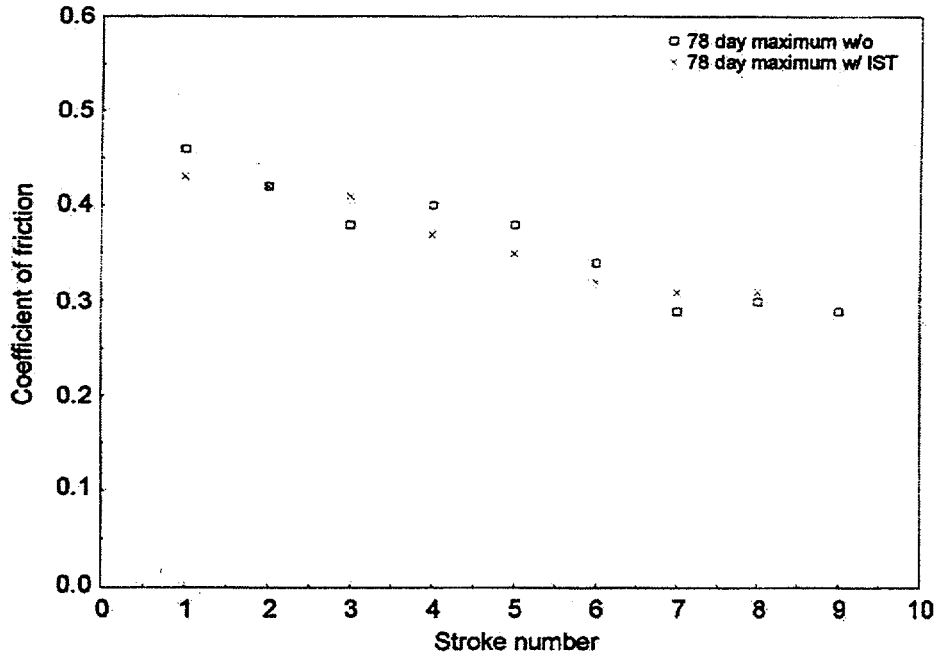

Figure 5. Coefficient of friction versus stroke for Stellite 6 specimens exposed to natural aging conditions; maximum values (top) and nominal values (bottom).

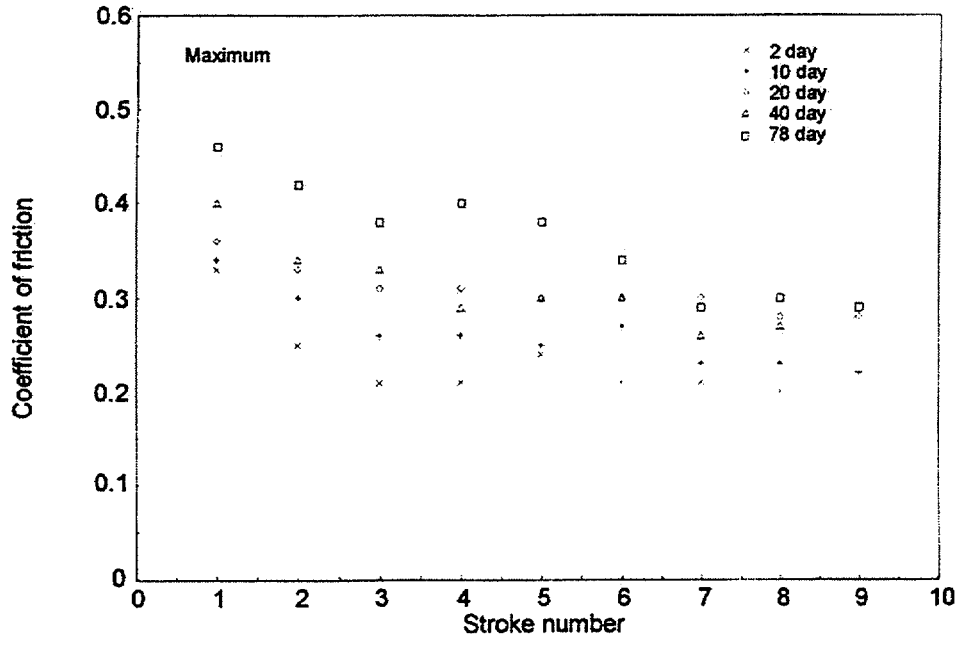

Figure 6. Maximum coefficient of friction versus stroke for naturally aged Stellite 6 specimens and specimens subject to in-service testing.

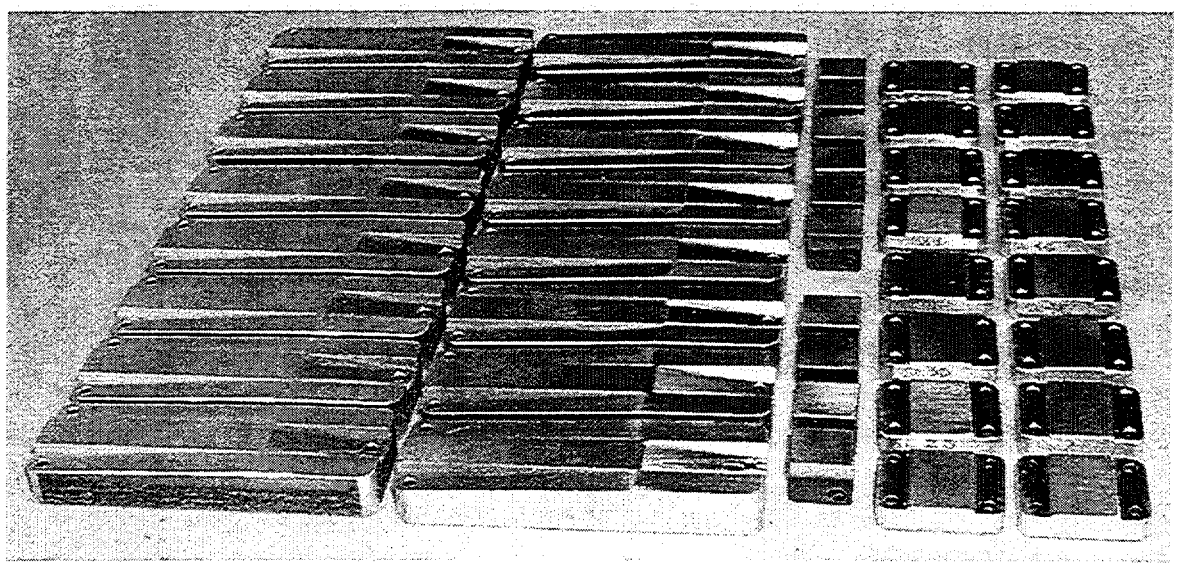

Figure 7. New Stellite 6 specimens prior to aging and friction testing.

Development of a dc Motor Model and an Actuator Efficiency Model

John C. Watkins, Michael G. McKellar, and Kevin G. DeWall
Idaho National Engineering and Environmental Laboratory

Abstract

For the past several years, researchers at the Idaho National Engineering and Environmental Laboratory, under the sponsorship of the U.S. Nuclear Regulatory Commission, have been investigating the ability of motor-operated valves (MOVs) used in nuclear power plants to close or open when subjected to design basis flow and pressure loads. Part of this research addresses the response of a dc-powered motor-operated gate valve to assess whether it will achieve flow isolation and to evaluate whether it will slow down excessively under design-basis conditions and thus fail to achieve the required stroke time.

As part of this research, we have developed a model of a dc motor operating under load and a model of actuator efficiency under load based on a first principle evaluation of the equipment. These models include the effect that reduced voltage at the Motor Control Center and elevated containment temperatures have on the performance of a dc powered MOV. The model also accounts for motor torque and speed changes that result from the heatup of the motor during the stroke. These models are part of the Motor-Operated Valve In Situ Test Assessment (MISTA) software which is capable of independently evaluating the ability of dc-powered motor-operated gate valves to achieve flow isolation and to meet required stroke times under design-basis conditions.

This paper presents an overview of the dc motor model and the actuator efficiency under load model. The paper then compares the analytical results from the models with the results of actual dc motor and actuator testing, including comparisons of the effect reduced voltage, elevated containment temperature, and motor heating during the stroke have on an MOV.

Nomenclature

A	=	Heat transfer area
C_1, C_2	=	Constants
C_p	=	Specific heat
e	=	Efficiency of the stem/stem-nut
emf	=	Back electromagnetic force
h_{cv}	=	Convection heat transfer coefficient
h_r	=	Radiation heat transfer coefficient
I_a	=	Armature current
I_{sh}	=	Shunt current
k, k_1, k_2	=	Constants
M	=	Mass

p = Pitch of the worm gear

r = Radius of the worm gear

r_m = Radius of the motor

R_a = Resistance of the armature, series and interpole

R = Resistance at temperature T

R_o = Resistance at temperature T_o

t = time

T = Motor temperature

T_{amb} = Ambient temperature

T_q = Motor torque

T_0 = Reference temperature

U = Heat transfer coefficient

V_a = Voltage across the armature

V_b = Voltage loss across the brushes

V_m = Voltage across the motor

V_{sh} = Voltage across the shunt

ϵ = Emissivity

ϕ = Magnetic flux

ϕ_a = Armature magnetic flux

ϕ_{sh} = Shunt magnetic flux

μ = Stem/stem-nut coefficient of friction

σ = Stefan-Boltzmann constant

ω_m = Rotational speed or the motor

Introduction

In response to regulatory initiatives, nuclear electric utilities are conducting in situ diagnostic testing of MOVs. The purpose of the tests is to provide assurance that the MOVs are able to operate (close and/or open) against design basis flows and pressures, and at design basis operating temperatures and voltages. The utilities generally use one of several commercially available diagnostic test systems to record pertinent diagnostic data during the in situ tests.

The United States Nuclear Regulatory Commission (NRC) requested that the Idaho National Engineering and Environmental Laboratory (INEEL) develop the capability to independently evaluate in situ diagnostic test data. The need for such capability is driven by the complexity of the situation:

- In situ test data are subject to individual interpretation. Many of the calculations necessary to evaluate the response of an MOV are not performed by the various diagnostic test systems
- The in situ test data are difficult, if not impossible, to use outside the diagnostic test system environment, because of the proprietary data formats
- Even if the data were available, large volumes of information need to be processed, and many of the calculations necessary to arrive at design-basis performance estimates rely on assessment methodologies that are difficult for either utility personnel or NRC inspectors to implement.

In response to the NRC request, MOV researchers at the INEEL developed the motor-operated valve in situ test assessment (MISTA) software; a package that achieves the needed test assessment capability by cross-linking proprietary diagnostic testing software with a commercial data analysis and display software package called DADiSP. The diagnostic vendors have either agreed to cooperate with this effort by providing the information necessary to translate their proprietary data formats to a more universal format that can be recognized by DADiSP, or else their data is already in a format that DADiSP can recognize.

The MISTA software is also capable of independently evaluating the ability of dc-powered motor-operated gate valves to achieve flow isolation and to meet required stroke times under design-basis conditions. MISTA uses INEEL's model of dc motor operation under load and INEEL's model of actuator efficiency under load, to perform the assessment. MISTA combines these models with data provided by the user (upstream pressure, differential pressure, motor control center voltage, actuator gear information, stem diameter, stem pitch and lead, etc., along with estimates for MOV variables such as disc friction, stem friction, etc.) as input. The focus of this paper is on how these two models were developed and validated. The actuator model will be discussed first followed by the dc motor model.

Development of the Actuator Model

The actuator model is based on a first principle evaluation of a Limitorque SMB type actuator and the physics that influence how it operates. Major components of the actuator are shown in Figure 1.

The input torque consists of the torque delivered by the electric motor to the input side of the gearbox, and the output torque consists of the torque delivered to the stem nut by the worm gear. The gearbox efficiency accounts for losses to friction at the helical gear set, the worm/spline interface, the worm/worm-gear interface, and the associated bearings. Typical efficiency values for SMB actuator gearboxes are in the range of 0.4 to 0.6. The more efficient the gearbox performance (the less the loss to friction), the higher the efficiency value. The gearbox efficiency value does not include motor effects or friction at the stem/stem-nut interface, which are separate calculations.

We begin the development of the actuator model by evaluating the torque losses at various locations within the actuator. We note that the torque at the worm is a combination of the torque out of the motor less torque losses due to the pinion gears and bearing friction losses. The torque at the worm gear will experience some losses at the upper and lower thrust bearing while being transferred to the stem. If we assume that most of the torque loss will occur between the motor and the worm, we can estimate the loss as the torque needed to reverse the worm gear without any output torque bring transferred from the actuator. This torque loss will be referred to as the hotel load.

Subtracting the actuator torque loss, or the actuator hotel load, from the motor torque trace and then multiplying the resulting value by the pinion gear ratio will give an estimate of the torque at the worm. Conversely, if we divide the stem torque by the worm to worm gear ratio, we can estimate the torque at the worm gear that was needed to generate the stem torque. The worm/worm-gear efficiency can then be estimated as the worm gear torque from the stem divided by the worm torque from the motor. This efficiency can then be used to estimate the friction between the worm and the worm gear using the following equation.

$$\mu = \frac{1-e}{\frac{2\pi r e}{p} + \frac{p}{2\pi r}} \qquad (1)$$

We can then plot the friction versus the worm gear sliding speed, similar to the method presented in reference [1] and shown in Figure 2. However, when we compare the results from one test with the results of another test, we find that a very poor relationship emerges, even for the same motor

and actuator combination. We then used our experience from the Stellite 6 friction testing and recognized that the load on the surfaces can influence the friction at the interface. As such, we adjusted the worm gear sliding speed to include the influence of load on the gears. The resulting relationship is shown in Figure 3. This figure contains the results of three tests, a 100% voltage test, an 80% voltage test, and a 60% voltage test using the same motor and actuator. While not shown, the same relationship exists when the actuator was at an elevated temperature. Since the results are repeatable regardless of either degraded voltage or elevated temperature conditions, this relationship can be used to estimate the worm/worm gear friction knowing the loaded sliding speed between the gears.

If we apply the above method to different actuators, different motors, and different gear sets within the actuator, we find that the friction to loaded worm gear sliding speed is reproduced. This gives us confidence that the actuator efficiency can be estimated using the above relationship between the worm to worm gear friction and the loaded sliding speed of the worm.

Use of the actuator model in MISTA

To estimate the actuator efficiency using Equation (1), a user would need to know the worm/worm-gear ratio, the pinion gear ratio, the effective radius of the worm, the centerline distance between the worm and the worm gear, and an estimate of the actuator hotel load. This information should be available from the actuator manufacturer. MISTA would then use the stem thrust at a given stem position and the user's estimate of the stem/stem-nut friction to estimate the stem torque. MISTA would then iterate on the motor speed at a given stem position until the worm to worm gear friction and the actuator efficiency converges. This friction can then be used to estimate the efficiency of the actuator and then, along with the actuator hotel load, used to estimate the torque required from the electric motor.

Development of the dc Motor Model

The dc motor model is based on a first principle evaluation of a dc motor and the physics that influence how it operates. The model is shown in Figure 4 and represents a cumulatively compound dc-motor, typical of the dc motors installed on MOVs.

Motor physics and development of the motor model

When a wire that is carrying a current is placed in a magnetic field, a force is exerted upon the wire. In a motor, this current carrying wire is part of the rotor, so the force creates a torque that is proportional to the magnetic field, or flux, and to the armature current (the current in the load-carrying wire) or,

$$T_q = k\phi I_a \tag{2}$$

The flux acting on the rotor of a cumulatively compound motor is proportional to the sum of the fluxes of both the series field and the shunt field. The flux is also proportional to the current through the shunt and the series fields, or

$$\phi = \phi_{sh} + \phi_a = k_1 I_{sh} + k_2 I_a \tag{3}$$

Substituting this relationship into Equation (2) yields a relationship between the torque output of a motor and the current in the shunt and armature, or

$$T_q = kk_1 I_{sh} I_a + kk_2 I^2_a \tag{4}$$

This expression can be used to estimate the armature current if the motor torque, the shunt current, and the constants are known. These constants are related to the geometry and magnetic properties within the motor and can be estimated by optimizing the motor's performance curves.

The rotation of the armature in the flux field also creates a counter or back electromagnetic force (emf) that opposes the rotation of the armature. The back emf is proportional to the flux and to the rotational speed of the armature, or

$$emf = k\phi\omega_m \tag{5}$$

Substituting the definition of flux from Equation (2) into Equation (5), the motor speed can be expressed in terms of the back emf, the armature current, and the motor torque, or

$$\omega_m = \frac{emf\, I_a}{T_q} \tag{6}$$

The voltage drop across the motor is equal to the sum of the back emf, the voltage loss across the brushes, and the armature current times the total resistance, R_a, of the armature, the series field, and the interpole resistance, or

$$V_m = emf + V_b + I_a R_a \tag{7}$$

This expression can be used to estimate the back emf if the motor voltage, brush voltage loss, and the armature current and total resistance are known.

Motor heatup and development of the motor model

During operation, dc motors will heat up while turning against a load. This heatup will become more severe as the motor speed slows and the stroke time increases. We have estimated the temperature response of the dc motor using a lumped thermal capacity model that includes:

- Heat input due to the electrical and mechanical losses in the motor
- Heat loss due to convection and radiation out of the motor
- The thermal capacity of the iron and copper in the motor, or

$$\frac{dT}{dt} = \frac{heat\ input - heat\ loss}{thermal\ capacity} \tag{8}$$

The heat input due to electrical and mechanical losses in the motor can be estimated as the difference between the electrical power into the motor and the mechanical power out of the motor, or

$$heat\ input = V_{sh}I_{sh} + V_a I_a - T_q\omega_m \tag{9}$$

The heat loss can be estimated as a heat transfer coefficient times the surface area of the dc motor times the difference in temperature between the motor and the ambient, or

$$heat\ loss = UA(T - T_{amb}) \tag{10}$$

The heat transfer coefficient is modeled as the sum of the convection and radiation heat transfer coefficients. During the optimization process, we determined that the heat conduction from the motor to the actuator was negligible; therefore, it was not included in the model. The convection and radiation heat transfer coefficients are, respectively

$$h_{cv} = C_1\left(\frac{T - T_{amb}}{2r_m}\right)^{C_2} \tag{11}$$

$$h_r = \varepsilon\sigma\,(T^2 + T_{amb}^2)(T + T_{amb}) \tag{12}$$

The thermal capacity of the motor can be estimated as the mass of the iron and copper times the specific heat, or

$$thermal\ capacity = MC_p \tag{13}$$

These expressions can be used to estimate the motor heatup if the constants are known. These constants are related to the geometry of the motor and can be estimated by optimizing the motor's performance curves.

From our testing, we observed that as a motor heats up, either due to ambient conditions or due to operation of the motor, its performance decreases. This heatup increases the internal resistances throughout the motor and contributes to the performance decrease. To account for this effect, the change in resistance can be estimated using the following expression; all resistances internal to the motor are adjusted using this relationship.

$$R = R_o\left[\frac{234.5+T}{234.5+T_o}\right] \tag{14}$$

The numerous unknown variables in the dc motor model can now be estimated by optimizing the manufacturer's motor performance curves. A typical speed versus torque and current versus torque performance curve is shown in Figure 5 and a typical temperature rise versus time curve is shown in Figure 6. Both of these curves are for a 25 ft-lb, 125-volt dc motor.

Model changes to accommodate field wiring

Prior to using the above to estimate the response of a dc powered MOV installed in the field, several modifications were necessary. These modifications include adding the effect of the wire and overload resistances and the effect that wiring differences have on the model. Figure 7 shows the revised first principle model with the above modifications included.

We also made one additional modification to the above. We were requested to develop a motor model that could be adjusted or fine-tuned to more closely match a motor that may be installed in the field based on the results of diagnostic testing. The generic motor performance curves were used to determine the various unknowns in the equations and, as such, the resulting response would reflect the generic information. Based on our understanding of how a dc motor operates and the factors that influence it, we were able to adjust selected parameters to approximate a slightly more powerful or slightly weaker motor relative to the generic information. This capability is obtained by adjusting two parameters that we refer to as the current control and the torque control. The current control adjusts the estimated armature current based upon the torque and the resistance of the armature. The torque control adjusts the resistance of the armature.

Use of the Actuator and dc Motor Models in MISTA

The required motor torque, the available voltage at the motor control center, and general MOV characteristics drive the dc motor model. Figure 8 presents a flow diagram that outlines the calculations performed at each stem position.

Comparisons of the actuator and dc motor models with the results of testing

To demonstrate the capabilities of the dc motor and actuator model, test data from our reduced voltage and elevated temperature dc motor and actuator testing was used to compare the actual response of the MOV with the estimated response obtained from

MISTA. Although only the results from a single motor and actuator are presented, we have used MISTA to simulate all the testing we performed, and the results from the other motors and actuators are very similar.

First, Figure 9 compares the prediction of actuator efficiency, motor torque, motor speed, motor voltage, motor current, and motor temperature for the 25 ft-lb, 125-volt dc motor at 100% voltage and ambient temperature with the results of the testing. The accuracy of the motor torque will depend heavily on the accuracy of the actuator efficiency, and the figure shows that the predicted actuator efficiency is very reasonable. The resulting motor torque is also reasonable. The additional motor comparisons presented in the figure indicate that the dc motor model provides a reasonable estimate of the motor response.

Additional figures showing selected results from the testing and similar results of the simulation are provided in Figures 10 through 12. These figures include the effect of reduced voltage only, the effect of elevated temperature only, and finally the effect of both reduced voltage and elevated temperature. In general, the results of the dc motor and actuator model provide a reasonable estimate of the response of the actual dc motor and actuator.

Conclusions

This paper presents the results of an INEEL research project to enhance the capabilities of the MOV in situ test assessment (MISTA) software. Two new first principle models have been developed and added to the software. The first model is based on a first principle model of an actuator that allows the efficiency of an actuator to be accurately estimated. The second model is based on a first principle model of a dc-powered electric motor that allows the response of the electric motor to be accurately estimated as the motor actuator closes a valve against pressure and flow loads. Both models allow the user to accurately estimate the response of a valve, actuator, and dc motor during the closure cycle of a motor operated valve.

References

Shigley, J. E., Mechanical Engineering Design, McGraw-Hill Book Co, Inc., New York, NY, 1963.

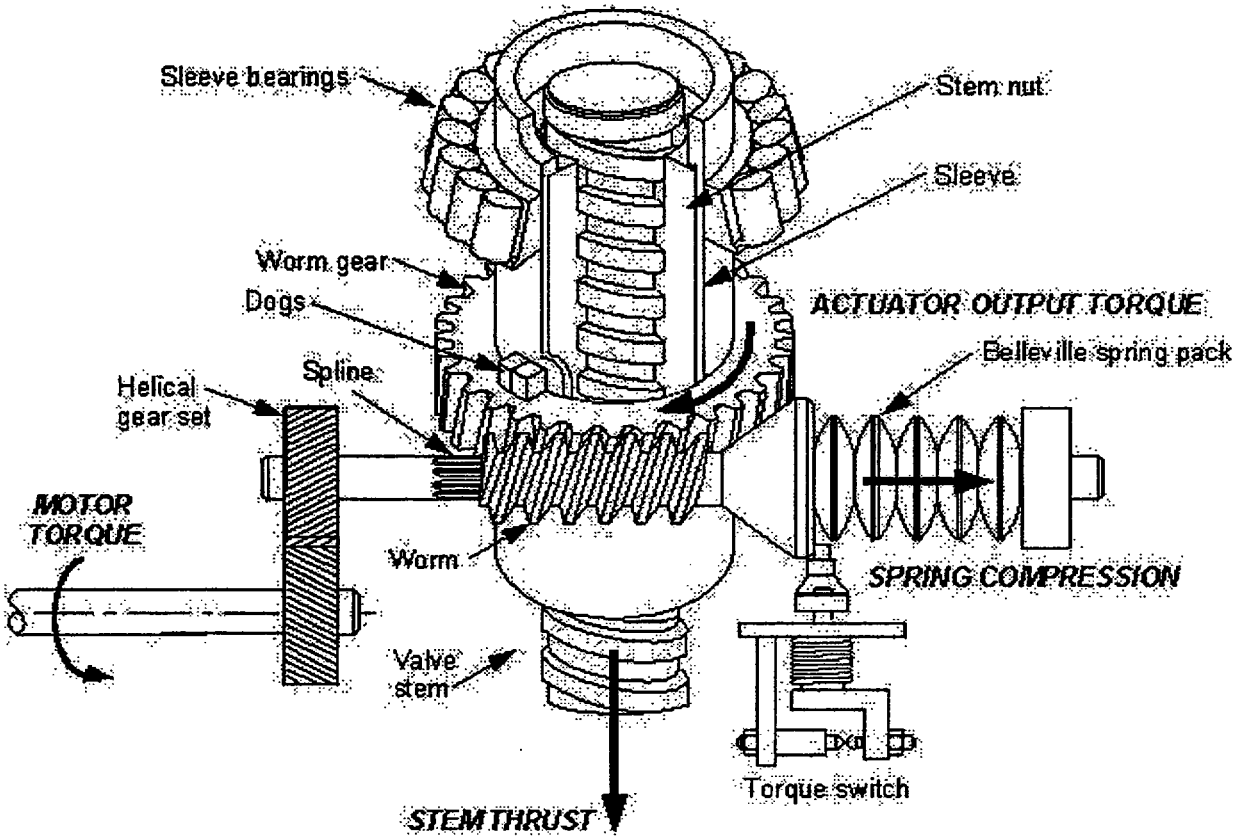

Figure 1. Major components of an MOV actuator.

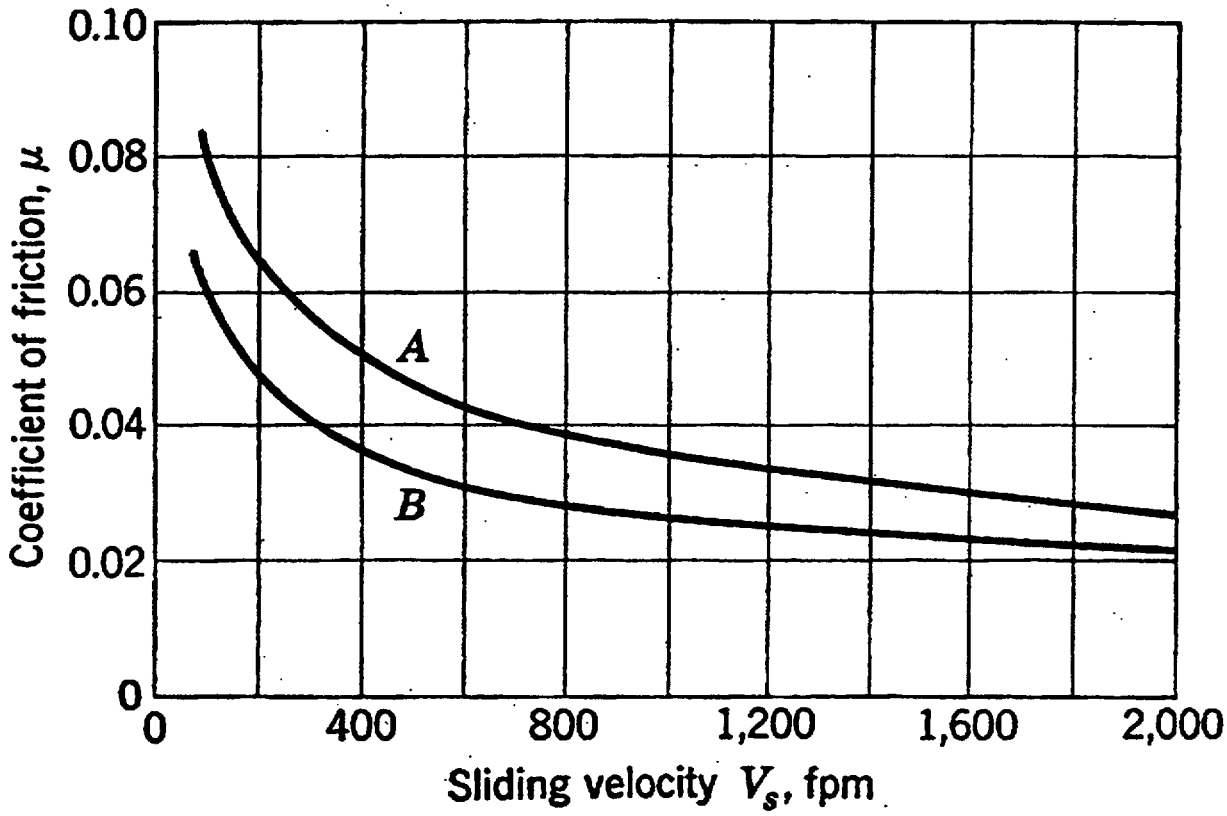

Figure 2. Worm to worm gear friction based on the sliding velocity of the gears.

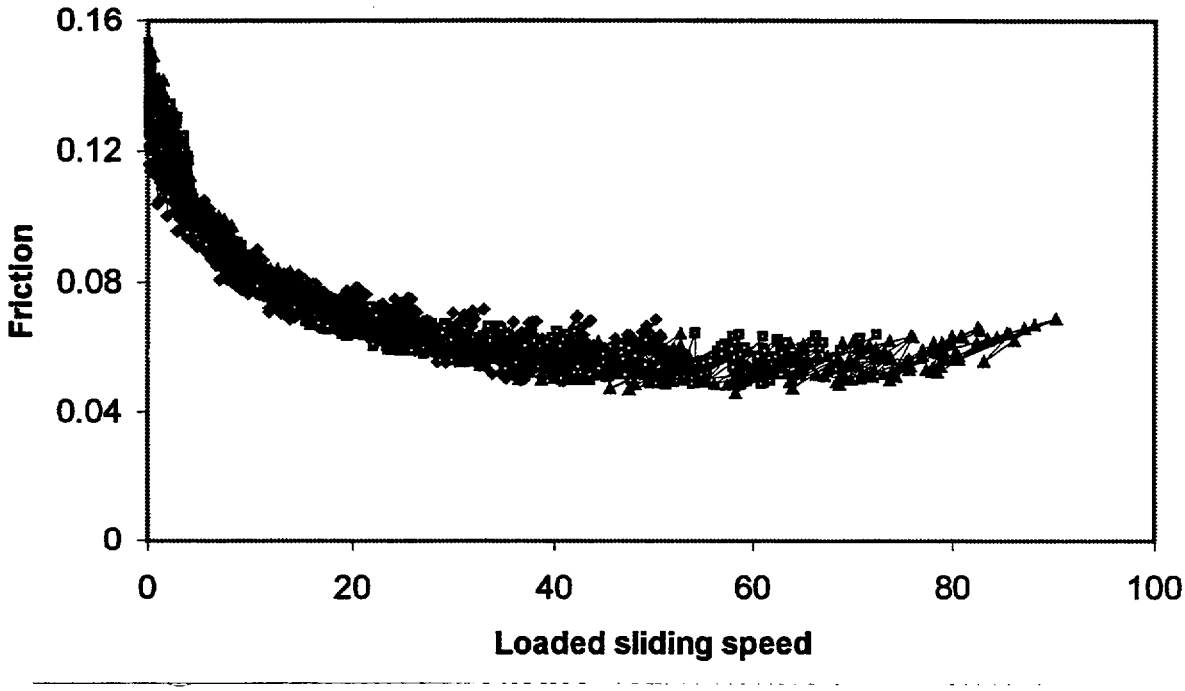

Figure 3. Worm to worm gear friction based on the loaded sliding speed of the gears

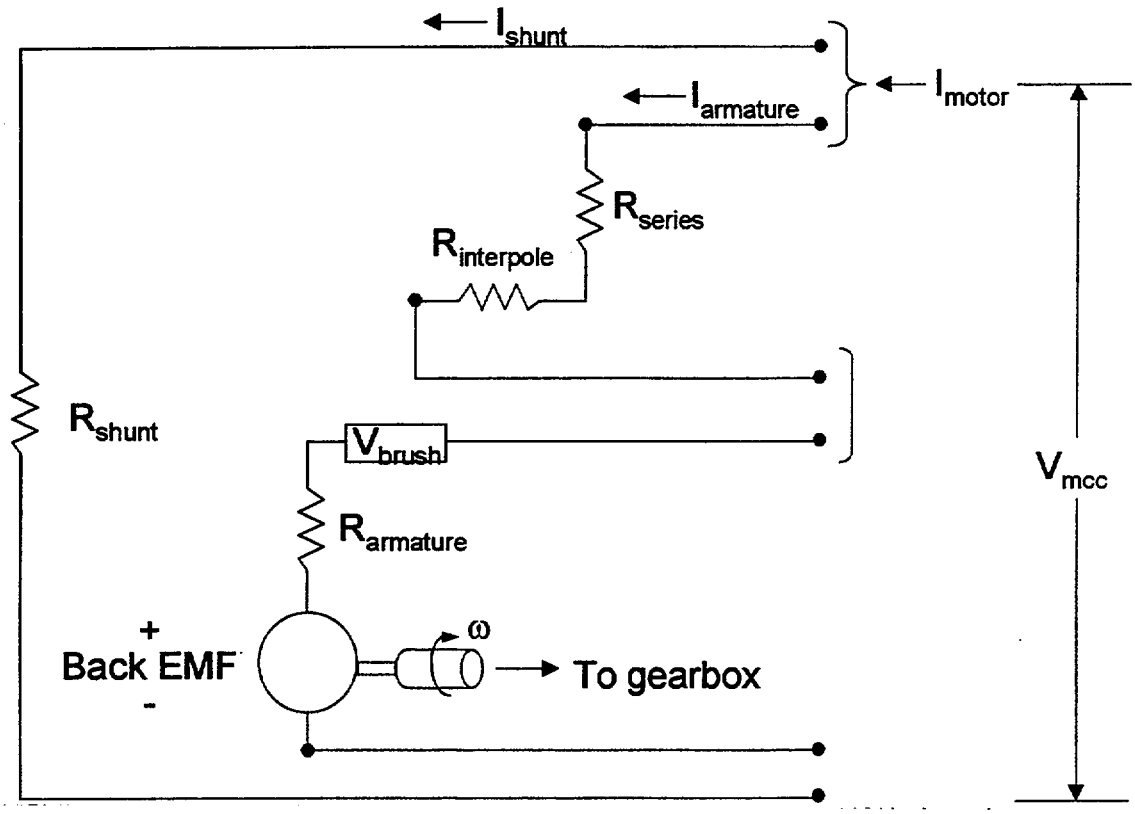

Figure 4. Electrical schematic of a typical MOV dc motor.

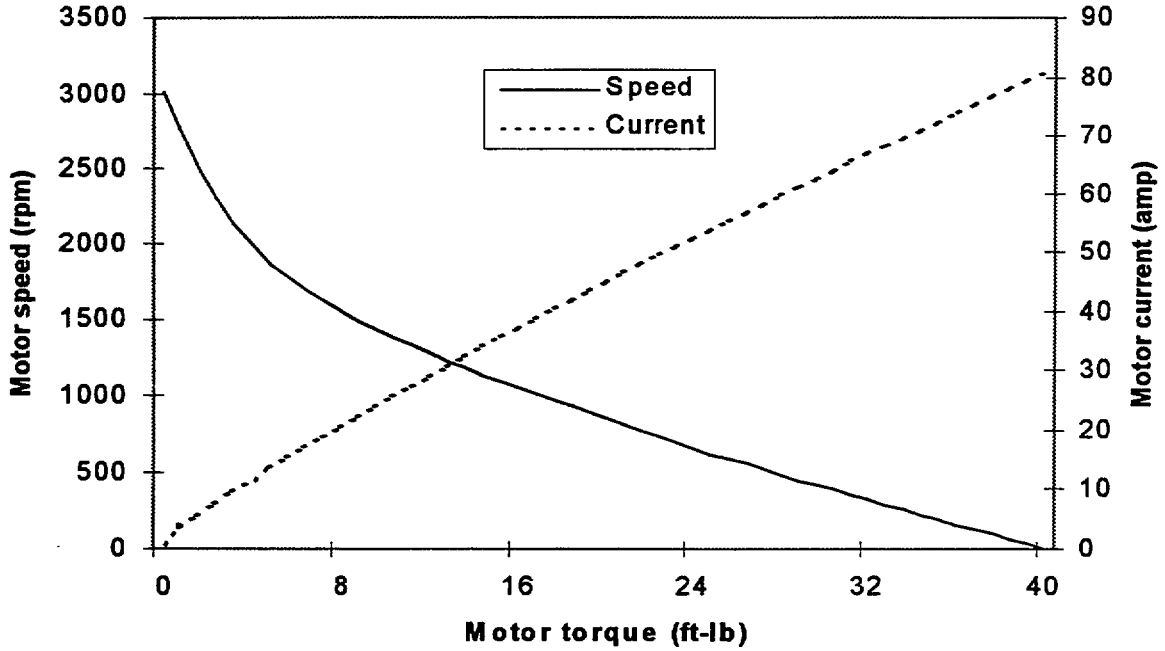

Figure 5. Typical dc motor performance curve.

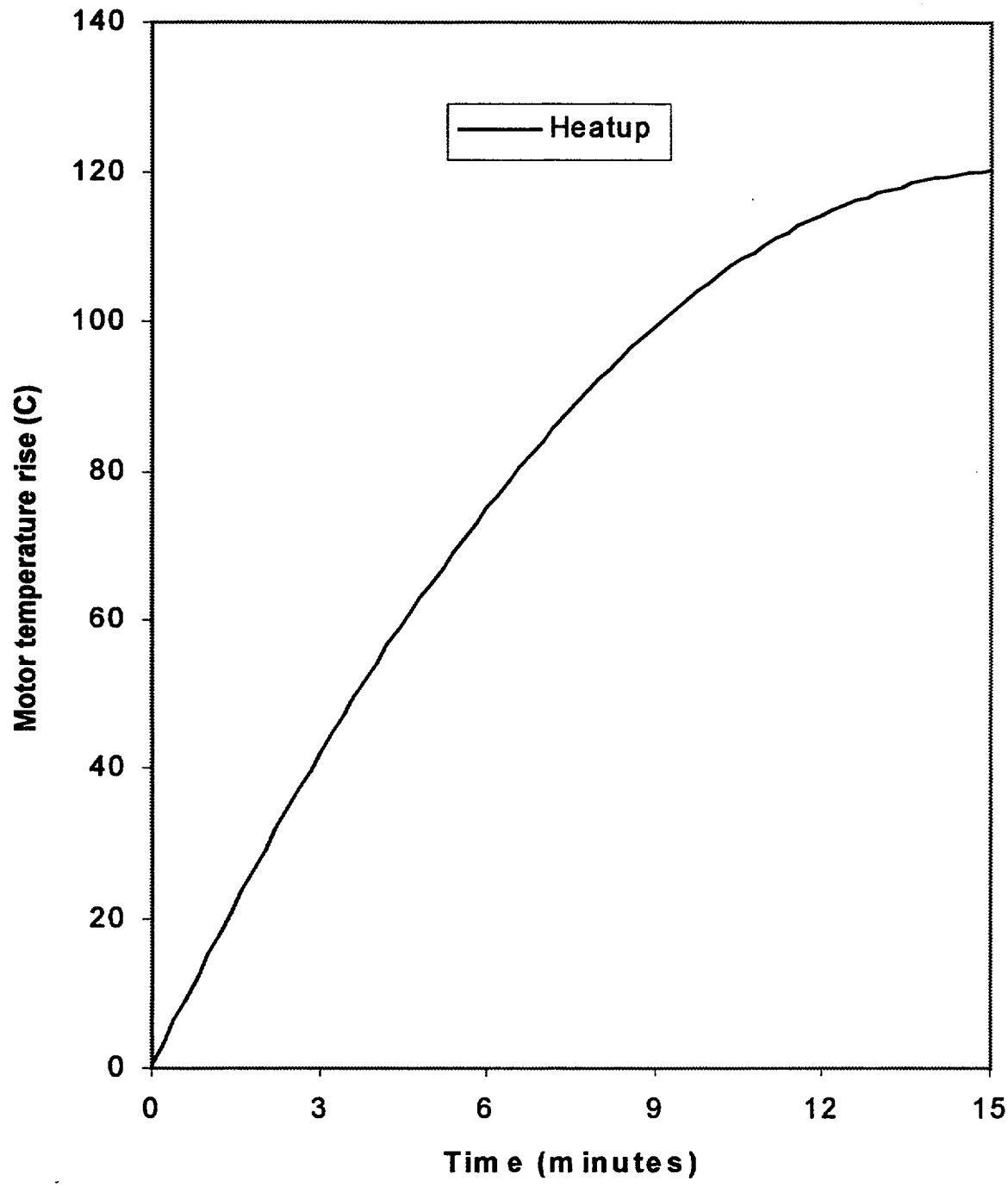

Figure 6. Typical dc motor heatup curve.

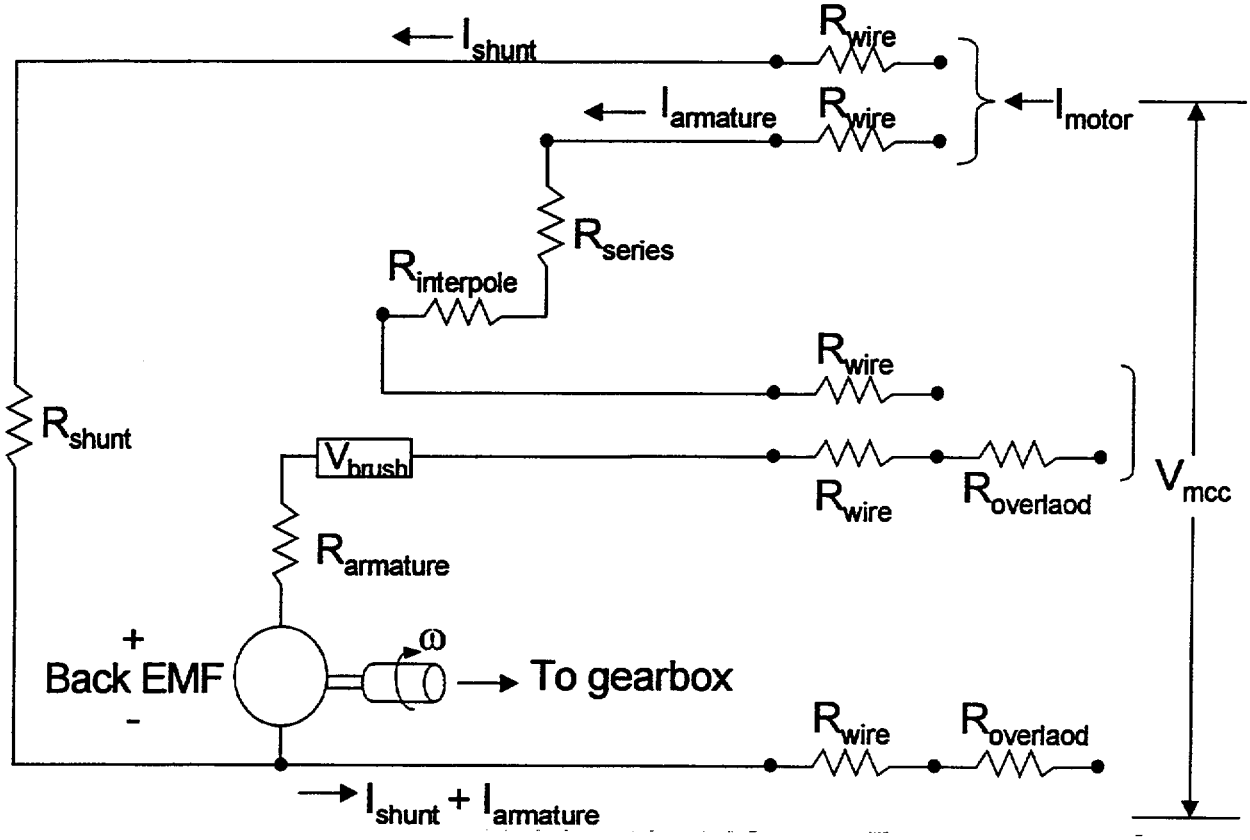

Figure 7. Electrical schematic of a typical MOV dc motor modified to reflect a typical field installation.

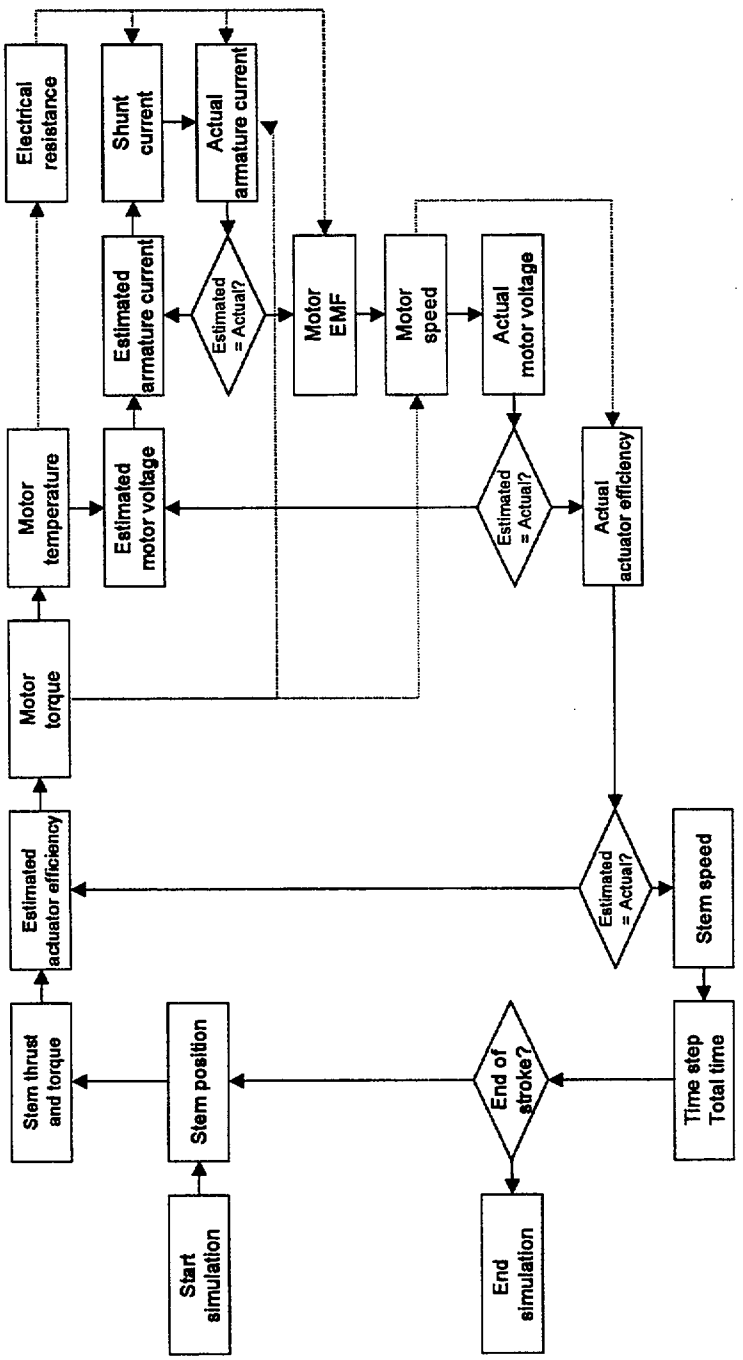

Figure 8. MISTA dc motor and actuator model calculations.

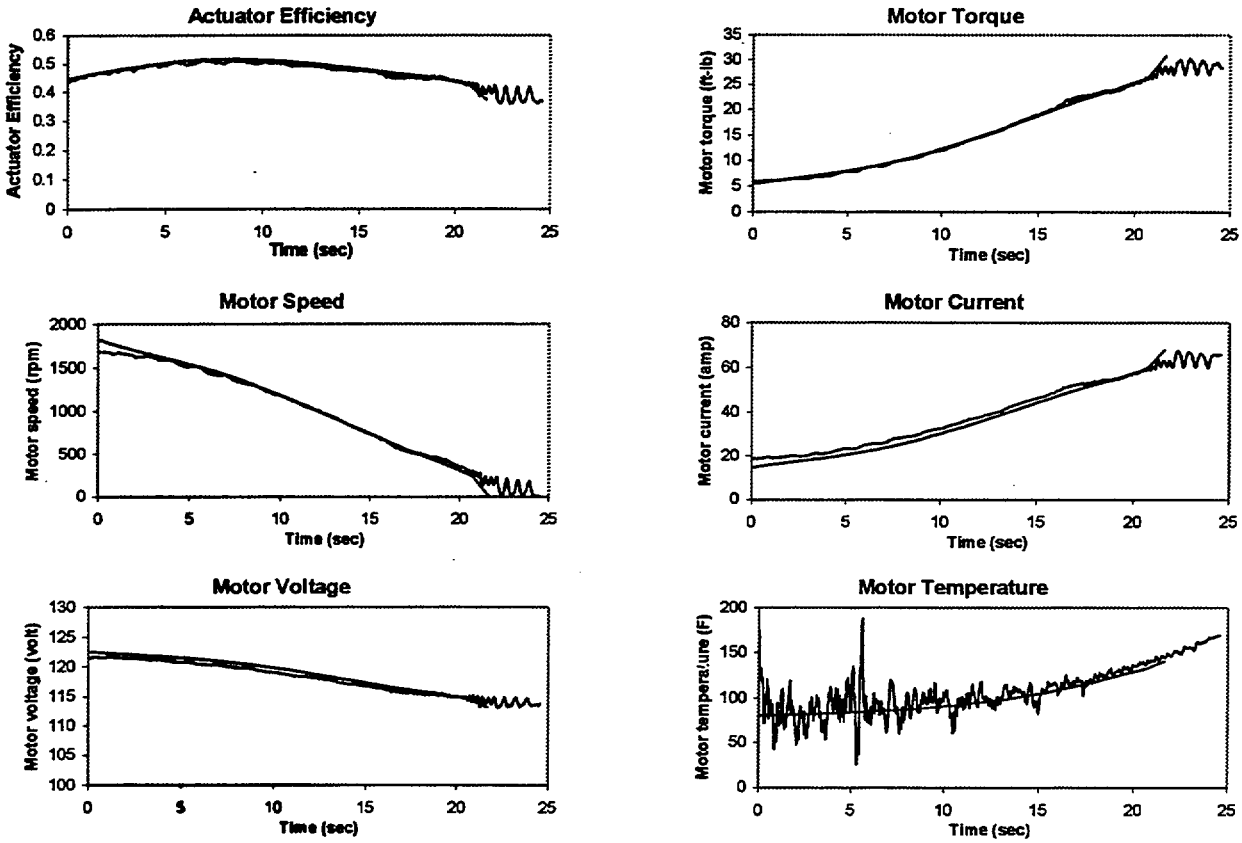

Figure 9. Comparison of actual dc motor and actuator response with the predicted results from the MISTA software.

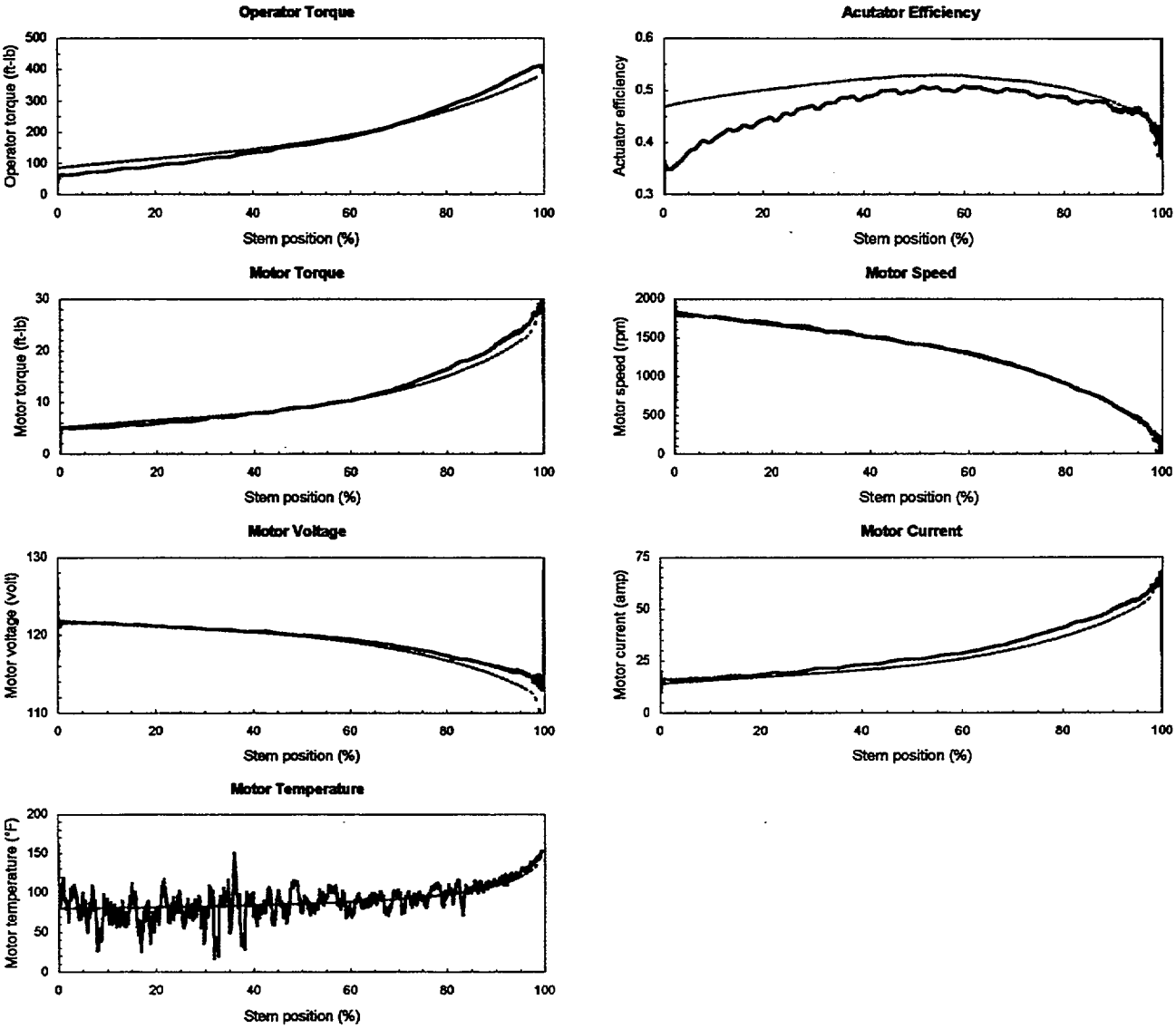

Figure 10. Comparison of actual dc motor and actuator response at 100% voltage and ambient temperature with the predicted results from the MISTA software.

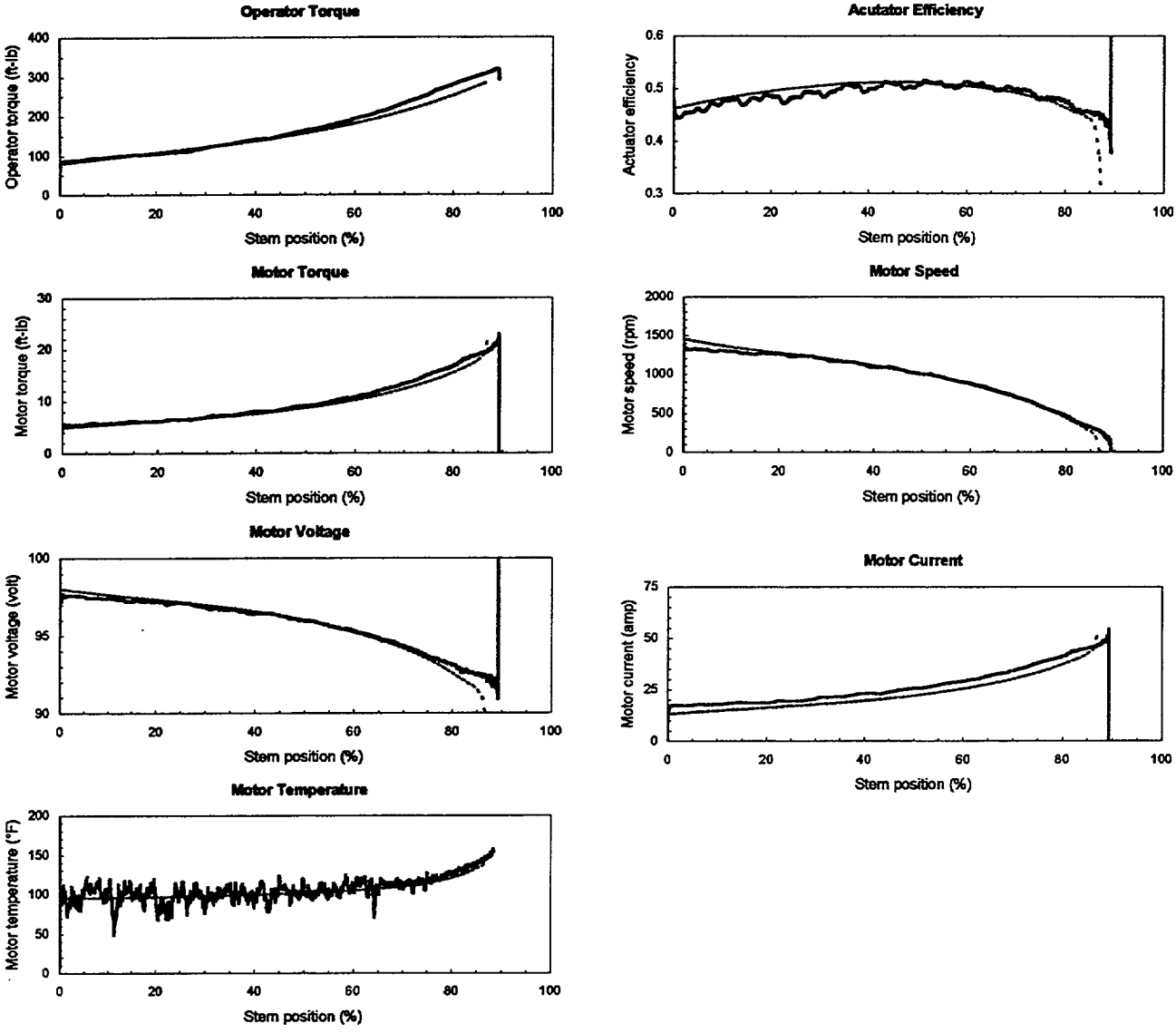

Figure 11. Comparison of actual dc motor and actuator response at 80% voltage and ambient temperature with the predicted results from the MISTA software

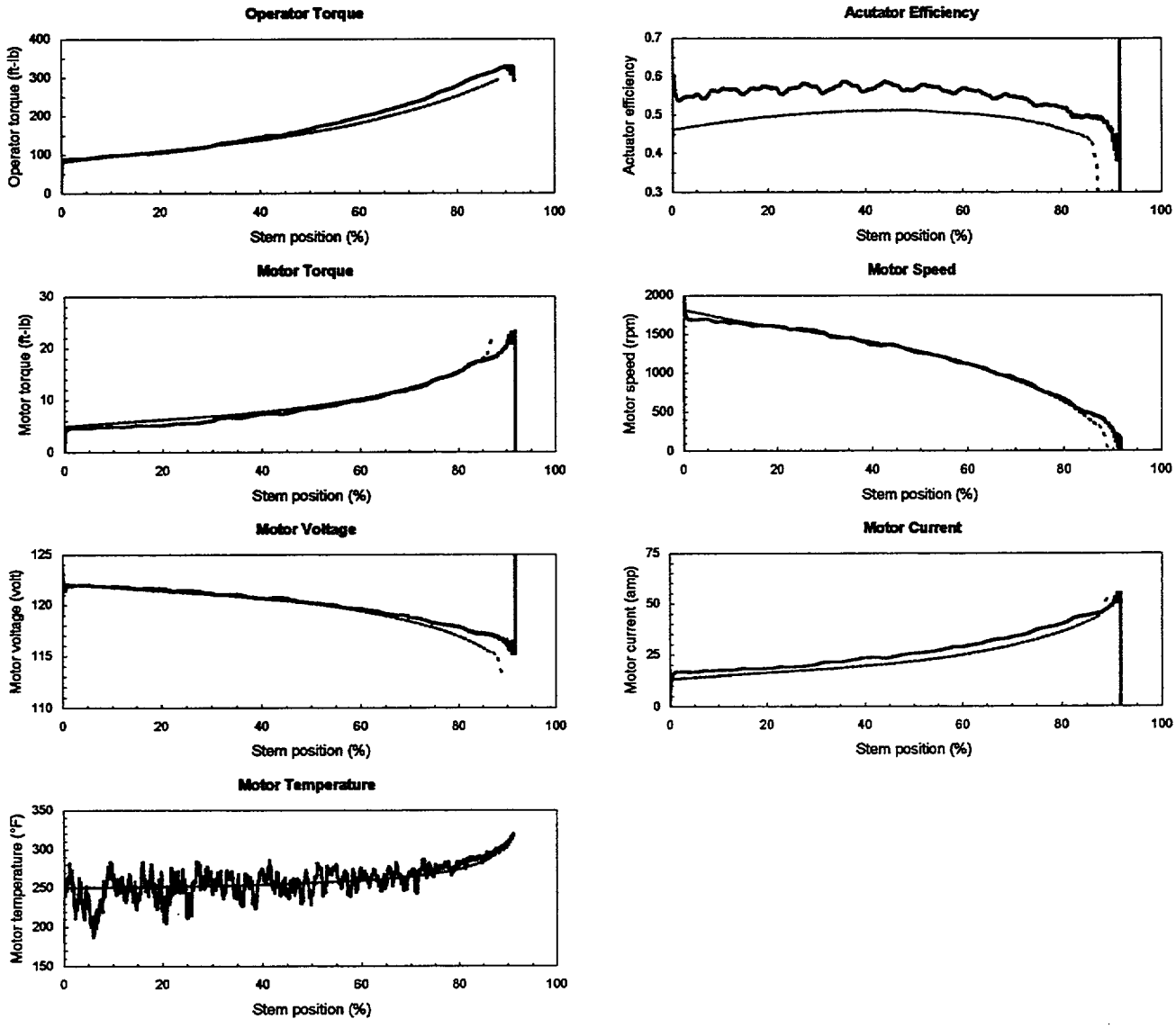

Figure 12. Comparison of actual dc motor and actuator response at 100% voltage and elevated temperature with the predicted results from the MISTA software.

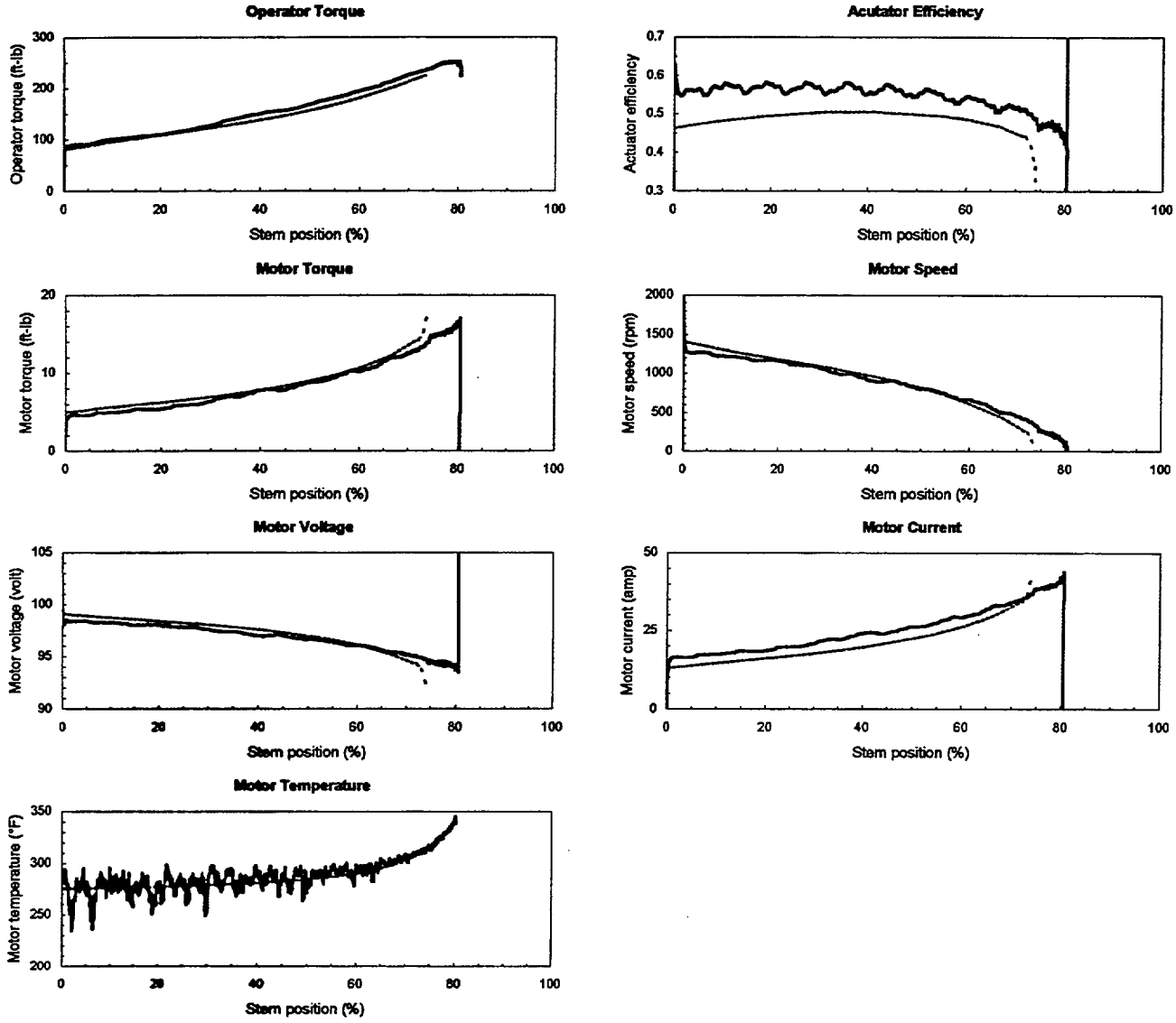

Figure 13. Comparison of actual dc motor and actuator response at 80% voltage and elevated temperature with the predicted results from the MISTA software.

The Development of In-situ Diagnostic Analysis System for Motor Operated Valves

Haruo Ito
The Japan Atomic Power Company

1. Introduction

The requirements for reliability improvement as well as cost reduction, "maximum reliability and minimum cost," have become one of the biggest issues in the nuclear plant maintenance field in the period of deregulation of the Japanese electric power market.

While these two requirements seem to be incompatible, machine designs for eliminating inefficiency together with structural and technological innovations in the conventional maintenance methods can realize both of them.

In the United States, in-situ machinery monitoring techniques have been developed, and recently various reports were published about maintenance cost reduction.

Also in Japan, many attempts have been made to shift to Condition Based Predictive Maintenance (CBM) from Time Based Teardown Maintenance (TBM) through introduction of in-situ diagnostic technology in order to improve economics of machinery maintenance at nuclear power plants. However, CBM will not work sufficiently unless there are obvious degradation mechanisms of the equipment and adequate diagnostic technology to detect them.

The in-situ diagnostic system developed by Japan Atomic Power Company (JAPC) is a useful tool for accurately checking the conditions of motor operated valves (MOVs), which are used in a large quantity as isolation valves and injection valves in safety related systems, in a short period of time not only during the periodic maintenance outage but also under normal operation.

This JAPC system can meet the recommendations of GL 89-10 and 96-05 by the NRC in the United States as well as the guidelines for operation and maintenance at nuclear power plants provided by Japan Electric Association Guide (JEAG)-4803.

This paper reports on the developmental work and actual experienced results of the newly developed in-situ diagnostic system at nuclear power stations of JAPC.

2. Problems with Conventional Maintenance for MOVs

2.1 Problems with TBM

To confirm the integrity of a great number of MOVs, the conventional approach was planned periodic teardown maintenance (TBM), where MOVs were regularly disassembled and inspected. However, this method has a disadvantage since it is not possible to tell whether the MOV is

healthy without disassembling it. And also, disassembling MOVs might invite new trouble such as human error by causing misassembly of healthy valves. This causes a potential for excessive maintenance costs.

In recent years, TBM that is thought to be excessive has hindered shortening of the periodic maintenance outage duration.

2.2 Analysis of Experienced Troubles

Out of 1,400 MOV inspections, including more than two cases per one valve and remarkable phenomena which were detected prior to failures, 564 cases of trouble have been found during the periodic maintenance outages at Japanese nuclear power plants since 1988, according to the conventional diagnoses conducted by Nippon Gear Company (NGC), a manufacturer of MOV driving units. As a result, 70% of the troubles were found as torque related matters.

Driving Unit Troubles Related Torque

1. Insufficient torque settings for opening/ closing: 242 cases
2. Improper torque switch setting of by-pass position: 81 cases
3. Improper motor brake operation: 12 cases
4. Worm shaft sliding troubles: 4 cases

Valve Unit Troubles Related Torque

1. Increased friction at gland packing of gate valve: 3 cases
2. Increased friction at gland packing of butterfly valve: 4 cases
3. Wear-out of baffle guide of ball valve: 5 cases
4. Wear-out of stem nut: 42 cases

The above results show that more effective preventive maintenance would be hoped, if there were some devices that could properly measure torque of the driving unit.

2.3 Problems with Conventional Diagnostic System

Conventional diagnostic devices for MOVs have been used as a part of maintenance during annual outages in Japan since the latter half of 1980.

Between 1987 and 1995, JAPC has tried to verify the performance and effectiveness of various types of diagnostic devices, including those developed in the United States, at the JAPC nuclear power plants. Finally, JAPC started diagnostic analysis of MOVs using NGC's existing diagnostic equipment called Super MAC since 1996 for practical use at Tsuruga power station.

The purpose of using the diagnostic system was to reduce the overall maintenance costs by verifying the integrity of MOVs and to review breakdown inspection and overhaul frequency of the conventional maintenance method. However, it was unavoidable to isolate both the MOV system and its power supply system because the conventional diagnostic system required attaching many sensors which must be disassembled as part of the mechanism. The result introduced poor work performance in that only two units per day could be diagnosed. Furthermore, the torque sensor which was temporarily mounted on the surface of MOVs did not have sufficient accuracy and was not suitable for a comprehensive diagnosis of the driving unit and the valve unit, or for trending the conditions of for MOVs.

It was also impossible, of course, to diagnose MOVs during plant operation. (See Fig. 2)

As diagnosing methods for MOVs which can detect load behavior of the valve, there are indirect methods such as motor current analysis and motor KW analysis. There are also direct methods such as using a strain gauge measurement which directly checks abnormal loads, thrust, and torque at the valve stems.

Since it is easy to measure electric current of motors, the current analysis method has been used widely in power plants in the United States as an economical and easy diagnostic method. However, theoretically, it has the demerits that quick changes in MOV condition cannot be traced clearly due to the large effect of current waveform attenuation caused by the motor mechanical inertia. Also, as compared with direct measurement methods, KW method can neither detect the load variations by distinguishing the load between opening and closing directions nor evaluate the holding torque applied to the valve stem when stopping the valve.

For the above reasons, JAPC decided to develop an In-situ diagnostic system that can accurately detect transitional torque behavior by upgrading the torque sensing technology, which was utilizing the strain gauge.

3. Outline of the Technical Development

3.1 Points of Technical Developments

As mentioned above, the method for attaching sensors from outside the driving units has restrictions from the viewpoint of uncomfortable attachment work and diagnostic accuracy. Therefore, it was not able to obtain condition monitoring of MOVs during plant operation.

The break-through point of these limitations is that the torque sensor is mounted inside the driving unit semi-permanently (build-in type) to achieve accurate diagnosis by directly checking the torque behavior during operation.

As shown in Fig. 3, the MOV has a mechanism that the entire load generated by the rotation of the motor is conveyed to the driving unit through the valve stem. Therefore, accurate diagnosis will become possible by mounting a torque sensor, a strain gage, at the point where the above load can be detected and obtain the torque signal including the abnormal loads applied to the valve stem.

3.2 Flow of Technical Developments

Technical development work has been carried out for almost three years. First of all, we verified the effectiveness of the built-in type torque sensor on an individual basis and when attached to a driving unit. The sensor was also reformed to easily obtain the torque signal while the MOV was in operation.

In the next step, mock failure tests were carried out based on assumed degradation and failure modes. Then, a diagnostic algorithm was developed by clarifying the relationship between the torque waveform and degradation and failure modes.

Mock failure tests based on past experienced troubles concentrated on detecting the wrong setting of torque and limit switches for valve protection devices, motor power amounts and degradation of the transmission system for the drive units, stem nut wear-out, defective gland packing, valve stem bending, valve suspension wear-out and sticking for the valve units through waveforms of torque sensor.

As for the diagnostic system, an all-in-one type device was developed with functions to predict the life of components according to degradation tendency management and to revise inspection plans such as overhaul

inspection periods in addition to diagnosis function.

Verification tests were made on SMB type and SBD type, with a shock absorbing spring, for driving units and on gate valves, butterfly valves and globe valves for valve units in order to confirm that the developed diagnostic device could be useful widely.

3.3 Built-in Type Torque Sensor

Limitorque type MOVs originally have a torque spring mechanism, as shown in Photograph 1, where the structure receives all the loaded torque applied to the valve stem.

Fig. 4 shows a cross section of such a system. The built-in type torque sensor is a part of installing the strain gauge on the component which receives the load in the torque spring mechanism.

The valve stem engages the worm gear via the worm shaft. When the motor rotates, the worm shaft moves left or right according to the load applied to the valve stem per each direction of opening or closing. The load acting on the torque spring allows the sensor to accept the tensile stress when in the opening direction and also the compression stress when in the closing direction. Since this load force is equivalent to the torque that is the multiple of the thrust of the valve stem and the radius of the worm gear, the device is called a "torque sensor." As the torque sensor is effectively applied and is mounted in the location of the principal mechanism of driving units, it is possible to accurately detect the load both in the opening and closing directions of the driving unit and the valve unit.

Built-in type torque sensors can easily be mounted by only replacing the existing component in the torque spring mechanism. So, once it is installed it is possible to measure the torque waveform during operation by just a connecting signal cable of the diagnostic equipment without any isolation.

3.4 Diagnostic Method

The diagnostic method is to check the degree of degradation by comparing the amplitude change and time change on the torque waveform with that of a normal MOV. Thus, this system can perform abnormality diagnosis and degradation tendency management.

Fig. 5 shows the typical torque waveform when a gate valve is moved from full open to the full closed position. The vertical axis shows the torque value, compression (+) and tension (-); and the horizontal axis shows the time.

If the valve is in the full-closed position, a seating force is applied to the valve stem in the compressed direction. When the motor is rotated, the worm will also rotate via the pinion gear and the load on the torque spring is relaxed. Then, the seating force on the valve stem is reduced and the torque value temporarily shows no load.

The worm gear is provided with a slight slip angle where the motor can achieve its full rotation in a short period of time and its full power is transmitted to the stem nut that moves the valve stem up. Since this situation is like the pounding of a hammer, which indicates the impact-type torque waveform, this point is called "hammer blow."

After absorbing the play away time of the gear transmission system, the force is transmitted to the stem nut, which pulls out the valve stem. The waveform changes at this moment indicate the pull out torque of the wedging disc. Subsequently, the valve stem moves in the open direction while receiving tensile force through the friction at the gland packing. When the valve reaches the full-open position,

where the valve unit back seat is effective, the tensile force continues to be applied to the valve stem because the motor is still rotating. When the torque reaches a pre-set value, the torque switch will be activated to stop the motor. However, there still is a slight amount of torque being applied to the valve stem due to the residual inertia of the motor rotor.

This is a very important point. If the torque switch does not work properly, the motor will experience a thermal trip, and if the torque pre-setting is not appropriate, an excess tension will be applied to the valve stem. Also, repeated operations under such conditions lead to fatigue build up, which might cause the wrench off of the valve stem.

In the waveform as described above, if the play away time of the transmission system becomes larger, the required time between the hammer blow and the valve pull out will be longer. If foreign matter causes hang up of the valve disc, the waveform of pull out torque will be higher. When the tightening of the gland packing is excessive, the running torque based on the friction will be raised. The change of running torque in a curved way means bending of the valve stem. The divergence of the torque switch setting can be detected by directly reading the holding torque value at the point where the power is shut off.

As mentioned above, visual diagnosis can be made through the torque waveform and can be used by anyone who understands the basic characteristics of MOVs.

3.5 Features of New Diagnostic System

The newly developed diagnostic system is called MOVDAS, or the "Motor Operated Valve Diagnostic Analysis System."

3.5.1 Hardware Function

Photograph 2 shows the MOVDAS diagnostic system. The diagnostic equipment is contained in an attache case together with the CPU and batteries, which does not require any outside power supply. It is lightweight at about 12 kg and does not need any additional tools like signal conversion boxes. The signal cable for the torque sensor is connected to a pre-mounted torque sensor. A micro-current meter is clamped to the motor power cable from the outside. A vibration sensor is attached to the end blanket of the motor with a magnet. So, one person can easily carry it to diagnose MOVs without isolating the system during plant operation.

3.5.2 Software Function

Fig. 6 shows the software functions of MOVDAS. Package software called "Test Point" is used to measure analog signal inputs of torque, electrical current, and vibration during normal operation. While in a maintenance outage, it also has an ability to measure the valve lift, stem thrust, the acting points of the limit switch and the torque switch, etc.

"Visual Basic" is used for the database software which consists of a database of various data such as the specifications, design data, inspection history, tendency and prediction management of degradation, and inspection plans of MOVs.

MOV lists, diagnostic results with regard to degradation, and inspection plan, etc. are printed as an output function.

4. Test Results

4.1 Results of Mock Failure Tests

Table 1 shows the results of a mock test of degradation and failure modes. The test indicated that it was possible to diagnose almost all the basic items of both the driving unit and the valve unit itself through only the analysis of the torque waveform.

Furthermore, highly reliable diagnosis was available in conjunction with the supplement of the micro-current measurement and vibration measurement that can easily be measured while MOVs are in operation.

Photograph 3 shows a simulation of the wear-out of the stem nut. Fig. 7 shows the MOVDAS waveform when wear-out takes place.

The time difference, ΔT, of backlash times of the gear transmission system between the normal condition and the wear-out condition can be obtained by the cursor operation of the torque waveform. Then, accurate wear-out as same as multiplying ΔT by the stem running speed can be given.

4.2 Tendency and Prediction Management

Measurement data stored in the database by cursor operation on the torque waveform are automatically transferred to the tendency and prediction graph. Fig. 8 shows a sample graph of wear-out of a stem nut. A prediction curve is generated from past data and can be compared with predetermined values. It is possible to evaluate the component life limit and to estimate the proper timing of replacement of parts, the rational inspection frequency and a rational maintenance plan as final output.

4.3 Application for Globe Valve

Fig. 9 shows a diagnostic torque waveform of a globe valve in the loop facility at the JAPC training center. The torque was constant until the valve reaches the full-closed position when there was no load, whereas a large upward pushing force by the fluid would be applied to the valve just before shutting off the valve in operation. This picture shows that the valve units with the driving unit have proper seating force greater than the fluid shut-off torque.

Thus, MOVDAS is able to determine whether the valve operates properly to accomplish its function by diagnosing the waveform under the actual load. It is thought that it will be possible to diagnose the degree of erosion of valve components and the integrity of the valve seating face condition in the future by strictly reading the torque waveform analysis.

4.4 Verification of Design Base Performance

By using MOVDAS, it is possible to evaluate design base performance that has been difficult under the conventional system. It is also possible to discover the design problem, which has often been overlooked, and to find similar chronic problems existing in MOVs and their components. Therefore, since the utility companies can always grasp the actual capacity of MOVs compared with design basis, it may contribute to the public understanding by guaranteeing the performance.

4.5 Experience of Actual MOV Diagnosis

JAPC has currently been gathering MOVDAS diagnostic data during operation at both Tokai #2 and Tsuruga power station where 30 torque sensors have already installed on MOVs.

This paper introduces two examples of diagnosis.

4.5.1 Experience for Pump Outlet Valve

Since MOVDAS has a design database, as described above, it is possible to evaluate the performance under actual loads in operation.

Here is an example diagnosis of the outlet valve of condensate booster pumps. Normally, two out of three pumps are always in operation and they are periodically changed over. The result of the diagnosis when the pump changed over showed that the outlet MOV of the stopped pump had enough torque allowance for the required torque. The reason was that there was little pressure difference between inlet and outlet of the MOV, because the outlet line of each pump was connected together. However, the diagnosis of the final stopped pump outlet valve when the plant was shut down for a maintenance outage, showed that a large ΔP was applied to the MOV. Although it was completely closed, the maximum required torque was very close to the preset value for actuating the torque switch and there was little leeway.

This means that the slightest operating conditions or the state of the valve unit could activate the torque switch, which might result in an incomplete closing of the valve unit. An investigation revealed that the preset torque value was lower than that which had been determined during the design process. Although there was enough allowance in terms of performance of the valve unit as well as the driving unit, this is an example that such a problem could go unnoticed unless diagnosed.

4.5.2 Problem on the Motor Brake for Driving Unit

MOVs in safety-related systems have high speed driving units because they are required to open and close in less than ten seconds. Designs have been introduced to mitigate the shock which takes place when those valves are seating. Generally, MOVs in safety-related systems have special motors equipped with a brake.

Fig. 10 shows the torque waveform of a gate valve when the valve moves to the close position. When the brake operates normally, the torque must be maintained like the A type of waveform after stopping the motor. In this case, however, the torque was not maintained as indicated by the B type of waveform. An investigation revealed that the cause was slippery oil adhering to the brake shoe surface and that the brake did not work properly. Furthermore, a degradation of the seal ring on the internal motor shaft and intrusion oil from the mechanical compartment side was found.

This phenomenon was discovered only by MOVDAS diagnosis.

5. Relations with Standards

5.1 Relations with NRC Recommendations

In the United States, a number of MOV troubles were experienced in the nuclear power plants in the past. Many of the causes were inappropriate switch settings regarding the maximum pressure differences of valve units, which lead to torque related troubles like incomplete opening. NRC was concerned about the reliability under design basis conditions of MOVs used in safety related systems and published GL 89-10, "Safety-Related Motor-Operated Valve Testing and Surveillance," in 1989, to recommend performance verifications under design basis

conditions relating to MOVs in safety related systems.

Further, NRC published GL 96-05, "Periodic Verification of Design Basis Capability of Safety-Related Motor-Operated Valves," in 1996 as a complete guideline for a regular periodic verification program, taking into consideration the increase of necessary thrust caused by degradation and the decrease of output power of driving units. Also, verification of the effectiveness of the program was requested. In order to meet these recommendations, diagnostic equipment that can precisely measure the thrust and the torque on the valve stem are needed during operation.

MOVDAS has an excellent technology that can meet them. Table 2 shows the failure phenomena pointed out in GL 89-10 and to what extent MOVDAS can handle them.

5.2 Japanese Regulatory Guidance of JEAG4803

JEAG4803 spelled out the shift from TBM to CBM following the ASME O&M standards in the United States, and organizes the basic philosophy and requirements that must be met. MOVs are described in Part C, "Valve Testing during Operation," which requires stroke time measurement testing while in operation depending on the category. Also, from the standpoint of upgrading accuracy of CBM it is preferred to measure the thrust, the torque of the driving units, and electrically related parameters. It is thought that MOVDAS is the only diagnostic device which clearly meets the above requirements.

6. Maintenance Costs Estimation Adopted CBM for MOVs

Since the effectiveness of this diagnostic technology has been verified, JAPC is studying a new maintenance plan for MOVs by taking into consideration CBM at its nuclear power plants. By means of importance evaluation, 80 to 90 MOVs per each unit, which are installed mainly in the safety-related systems, have been selected for diagnosis. Including other MOVs, the maintenance method is being progressed from the conventional TBM to the general inspection focusing on diagnosis. It will lead to rational MOV maintenance in accordance with the degree of degradation by predicting the life of components through CBM.

Cost evaluation has shown that, although initial costs for purchasing built-in type torque sensors and diagnostic equipment are comparatively higher than those for conventional maintenance, the cost merits for CBM will come out soon since the disassembling inspections which occupy the major portion for TBM can be eliminated. Also, although TBM inspections of the driving unit and the valve unit were separately conducted as conventional maintenance, diagnosis of the driving unit together with the valve unit at the same time for the developed CBM can realize a rational maintenance plan.

7. Conclusion

As described above, this new diagnostic system has enough capability to detect failures and to diagnose degradation of MOVs. As shown in Table 1, it has been verified that it is basically possible to diagnose not only the driving unit but also the valve unit all together by only using the torque waveform analysis.

Since diagnosis by MOVDAS can be performed in plant shutdown as well as during operation in a short period of time, it can be applied to performance verification by periodic tests and to guarantee design base performance.

Furthermore, it can contribute to decreased radiation exposure while inspecting MOVs in high radiation areas.

Also, in view of direct detection of machine conditions and determining internal machine condition, it is believed that MOVDAS will give transparency to the technology to improve reliability and contribute to public acceptance.

Still more, since conventional designs of driving units have enough capacity margin, rationalization of designs as an intelligent driving unit, combining this sensing technology with IT, will enable further cost reduction in the future by downsizing the driving unit. Also, in new plant designs, by mounting torque sensors at the initial stage of MOV manufacturing and by grasping the continuous performance of MOVs, it is considered that it can be possible to continue performance guarantees by the plant vendor at the time of factory test, installation and startup tests. Consequently, the power utilities may be guaranteed continuous performance of MOVs after the start of commercial operations to be cost effective.

Studies will be continued to refine this system by accumulating actual data.

References

1. Technical data and operational manuals for Limitorque Actuator by Nippon Gear Company, Ltd.
2. Generic Letters 89-10 and 96-05 by NRC.
3. Operation and maintenance guides for BWR and PWR, JEAG4803–1999 by Japan Electric Association.
4. Basic study of abnormality diagnosis by current analysis for motor operated system by Toshio Toyoda published in Japan Facility Management Association.

Table 1. Result of mock failure tests		
	Items of diagnosis	**Applied torque waveform**
1. Basic parameter	Stroke time	Running time
2. Switches	Actuating point of limit switch	Running time
	Actuating point of torque switch	Holding torque
	Incorrect bypass settings	Torque waveform
3. Motor	Insufficient motor power	Torque waveform
4. Transmission system	Excessive running torque	Running torque
	Defective gear	Torque waveform
	Wear out of stem nut	Play time
	Loose locking nut	Play time
5. Gland	Loose and tightness of packing	Running torque
6. Valve unit	Seating force	Seating torque
	Stem bending	Running torque
	Sticking of valve	Pulling out torque
	Disc suspensions wear out	Play time

Table 2 Summary of Common Motor-Operated Valve Deficiencies, Misadjustments, and Degraded Conditions with MOVDAS

	In Operation	In Outage
1. Incorrect torque switch bypass settings	App. (part)	App.
2. Incorrect torque switch settings	App.	App.
3. Unbalanced torque switch	App.	App.
4. Spring pack gap or incorrect spring pack preload	App.	App.
5. Incorrect stem packing tightness	App.	App.
6. Excessive inertia	App.	App.
7. Loose or tight stem-nut lockout	App.	App.
8. Incorrect limit switch settings	App.	App.
9. Stem wear	App.	App.
10. Bent or broken stem	App.	App.
11. Worn or broken gears	App.	App.
12. Grease problems (hardening, migration into spring pack, lack of grease, excessive grease, contamination, non-specified grease)	App. (part)	App.
13. Motor insulation or rotor degradation	Not App.	See note
14. Incorrect wire size or degraded wiring	Not App.	See note
15. Disk / Seat bending including thermal binding	App.	App.
16. Water in internal parts or deterioration thereof	Not App	App.
17. Motor undersized for degraded voltage conditions	App.	App.
18. Incorrect valve position indication	App. (visual)	App.
19. Misadjustment or failure of handwheel declutch mechanism	App.	App.
20. Relay problems (incorrect relays, dirt in relays, deteriorated relays, miswired relays)	App. (part)	App.
21. Incorrect thermal overload switch setting	Not App.	See note
22. Worn or broken bearing	App.	App.
23. Broken or cracked limit switch and torque switch	Not App.	See note
24. Missing or modified torque switch components	Not App.	See note
25. Improperly sized actuators	App.	App.
26. Hydraulic lockup	App.	App.
27. Incorrect metallic materials for gears, keys, bolts, shafts	Not App.	See note
28. Degraded voltage, within design basis	App.	App.
29. Defective motor control logic	App.	App.
30. Excessive seating or back seating force application	App.	App.
31. Incorrect reassemble or adjustment after maintenance and / or testing	App.	App.
32. Unauthorized modifications or adjustments	App.	App.
33. Torque switch or limit switch binding	App.	App.

(Abbreviation)
App. – MOVDAS is applicable in this case.
Not App. – MOVDAS is not applicable in this case.
(Note) General inspection such as visual inspection, meggering, replacement of waste parts.

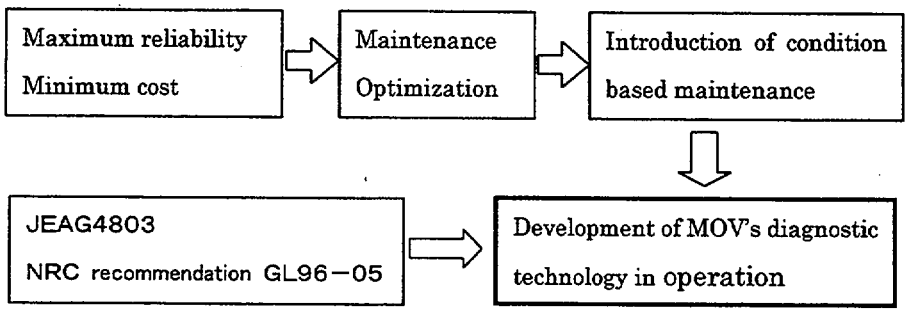

Figure 1 Needs for technology development

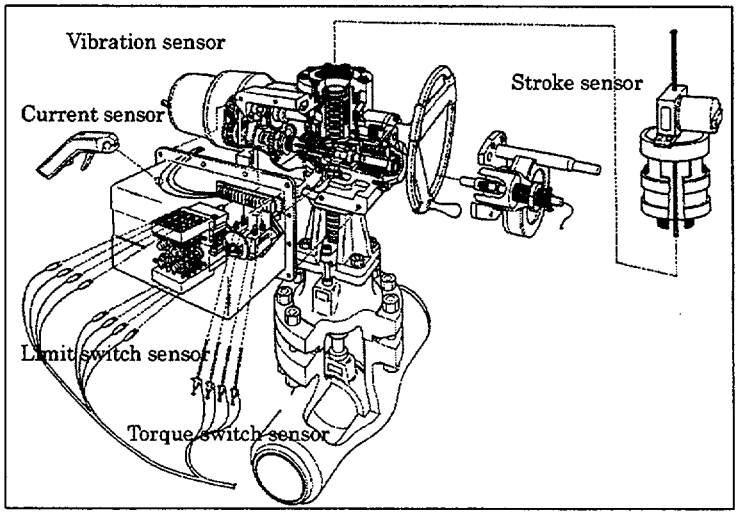

Figure 2 Sensors required for conventional diagnosis

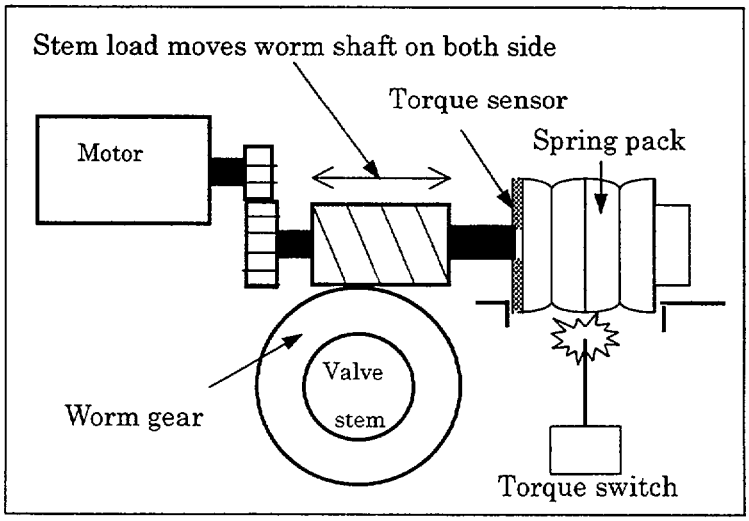

Figure 3 Mechanism of MOV

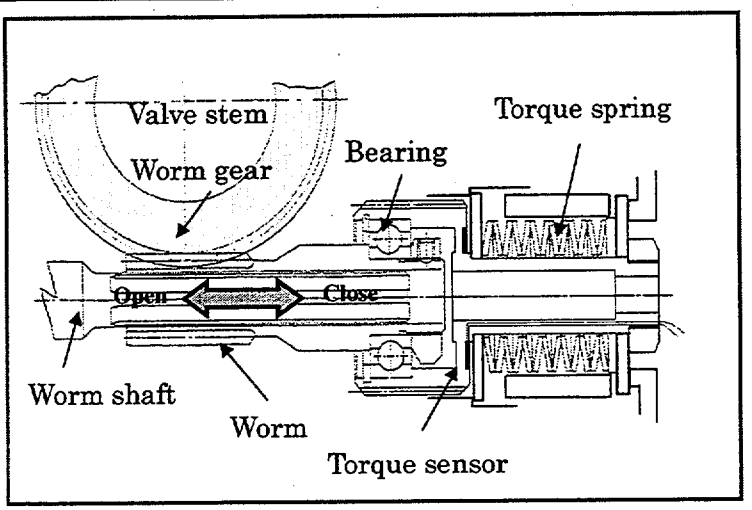

Figure 4 Built-in type of torque sensor

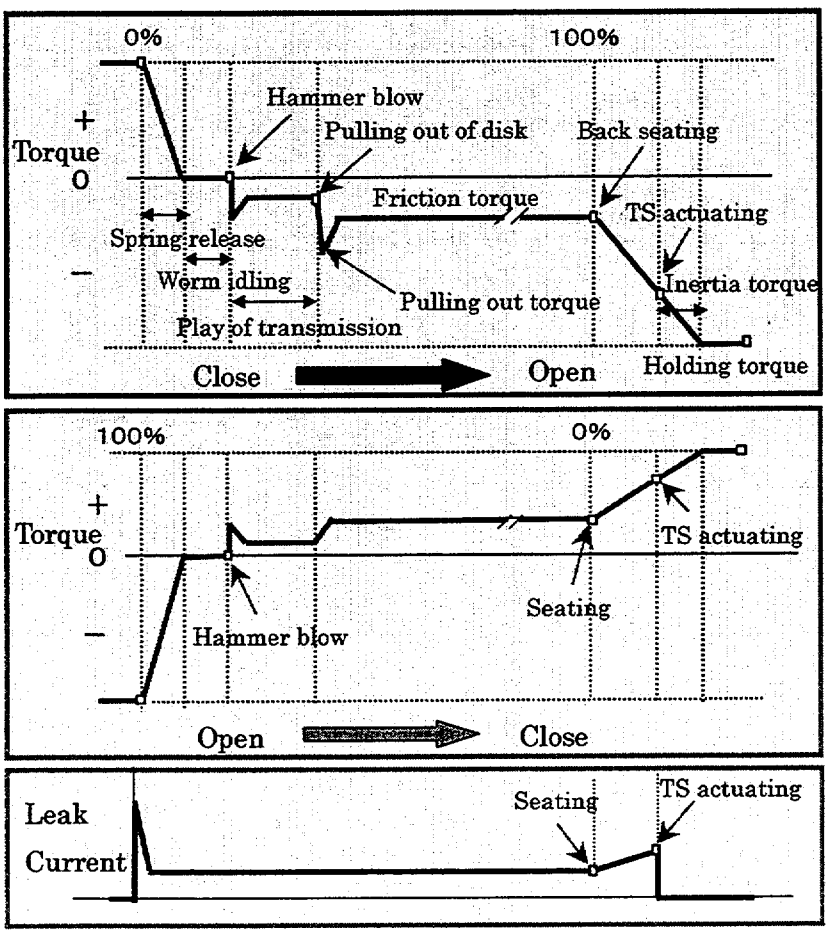

Figure 5 Typical torque waveform of gate valves

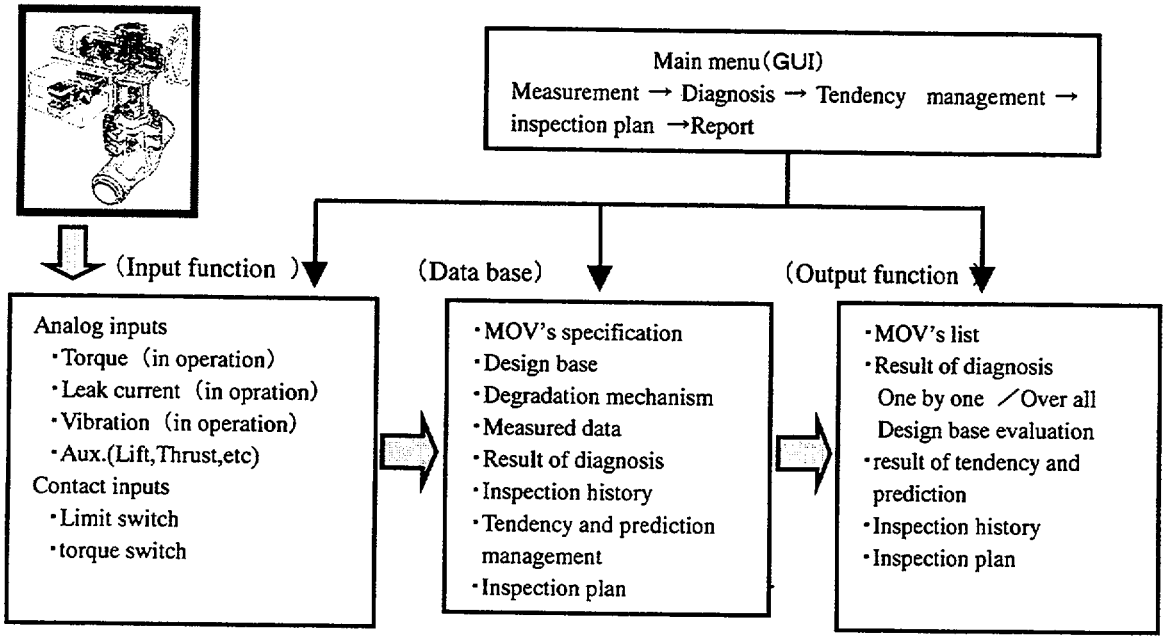

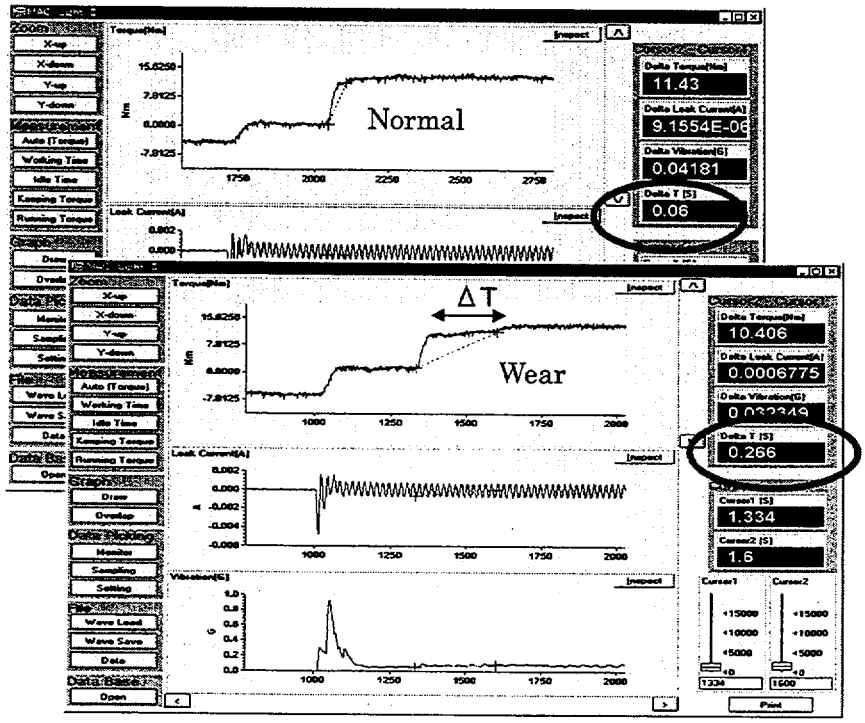

A amunt of wear=(0.266-0.06)sec × 6.00mm/sec=1.236mm

Figure 7 Mock failure of stem nut wear

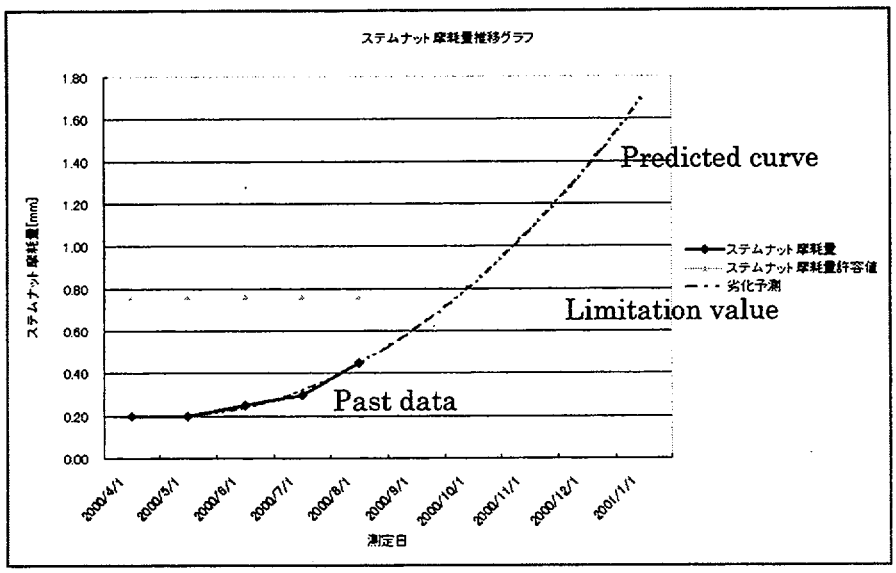

Figure 8 Tendency management graph of stem nut wear (example)

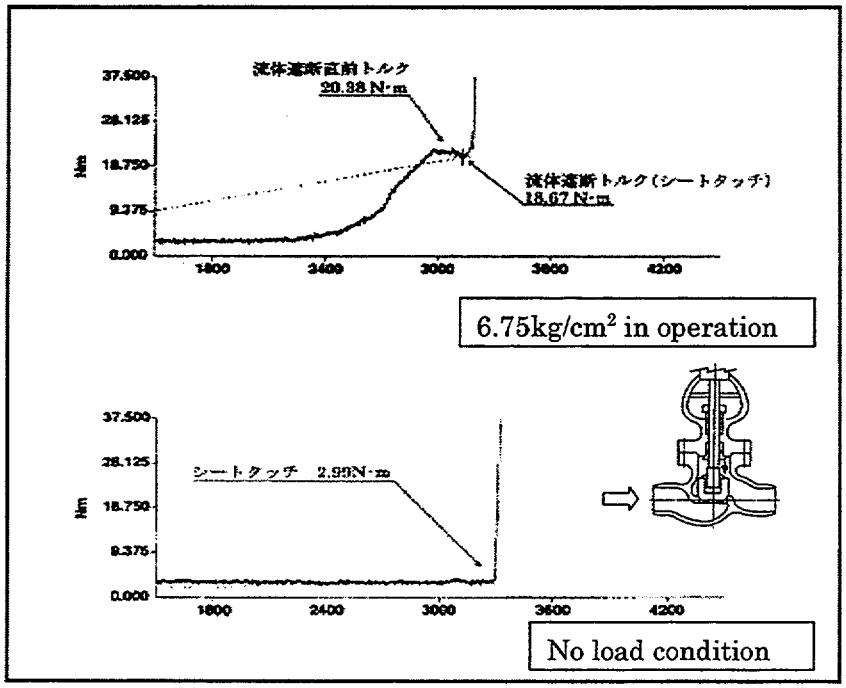

Figure 9 Torque waveform of gate valve

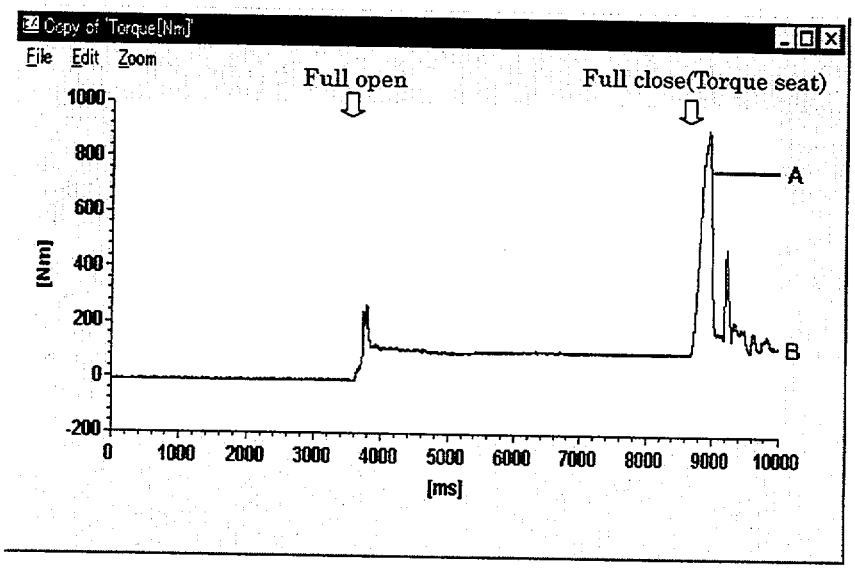

A: Normal (Torque holding by brake)

B: Unusual(Brake didn't work)

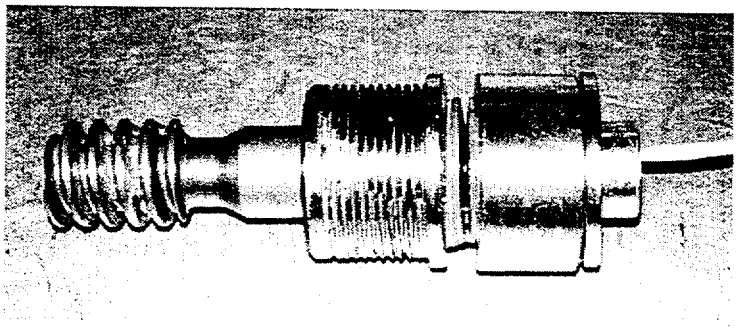

Photograph 1 Torque spring mechanism

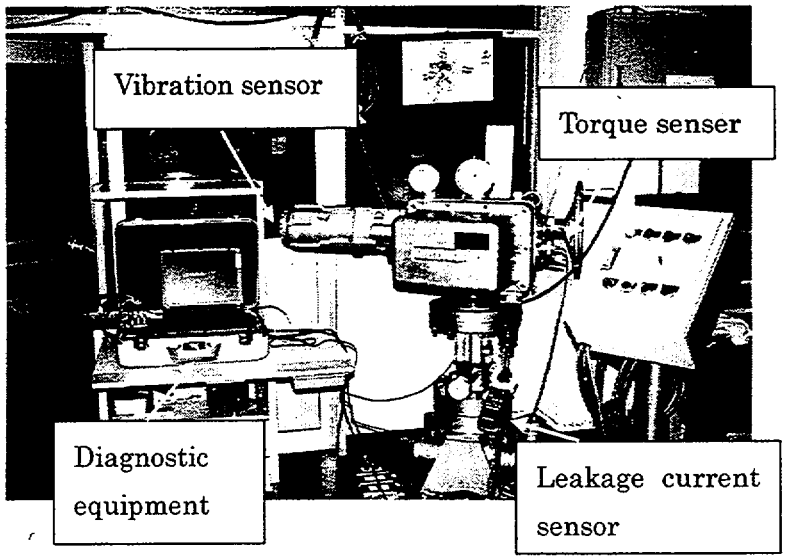

Photograph 2 MOVDAS diagnostic system

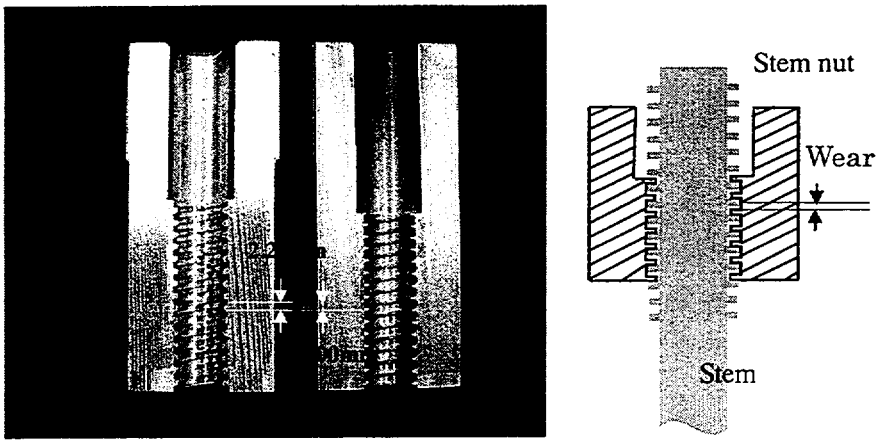

Photograph 3 Simulation of stem nut wear